Report number: 2024-1

EAN number: 978-87-7595-122-2

NorDust II

Nordic Road Dust Project Phase II

Cover photo: Satu AB and Mats Gustafsson, VTI

Project: NORDUST II Nordic Road Dust Project Phase II
Date: Date the report was finished and submitted.
Report title: Nordic Road Dust Project, Phase II (NORDUST II)
Report number: 2024-1 EAN-number: 978-87-7595-122-2
Project manager: Karl Idar Gjerstad, Statens vegvesen, Norway *Steering group:* Brynhild Snilsberg, Statens vegvesen, Norway Páll Valdimar Kolka Jónsson, Vegagerðin, Iceland Taiju Virtanen, Väylävirasto, Finland Hung Nguyen, Trafikverket, Sweden Michael Ruben Anker Larsen, Vejdrektoratet, Denmark
Members of the scientific group: Mats Gustafsson, Göran Blomqvist, Ida Järlskog, Nina Svensson (VTI) Sami Kulovuori (Metropolia) Bruce Rolstad Denby, Eivind Grøtting Wærsted (MET Norway) Ana Stojiljkovic, Niko Karvosenoja (SYKE) Henrik Grythe, Karl-Espen Yttri (NILU) Throstur Thorsteinsson (University of Iceland) Christer Johansson (University of Stockholm, SLB-analys) Michael Norman, Magnuz Engardt, Anton Josefsson (SLB-analys)
Financial partners: • Statens vegvesen • Trafikverket • Väylävirasto • Vegagerðin • Vejdirektoratet
Scientific partners: • Swedish National Road and Transport Research Institute (VTI) • Metropolia University of Applied Sciences • Stockholm luft- och bulleranalys (SLB-analys) • Finnish Environment Institute (SYKE) • University of Stockholm • Norwegian Meteorological Institute (MET Norway) • Norwegian Institute for Air Research (NILU) • University of Iceland

Summary:
The NORDUST II project has aimed to enhance knowledge about road dust emissions through extensive investigations, including laboratory and field studies, measurements, modeling, and future scenarios.
An initial work package summarized current knowledge on mitigating road dust emissions. It found that dust binding solutions are most effective during acute dust episodes, while sweeping is beneficial on a seasonal basis. Preventive measures during autumn and winter can reduce airborne dust in spring. A core component of the project was experimental parameterization of processes in the NORTRIP emissions model. Studies revealed that vehicle weight and speed significantly influence particulate matter (PM) emissions, with heavier vehicles and higher speeds increasing emissions. The type of tire and road surface properties also play crucial roles.

Experiments showed that winter sand is quickly crushed into finer fractions when driven over, but only a small portion of the sand mass is crushed. Coarse particles are removed more efficiently than finer particles at low speeds, but all particles are removed at speeds above 20 km/h. A field test in Linköping, Sweden, examined the removal of the dust binder CMA by traffic. Results indicated that the NORTRIP model could largely replicate the impact of traffic migration on CMA concentrations. A 16% reduction in PM10 concentrations was observed with dust binding.

The project also explored the correlation between road dust load and PM concentrations in the air, noting that dust load is typically lower in wheel tracks due to higher suspension forces. Studies found that tire wear particles have a unimodal size distribution, with a peak between 1 µm and 4 µm, making them a significant source of microplastics. Future scenarios with increased shares of electric vehicles (EVs) in Stockholm, Helsinki, and Trondheim were modeled. Heavier EVs increase non-exhaust emissions, particularly if the use of studded tires remains constant. Reducing studded tire use can, however, lead to lower emissions.

Initial tests in Iceland characterized road dust load, showing patterns similar to other Nordic countries. The NORTRIP model was used to assess the impact of mitigation measures on particulate matter pollution in Reykjavik. The NORTRIP model has been refined through various studies and applied to analyze future scenarios and mitigation measures. The model's parameters have been adjusted for better accuracy and have been used to evaluate the impact of changes in the vehicle fleet.

The NORDUST II project has significantly advanced the understanding of road dust emissions and effective mitigation strategies. It has developed tools for modeling and predicting future emissions under various scenarios, focusing on the parameterization of emissions, the impact of vehicles and tires, and the effects of electrification.

Web accessibility statement:
This report has been made web accessible.

Keywords: PM10, road dust, emission, dust binding, mitigation, winter maintenance, road operation

Language: English

Number of pages: 202

Content

Background

Road dust is an important source to airborne particles in the Nordic countries. It consists of wear products from road pavement, tyres, brakes, traction sand, salt and dust dragged in from adjacent unbound roads or deposited from nearby or long distance dust sources, like building sites and farmland. The cold climate in the Nordic countries enhances the formation of road dust compared to most European countries, since it promotes the use of studded tyres, which abrades the road surfaces, and winter maintenance where dust forming material is added to the road surfaces.

When limit values for airborne particles were introduced, first for PM10, then for PM2.5[1], and more wide-spread measurements and air quality modelling in Nordic cities where made, it was soon obvious that non-exhaust particles dominated the concentrations and especially so when PM10 limit values were exceeded. Exceedances were most common in late winter and spring. Numerous research initiatives stared to build up the knowledge about sources, emissions, exposure and mitigation possibilities. For many years the initiatives were mainly national. In Norway and Sweden, efforts were focusing on road wear and use of studded tyres (e.g. Norman & Johansson, 2006, Hussein et al., 2008, Gustafsson et al., 2007), while in Finland, a strong research focus was resuspension, tyres and the interaction between road surface and traction sand (e.g. Kupiainen & Tervahattu, 2004, Räisänen et al., 2005, Tervahattu et al., 2006).

An increasing collaboration between Nordic researchers in the area was further intensified through the project NOn-exhaust Road TRaffic Induced Particle emissions (NORTRIP), financed by the Nordic Council of Ministers (Johansson et al., 2012). The project initiated the development of an emission model, also called NORTRIP, which, as opposed to the then current emission models, could handle the complex factors influencing road dust emissions. These include e.g. wear processes, dust removal processes, road surface properties and conditions as well as road operation and meteorology. Many of the processes were very rudimental described due to lack of data that could be used for parametrisations in the model. Consequently, there was a need for research that could help fill the knowledge gaps.

In 2016, the project Nordic road dust project (NORDUST), financed by NordFoU, was initiated by the Nordic road administrations. It included a range of field and laboratory tests with the intention to produce data that could be used for improved parametrisations in the NORTRIP model. Tests included e.g. PM emissions from different studded tyre types, winter sand, sweeping efficiency, dust binding and flushing tests (Gjerstad et al, 2019). Some tests were successful, and results could be implemented in the model, while others were inconclusive and called for further improved research approaches. The research needs were compiled into what became a NORDUST II application, which was approved by NordFoU in 2020.

An important learning from the first project was the value of on-site common activities. Due to the pandemic, that unfortunately co-incided with the project period, most work had to be done in national isolation. The resulting report is structured as a compilation of the work performed within each work package.

[1] DIRECTIVE 2008/50/EC OF THE EUROPEAN PARLIAMENT AND OF THE COUNCIL of 21 May 2008

References

Gjerstad, K.I., Gustafsson, M., Blomqvist, G., Denby, B., Elmgren, M., Grythe, H., Janhäll, S., Järlskog, I., Johansson, C., Kulovuori, S., Kupiainen, K., Lundberg, J., Malinen, A., Norman, M., Ritola, R., Silvergren, S., Stojiljkovic, A., Sundvor, I., Þorsteinsson, Þ., Stefani, M., Vogt, M., 2019, NORDUST : Nordic Road Dust Project, http://urn.kb.se/resolve?urn=urn:nbn:se:vti:diva-14950

Gustafsson, M., Blomqvist, G., Gudmundsson, A., Dahl, A., Jonsson, P., Swietlicki, E., 2009. Factors influencing PM10 emissions from road pavement wear. Atmospheric Environment 43, 4699-4702, 10.1016/j.atmosenv.2008.04.028.

Hussein, T., Johansson, C., Karlsson, H., Hansson, H.-C., 2008. Factors affecting non-tailpipe aerosol particle emissions from paved roads: On-road measurements in Stockholm, Sweden. Atmospheric Environment 42, 688-702.

Johansson, C., Gustafsson, M., Blomqvist, G., Bennet, C., 2012, NORTRIP - Non-exhaust road traffic induced particle emissions : development of a model for assessing the effect on air quality and exposure, 1103341X (ISSN), Stockholms universitet. Institutionen för tillämpad miljövetenskap, http://urn.kb.se/resolve?urn=urn:nbn:se:vti:diva-5289

Kupiainen, K., Tervahattu, H., 2004. The effect of traction sanding on urban suspended particles in Finland. Environmental Monitoring and Assessment 93, 287-300.

Norman, M., Johansson, C., 2006. Studies of some measures to reduce road dust emissions from paved roads in Scandinavia. Atmospheric Environment 40, 6154-6164, https://doi.org/10.1016/j.atmosenv.2006.05.022.

Räisänen, M., Kupiainen, K., Tervahattu, H., 2005. The effect of mineralogy, texture and mechanical properties of anti-skid and asphalt aggregates on urban dust, stages II and III. Bulletin of Engineering Geology and the Environment 64, 247-256, 10.1007/s10064-004-0267-0.

Tervahattu, H., Kupiainen, K.J., Räisänen, M., Mäkelä, T., Hillamo, R., 2006. Generation of urban road dust from anti-skid and asphalt concrete aggregates. Journal of Hazardous Materials 132, 39-46, 10.1016/j.jhazmat.2005.11.084.

Work package 1: Compilation of best road operation practices to mitigate PM_{10}

Introduction

The scale of the road dust problem is different in different locations. Generally, the magnitude of the road dust problem is more pronounced in streets with high traffic volume, high driving speeds, and a greater need for traction control. On the other hand, suspended dust is more easily diluted in the ambient air in areas that are in an open environment. It is essential to take actions where they are most needed to protect health, increase comfort and reduce harm to the environment.

The amount of dust that becomes airborne in spring when surfaces dry up can be reduced by preventing the build-up of dust deposits during wet periods in autumn and winter as well as preventing suspension in spring.

The aim of Work package 1 is to compile best practice guidelines for road maintenance operations used to control road dust emissions based on results from relevant studies and projects.

Methods

Results from seventeen national and international studies and projects aimed to determine the impact of different road maintenance operations on road dust emissions and air quality have been reviewed. A brief description of studied measures, methods used and main results from different sources are summarized in Table A 1.

Results and discussion

Best practice guidelines for the use of traction control materials, dust binding and street cleaning are compiled in Table 1 to Table 3, respectively.

Traction control materials

In Nordic conditions, traction control methods are used during winter to improve traffic safety. These include the use of winter tyres and the application of traction salt and sand. Traction control measures should be optimized to have the least direct or indirect impact on air quality and, at the same time, maximize the benefits for traffic safety.

The most extensive tests to evaluate the impact of traction sanding on PM10 emissions were conducted in Finland. These tests assessed different sanding materials in terms of quality and grain size. In the NorDust project, sand crushing and sand migration tests were conducted. Best practice guidelines for the use of traction control materials compiled in Table 1 address the use of traction sanding.

Table 1 Best practice guidelines for the use of traction control materials

Material selection	It is recommended to use abrasion-resistant stone material for sanding, from which the smallest grain sizes (<1-2 mm) have been removed by wet sieving. Wet sieving removes the smallest particle fractions more efficiently than the dry method. Non-sieved and fine sanding materials should be avoided, as they contain a large amount of material that can directly contribute to PM10 emissions. It should be considered that the same fine fractions that are prone to contribute too PM_{10} also give better friction than coarser fractions on hard snow and ice (Bolme, 2018). Quality assurance should be developed to quickly detect and replace poor or non-compliant sanding material.

	Traction salt should be used as an alternative to sand whenever allowed by weather conditions. When using salt, the potential environmental impact should be considered (e.g., the impact on groundwater). The salt is not effective at temperatures below -6 ° C. The use of alternative traction control materials can be considered.
Optimization of sanding	Sanding should be considered only in areas where it is most beneficial, such as side-walks, bike lanes, stairs, intersections, inclined streets, and bus stops. If it is necessary to apply sand or gravel along the entire street length, the application rate (g m^{-2}) should be optimized in accordance with weather and driving conditions. For example, excess sanding material will not improve traction but will quickly be removed to surrounding and may cause damage, e.g., stones stuck in the tyres come loose and fly away at high speeds. To minimize the impact of sanding on the air quality, material accumulated during the winter should not be left in the street environment longer than is necessary. Scheduling of the sand removal should be made taking into account dust problem, temperature variations (night frosts), and the associated need for traction control.

Dust binding

Dust binding can significantly reduce street dust emissions and prevent peaks in the ambient PM10 concentrations in street environments where the dust load is high and road dust emissions represent a major contributor to PM10 levels. However, dust binding is not a long-term solution but gives maintenance time to take necessary steps during the spring season to keep streets clean. Efficient dust suppression requires repeated application and treatment over large areas. Proper timing of application will ensure maximal effects.

In recent years, different options for the application of dust binding solutions in terms of timing, application method and solution concentrations have been tested in Nordic countries. For example, the impact of fixed-schedule dust binding during springtime and extended block-wise operations were tested in Sweden. In Finland, the dust binding potential of the targeted application method was compared with the whole lane application method. Additionally, reviewed international reports provided some results from Central European and Mediterranean countries. In these studies, the impact of dust binding was evaluated for both paved and unpaved roads and industrial sites.

Table 2 compiles best practice guidelines for dust binding operations based on the findings from relevant studies.

Table 2 Best practice guidelines for dust binding operations

Application method	Dust binding solution can be applied to the whole lane width or targeted to areas with higher dust load. The WDS measurements indicate that the dust load is often highest close to the curb, between lanes and wheel tracks. The choice of application method will depend very much on the street surface conditions at the time of the operation. Whole lane treatment has a stronger dust emission reduction potential but may reduce friction, especially if a solution with a high concentration is used. Targeted dust binder application has practical advantages. For example, the amount of chemicals used in targeted spreading is significantly lower, decreasing cost, environmental stress risks and corrosion to infrastructure or vehicles. For example, the targeted spreading technique may be used more frequently for dust binding to minimize harmful side effects and the whole lane dust binding can be used as

	an efficient tool during the worst street dust days. Dust binding of the whole lane width supresses also emission of directly emitted wear particles, while targeted dust binding to kerb supresses suspension of this dust load.
Materials	The main dust suppressants that have been tested on paved roads and show similar efficiencies in reducing PM10 concentrations are magnesium chloride (MgCl2), calcium chloride (CaCl2), calcium magnesium acetate (CMA) and potassium formate (referred to as KF). Potential hazards to the local environment (damage to vegetation and human health, and contamination of soil and groundwater) should be considered when choosing dust suppressants, CMA and KF being eco-friendly options. The dust binding ability of a solution depends on its concentration. Stronger solutions have a longer-lasting effect but are more expensive and might increase the slipperiness of the surface. CMA and MgCl2 is normally used in saturated solutions (20-25%), while CaCl2 is used in 10% solution. Typically, the recommended application dose of the dust suppressants in the reviewed studies is 10 g m^{-2}. A higher application dose was used for targeted dust binding in Finland.
Timing	The timing of the dust binding treatments should be optimized by utilizing information about weather forecasts, air quality and expertise in winter road maintenance rather than according to the fixed schedule. The application should be done in dry weather without precipitation forecast and with the expected rising trend of PM concentrations. The efficiency of the treatment is highest at high air humidity (close to 80%). Nevertheless, application during lower humidity conditions, which are common during high PM_{10} episodes, will still have a positive but shorter-lasting effect. Because relative humidity typically fluctuates throughout the day, it is recommended to schedule the application of dust suppressant at night or very early in the morning before rush hour or in the evening /night before a day with expected high road dust emissions. If the dust binding is carried out in the middle of a very dry and sunny day, the solution will dry out quickly, reducing the treatment's effectiveness. It is also less suitable to apply dust binding agents when traffic is high due to risk for uneven application in stop-and-go traffic which can risk lower friction. Also, the risk for spraying other vehicles with sometimes corrosive solutions is high and not suitable nor effective. Additionally, the solution will quickly be removed from the street surface if it is applied before heavy rain. The observed effect of the dust binding treatment typically lasted 2-3 days, after which application should be repeated. In the Helsinki Metropolitan Area, the dust-binding agent has been reactivated by spraying a layer of water on top of the dust binding solution applied on the previous day. The efficacy or duration of this measure has not yet been studied.
Site prioritization	Dust binding should be performed especially at sites where i) exposure to dust is the largest and ii) the highest amount of dust is available for suspension. Street categorization based on the intensity of use (e.g., population density, vehicle density) may be used to determine the order in which streets will be treated.

	Dust binding should be avoided on streets with trams, since the agent can cause slipperiness on the tracks (e.g. Statens Havarikommisjon for Transport, 2011)

Street cleaning

Different tests have shown that the significance of street cleaning for road dust mitigation is due to its long-term impact on PM10 emissions rather than due to its impact on a day-to-day basis. Typically, street cleaning includes street sweeping (dry or wet), street flushing or their combination. Street sweeping equipment utilizes brooms to loosen dirt and debris from the road which is removed from the street surface by rotating brooms or sucked into the hopper using a vacuum nozzle. Flushing describes high-pressure water spraying onto a road surface to loosen dust and wash it off the street surface. Street cleaning reduces dust load and, thus, its subsequent suspension.

In Nordic countries, different street cleaning solutions have been tested. For example, in Norway, tests were made with a sweeper with dust-free performance without the use of water (DISA-CLEAN 130), different vacuum sweepers with flushing booms or rotating nozzles, and washing arms for cleaning sidewalks and side areas. Additionally, methods and equipment for cleaning tunnels were evaluated. In Sweden, the air quality impact of vacuum sweeping with or without flushing was assessed. In Finland, a street scrubber with captive hydrology (PIMU) (a sweeper that uses high-pressure washing to remove dust and debris from the street surface, which together with the water forms a liquid sludge, which is removed from the surface by a strong vacuum), and rear grit suction unit were tested and compared to a traditional vacuum sweeper.

Results from different tests show that street sweeping alone did not have much effect unless combined with high-pressure water flushing. The short-lived reduction of PM10 emissions that was sometimes observed after sweeping can be attributed to the water spraying that temporarily reduces the release of PM10 into the air. The most significant reduction of dust load was achieved when the initial level was high. Street cleaning operations in spring should be organized according to the magnitude of the dust problem, resources, and weather conditions.

Table 3 compiles guidelines for best practices for street cleaning based on the findings from the relevant studies.

Table 3 Best practice guidelines for street cleaning operations

quipment	Vacuum sweepers are preferable to simple mechanical sweepers. However, because sweepers can potentially increase PM10 concentrations during operations due to the re-suspension, vacuum sweepers should be supplemented with water spraying. Solutions for the control of the PM10 emission from the air outlet of the sweepers need to be considered. Different techniques exist, including cyclones, bag filters and electrostatic precipitators. Using vacuum sweeping in conjunction with high-pressure water flushing has given the best results in dust load reduction. Heavy suction is effective for removing loose road dust, and high-pressure flushing is important to loosen road dust from the texture of the asphalt. Water flushing can be integrated into the street sweeper or manually applied using hose-pipes to improve cleaning results. Reduction of ambient PM10 due to water flushing is short-term. If used in response to poor air quality as a single measure, flushing should be conducted early in the morning before the beginning of the morning rush hour for the best effects.

	Reducing the driving speed of the cleaning vehicles provides better cleaning results but affects progress (time needed) and resource use.
Timing	Efforts should be made to decrease the upbuilding of dust deposits during long, wet seasons (basically autumn and winter). This would reduce the amount of dust that becomes airborne when surfaces dry up. During the winter, deposited snow should actively be removed from the street environment. Snow deposited on the shoulders of the street can have up to 20 times the solids content compared to pure snow and will act as a dust source if allowed to melt in the street environment. Street washing results are best when the dust load level on the street surface is high. It is advisable to start washing the streets in the spring as soon as the weather permits, considering traffic safety, so that the dust load decreases before the start of the heavy dust season. If street washing is delayed, it may become ineffective as a measure in terms of the cost-effectiveness and dust reduction potential. In case it is not yet possible to start street washing due to temperature variations and night frosts, the dry brushing method can bring forward the removal of accumulated traction sand from the street environment and, thus, prevent the formation of finer dust that is formed by grinding sand under tyres of passing vehicles. The use of dry high-vacuum cleaning without water spraying is a functional and efficient alternative during sub-zero temperatures. In case of washing delay due to night frosts, dust binding can be used to prevent dust suspension before the weather conditions improve. Street washing may need to be repeated, especially in high-trafficked areas, as new dust is formed if studded tyres are still in use or transported from the surrounding area to the streets. Street cleaning operations should be coordinated between all operators working in the same area to conduct cleaning simultaneously. Otherwise, sand and dust will likely migrate from the dustier streets to those already cleaned. Also consider dust from construction areas. Cleaning of sidewalks and bike lanes should be done before or simultaneously with cleaning operations on the traffic lanes, i.e., the best results will be achieved if the whole width of the street is cleaned.
Site prioritization	It is recommended to perform block-wise cleaning, i.e., a wider area rather than a single street cleaning. If this is not possible due to, e.g., lack of resources, street categorization based on the intensity of use (e.g., population density, vehicle density) may be used to determine the order in which streets will be cleaned.

Conclusions

Efforts should be made to prevent the build-up of dust deposits during wet periods in autumn and winter. This would decrease the amount of dust that becomes airborne in spring when surfaces dry up. Due to the need for traction control in Nordic conditions, methods can include, for example, studded tyre restrictions, optimization of the use of traction control materials in terms of quality and amounts, and timely street cleaning operations. In acute dust episodes, the best way to control road dust emissions is the application of dust binding solutions. In addition to the visual observation of the street surface conditions, information about weather forecasts, air quality, and winter road maintenance expertise should be utilized when planning road dust mitigation measures.

References

Bolme, I. 2018. Sandfraksjoners betydning med tanke på friksjon - Feltforsøk Bjorli, SVV Rapport 647. https://vegvesen.brage.unit.no/vegvesen-xmlui/bitstream/handle/11250/2674333/Sandfraksjoners%20betydning%20med%20tanke%20pa%20friksjon%20SVV%20rapport%20647.pdf?sequence=1&isAllowed=y

EU LIFE+ 2014. REDUST 2014. Demonstration test final report: Main results and conclusions. Deliverable product of the REDUST LIFE+ project Actions 1 and 2, https://webgate.ec.europa.eu/life/publicWebsite/project/LIFE09-ENV-FI-000579/best-winter-maintenance-practices-to-reduce-respirable-street-dust-in-urban-areas-demonstration-of-best-practices-strategy-development-and-implementation

EU LIFE+ 2016. AIRUSE: Testing and development of air quality mitigation measures in South Europe. Deliverable products of the AIRUSE LIFE+ project Action B7 and Action B8. https://airuse.eu/project/deliverables/

Gjerstad, K. I., Gustafsson, M., Blomqvist, G., Denby, B.R., Elmgren, M., Grythe, H., Janhäll, S., Järlskog, I., Johansson, C., Kulovuori, S., Kupiainen, K., Lundberg, J., Malinen, A., Norman, M., Ritola, R., Silvergren, S., Stojilkovic, A., Sundvor, I., Thorsteinsson, T., Stefani, M. & Vogt, M. 2019. NORDUST: Nordic Road Dust Project. NordFoU 2019-01. NordFoU. http://api.vejdirektoratet.dk/sites/default/files/2022-08/NorDust%20Final%20report.pdf

Gustafsson, M., Blomqvist, G., Elmgren, M., Janhäll, S., Johansson, C., Järlskog, I., Lundberg, J., Norman, M. & Silvergren, S. 2018. Driftåtgärder mot PM10 i Stockholm : utvärdering av vintersäsongen 2016-2017. VTI rapport. Linköping: Statens väg- och transportforskningsinstitut, https://vti.diva-portal.org/smash/get/diva2:1255974/FULLTEXT02.pdf

Gustafsson, M., Blomqvist, G., Elmgren, M., Johansson, C., Järlskog, I., Lundberg, J., Norman, M. & Silvergren, S. 2019a. Driftåtgärder mot PM10 i Stockholm : utvärdering av vintersäsongen 2017–2018. VTI rapport. Linköping: Statens väg- och transportforskningsinstitut, https://www.diva-portal.org/smash/get/diva2:1287718/FULLTEXT02.pdf

Gustafsson, M., Blomqvist, G., Janhäll, S., Johansson, C., Järlskog, I., Lundberg, J., Norman, M. & Silvergren, S. 2017. Driftåtgärder mot PM10 i Stockholm : utvärdering av vintersäsongen 2015-2016. VTI rapport. Linköping: Statens väg- och transportforskningsinstitut, https://vti.diva-portal.org/smash/get/diva2:1111887/FULLTEXT01.pdf

Gustafsson, M., Blomqvist, G., Järlskog, I., Lundberg, J., Niska, A., Janhäll, S., Norman, M., Eneroth, K. & Johansson, C. 2019c. Optidrift : optimerad vinter- och barmarksdrift för bättre luftkvalitet. VTI rapport. Linköping: Statens väg- och transportforskningsinstitut, https://www.diva-portal.org/smash/get/diva2:1296413/FULLTEXT04.pdf

Monrabal-Martinez, C. & Berge, K.A.H. 2019. Metodeutvikling av tunnelvask. Multiconsult. https://hdl.handle.net/11250/2731622

OECD (2020), Non-exhaust Particulate Emissions from Road Transport: An Ignored Environmental Policy Challenge, OECD Publishing, Paris, https://doi.org/10.1787/4a4dc6ca-en

Reitan, K. M., Lysbakken, K.R., Gryteselv, D. & Snilsberg, B. 2018. Driftstiltak mot svevestøv i Trondheim kommune: Erfaringsrapport for tiltak før og etter 2013. Statens vegvesens rapporter 348. Statens vegvesen. https://hdl.handle.net/11250/2659509

Ritola, R., Kulovuori, S., Stojiljkovic, A. and Karvosenoja, N. Katupölyn lähteet, päästövähennyskeinot ja ilmanlaatuvaikutukset. 2021. KALPA3-tutkimushankkeen loppuraportti, Suomen ympäristökeskuksen raportteja, 28/2021, https://helda.helsinki.fi/bitstreams/59853fa1-c608-423b-9680-5726421858c5/download (in Finnish, summary in English)

Snilsberg, B. & Gryteselv,D. 2017. Renholdsforsøk 2016: Strindheimtunnelen og Haakon VII gate i Trondheim Stordalstunnelen i Møre og Romsdal. Statens vegvesens rapporter 432. Statens vegvesen. https://hdl.handle.net/11250/2670383

Snilsberg, B. & Gryteselv,D. et.al. 2016. Renholdsforsøk i tunnel og gate i Trondheim våren 2015-Strindheimtunnelen og Haakon VII gate. Statens vegvesens rapporter 619. Statens vegvesen. https://hdl.handle.net/11250/2673147

Snilsberg, B., Gryteselv, D., Sætermo Veivåg, I-L., Lamo Hauan, T., Dalseth Austigard, Å. 2018. Renholdsforsøk 2017 : Uttesting av renholdsmaskiner i gate i Trondheim. Statens vegvesens rapporter 534. Statens vegvesen. https://hdl.handle.net/11250/2671430

Snilsberg, B., Sætermo Veivåg, I-L. & Gryteselv, D. 2017. Renholdsforsøk 2017: Uttesting av ny spylebom i tunnel og gate i Kristiansund. Statens vegvesens rapporter 536. Statens vegvesen. https://hdl.handle.net/11250/2671648

Statens Havarikommisjon for Transport, 2011. Rapport om sammenstøt mellom trikk og buss ved Ilevollen i Trondheim 5. november 2009. Rapport JB2011/01. https://havarikommisjonen.no/Bane/Avgitte-rapporter/2011-01.

Statens vegvesen. 1997. Renhold i tunneler: prosjektrapport. https://vegvesen.brage.unit.no/vegvesen-xmlui/bitstream/handle/11250/192785/renhold_i_tunneler.pdf?sequence=1&isAllowed=y

SYKE. 2023. PÖLYBAT 1&2: Katupölyn torjunnan parhaat käytännöt käyttöön, https://www.syke.fi/fi-FI/Tutkimus__kehittaminen/Tutkimus_ja_kehittamishankkeet/Hankkeet/PolyBAT_Katupolyntorjunnan_parhaat_kaytannot_kayttoon (in Finnish, summary in English)

Appendix 1

Table A 1 Summary results from relevant projects and studies.

Country	Project/Report	Studied measures	Aim/Test description	Methods	Main results
Finland	[1] REDUST (2011-2014) LIFE 3.0 - LIFE Project Public Page (europa.eu)	Street cleaning	Demonstration of PM10 reduction potential for three street cleaning techniques: street sweeper, street scrubber, and combination (sweeping+flushing+scrubbing).	Sniffer	Street scrubber and combination cleaning technique were more efficient in decreasing PM10 emissions than street sweeping. However, the results were highly dependent on the initial emission levels. The cleaning is more efficient when performed early in the spring, i.e., when the road dust emission levels are still high.
		Dust binding	Demonstration of PM10 reduction potential of dust binding depending on i) different types of application procedures, ii) different concentrations of dust binding solution and iii) different types of dust binding solutions.	Sniffer	i) Observed PM10 emission reduction was from 10%-40% one day after treatment. The reduction potential for the "whole lane" treatment is strong even on low initial street dust levels compared to applications targeted only to the kerb area and lasted longer. The effect of dust binding was detected 2-3 days after treatment for the whole lane application. ii)The efficiency of dust binding is not necessarily dependent on the concentration of the $CaCl_2$ solution. iii) $CaCl_2$ demonstrated higher PM10 reduction potential. However, the difference is more likely explained by the

				application of the solution (wider spray for CaCl2 than for potassium formate) than by the type of solution.
	Sanding	Demonstration of the impact of i) grain size and ii) sieving method (dry or wet) on PM10 formation under the vehicle tyres.	Sniffer	i)The test did not unambiguously demonstrate the benefits of coarser grain size to PM10 formation. ii) Wet sieving of the sanding may reduce PM10 formation.
[2] KALPA I- III (2016-2020) Katupölyn lähteet, päästövähennyskeinot ja ilmanlaatuvaikutukset. KALPA3-tutkimushankkeen loppuraportti (helsinki.fi)	Street cleaning	Demonstrate the impact on suspension emissions of PM10 and dust load: i) Vacuum sweeper vs. street scrubber (PIMU) vs. street scrubber (PIMU) with rear grit suction unit ii) Snowek Trombia sweeper in street environment iii) Road shoulders cleaning using street scrubber	Sniffer Vectra WDS	i) Rear grit suction unit makes cleaning somewhat faster but doesn't reach the dust deposited elsewhere than on the driving lane (e.g., close to kerbs). With low initial dust levels, there is no significant difference between the cleaning results for the two methods. Achieved dust load reduction was from 20% - 40% with PIMU and rear grit unit, whereas no reduction was observed for the traditional vacuum sweeper. ii) Snowek Trombia was able to reduce road dust load (WDS) in sections with high initial values (kerb area and between wheel tracks) but did not affect measured suspension emission (Sniffer) of PM10. iii) Significant reduction of dust load (50%-80%) and emission of PM10 on

					the shoulders but, as expected, no effect on emissions from the traffic lanes.
	[3] PölyBat (2020) Suomen ympäristökeskus > PÖLYBAT 1&2: Katupölyn torjunnan parhaat käytännöt käyttöön (syke.fi) (syke.fi) (in Finnish)	Winter road maintenance operations in different Finnish cities.	The project aim was to summarize the current state of street cleaning and maintenance practices in Finland and to enhance the dissemination of best practices to municipalities and contractors, including stakeholders who have not been actively involved in street dust research activities.	Survey and desktop work	The survey was conducted in Finland's 22 biggest cities (by population) among municipality authorities and contractors to collect information about current street cleaning and maintenance practices and general knowledge and awareness regarding road dust-related issues. Sixteen answers were received: Helsinki (6), Espoo, Tampere, Vantaa, Turku, Pori, Joensuu, Kuopio (2), Lahti, Jyväskylä. Methods and materials used vary depending on the size of the city and available resources. Only one of the smaller cities reported NOT using dust binding, but they were also testing it for the first time in season 2020-21. The same city reported not following air quality measurement results in connection to road maintenance.
Sweden	[4] Stockholm_prj_2015-2016: Driftåtgärder mot PM10 i Stockholm : utvärdering av vintersäsongen 2015–2016 (diva-portal.org)	Dust binding with CMA (extra dust binding during daytime and extended block-wise dust binding), dry vacuum suction sweeping with a high power vacuum.	Actions aiming at lowering PM10 concentrations taken by Stockholm City during 2015–2016. Analysis between dust load, PM10 and impacting factors. Condition-based calculation method.	WDS, Air quality measurements, NORTRIP modelling	Dust binding in spring is important for keeping the PM10 levels down, while dust binding in autumn and winter is more often "unnecessary" (in terms of PM10 exceedances). Further efforts are needed to understand better the connection between dust load and direct emission, PM10,

// Operational measures against PM10 in Stockholm - Evaluation of the winter season 2015–2016				and different mitigation actions in different meteorological conditions. Evaluation of the impact of daytime dust binding was complicated since CMA was also used on the reference street. Block-wise dust binding and vacuuming could not be evaluated due to contamination from a construction site.
[5] Stockholm_prj_2016-2017 [Driftåtgärder mot PM10 i Stockholm : utvärdering av vintersäsongen 2016/2017 (diva-portal.org)]() // Operational measures against PM10 in Stockholm - Evaluation of the winter season 2016–2017	Dust binding with CMA (fixed schedule, three nighttime plus in March two daytime spreadings/week), vacuum suction sweeping with Disa-Clean (once a week). Block-wise treatment.	Actions aiming at lowering PM10 concentrations taken by Stockholm City during 2016–2017.	WDS, Air quality measurements	Additional daytime dust binding lowered the daily average PM10 concentration by 6%. Block-wise CMA treatment did not have an apparent effect. Dust binding efforts could have better efficiency if optimized with forecast-based measures. Re-paving of Folkungagatan has resulted in a heavy increase in dust load levels but lower PM10 levels than in previous seasons. The link between dust deposits on the road surface and ambient PM10: As observed in previous seasons, the connection between PM10 and street dust storage is not apparent. High DL180 levels do not necessarily indicate

				that high PM10 levels will co-occur. The connections are more complex. How can we reduce the building up of dust deposits during autumn-winter (wet conditions)? Regular cleaning and the special vacuum cleaner used in Stockholm are not so effective when there's a damp road surface. Modern high-pressure washing cleaning machines could be more effective in the fall (when below-zero temperatures are not expected). However, the low working speed of scrubbers is considered a challenge.
[6] Stockholm_prj_2017-2018 [Driftåtgärder mot PM10 i Stockholm : utvärdering av vintersäsongen 2017–2018 (diva-portal.org)] // Operational measures against PM10 in Stockholm - Evaluation of the winter season 2017–2018	Fixed schedule for CMA treatments: three nights a week, ending in April. No sweeping.	Actions aiming at lowering PM10 concentrations taken by Stockholm City during 2017–2018.	WDS, Air quality measurements	CMA is being used on many days when the PM10 limit value would not have been exceeded, while days with PM10 exceedances are missed, several of which were in May, when the dust binding has ended for the season (due to the risk of lowering friction). Still increased dust load levels but lower PM10 levels at Folkungagatan (see results for 2016-2017). Strategy-wise, it is advised that efforts should be made to decrease the upbuilding of dust deposits during long, wet seasons (basically autumn and

				winter). This would reduce the amount of dust that becomes airborne when surfaces dry up. Due to the need for traction control, methods are limited but include, e.g., the limitation of the use of studded tyres, paying attention to traction control materials (and amounts used), and the possibility to sweep/clean surfaces as early as possible. The city is also advised to look at long-term solutions, like increasing compliance with studded tyre bans and studying whether new pavements can reduce PM10 levels on the city streets.
[7] Optidrift 2019: Optidrift : optimerad vinter- och barmarksdrift för bättre luftkvalitet (diva-portal.org) //Optimized winter and "bare ground"(?) operation for better air quality	A criterion-based analysis of dust binding occasions, data from seasons 2014 - 2018. Three evaluations of the effect of a different coil and cleaning variants on road surface dust storage were carried out with WDS II.	Possibilities to optimize street maintenance operations with regard to air quality and road dust.	Workshop with focus groups (industry, machine operators), survey (dust binding methods in different municipalities), WDSII, Nortrip-model (optimization tests)	Optimization tests (using the Nortrip model) showed that good forecasting of dust binding is important for good results. Frequent dust binding during periods with exceptionally high PM10 levels can give better results than just dust binding the days with the highest levels. Daytime dust binding did not produce an extra effect while flushing with water during the days when dust binding was not made could further reduce the PM10 levels.

					Coil and cleaning variants: The positive effect of the methods requires that there is relatively much dust on the road surface. The study uses a reduction percentage from previous Swedish studies: (Gustafsson et al., 2014) "Previous projects with dust binding have shown that laying out CMA not only affects on the same day, but the effect can last for several days. However, the greatest effect was observed on the first day: a 20%–40% reduction in PM10 levels. A decrease of up to 15%–30% is observed the day after."
Norway	[8] Renhold I tunneler //Cleaning in tunnels (1997)	Cleaning of tunnels (walls, roof, other surfaces) 1) low-pressure washing (up to 15bar) 2) high-pressure washing (75 to 150 bar) and 3) high-pressure washing combined with brushes	Norway has built more tunnels and started using different "coating" materials for walls, roofs, etc (as opposed to rock surfaces). The aim was to test available cleaning methods (equipment) and their efficiency, principles of usage and available resources. Additionally, to estimate possible cleaning methods	Tested methods were estimated based on their capacity, usage of water, resource efficiency and cleaning result. The report uses the word "smuts", which translates to "dirt". Results were estimated	Tunnel walls won't clean up unless soap/chemicals are used together with washing. This is true whether cleaning with low- or high-pressure washing. Soap should be applied at least 4-6min before washing with water. Satisfying results with low-pressure washing is only achieved if used with soap/chemicals and some type of mechanical cleaning (brushes). With high-pressure washing, the distance

		and their efficiency for tunnels and create a cleaning standard. Several different types of equipment were tested in several locations—also, the extent/scale of cleaning varied. "Soap/chemicals" (in Kristiansand) and cleaning of tyres (in Oslo) were tested.	based on visual inspection ("reference dirt level").	between the water nozzles and the wall needs to be correct (not too long). There are no significant differences between the "amount of dirt" (or dirt accumulation) between concrete and asphalt-paved tunnels. Kristiansand (using soap/chemicals): road surfaces stayed clean, but dirt accumulated on, e.g., sidewalks. Oslo (tyre cleaning): cleaning of tyres did not end up in very high efficiency and won't compare to traditional cleaning of road surfaces. However, the test showed that a combination of wet road surface and studded tyres causes a lot of dirt accumulation, whether the road has recently been cleaned or not. Dirt accumulation and, thus, the need for cleaning during studded tyre season is highly dependent on the wetness conditions.
[9] Driftstiltak mot svevestøv I Trondheim commune Brage - Statens vegvesen: Driftstiltak mot svevestøv i Trondheim kommune:	The report describes a whole strategy/approach for better street dust management within a city/community. The report does not provide data on dust reductions achieved by individual tests/methods.	The report's purpose is to share experiences from Trondheim regarding important framework conditions, scope, implementation of measures, methods, and equipment. Several measures have been taken, e.g., a newly defined	Interview results from different operators in Trondheim. Air quality monitoring results.	Street dust levels have been lowered in Trondheim in recent years. There is a reason to believe that operational measures have contributed to positive development. Experience from Trondheim:

Erfaringsrapport for tiltak før og etter 2013 (unit.no) //Road dust and air quality in Trondheim. Maintenance measures against road dust taken before and after 2013. 2018. Report no. 348.	Some methods that have been applied to mitigate the street dust problem in general are: - Wall-to-wall cleaning (as a preventive measure when the concentrations are not yet high) - Mg2 solution for dust suppression (spreading is carried out with a nozzle spreader on areas with dust depot, and not just in the roadway) - Dry vacuum cleaning	"dust regime" (i.e., preparedness period for maintenance) from 1. Oct – 1. June, which is a longer than standard preparedness period for winter maintenance. Focus from a frequency-based operation to a more preventive demand-based operation, where measures are carried out to the greatest possible extent during periods of low airborne dust.		It is more effective to take preventive measures instead of taking measures when the air quality is poor. As a preventive measure in periods with little airborne dust, cleaning is performed using "wall-to-wall" cleaning, which includes noise barriers, sidewalks, pedestrian/cycle roads, signs, banquets, curbs, driving areas and house walls up to approx.—0,5 m. Results for individual methods or tests are not included in the report. On a strategic level, Trondheim has experienced many administrative changes and the development of methods, procurement practices, budget increases, etc. - The authority and the executor are in the same organization - There is the same executor on the county road network and the municipal road network - Trondheim bydrift has been accepted for using sufficient resources to comply with the air quality requirements. This has made it possible to focus on self-development, procurement, testing and maintenance of suitable equipment. Trondheim city management has also gained experience, competence, and a stable workforce. All these have led to better air quality/road dust problem management.

[10] Renholdsforsøk i tunnel oggate i Trondheim våren 2015 [Brage - Statens vegvesen: Renholdsforsøk i tunnel og gate i Trondheim våren 2015: Strindheimtunnelen og Haakon VII gate (unit.no)] // Road cleaning in tunnel and street in Trondheim, spring 2015	Methods and equipment for cleaning tunnels and roads. Altogether 6 test fields: 3 at each location, Haakon street and Strindheimtunnel.	Haakon street: Machine 1: Front broom, transverse centre broom and curb broom. Rotating spray nozzles and powerful suction ("rotor-clean"). Driving speed 2-3 km / h. Machine 2: Front broom, transverse centre broom and curb broom. Driving speed 7-8 km/h. Machine 3: Transverse centre brush, curb brush and weed brush. High-pressure flushing and powerful suction. Driving speed 7-10 km/h. Strindheimtunnel: Field 1: Sweeping with Machine 1. Soap application. Flushing of light sources. Wall washing with a polishing brush. Sweeping with Machine 1. Field 2: Sweeping with Machine 2. Soap application. Flushing of light sources. Wall washing with a brush. Sweeping with Machine 2.	Field test documentation methods: WDS (wet dust sampler), measurement of brightness in the tunnel, measurement of texture of the roadway and measurement of residual moisture on the roadway. In addition, environmental analyses from washing water and sludge samples.	WDS results: Strindheimtunnel: The amount of dust on the road increases after cleaning for all three sweepers. This may be due to large amounts of dust being washed down from ceilings and walls, which the sweepers do not pick up well enough afterwards. In addition, soap used on tunnel roofs and walls that run down the road after washing can cause dust cemented in the road surface texture to loosen easier and become available for suspension after washing. The tunnel also has a coarser surface texture (SMA16) than Haakon VII gate (SMA11). Haakon VII gate: In a street environment, the amount of dust is reduced by 92% for Machine 1 and 65% for Machine 3, while Machine 2 fails to reduce the amount of dust on the road. For Machine 3, the cleaning effect is poor on the left side of the car (towards the middle of the roadway), which gave a lower average result. Heavy suction seems most effective at removing road dust, but rotating nozzles with high-pressure flushing are important to loosen the dust from the road. Lower driving speed provides better cleaning results on the roadway but

		Field 3: Sweeping with Machine 3. Soap application. Flushing of light sources. Wall washing with high-pressure flushing with water in combination with high-pressure air. Sweeping with Machine 3.		affects progress (time needed) and resource use. Experience from tunnel washing shows that one should focus less on the dust that is stuck in the texture of the asphalt and instead concentrate the cleaning on looser dust on the roadway, banquets and accident/safety pockets. There should be a greater frequency of sweeping roadways, banquets, accident pockets and the like, and fewer complete washing in the tunnel.
[11] Renholdsforsøk 2016 Brage - Statens vegvesen: Renholdsforsøk 2016: Strindheimtunnelen og Haakon VII gate i Trondheim Stordalstunnelen i Møre og Romsdal (unit.no) // Road cleaning in tunnel and street, 2016. Report no. 432	Cleaning experiments on three sites: Haakon VII street and two different types of tunnels (one with concrete vault and another with metal plates on the wall), Strindheimtunnel (3 fields) and Stordaltunnel.	In Haakon VII, street cleaning on 7 test fields with two different types of machines: i) machine with dry vacuum suction with PM2.5 filter and without brushes (Disa-Clean). Dry suction was tested with applying water before suction (Fields 2&3) and with a high-pressure washer before suction (Field 4). ii) a sweeper with rotating high-pressure nozzles combined with vacuum cleaner "rotorclean" (ValAir) at two working speeds.	Measurement parameters and methods: Cleanness (WDS), light emission, rutting, unevenness, texture, friction and humidity.	Haakon street: Results from measurement with WDS II show that Disa-Clean with high-pressure washing at 10 km/h and rotor clean at 3 km/h were the most effective. Rotorclean at 3 km/h is 57% more efficient than at 10 km/h. Disa-Clean in combination with high-pressure washing at 10 km/h is 35% more efficient than rotorclean at 10 km/h. Also, Disa-Clean, in combination with the application of water before suctioning at 10 km/h, is 10% more efficient than rotorclean at 10 km/h. This means Disa-Clean is more efficient than rotorclean at higher working speeds.

		Field 1: Disa-Clean, dry suction, 10km/h Field 2: Disa-Clean, wet suction, 10km/h Field 3: Disa-Clean, wet suction, 10km/h Field 4: High pressure flushing + Disa-Clean 10 km/h Felt 5: Beam rotorclean 10 km/h Felt 6: Beam rotorclean 3 km/h Strindheimtunnel: washing with or without soap at two speeds at three fields. Cleaning process: i) Sweeping with Beam (front broom on banquet and rotor clean on street surface). ii) Soap application fixtures, ceil-ings and walls (on two of the three fields), followed by rinsing of fixtures, ceilings and walls. iii) Sweeping with Beam (front broom at the banquet and rotor clean on the road.)		Heavy suction is effective for removing loose road dust, and high-pressure flushing is important to loosen road dust from the texture of the asphalt. The fixed nozzle row seems to enable higher propulsion speed and a better cleaning effect than rotating flushing nozzles. Lower working speed provides better road surface cleanliness but re-duces progress and increases resource consumption. (Similar conclusions as in the 2015 report) Strindheimtunnel: WDS II measure-ments were performed i) before clean-ing, ii) after only the banquets and the road surface had been cleaned once and iii) after the full wash was com-pleted. The experiment shows no ap-parent effect on the cleanliness of the roadway with or without the use of soap. The distribution of dust across the road is similar before and after cleaning: lit-tle at the banquet, much at the road-side, little in the wheel tracks and a lit-tle between wheel tracks and between lanes. The brush system of the sweeper comes close enough to the banquet but does not work well enough to move the dust towards the suction system of the sweeper.

		Stordaltunnel: only walls cleaned with two different brush types (polishing and washing brushes), two types of soaps, high and low-pressure washing and high and low working speeds—six different cleaning/field combinations.		Experience from tunnel washing shows that one should perhaps have less focus on the dust that is stuck in the texture of the asphalt and instead concentrate the cleaning on looser dust on the roadway, banquets and accident/safety pockets. There should be a greater frequency of sweeping roadways, banquets, accident pockets, and fewer complete washing in the tunnel**.** (The same conclusion as in the 2015 report.)
[12] Renholdsforsøk 2017 Uttesting av ny spylebom i tunnel og gate i Kristiansund [Brage - Statens vegvesen: Renholdsforsøk 2017: Uttesting av ny spylebom i tunnel og gate i Kristiansund (unit.no)]() //Road cleaning in tunnel and street, 2017: Testing of a cleaning unit with high-pressure nozzles. Report no. 536	The report provides results from testing one flushing boom in combination with side nozzles to clean sidewalks, banquets and the area next to the curb/banquet. Tests were performed in one street and one tunnel.	Street and tunnel: one field was cleaned as a reference without using a flushing boom but with side nozzles. The side nozzle flushes against the curb/banquet, covering a horizontal area of approximately 20-30 cm and vertically towards the curb/banquet. The pressure was 130 bar. Street: the side boom was used with an extension (a total of 7 beam nozzles) to clean the area on the sidewalk and up to and on top of the curb at a pressure of 70 bar. Tunnel: the side boom was used without extension (3 jet	WDS	WDS results for the street: cleaning without a flushing boom and with a high-pressure nozzle towards the curb reduced the amount of particles (particles less than 180 µm) close to the curb by 73% and approximately 40% in the right wheel track. Cleaning with a flushing boom (70 bar) and a high-pressure nozzle towards the curb reduced the amount of particles (particles less than 180 µm) close to the curb by 89% on the sidewalk approx. 65%, in the right wheel track approx. 19%. The reduction of dust was most significant when the flushing boom was used. Right wheel tracks: reduction in the amount of dust was more significant without the use of a flushing boom.

		nozzles) to clean the area on and next to the banquet at a pressure of 70 and 130 bar. Working speed during the experiments was approx. 3 km/h.		This may indicate that the flushing boom flushes particles from the edge towards the right wheel track. The total amount of dust (particles less than 5 mm) shows the same distribution across the road surface as for smaller particles (particles smaller than 180 µm) WDS result for the tunnel: There is low efficiency for cleaning without a boom and only with a high-pressure nozzle close to the banquet. The decrease in the amount of particles (less than 180 µm) after washing was approximately 2%. Cleaning using a flushing boom with 70 bar pressure and a high-pressure nozzle towards the banquet reduced the amount of particles (particles less than 180 µm) close to the banquet by 40%. The amount of dust in the right wheel track was reduced by approx. 65%. Cleaning with a high-pressure flushing boom (130 bar) and a high-pressure nozzle reduced particle amount (particles less than 180 µm) close to the banquet by 40% (same as for lower washing pressure). The amount of particles increased by approx. 77% in the right wheel tracks after washing. Perhaps the

				high pressure on the spray boom can move more dust to the right wheel track.
[13] Uttesting av renholdsmaskiner i gate I Trondheim Brage - Statens vegvesen: Renholdsforsøk 2017 : Uttesting av renholdsmaskiner i gate i Trondheim (unit.no) // Testing of road and street cleaning systems in Trondheim 2017. Report no. 534	Trondheim Municipality and the Norwegian Public Roads Administration challenged the industry. (contractors, manufacturers and suppliers of cleaning machines) to think and develop efficient equipment adapted to the Nordic climate. Machines were tested in Trondheim in 2017. Altogether, 15 test areas with different cleaning combinations were tested.	Six different machines for cleaning the road surface (Machines 1-6) and two "washing arms" for cleaning sidewalks (Washing arms A and B). 1. Beam S, Washer and vacuum cleaner or RotorClean, plus side nozzle 2. Johnston C401, a sweeper with two front brooms and suction (not designed for collecting finer dust) 3. Macro M60 sweeper with rotating brooms, suction, and possibility for damping 4. DisaClean 130 High Vacuum Dry Road Sweeper 5. Beam (Kjelsberg), mounted on Beam S14000, four rotors with 16 wide jet nozzles, followed by suction. Includes fold-out high-pressure flushing boom (2 spray nozzles) in the middle of the car that can be	The following was assessed: - cleaning efficiency (WDS, (particles less than 180 µm)) - concentrations of PM in process air and next to the road (Met One 831) - noise level - vibration - moisture (Wettex) - Particle Size (Analyzer Cilas 1190)	WDS results: Beam S, with the flushing boom on the first crossing and side nozzle on the second crossing, reduced the amount of dust most effectively with a reduction of approx. 84%. The most efficient methods in this experiment for cleaning the entire road surface were Beam Kjelsberg with RotorClean and side boom at 10 km/h and ValAir with flushing row, suction and side nozzle at 5 km/h. These cleaning machines reduce both the fine dust and the coarse particles well. The flushing boom mounted on ValAir and the flushing arm for Trondheim bydrift effectively removed the fine material (<180) from the sidewalks. The reduction was 53% and 57%, respectively. Dust concentration in the ambient air: Results are described only qualitatively. The potential for very high concentrations and exposure can be reduced with dampening and cleaning when there are not as many other traffic/street users as possible.

			used simultaneously as the rotor system. 6. ValAir BalHydro 15 Rotor-Clean, RotorClean or washer w / suction, side nozzle, flushing boom. 230bar A) ValAir washing arm B) Trondheim bydrift washing arm for cleaning sidewalks and side areas (2.5m reaches for 7m)		
	[14] Metodeutvikling av tunnelvask 2019 //Method development for tunnel washing 2019	Several tunnels in Norway to see the efficiency of traditional washing methods vs. new potential cleaning technology		Inspections, input and experience from relevant operating personnel and literature review	Report lists: - best methods to reduce the amount of soap and water needed in cleaning - advice on how to document that the cleaning results are good enough quality-wise - "best-practice guide" with pictures of good and poor execution/washing results/degree of contamination - suggestions for the assessment of washing frequency
Other	[15] AIRUSE LIFE+ (2012-2016) AIRUSE	Impact of street cleaning (sweeping and washing) and dust binding (CMA and $MgCl_2$). Also, use of nano-polymer solution at an urban unpaved area (public park of Barcelona).	AIRUSE provides National Authorities of Southern European countries with appropriate measures to reduce PM2.5 and PM10 concentrations in the air.	Experimental tests to investigate air quality benefits, literature review	Experimental tests in South European cities: -Street washing (combined with a preliminary sweeping) was found to be the most effective measure in all the tested roads (urban paved, industrial paved and unpaved). At the urban paved road, the reduction in daily mean PM10

				levels measured at kerbside sites was 7-10%. -There is no clear air quality benefit due to CMA or MgCl2 application, likely because of high solar insulation and low RH. -Results confirm that at specific locations, such as unpaved areas strongly affected by (natural or anthropogenic) dust resuspension, a dust suppression strategy with nano-polymers can help to attain PM10 standards. The literature review gives results of different street cleaning and dust binding tests on paved, unpaved and industrial sites conducted in selected EU countries and Canada. Also, a review of PM10 certification of road sweepers is included.
[16] NORDUST (2016-2019) [NORDUST: Nordic Road Dust Project (diva-portal.org)]()		Hornsgatan, Stockholm: A combination of high-pressure water flushing followed by DisaClean vacuum sweeper at 11 a.m. Fleminggatan: Nighttime Cleaning with DisaClean vacuum sweeper. Koisotie, Vantaa:	WDS Sniffer	Hornsgatan: The direct effect of flushing the road surface with water was apparent. The concentrations of PM10 dropped substantially and remained low for an hour before reaching back to similar levels as before the cleaning. The water flushing, followed by vacuum sweeping, removed dust, especially from the area between wheel tracks. Only minor increases in dust load are

		- Cleaning test to evaluate the efficiency of reducing PM10 emission by two machines, PIMU (Scrubber with Captive Hydrology) and CityCat 5006 (compact sweeper). - Sanding test to evaluate the impact of sanding on PM10 emissions and evaluate sand crushing under tyre.		noted, especially in the left wheel track and the biking lane. Fleminggatan: The results of the vacuum sweeping test show a general increase in dust load after sweeping across the whole street transect. This implies that dust is redistributed across the driving lane and added from upstream of the transect or adjacent surfaces, like the sidewalk. Koisotie: In the cleaning test, both machines decreased PM10 emissions on the day of the treatment. The mean reduction was 35% and 54% for the CityCat 5006 and PIMU, respectively. The effect for the CitCat 5006 was limited to several hours. For PIMU, emissions lower than the initial levels were detected one day after the treatment. Unlike the Vectra measurements, the WDS profiles could not show any apparent differences in dust load (approximated through turbidity) between profiles before and after cleaning. Applying sand increased measured PM10 emissions by 180% after 100 vehicle passages, 250% after 3 hours and an additional 50 vehicle passages. However, sand was applied on a dry street surface, which does not resample application in real-life conditions. Also, the

				migration of sand along the street was observed. The crushing experiment resulted in ambiguous results. The sieved coarse material (0.063–8 mm) did not change much between the crushing rounds. A general tendency towards smaller fractions compared to the uncrushed material can be seen but is not consequently being finer and finer as one would expect.
[17] OECD report (2020): Non-exhaust Particulate Emissions from Road Transport - An Ignored Environmental Policy Challenge Non-exhaust Particulate Emissions from Road Transport: An Ignored Environmental Policy Challenge | en | OECD	This report synthesizes the state of knowledge on the nature, causes and consequences of non-exhaust particulate emissions from tyre, brake, and road wear, as well as road dust resuspension. It also simulates how particulate matter emissions from non-exhaust sources will evolve in future years and identifies existing technological and policy measures to mitigate these emissions. Finally, the report proposes a policy framework for internalizing the social costs associated with these emissions.			A role of street sweeping, street washing, and dust binding are included as measures to reduce road dust resuspension. The report provides a brief overview of results from studies conducted to evaluate the impact of these measures on road dust emissions and air quality.

Work package 2: Measurements for model parametrisations and processes

Introduction

An important aim with the NorDust projects has been to contribute with new knowledge and data that can be parameterized and used to improve the NORTRIP model. This work package focuses on improving the parameterizations of some of the model processes which are based on very little or no measurement data.

Due to the increasing weight of vehicles, related both to trends like SUV:s and the ongoing electrification of the vehicle fleet, the influence of weight on emissions is of importance to describe for better scenarios on how this development will affect PM concentrations and public health. Recent studies have pinpointed the risk of an increased tyre wear due to electric vehicles being heavier than fossil fuelled vehicles (Timmers & Achten, 2016, Beddows & Harrison, 2021, Fussel et al., 2022). No study has, to our knowledge, been made on the effect on road wear, especially in connection to use of studded tyres. This work package therefore addresses this issue using both a laboratory and a field measurement approach. Two unique resources are used: the VTI road simulator and Metropolia's Sniffer vehicle.

Traction sanding is known to be a potentially important source to airborne particulate matter (Gertler et al., 2006, Kupiainen et al., 2016, Gulia et al., 2019), but its contribution is strongly depending on material properties, traffic situation, meteorology, and the following road surface conditions. A crucial question is how the material interacts with traffic by both being crushed into finer fractions by vehicle tyres and by being moved away from the wheel tracks by traffic. Also, the fragmentation resistance in relation to the asphalt properties seem to be of importance. Kupiainen et al. (2016) showed, by using winter sand with a markedly different petrography compared to the rock aggregates in the pavement combined with source apportionment analysis, that the sand contributed to 25% of urban PM10, while the pavement contributed to 40-50%. A few percent of these were estimated to originate in the "sandpaper effect", i.e. the traction sand causing additional wear of the pavement. In the sand crushing experiments in the previous NORDUST project (Gjerstad et al., 2019) it was found that studded tyres seem to mainly increase the relative abundance of finer fractions (0.0125-2000 µm) compared to friction tyres, while the coarser fractions did not show any obvious signs of crushing. Using the VTI road simulator, a more detailed analysis of the crushing processes has been made. Also, winter sand is well known to be removed from wheel tracks by traffic, why it is seldom used on highly trafficked and high-speed roads, where the positive traction effects are short-lived. We have found no literature describing the removal rate of sand from the wheel tracks, which would be a useful for modelling purposes. Therefore, a dedicated sand removal test has been performed in the road simulator.

Dust binding has been studied in several previous studies and is known as a well-functioning acute mitigation measure at high PM10 concentrations in street with high road dust contribution to PM10 (e.g. Norman & Johansson, 2006, Aldrin et al., 2008, Gustafsson et al., 2010). Common dust binders used in the Nordic countries are chloride salts like $MgCl_2$ and $CaCl_2$ and organic salts like calcium magnesium acetate (CMA) and potassium formate (KF). What is less known is how the dust binder road surface load is affected and redistributed by traffic after application. Knowledge on these matters is of importance to modelling the dust binder effect and can also contribute to more effective mitigation. In the work package, a detailed road surface follow-up of a dust binder application was made to better understand this process. Also, the effect on PM10 was analysed.

Influence of vehicle weight on particle emissions, road simulator tests

Methods

The VTI road simulator

To study the influence of vehicle weight on PM emissions, the VTI road simulator was used (Figure 1). The simulator is a carousel-like equipment with four wheels rotating on a circular track, which can be equipped with any kind of pavement and personal car tyres. It can be run in up to 70 km/h and the hall can be cooled down to below 0°C.

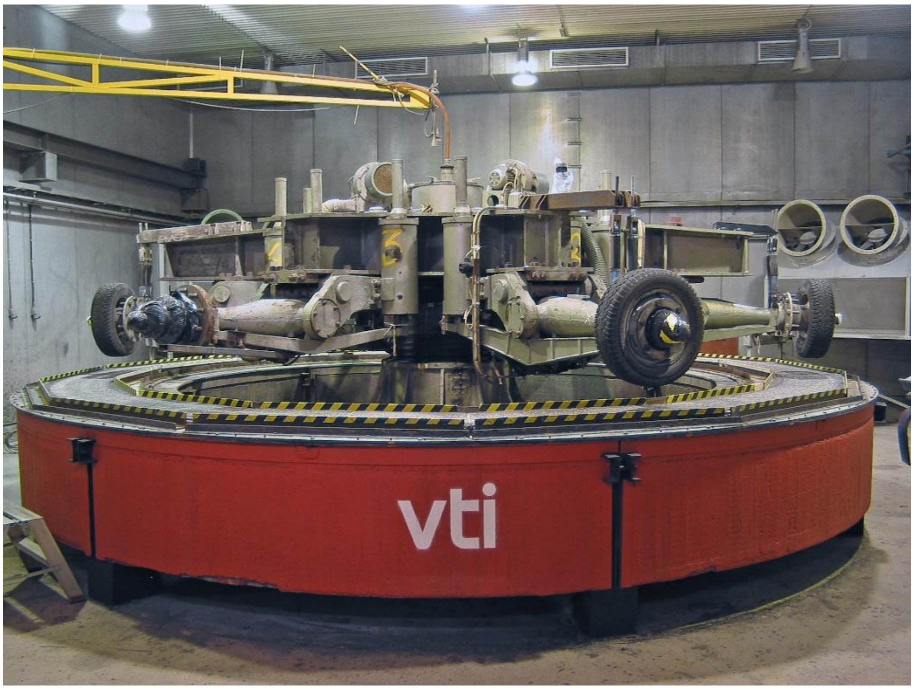

Figure 1. The VTI road simulator. Photo: Mats Gustafsson, VTI.

Test set up and conditions

For the tests a previously tested mixed cement concrete pavement ring was used consisting of seven different concrete recipes. The tyres used were two types of studded tyres (Nokian Hakkapeliitta 9 and Kumho WinterCraft Ice) (Table 4). The chosen start temperature was set to be in the range -5°C to 0°C. The test sequence included two 60 km/h runs for an hour each followed by two 40 km/h runs for an hour each (Figure 2) for each load setting. Just before the end of each hour of a speed sequence, a large filtering fan was turned on to reduce deposition that might suspend in the following speed sequence. The cooling system was also turned on to lower the temperature below zero before next speed sequence (Figure 3). At the end of the last run at 40 km/h in the test sequence, the speed was increased to 70 km/h and the filtering fan was turned on again as well as an evacuation fan in the ceiling. This was done to suspend any accumulated dust and filter and evacuate as much as possible of remaining dust before next speed test. The cooling system was also turned on to "reset" the system temperature for the next test.

Table 4. Studded tyres used in the tests

Manufac-turer	Name	Mass (g)	Tread depth (mm)	Number of studs	Stud protru-sion (mm)	Rubber hardness (shore)
Kumho	WinterCraft Ice	11261	9,2	150	1,2	59,89
Nokian	Hakkape-liitta 9	8961	7,9	190	0,8	50,8

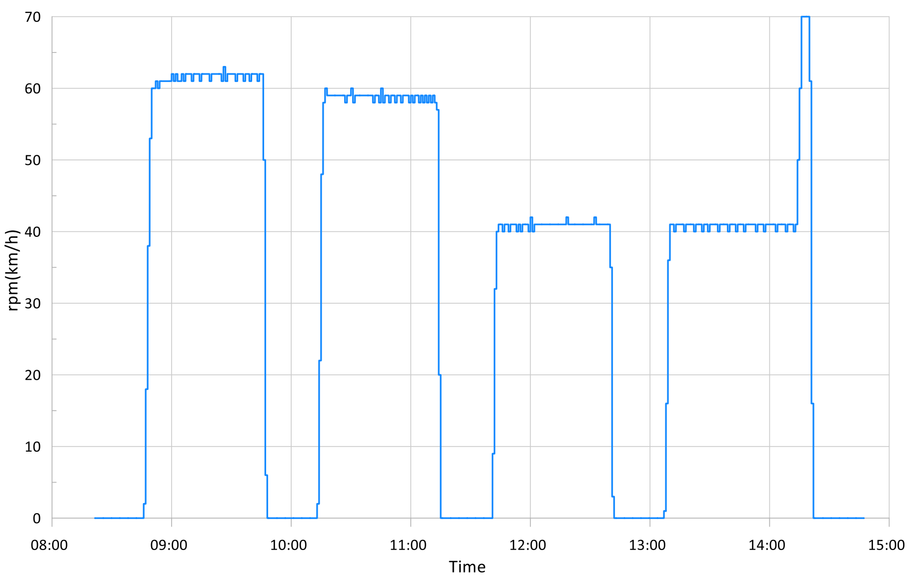

Figure 2. Speed sequence used for weight tests in the VTI road simulator.

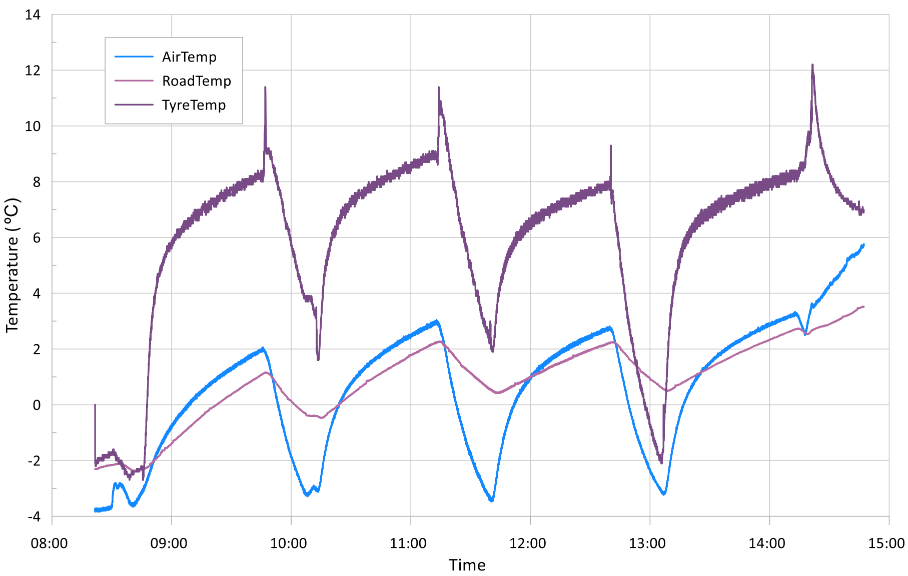

Figure 3. Temperatures in road surface, air and tyre surface during a test sequence.

Stud protrusion can vary during a test. Both the wear and movements in the stud mount in the rubber contributes to changes. Since stud protrusion is affecting wear and PM emission a method has been developed to deal with the problem (Göransson et al, 2018). By using the concept of “stud laps” where one lap in the simulator with a mean stud protrusion of 1 mm is counted as one stud lap. The number of stud laps is the product of laps and stud protrusion in mm. Since all tests are run the same amount of laps in the simulator (12 000), the stud laps are directly correlated to stud protrusion. In the analyses, PM10 concentrations and emission factors have therefore been corrected for differences in stud protrusion. Stud protrusion was measured in-between each load test using a digimatic indicator (Mitutoyo IDU25) on the same 10 studs on each tyre. During the tests, the stud protrusion developed as shown in Figure 4, left. As can be seen, the stud protrusion is decreasing, even though very little during these tests. Also four tread depths were registered using the same device in four positions round each tyre, resulting in 16 measurement point, before and after each test. While the Kuhmo tyres show a decreasing tread depth during the tests, the Nokian tyres did not show an obvious trend (Figure 4, right).

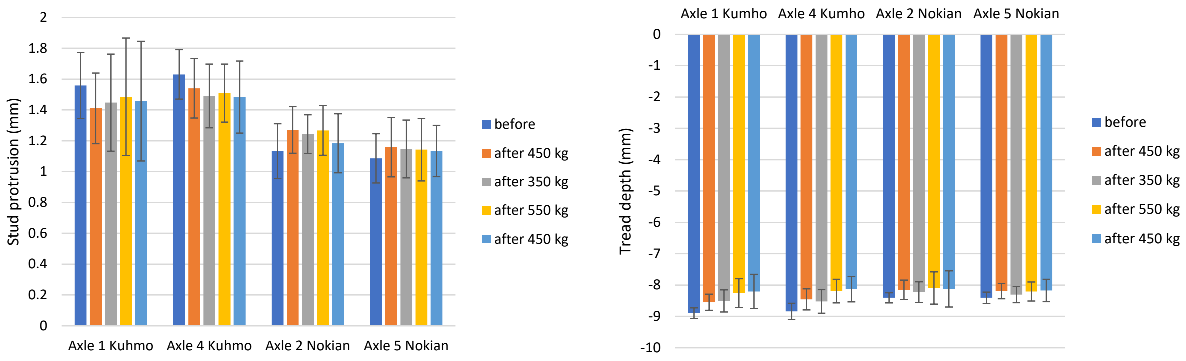

Figure 4. Stud protrusion (left) and tread depth (right) development during the load tests. Error bars are one standard deviation.

The load of each axle in the simulator can be adjusted. Standard load per axle is 450 kg, resulting in a total load of 1800 kg, since there are four tyres mounted on the simulator to investigate the effect of different loads, the standard load was complemented with 350 kg and 550 kg per axle, resulting in 1400 and 2200 kg total loads respectively.

The wear of the pavement slabs before and after the full test was measured in profiles across each slab using a laser device. The differences were negligible as can be seen in Figure 5.

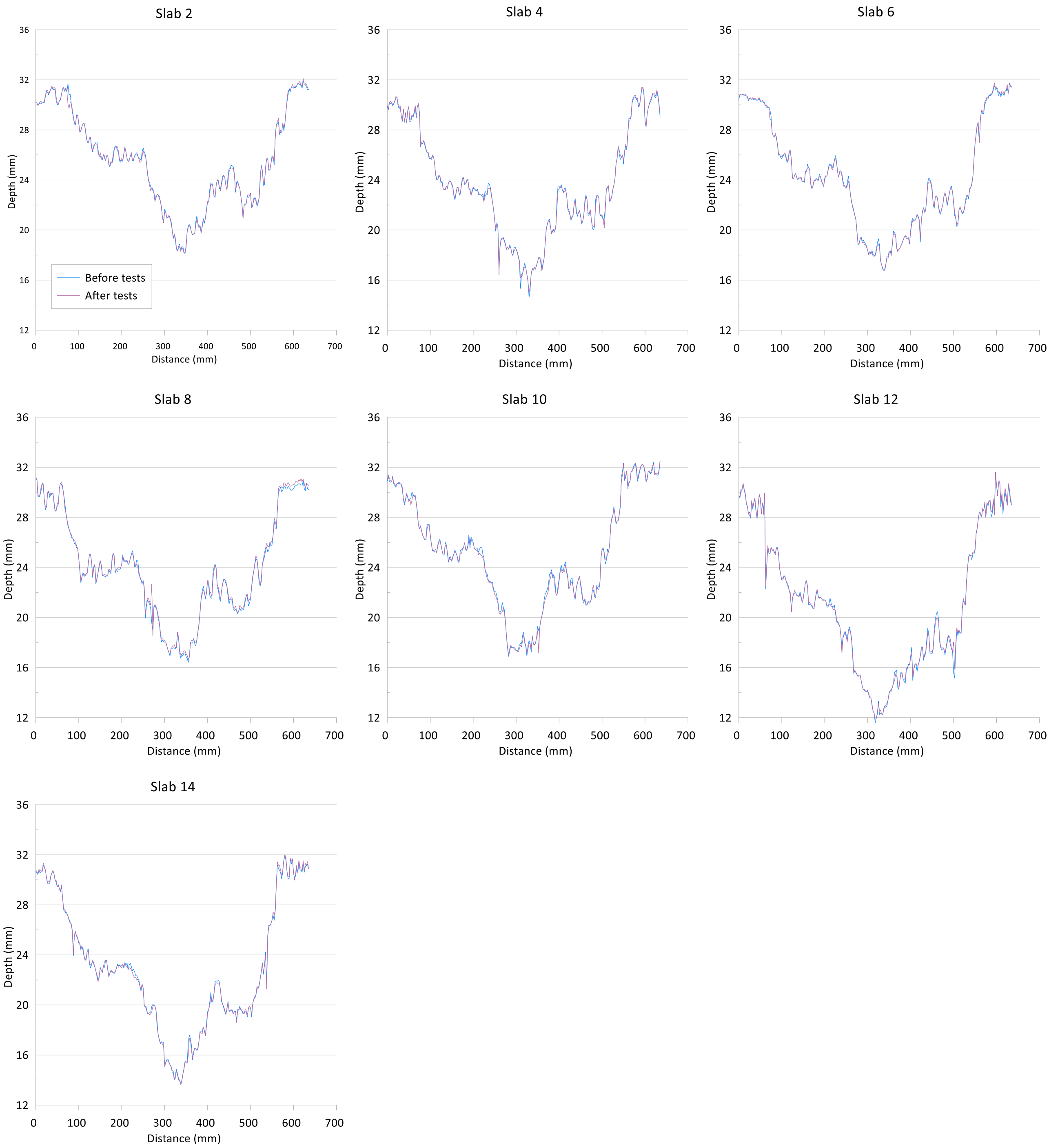

Figure 5. Profiles across seven slabs in the simulator before and after full test (all loads).

Macro texture, defined as mean profile depth (MPD) along the track was recorded using a laser device mounted on one of the two “free” axles in the simulator. This was made before and after each weight test. The mean MPD decreases during the test and the decrease is faster in the beginning of the test and successively slower, but there seems to be no correlation to mass load (Figure 6).

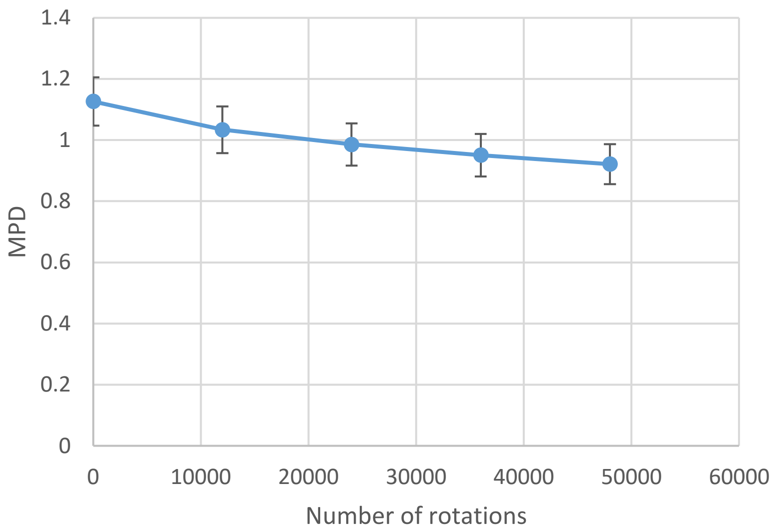

Figure 6. Macro texture (mean profile depth, MPD) during the tests. Error bars are one standard deviation.

Plotting the change in MPD (ΔMPD) to accumulated number of rotations shows a decrease best fitted with a power function and no relation can be seen with mass load on axles (Figure 7, left). A better correlation can be seen to mean stud protrusion, where a higher protrusion results in a larger change at the same number at the same number of rotations (Figure 7, right).

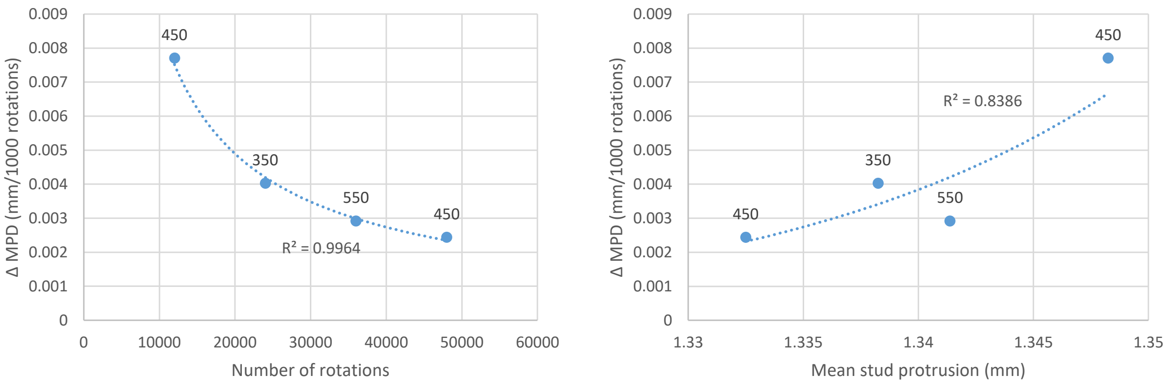

Figure 7. Δ MPD plotted to rotations (left) and to mean stud protrusion (right). Lables are axle load.

Particle measurements

During the measurements, particle concentrations and size distributions were measured using TEOM (1400a, Ruprecht & Pataschnik), Aerosol Particle Sizer (APS, TSI Inc), Scanning Mobility Particle Sizer (SMPS, TSI Inc) and AQ-Guard (Palas). Also, ambient, road surface and tyre surface temperatures were registered continuously.

Results and discussion

PM10 concentration and emission increase both with speed and with increasing load. Concentration differences between minimum and maximum loads are similar at both tested speeds, approximately 1.3 mg/m^3. The differences in emission factors tend to increase with load and is about 0.3 mg/vkm at 350 kg/axle and 0.5 mg/vkm at 550 kg/axle (Figure 8). It should be noted that the emission factor calculation from concentration curves from the road simulator is very sensitive to chosen initial assumptions made in the curve fitting and small changes can result in large differences in emission factor. Also, the constant rotation induces a turn-slip in the contact that exaggerates the wear, why the absolute numbers should be treated with care.

The initial test at 450 kg/axle has higher concentration and emission factor than the finalising 450 kg/axle test. A probable explanation is the higher macro texture in the first test, which implies a rougher surface more prone to release fragments. The ΔMPD decreases continuously during the test sequence, indicating a stabilisation of the macro texture, which would favour a lower particle emission.

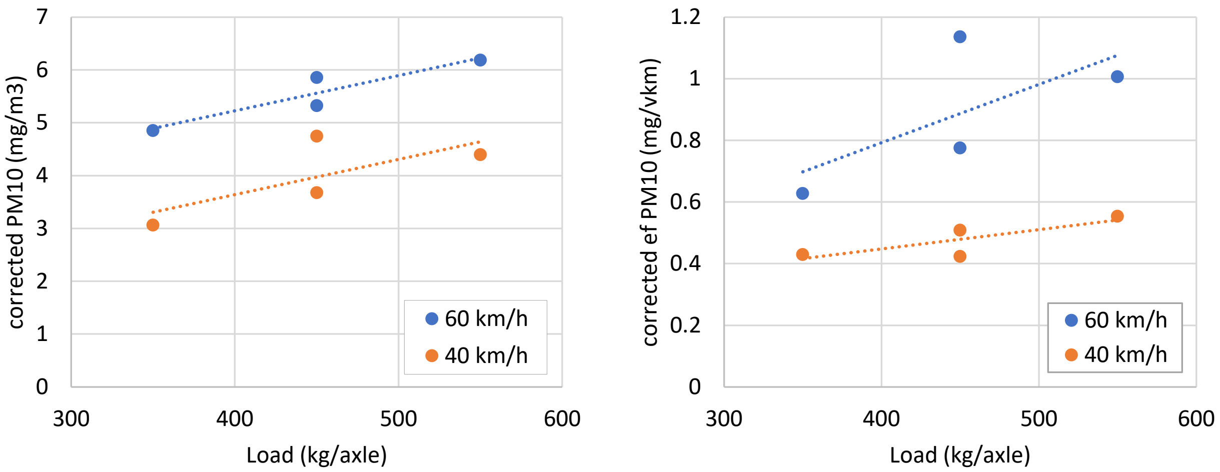

Figure 8. PM10 mean concentrations and emission factors for three axle loads and two speeds.

Particle number concentration is totally dominated by ultrafine particles. At 60 km/h a weak correlation to axle load can be seen but at 40 km/h, there is no correlation. PNC is significantly higher at 60 km/h than at 40 km/h (Figure 9).

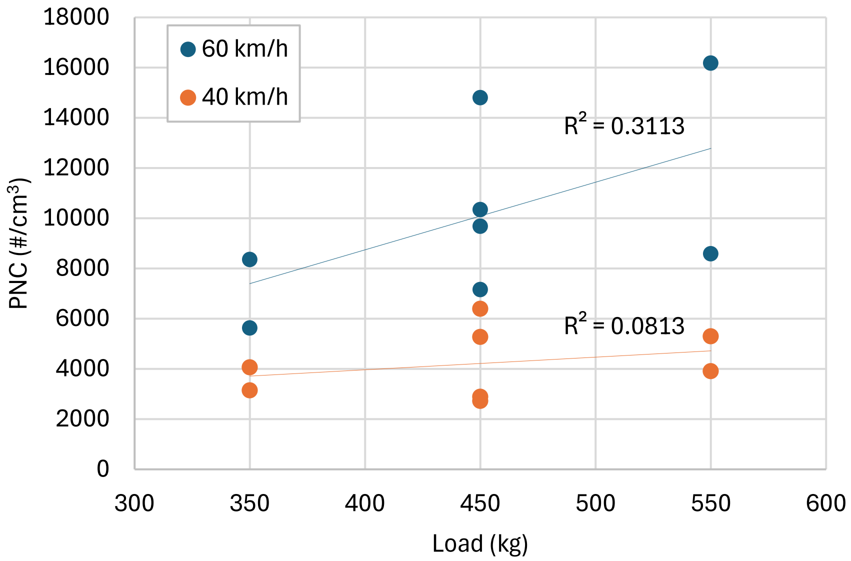

Figure 9. Particle number concentration as measured by SMPS (5.94–224.7 nm) in relation to axle load and speed.

Measurement of particle size distributions show that both particle number and mass concentrations in general increase at higher load and higher speed, while the influence on the distributions' shape is rather small (Figure 10). At 40 km/h, the influence on number distribution, both in concentration and shape, is marginal. Mass size distribution have a primary mode at 2–3 µm and a secondary at about 5–6 µm. At higher speed the coarser mode is slightly more pronounced. At 550 kg axle load, an additional coarse mode above 10 µm can be seen at both speeds in Figure 10. It should be noted that the coarser part of the distribution is affected by the PM10 cut-off, why this coarse mode is likely to be vastly more prominent in the full size distribution of the road abrasion wear. Number distributions are unimodal and have a maximum at around 20–30 nm at all axle loads. Number concentrations increase more with speed than mass concentrations and the differences between load is markedly higher at higher speed. A small secondary maximum can be seen at around 150–200 nm. The origin of these ultrafine particles has been speculated to be volatilisation and following condensation of softening oils (Dahl et al., 2006). Since they do not appear in high concentrations when testing studless winter or summer tyres (e.g. Grigoratos et al., 2018), a connection to the studs is expected. If oils are the source, they are volatilised from the friction between studs and rubber as the studs move in their attachments. Another possible process could be spark formation between rocks and stud metals which could result in metal particle formation.

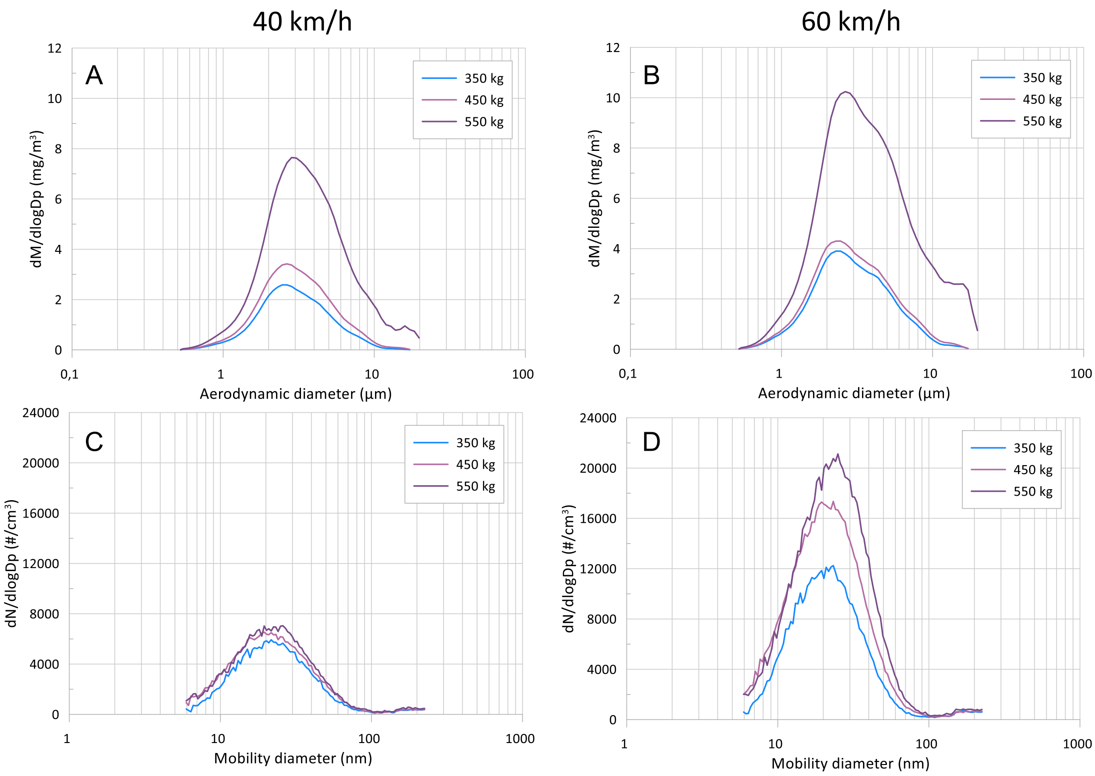

Figure 10. Mass size distributions (A and B) and and number size distributions (C and D) at different speeds and axle loads.

The ratio of PM2.5 to PM10 is of interest for modelling purposes and estimations of health effects. In these measurements we have used two different instruments, which can be used to study the ratio. The APS gives mass size distributions for PM10 based on a density of 2.8 g/cm^3. A subset up to 2.5 µm of the mass size distribution can be divided by the mass of the full distribution to achieve the ratio. The AQguard instrument delivers PM10, PM4, PM2.5 and PM1 as output from which the ratio can be calculated. The instrument is optical and PM values are based on particle counts combined with instrument-specific algorithms. The PM2.5/PM10 ratio calculated from the APS data shows no obvious relation to axle load and speed and is in the range 30–35%. The AQguard results (available only for 450 and 550 kg axle load) suggest a slightly lower PM2.5/PM10 ratio around 23–27%. In the AQguard data, higher speed generates a higher share of

PM2.5. Higher load, at least at the highest load of 550 kg per axle, generates a lower share of PM2.5 (Figure 11). This is likely to be a result of the additional coarse peak seen in Figure 10 at 550 kg.

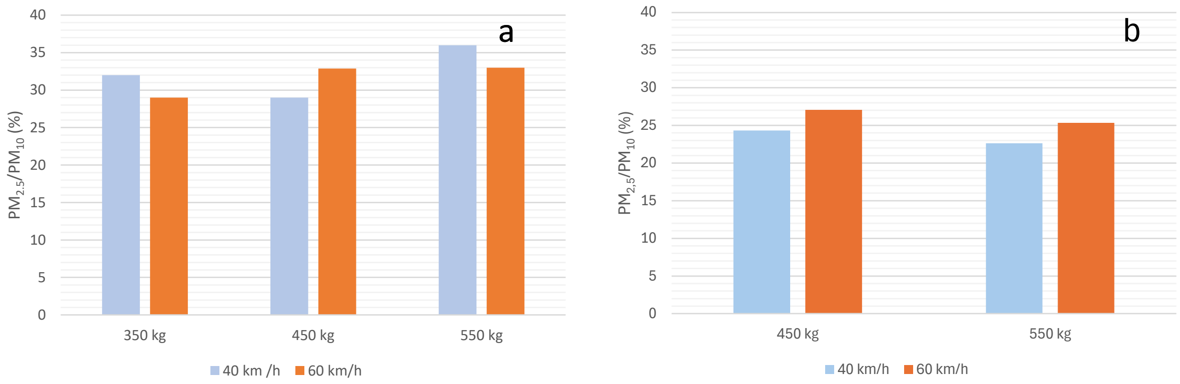

Figure 11. Ratio between PM2.5 and PM10 calculated from APS instrument (left) and based on AQguard data (right).

Higher load and higher speed means that the studs hit the pavement with a higher force which imply a higher wear. It is also plausible that the higher stud force is able to abrade larger fractions of the specific pavement material. This effect might be depending on rock properties.

Conclusions

From the load tests in the road simulator it was concluded that:

- Higher axle load yields higher particle mass and number emissions
- Higher speed yields higher particle mass and number emissions
- Mass size distributions are bi- or trimodal and have a primary peak at 2–3 µm, independent on speed or axle load. The highest axle load (550 kg) yields an additional secondary coarse particle mode.
- Number size distributions are unimodal and peak at 20–30 nm, independent on speed or axle load.

Influence of weight on particle emissions, field tests

Methods

To investigate the effects of vehicle weight and speed on particulate matter (PM) emissions in real-world settings, an instrumented vehicle known as "Sniffer," provided by Metropolia, was used (Figure 12A-B). The "Sniffer" vehicle is known for its use in exhaust emissions bloom chasing (Pirjola et al. 2004), and usage in road dust studies, where sampling is conducted through an inlet located behind the vehicle's rear left wheel (Pirjola et al., 2009).

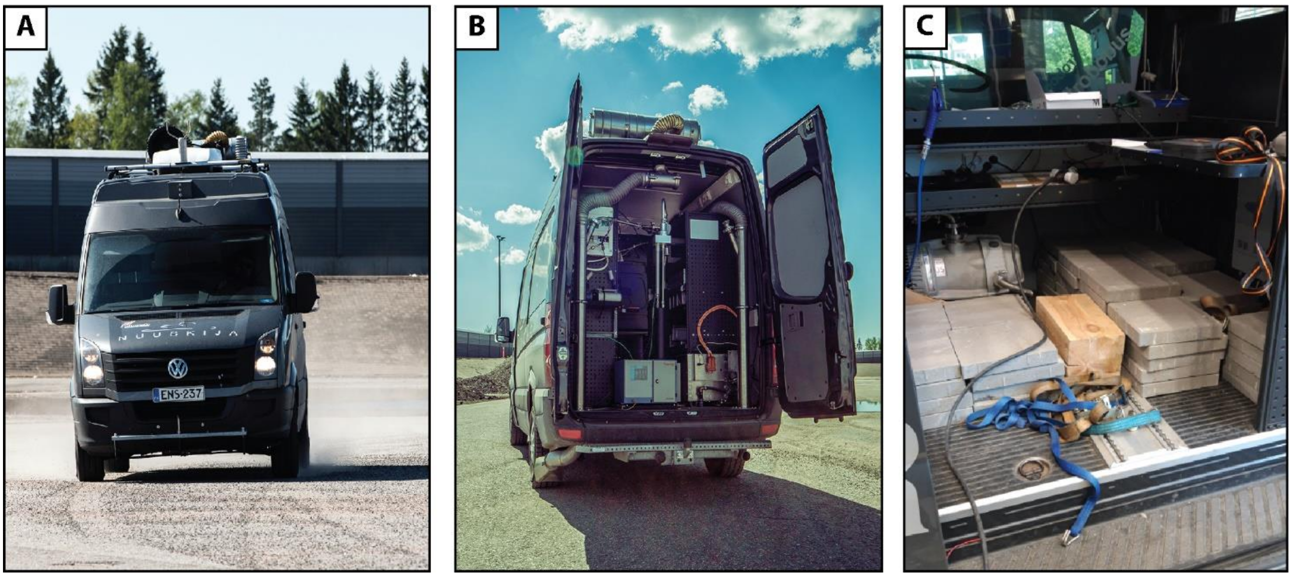

Figure 12: A-B: Metropolia's 'Sniffer' Vehicle. C: Some extra weights used in vehicle weight campaigns. Photos: Sami Kulovuori.

This study involved four distinct investigative campaigns at three different locations to assess the impact of varying vehicle weights and speeds on PM emissions (Table 5). Two of these campaigns, conducted at Site A (Figure 13A), were dedicated to investigating the impact of vehicle weight on PM emissions. The remaining two campaigns were conducted at site B (Figure 13B) and C (Figure 13C), in which the impact of vehicle speed on PM emissions was investigated.

Table 5: Summary of measurement campaigns

CAMPAIGN	SPEEDS (KM/H)	WEIGHT (KG)	SEASON	WDS	TYRES
A: VEHICLE WEIGHT IMPACT ON PM EMISSIONS	30, 50, 70	3500,4050, 4600,5150	Spring, Summer	Yes (Summer)	Friction, Studded
B: VEHICLE SPEED IMPACT ON PM EMISSIONS	80, 90, 100, 110, 120	3500	Summer	No	Friction, Studded
C: VEHICLE SPEED IMPACT ON PM EMISSIONS	20, 40, 60, 80, 100, 120	3500	Autumn	Yes	Summer, Friction, Studded

Campaigns

All campaign sites (A, B, and C) were separated into three distinct zones: acceleration/deceleration zones and measurement zones where the speed of the vehicle was maintained constant. The tyres used in the measurement campaigns were Continentals Vancontact 100 (summer) VanContact Viking (friction) and VanContact Ice (studded). All of the tyres were sized as 235/65/R16, and the tyre pressure was kept constant at four bars throughout all of the measurement campaigns.

During the campaigns, particle size distribution was observed using an optical particle sizer (TSI OPS 3330), and particle mass concentrations (PM2.5, PM_{coarse}, and PM10) were measured using a tapered element oscillating microbalance (TEOM 1405-D, Thermo Scientific) and with DustTrak II (TSI DustTrak II 8830) from behind the wheel. Ambient temperature and relative humidity (Vaisala, HMP45A), wind speed, and wind direction (Vaisala WS425, when stationary) were also recorded at the top of the vehicle. Additionally, the concentrations of ambient PM10 (TSI DustTrak II 8830), NO_X (Horiba APNA-360), and CO_2 (Li-Cor, Li-820A) were measured from the front of the vehicle.

Wet Dust Sampling (WDS) measurements were conducted using cross-sectional sampling on the road, with a sampling interval of 25 cm. From the collected samples only, turbidity was measured with Hanna Instrument Turbidity Meter (HI-88703-02) and converted to dust load (DL < 180 µm) using a conversion function from VTI.

Vehicle weight campaigns (Site A)

Campaigns were conducted on road number 130 (Hämeenlinnantie, 19000 Nurmijärvi, Finland) where the average daily vehicle count is 3700 veh/d, with 10% of heavy-duty vehicles. Measurements were conducted in spring and summer, with friction and studded tyres, at three different speeds (30, 50, and 70 km/h), and four different vehicle weights (3500, 4050, 4600, and 5150 kg) (Figure 13A).

Measurements were performed on 3 consecutive days. One speed was driven by both tyres for all weight classes. The vehicle weight was increased after the given weight was driven with both tyres by placing concrete tiles (11 kg/pcs) in 550 kg increments inside the vehicle (Figure 12C). Owing to the additional weight on vehicle impacts and the location of the inlet in relation to the ground, air suspensions were used to compensate for the drop in inlet height, which was set to 7 cm from the ground for each weight. Additionally, WDS measurements were performed during the summer campaigns.

High-speed campaign 1 (Site B)

The campaign was conducted on highway number 3 (Hämeenlinnanväylä, between off ramps 11-13, Finland), where the average daily vehicle count was approximately 34000 veh/d with 8% heavy-duty vehicles. Measurements were performed on two consecutive days in the summer using studded and friction tyres, with speeds varying from 80 to 120 km/h (Figure 13B).

High-speed campaign 2 (Site C)

The campaign was conducted on road number 12577 (Kievarintie, 32560 Virtaa, Finland), where the average daily vehicle count was approximately 355 veh/d with 10% heavy-duty vehicles. Measurement campaigns were conducted during late autumn using summer, friction, and studded tyres, with speeds varying from 0 to 120 km/h. Additionally, Wet Dust Sampling was performed on-site (Figure 13C).

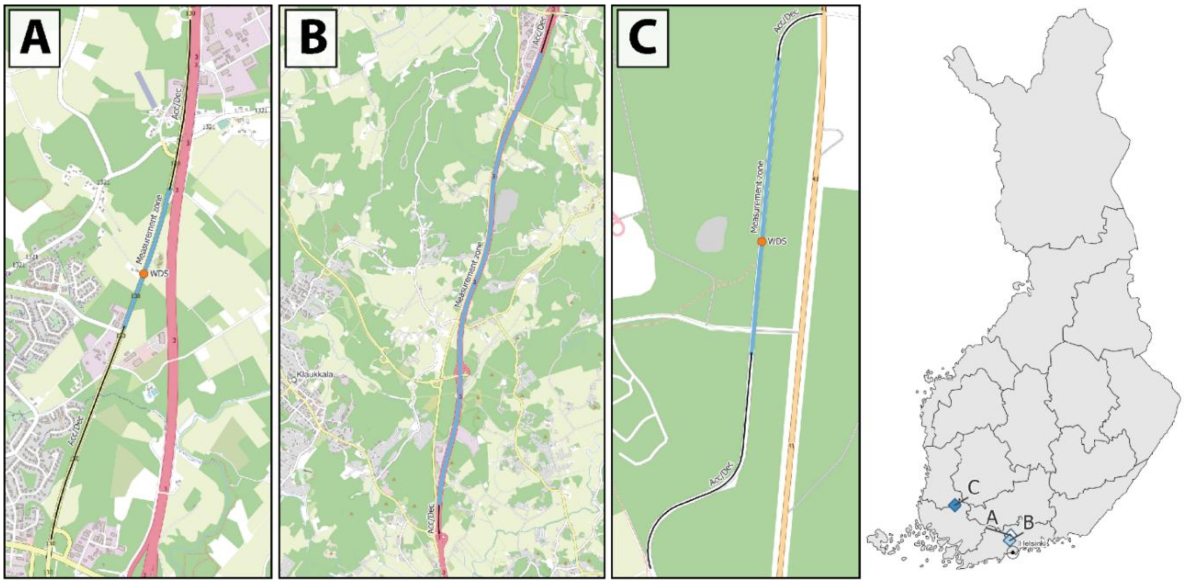

Figure 13: Different zones in measurement sites with WDS sampling locations. A: Weight test campaign, B: High-speed test campaign 1, C: High-speed test campaign 2.

Data processing

The collected data were processed using three common filters for each dataset. The first common filter used in the data processing was speed filter (Equation 1), where v is recorded the vehicle speed (km/h), and v_{target} is the targed speed for the measurements (km/h), the difference between the recorded and traged speed should be within 3 km/h.

$$\left|v - v_{target}\right| \leq 3 \tag{1}$$

The second common filter used for the data was, inner quartile range (IQR) filter, where IQR was calculated using Equation 2, where Q_3 represents the 75th percentile, and Q_1 represents the the 25th percentile. The lower and upper bounds were determined (Equation 3) using constant k (1.5). To filter out outliers from the data, equation 4 was applied to the datasets.

$$IQR = Q_3 - Q_1 \tag{2}$$

$$\begin{gathered} Lower\ bound: LB\ Q_1 - k\ \times IQR \\ Upper\ Bound: UB\ Q_3 + k\ \times IQR \end{gathered} \tag{3}$$

$$Outlier\ if\ x < Q_1 - 1.5\ \times IQR\ or\ x > Q_3 + 1.5\ \times\ IQR \tag{4}$$

The third common filter applied to the datasets was that the recorded data point (latitude and longitude) was within the boundaries of the measurement zone. For this, ray casting algorithm was used which can be expressed as follows, let point in question be $P = (x_p, y_p)$, and polygon in question be sequence of vertices $\{(x_1, y_1), (x_2, y_2) \dots, (x_n, y_n)\}$, where each vertex is (x_i, y_i) is connected to (x_{i+1}, y_{i+1}) and (x_{n+1}, y_{n+1}) = (x_1, y_1) to form closed polygon. Point´s location relative to the polygon can be defined as function $f(P, Polygon)$ (Equation 5), where E_i, represent the edge from x_i, y_i to x_{i+1}, y_{i+1} and $I(P, E_i)$ is indicator function defined as in Equation 6.

$$f(P, Polygon) = \begin{cases} \text{Inside}, & if\ \sum_{i=1}^{n} I(P, E_i)\ \ mod\ 2 = 1 \\ Outside, & Else \end{cases} \tag{5}$$

$$I(P, E_i) = \begin{cases} 1, & if\ horizontal\ ray\ starting\ at\ P\ intersects\ E_i \\ 0, & Else \end{cases} \tag{6}$$

The intersection test checks if the y-coordinate of P is between the y-coordinates of the endpoints E_i and if the x-coordinate of the intersection point of the ray and E_i is greater than x_p.

The sniffer emissions factor (EF), is expressed in grams per vehicle kilometre travelled $\left(\frac{g}{VKT}\right)$, and is calculated using Equation 7:

$$EF = \frac{m \times Q}{v} \times \frac{1}{fA} \times 4 \tag{7}$$

where m is the mass concentration difference $\left(\frac{g}{m^3}\right)$ and it is calculated as (Equation 8):

$$m = \left(C - C^{'}\right) \times 10^{-6} \tag{8}$$

where, C is the measured mass concentration behind the tyre $\left(\frac{\mu g}{m^3}\right)$ and $C^{'}$ is the measured ambient mass concentration (front of the vehicle while moving or stationary) $\left(\frac{\mu g}{m^3}\right)$. A factor of 10-6 was used to convert micrograms into grams. In Equation 7, Q is the total flow rate of the sampling system $\left(\frac{m^3}{h}\right)$, v is the vehicle speed $\left(\frac{km}{h}\right)$, and fA is the correction factor. Factor 4 in Equation 7 considers all four tyres of the vehicle.

Calculations assume that the concentration behind each individual tyre is the same, even though there might be variations depending on the road surface dust load, vehicle weight distribution, etc. which would affect the suspension of dust behind each tyre.

Results and discussion

Campaign A

Campaigns were held during spring and summer time (April and June), spring campaign temperatures were somewhat consistent during the measurements ranging from 10 to 15 ºC during the days. The relative humidity was between 30 and 58% during the measurements. In the summer campaign, the average daily temperatures were 20, 22 and 25 ºC, and the average daily relative humidity was 36, 43, and 40%, respectively (Figure 14). In both campaigns, the sky was clear, and the road surface was dry throughout the sections.

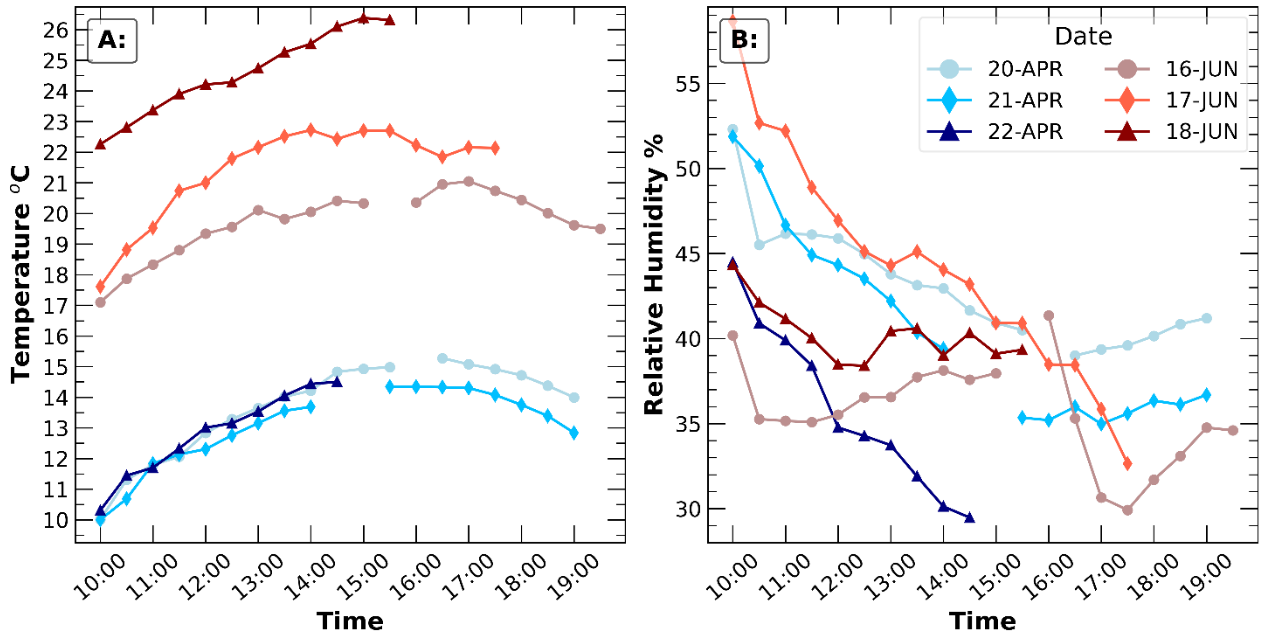

Figure 14: Daily ambient 30-minute average (A) temperature (ºC) and (B) relative humidity (%), during measurement campaigns on road number 130 (Hämeenlinnantie), measured with Sniffer.

The dust load on the road surface was low during the summer campaign, and most of the dust was located outside of the wheel tracks, concentrating towards the middle and outer sides of the driving lanes (Figure 15A). The mean dust load in the south direction was 18,8 g/m^2 and for the north direction,11.9 g/m^2 (Figure 15B. In the northbound lane, the mean dust load on the left wheel track (Figure 15A, 225-275 cm from the edge of the driving track), where the Sniffers inlet is located, was 5.5 g/m^2, while on the right wheel track (Figure 15A, 75-125 cm from the edge of the driving track), it was 9.7 g/m^2. In the southbound lane, the mean dust load on the left wheel track (Figure 15A, 425-475 cm from the edge of the driving track) was 22.1 g/m^2, compared to 7.2 g/m^2 on the right wheel track (Figure 15A, 575-625 cm from the edge of the driving track).

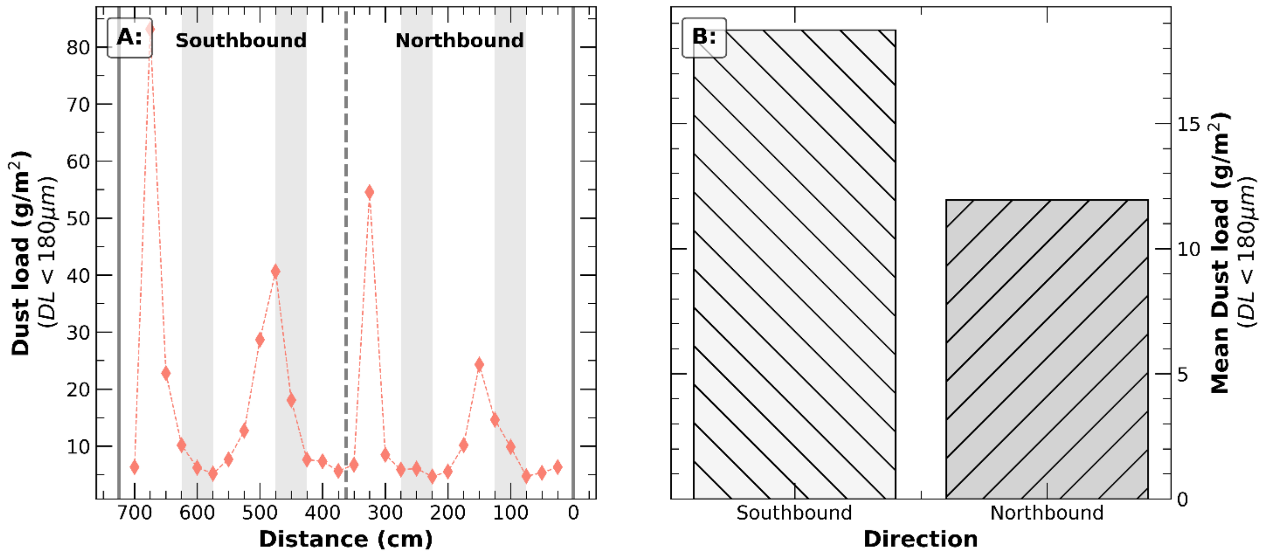

Figure 15: A: Point-specific dust load during summer during the weight effect campaign in Nurmijärvi. B: Mean driving lane-specific dust loads during the summer campaign.

The measured mean PM10 concentrations were significantly higher in spring than in summer, which was expected due to the diurnal change in road surface dust load. As seen in Figure 16, the vehicle speed influences the measured suspension for both campaigns with both tyres, even though the effect is not significant in the summer campaign with friction tyres and lower speeds (Figure 16B). By increasing vehicle weight we can see a similar effect as with speed in both campaigns, even though the difference between the tyres on PM10 concentrations in the spring campaign is not huge, and for instance, with 5150 kg (Figure 16A), the concentration is higher with the friction tyre than with the studded tyre.

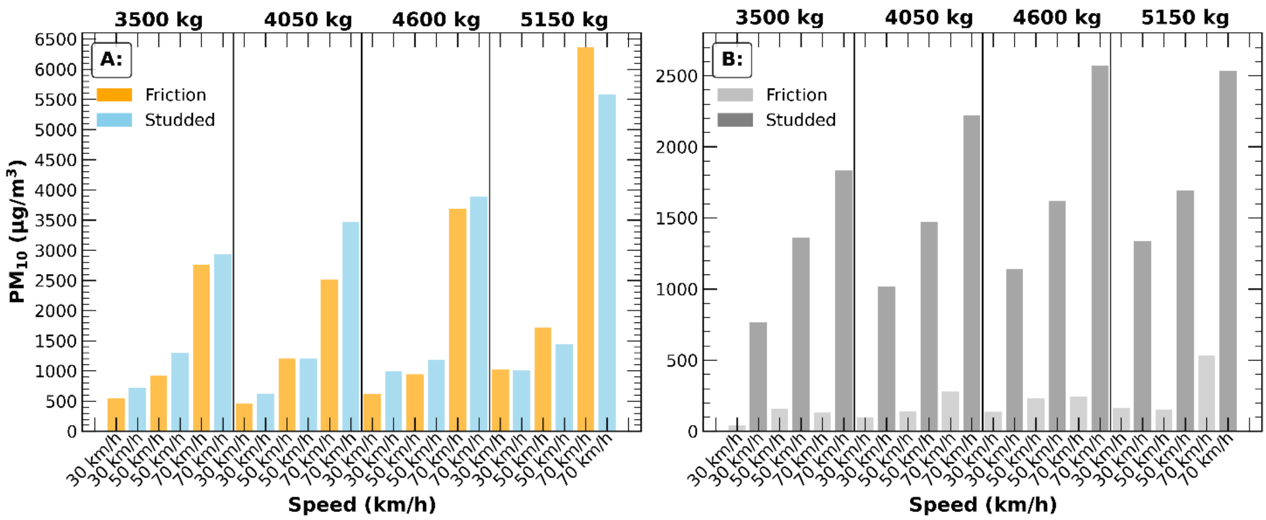

Figure 16: Measured mean PM10 concentrations with studded and friction tyres for different speeds and vehicle weights. A: Spring campaign. B: Summer campaign.

The PM2.5 share of PM10 did not behave similarly to the PM10 concentrations, although a linear increase with speed with a given weight and studded tyres is observable in Figure 17B. During the summer campaign, the PM2.5 share was between 8 to 15% of PM10, and in the spring campaign between 8 to 21%, with mean PM2.5 share with studded tyres being 12 and 10%, and with friction tyres 13 and 14%, respectively during the campaigns.

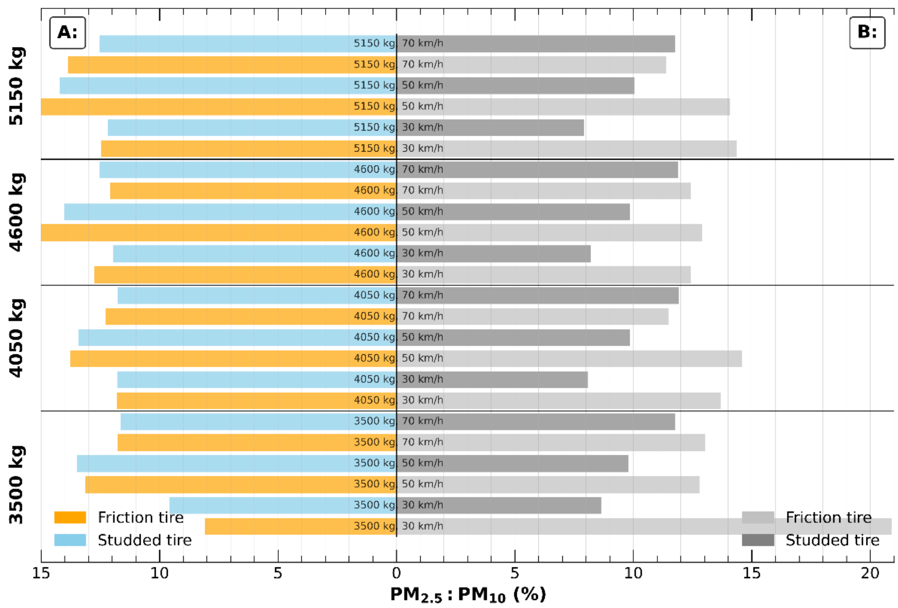

Figure 17: Mean measured PM2.5 share of PM10 during spring (A) and summer (B) campaigns.

As observed in the PM10 concentrations in Figure 16, vehicle weight had an effect on particle mass size distributions with increasing concentrations (Figure 18). Differences between different weight classes were minor between the tyres in the spring campaign (Figure 18A), but noticeable in the summer campaign (Figure 18B). During the summer campaign, we can also observe that the weight effect has a minor difference between the two highest weights and speeds with the studded tyre, and a similar leveling-out effect can also be observed at 50 km/h (Figure 16B).

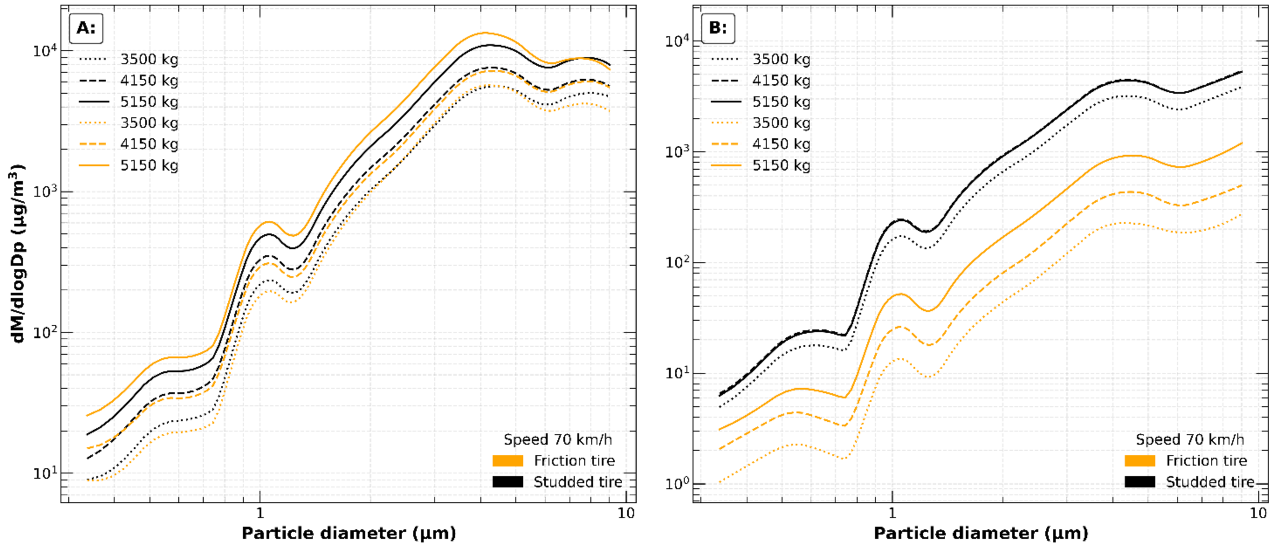

Figure 18: Mean particle mass size distribution at a constant speed. A: Spring campaign. B: Summer campaign.

In the spring campaign, we observed 3 peaks in the size distributions, at around 1.2, 4.5, and 7.5 μm, respectively (Figure 19), and similarly in the same spots in the summer campaign except that 7.5 μm, peaks vanished or shifted out of range. Similar observations were made in the road simulator (Figure 10); even though the exact locations of the peaks are not identical, two peaks can be observed in the coarse fraction of the size distributions in both tests with the studded tyres.

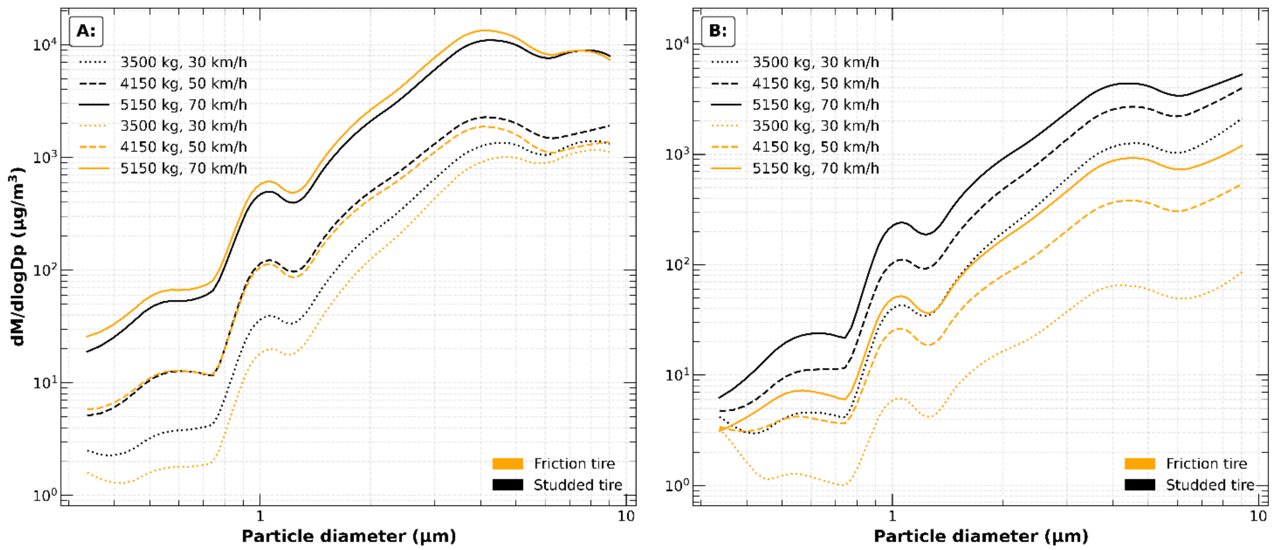

Figure 19: Mean particle size distribution with varying speeds and weights. A: Spring campaign. B: Summer campaign.

When looking at how the mass size distributions (Figure 18, Figure 19) or PM10 concentrations (Figure 16) changes with different speeds, weights, and tyres, we can observe that increasing the vehicle speed or vehicle weight increases the measured concentrations with each tyre. This is due to changes in tyre forces and moments what are dependable i.e. velocity, weight, slip angle, tyre and road properties as well ambient conditions etc. that will affect road dust suspension.

When the road surface dust load is low, as in the summer campaign (Figure 16), we can see that the difference in measured concentrations with studded and friction tyres is large (Figure 15B, Figure 18B, and Figure 19B), thus indicating that the difference in concentrations is caused by the direct road surface wear of the studded tyres. This is the main mechanism of the higher emission rate for the studded tyre; thus, resuspension of the dust load is the main mechanism for all studdless tyres. This effect can be observed clearly inFigure 19B, where the observed mass size distribution (particle size >≈ 1.3 µm) with the lowest weight and lowest speed with studded tyres is higher than that with the highest weight and highest speed with the friction tyre.

However, when the road surface dust load increases, the difference between the tyres and observed concentrations levels out or in some cases might be reversed, indicating that the resuspension of the accumulated dust on the road surface during winter is the main mechanism that increases the observed concentrations. This also means that when the road surface dust load is sufficiently high, resuspension of this dust overshadows the direct road surface wear effect of the studded tyres.

Campaign B

During the measurements, temperatures ranged from 22 to 25 and 24 to 26 $^{\circ}C$, and relative humidity from 67 to 51% and 55 to 42%, between the 11th and 12th of August (Figure 20). The increase in temperature and decrease in relative humidity during the measurements were not considered to have affected the outcome of the results.

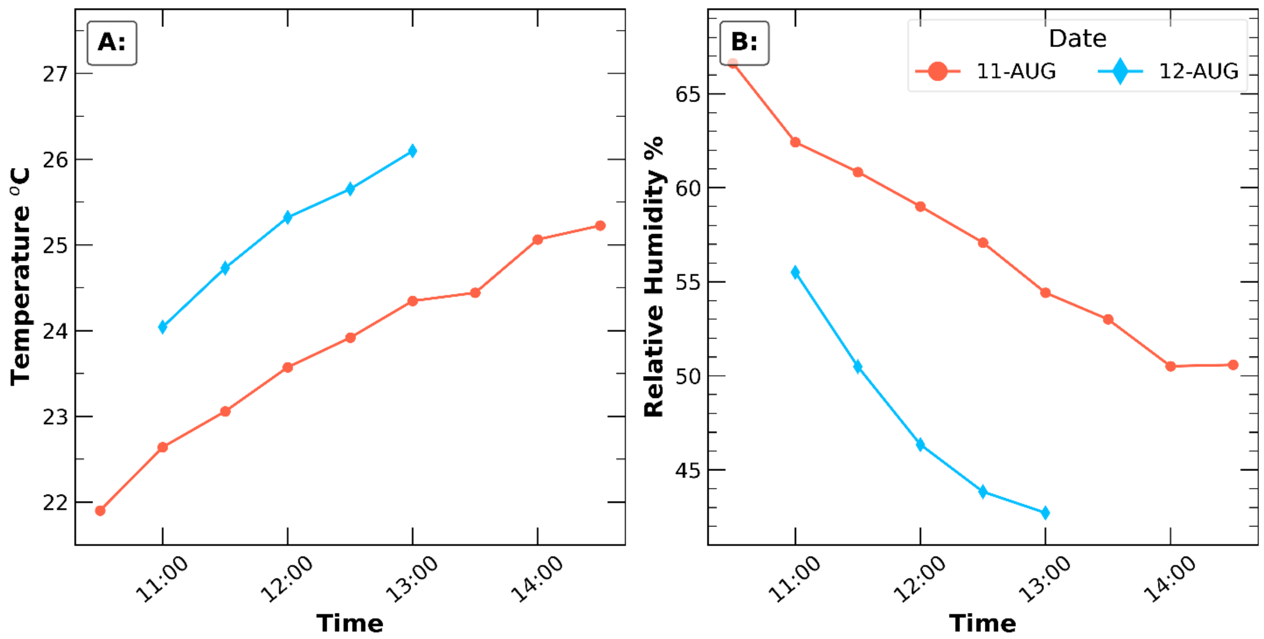

Figure 20: Daily ambient 30-minute average (A) temperature (ºC) and (B) relative humidity (%) during measurements (blue = friction tyres, red = studded tyres) in road number 3 (Hämeenlinnanväylä), measured with Sniffer.

The measured PM10 concentrations with friction tyres were low, indicating that the road surface in the driving lanes did not have a significant amount of dust left on the surface, and the observed concentrations from friction tyres can be considered as direct emissions caused by the selected tyre type. PM10 concentrations increased linearly from 80 to 120 km/h, from approximately 1100 to 3500 $\mu g/m^3$ and from 150 to 600 $\mu g/m^3$ with studded and friction tyres, respectively (Figure 21).

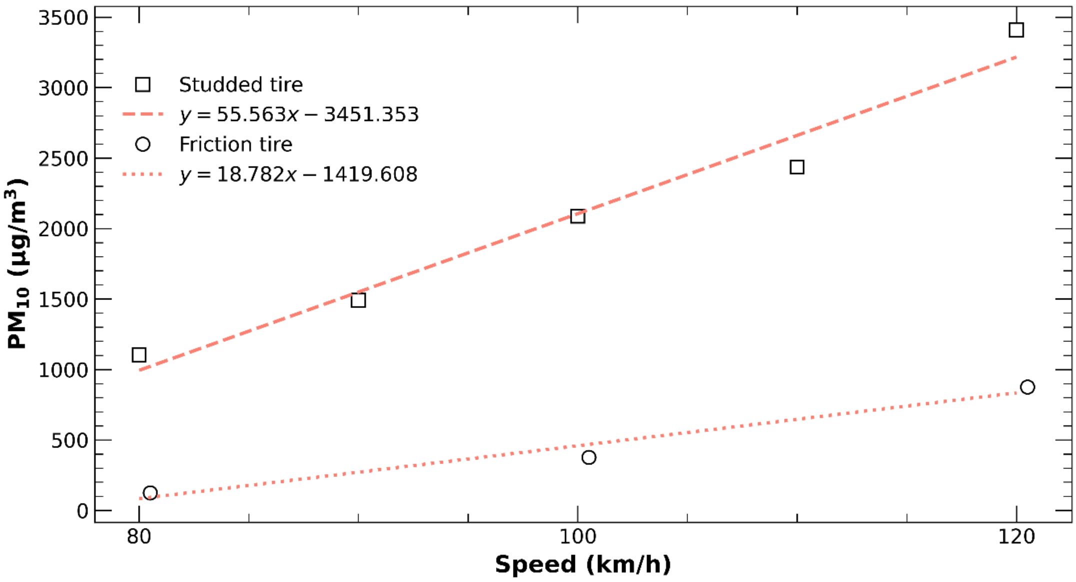

Figure 21: Mean PM10 concentrations as a function of speed with studded and friction tyres.

Similar to campaign A, two distinct peaks can be observed from the particle mass size distributions of the coarse fraction with both tyres. These peaks are approximately 4, 5 and 9 μm, even thou with the friction tyres with 80 km/h the peaks are not as clear as in other speeds. Both tyres also had a peak of around 1 μm, which is also observed in campaign C. As shown in the PM10 concentrations, the difference in the concentrations between the studded and friction tyres was an average factor of eight.

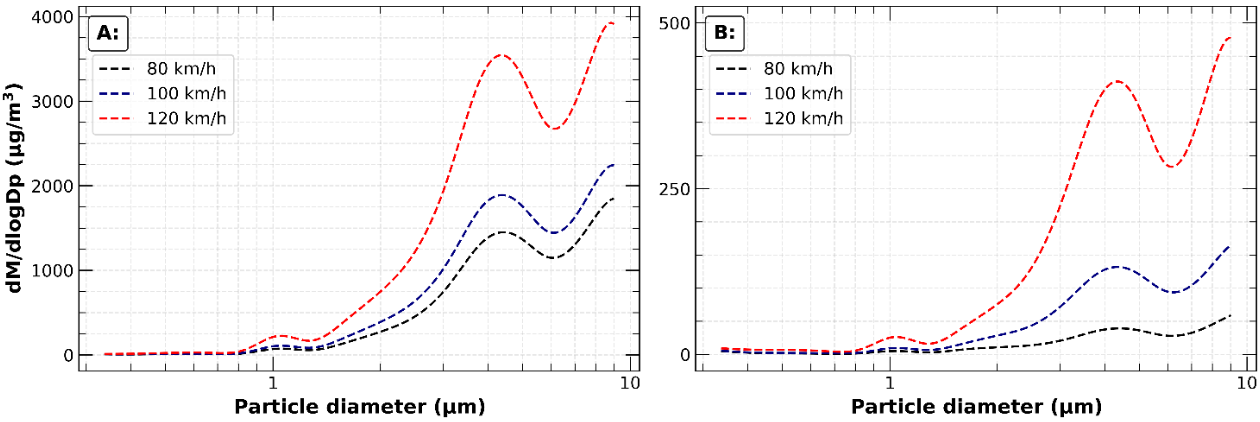

Figure 22: Mean particle mass size distributions at 80,100 and 120 km/h for studded (A) and friction (B) tyres.

Campaign C

During the measurements, the temperature ranged from morning 17.5 ºC to afternoon 22.5 ºC and the relative humidity was around 57-59% during the measurements. During the day, the sky was mostly clear, except from 12:00 to 14:00, when the sky was mostly cloudy, which resulted in a drop in the ambient temperature (Figure 23). Road surface temperatures were between 16-27 ºC (measured with Fluke 62 mini, IR thermometer) in the morning/evening and afternoon, respectively.

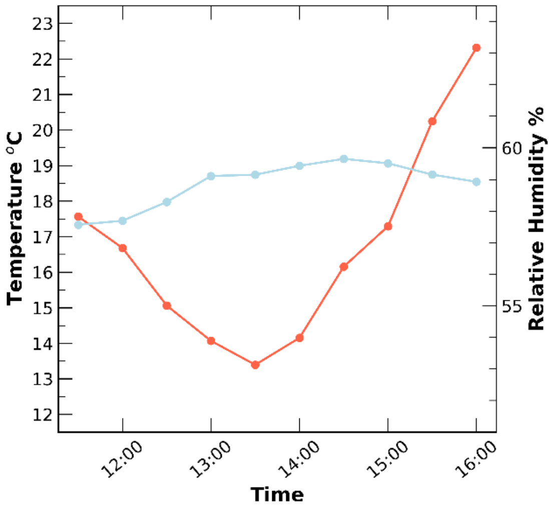

Figure 23: Ambient 30-minute average temperature (ºC) and relative humidity (%) during measurements, in road number 12577 (Kievarintie), measured with Sniffer.

Similarly, as in the weight effect campaign, the dust load was low at the site during the campaign. The mean dust load was 6.6 in the southbound lane and 5.8 g/m^2 in the northbound lane (Figure 24B). The dust load was quite consistent in both wheel tracks, 4.9 and 4.3 g/m^2 on left wheel tracks, and 4.7 and 5.2 g/m^2 on right wheel tracks, in north and south directions respectively. The highest dust load was observed in the middle part of the road and between the wheel tracks (Figure 24A).

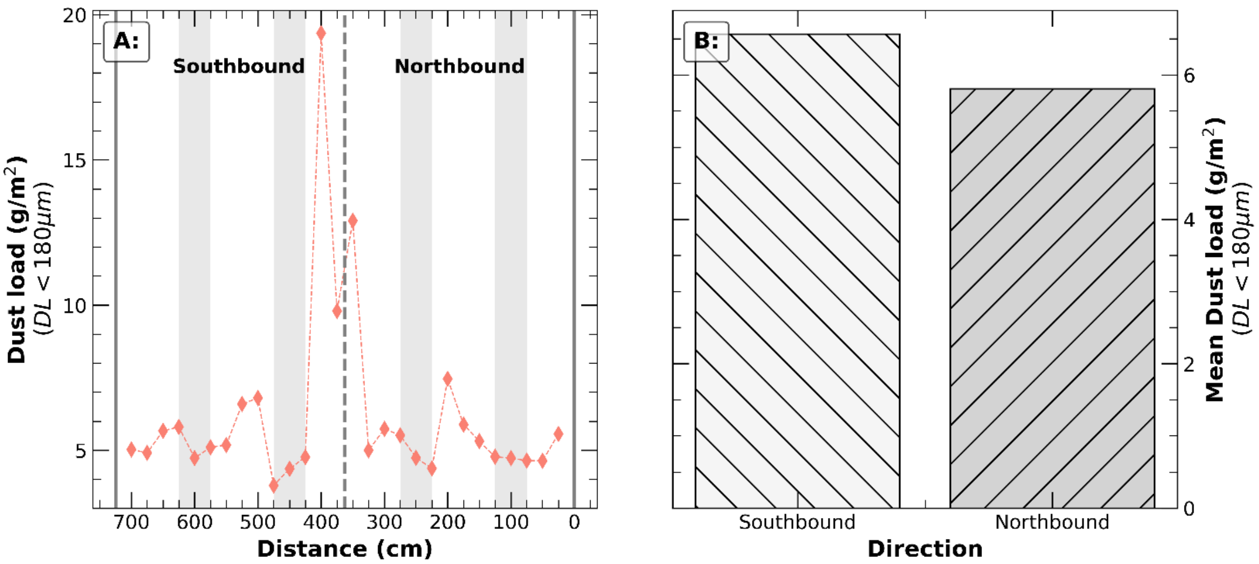

Figure 24: Point-specific dust load during the speed effect campaign in Virtaa. B: Mean driving lane-specific dust load during the campaign.

The measured mean PM10 concentrations with studded tyres varied from 2000 $\mu g/m^3$ to 11 000 $\mu g/m^3$, and increased linearly with speed as seen in Figure 25A. For friction tyres, mean PM10 concentrations ranged from around 50 $\mu g/m^3$ to 1200 $\mu g/m^3$ (Figure 25B), and with summer tyres concentrations ranged from 150 $\mu g/m^3$ to 1700 $\mu g/m^3$ (Figure 25C), with speed of 20 to 120 km/h respectively.

Concentrations with friction and summer tyres increased quadratically as a function of speed (Figure 25B-C) compared to the linear increase in studded tyres (Figure 25A). The highest concentrations were measured with studded tyres and the lowest with friction tyres, and the overall average difference across the whole speed range between the tyres was 13.6 and 8.7 times higher measured concentrations for studded tyres in comparison to friction and summer tyres, respectively.

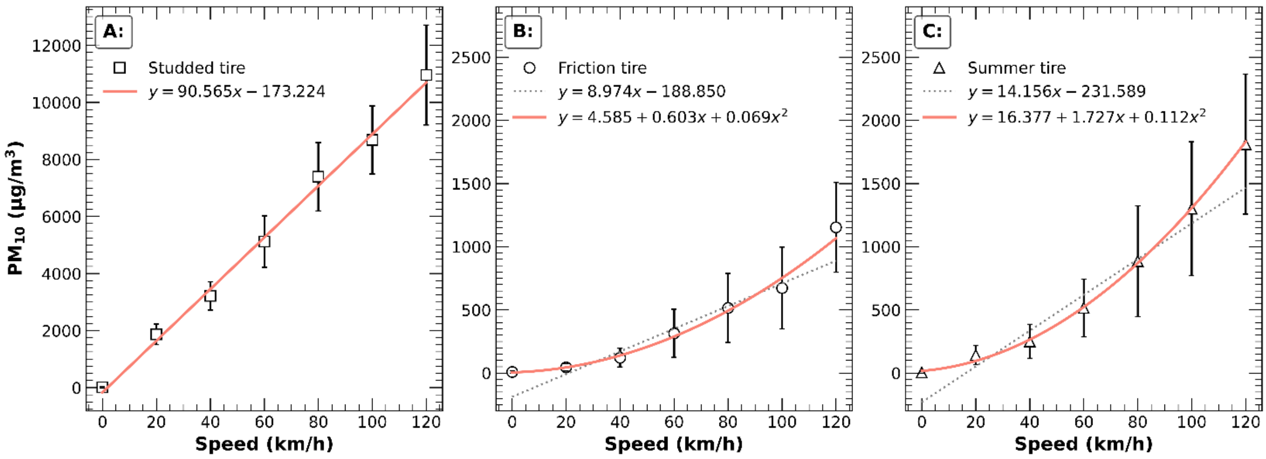

Figure 25: Measured mean PM10 concentrations and linear and quadratic fits at different speeds. A: Studded tyre, B: Friction tyre, C: Summer tyre

As the PM10 concentration figures show, the concentrations increase as a function of speed; a similar increase can be seen in the particle mass size distributions for each type of tyre across the size distributions (Figure 26). For each tyre, 3 peaks were observed from the mass size distributions around 1.2, 4.5 and 7.5 µm (darker blue color in Figure 26A,B,C), all distributions started leveling out after the last peak. The highest concentrations are measured around 4.5 µm, where the concentration is 1.15 times higher than at the second highest peak formed around 7.5 µm

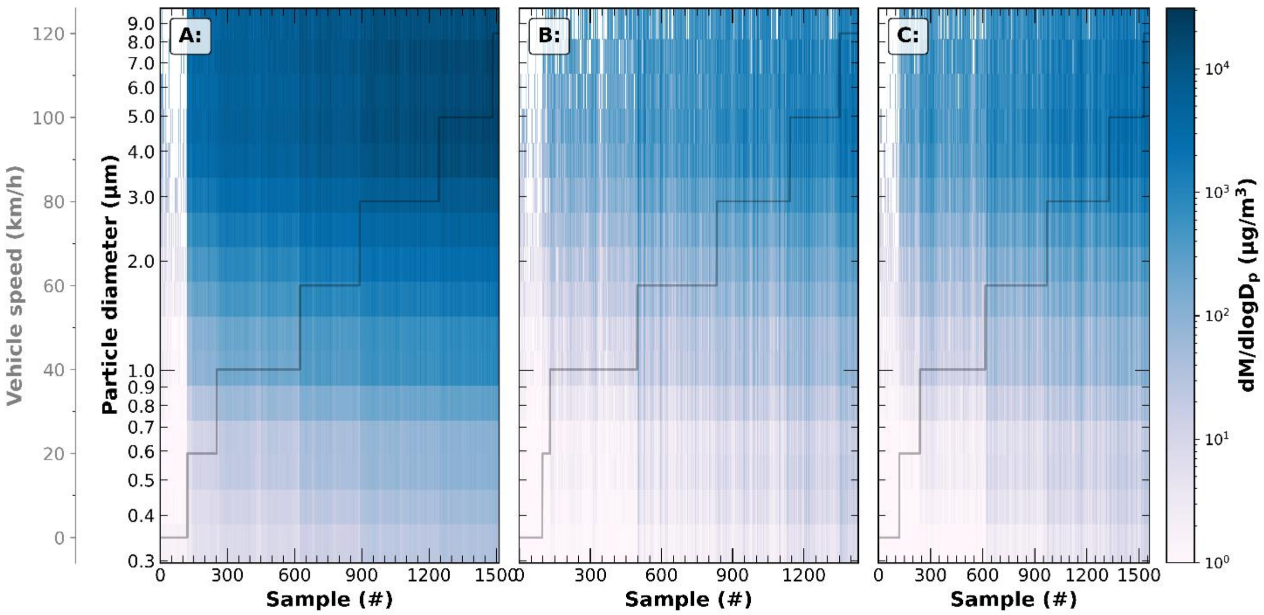

Figure 26: Measured particle mass size distributions as function of time with vehicle speed. A: Studded tyre, B: Friction tyre, C: Summer tyre.

When considering Sniffer's PM2.5 share of PM10, we observed that the ratio decreased as a function of speed for all measured tyres (Figure 27). The share of PM2.5, was approximately 13% at 20 km/h and decreased linearly across the range, ending up to approximately 9% at 120 km/h. In the stationary state (0 km/h in Figure 27), the PM2.5 share is approximately 50%, which can be explained by the fact that the vehicle was idling during stationary measurements and some of the exhaust fumes most likely entered the inlet, thus affecting the PM2.5 share to some extent. There is also no contribution of coarse resuspended particles from tyre and road interface, which also contributes to a higher share of PM2.5.

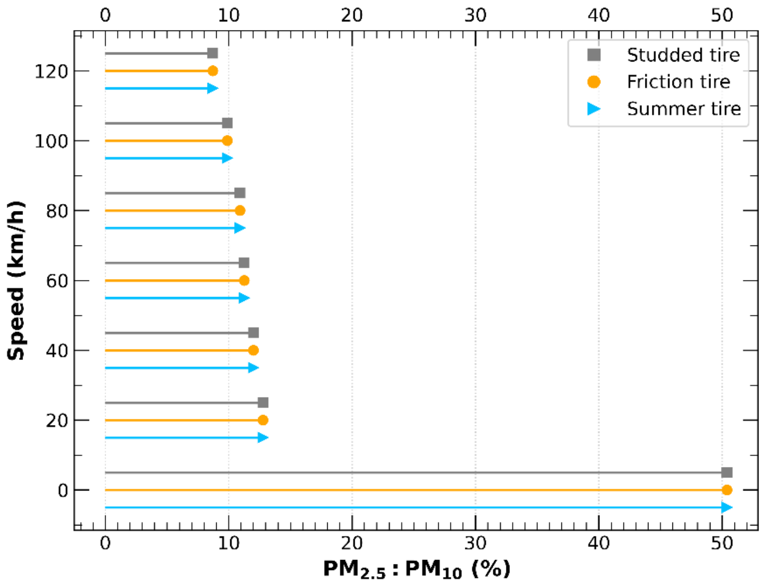

Figure 27: Mean PM2.5 share of PM10 during measurements at different speeds and tyres.

Emissions factors

The emission factors were calculated using (Equation 7) for campaigns A and C. In campaign A, emission factors were represented as a function of weight for spring and summer (Figure 28-Figure 29) and for campaigns B (Figure 30) and C (Figure 31) as a function of speed. In campaign A, the emission factors for both tyres were quite close during springtime. The friction tyres emit around 0.8, 0.9, and 1.3 times compared to the studded tyres (Figure 28A-C), with speed classes of 30, 50, and 70 km/h, respectively.

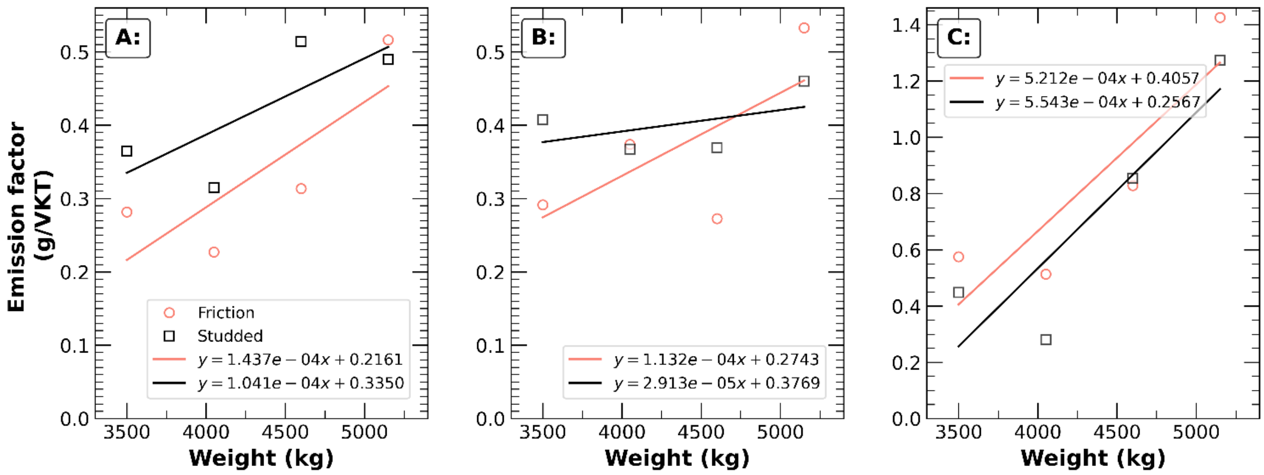

Figure 28: Calculated sniffer emission factors for friction and studded tyres as a function of weight during springtime in campaign A. A: Speed 30 km/h, B: Speed 50 km/h, C: Speed 70 km/h.

In the summertime, the difference in the emissions factors between the tyres is much clearer, with friction tyre emissions being around factors of 0.09, 0.11, and 0.12 compared to the studded tyre emissions for each speed class (Figure 29A-C). In both campaigns, a linear increase in emissions can be seen as a function of vehicle weight, as shown in the PM10 concentrations in Figure 16.

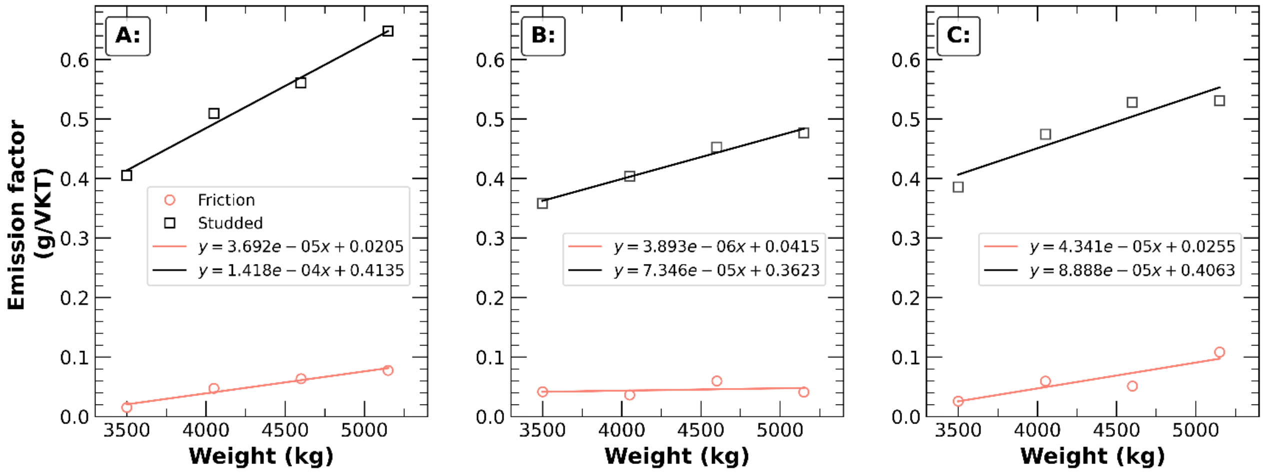

Figure 29: Calculated sniffer emission factors for friction and studded tyres as a function of weight during summer in campaign A. A: Speed 30 km/h, B: Speed 50 km/h, C: Speed 70 km/h.

A linear relationship of emission factors as a function of speed can be observed in most cases in campaign A, especially in springtime, where only one of the weight classes has no increasing linear relationship (studded tyres at 4050 kg).

During summer, the emission factors behaved differently and no clear indicator for the linear increase in emissions factors and speed could be established; instead, emissions factors seem to be more constant or decreasing in nature. The reason for this might be that the data collected during the summer campaign is not as good as in the springtime and other campaigns (B and C), causing the calculations to be not in line with the assumptions. The emission factors from Campaign A are summarized in Table 6-Table 7.

Table 6: Sniffers emissions factors, for studded tyres, with each weight and speed class in campaign A.

Season	Tyre	Weight (kg)	Speed (km/h)	EF (g/vkm)
Spring	Studded	3500	30	0.365
			50	0.407
			70	0.448
		4050	30	0.315
			50	0.367
			70	0.280
		4600	30	0.514
			50	0.369
			70	0.854
		5150	30	0.489
			50	0.460
			70	1.273
Summer	Studded	3500	30	0.405
			50	0.358
			70	0.386
		4050	30	0.509
			50	0.404
			70	0.474
		4600	30	0.560
			50	0.453
			70	0.528
		5150	30	0.648
			50	0.477
			70	0.531

Table 7: Sniffers emissions factors, for friction tyres, with each weight and speed class in campaign A.

Season	Tyre	Weight (kg)	Speed (km/h)	EF (g/vkm)
Spring	Friction	3500	30	0.282
			50	0.291
			70	0.575
		4050	30	0.227
			50	0.374
			70	0.513
		4600	30	0.314
			50	0.273
			70	0.828
		5150	30	0.516
			50	0.533
			70	1.426
Summer	Friction	3500	30	0.015
			50	0.042
			70	0.026
		4050	30	0.047
			50	0.036
			70	0.060
		4600	30	0.064
			50	0.060
			70	0.051
		5150	30	0.078
			50	0.041
			70	0.108

In campaign B, the emission factors for both the studded and friction tyres increased linearly with vehicle speed. For studded tyres, emissions factors ranged from around 0.16 to 0.26 g/VKT and for friction tyres from around 0.003 to 0.03 g/VKT, respectively (Figure 30).

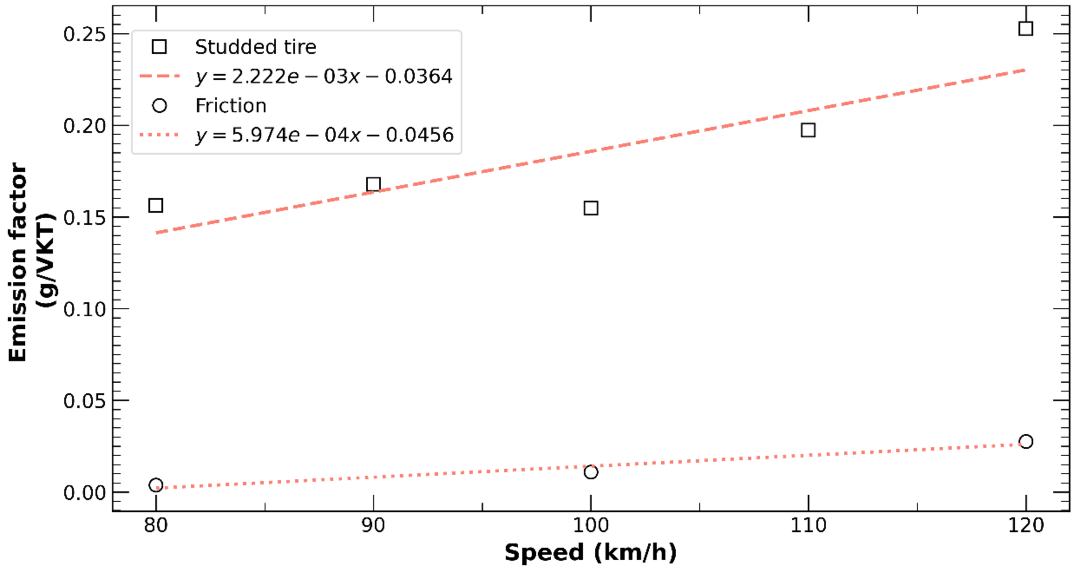

Figure 30: Sniffer emission factors for studded and friction tyres as a function of speed during VT3 campaign.

Similarly, as in campaigns A and B, a linear relationship was observed with emission factors as a function of speed in campaign C (Figure 31). For studded tyres (Figure 31A) emissions factors ranged from 1.1 to 1.3 g/VKT, for friction tyres ((Figure 31B) from 0.07 to 0.12 g/VKT, and for summer tyres (Figure 31C) 0.09 to 0.2 g/VKT, across the speed range, respectively.

The difference between studded and friction tyres was similar in other campaigns, with studded tyre emissions being at least tenfold higher than studdles tyres. Notably, the summer tyre emissions factor was higher than that of the friction tyres, which might be due to the rubber compound and tread pattern differences. Friction tyres are generally softer all around (tread and side walls softer) and they have more complex tread pattern designs with more cavities compared to summer tyres.

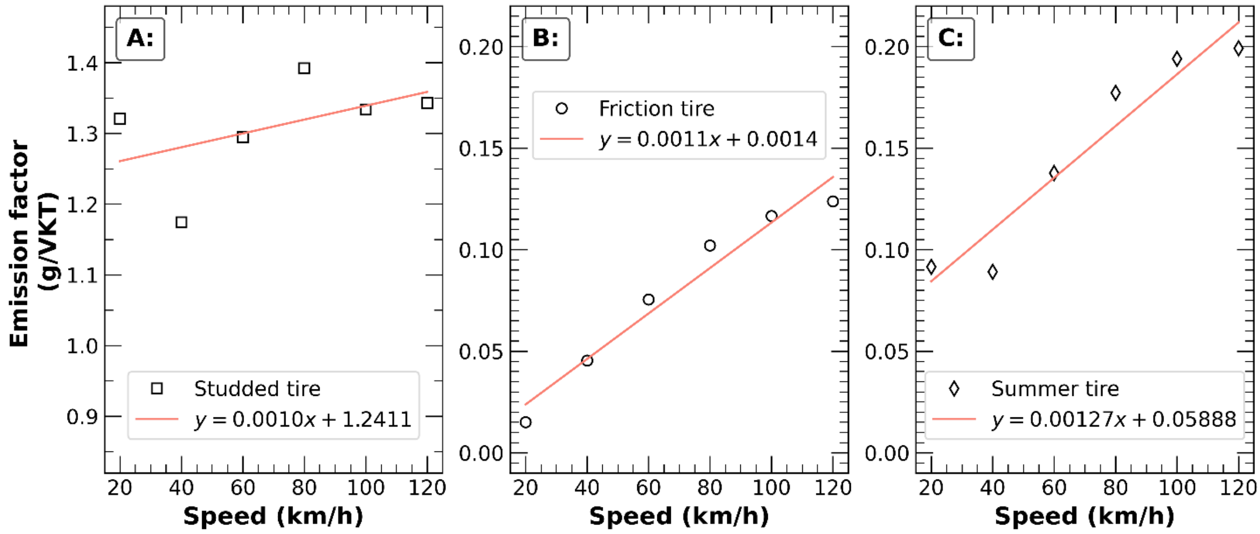

Figure 31: Sniffer emission factors from campaign C as a function of speed for different tyres. A: Studded tyre, B: Friction tyre, and C: Summer tyre. Emission factors are displayed as grams per. vehicle kilometre traveled (g/VKT).

Conclusions

Through deployment of the "Sniffer" vehicle, we conducted four comprehensive investigative campaigns across three diverse real-world settings. This approach allowed us to capture a broad spectrum of data, providing a detailed understanding of how these variables collectively influenced PM emissions. This study's findings present a compelling case for the significant role that vehicle weight and speed play in contributing to PM emissions. The data clearly indicate that increases in vehicle weight and speed correlate with higher PM emissions, highlighting the need for regulatory measures to address these factors. Implementing speed restrictions in pollution-sensitive areas and encouraging the use of lighter vehicles could serve as effective strategies for mitigating PM emissions, thereby enhancing urban air quality and public health.

Moreover, research highlights the critical impact of tyre type on PM emissions, with studded tyres identified as a major contributor compared with studless tyres. This discovery points towards the necessity of guiding consumer and industry practices towards the adoption of less polluting tyre types through informed policy-making and regulatory incentives.

The broader implications of our findings suggest that addressing vehicular PM emissions requires a multifaceted approach. This approach should encompass not only advancements in vehicle technology and design but also strategic urban planning and comprehensive public policy initiatives. This study underscores the importance of continued research in this area, particularly in understanding the evolving dynamics of vehicle emissions in the context of new automotive technologies and changing urban infrastructure.

In conclusion, our in-depth investigation provides a robust evidence base for formulating targeted strategies to reduce vehicular PM emissions. By addressing the intertwined factors of vehicle weight, speed, and tyre type, policymakers, automotive industry stakeholders, and urban planners can forge a path toward sustainable urban mobility. Such concerted efforts are essential for achieving significant improvements in air quality, ultimately safeguarding the health of urban populations and the integrity of our environment for future generations.

Crushing of winter sand, road simulator test

Methods

For winter sand crushing tests, the VTI road simulator was used (Figure 32). A standard, authentic winter sand material, from the city of Karlstad, Sweden, was used. The material was a 2-6 mm sieved crushed gneissic granite from the Alster quarry. The material was thoroughly washed (Figure 33) before the tests to minimize the occurrence of finer fractions below 2 mm.

The simulator track was the same cement concrete pavement used in the wight tests described above and consisting of seven different cement concrete recipes. The tyres used were summer tyres with dimension 205/55 R16 (Michelin Primacy 4 and Pirelli Cinturato P7), since these do not have siping, typical for winter tyres, that risk to accumulate sand grains and affect the results. Inflation pressure was set to 2.5 bars.

Figure 32. The VTI road simulator with plastic cover to collect sand leaving the track during tests. Photo: Mats Gustafsson, VTI.

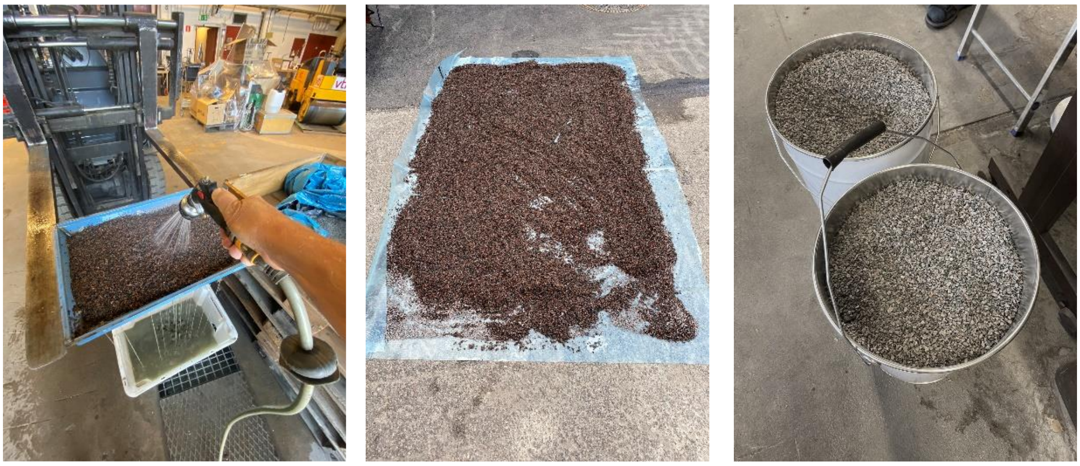

Figure 33. Washing and drying of the test sand and the resulting material. Photo: Mats Gustafsson, VTI.

The resulting sieving curve can be seen in Figure 34, confirming very small amounts of material above 6 and below 2 mm.

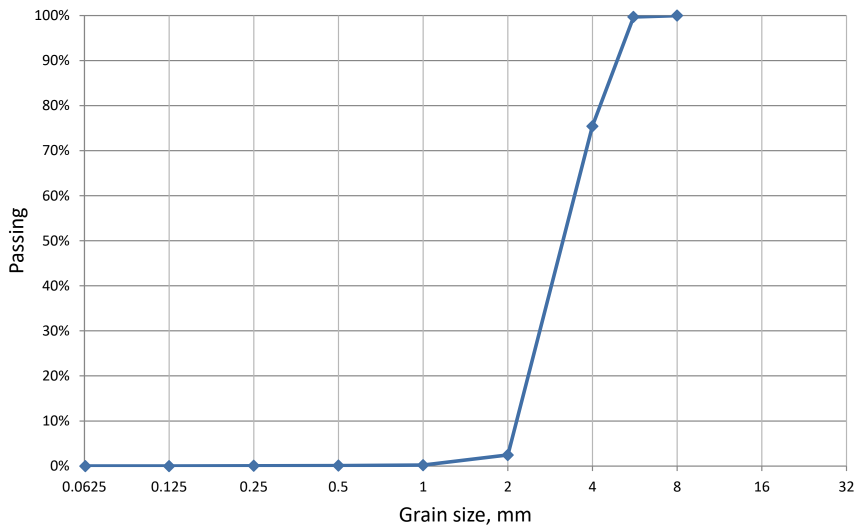

Figure 34. Accumulated size distribution of washed wintersand used in tests.

On the simulator track, 400 g (corresponding to about 2 kg/m^2) of the material was distributed evenly on each slab. The amount is high compared to what is used on roads, but since a continuous loss was expected, it was considered a suitable amount to be able to sample and analyse remaining material after each test run. To keep the sand from leaving the track a very low speed was used (2 km/h). Additionally, a specially built brush swept the verges of the track to push back any sand about to leave the track (Figure 35). The first four tests were identical, with 25 rounds generating 100 wheel passages at 2 km/h. During the fifth test, the speed was 3 km/h. The three final tests were run in 2 km/h but the number of rounds and wheel passages was increased to 100 and 400 respectively (Table 8). After each round, the material left on a slab was sampled using a vacuum cleaner with a modified interior set-up to sample the main particle amounts in a single bucket containing 1 l of water (Figure 36). Due to some splash, the method eventually included thorough sprinkling, with controlled amount of added water, of the interior to recover as much as possible of the vacuumed material.

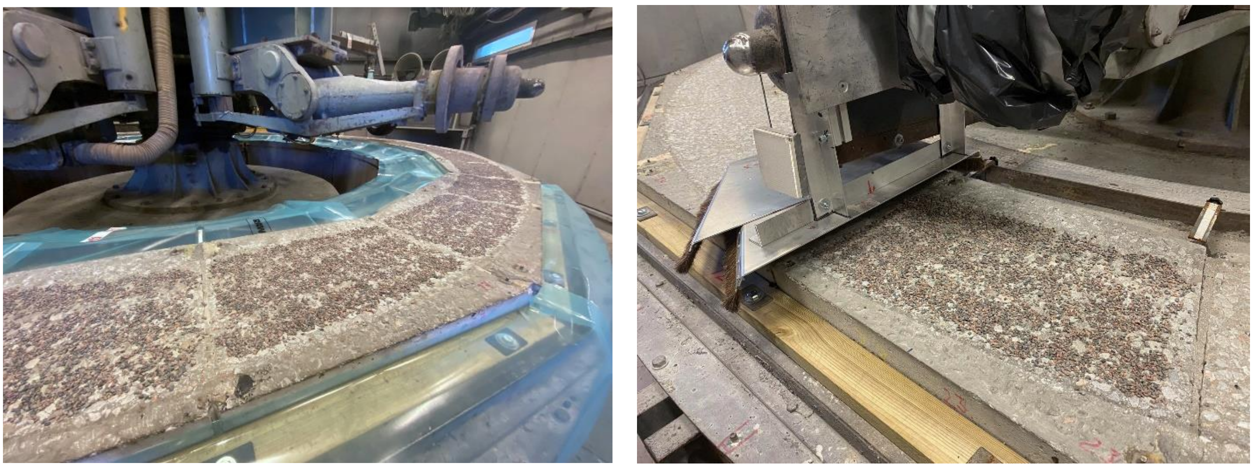

Figure 35. Left: sand evenly spread on the test track. Right: brush constructed to keep the sand on the track. Photo: Mats Gustafsson, VTI.

Figure 36. Vacuum cleaner used for sampling remaining sand on track. Right: modified interior to direct sample into bucket with water. Photo: Mats Gustafsson, VTI.

Sampling started with sampling slab no 1 (see Figure 37) before the crushing tests was started to ensure the vacuuming could sample the amount put out. 399 g was sampled from the originally 400 g, which was considered as sufficiently efficient. The crushing tests was started with a 25 rounds (100 wheel passages) test at 2 km/h after which slab no 3 was vacuumed and analysed.

Table 8. Crushing test rounds and position of sampled slabs on the track.

Sampled slab	Rounds	Wheel passages	Accumulated wheel passages	Speed (km/h)
1	0	0	0	0
3	25	100	100	2
5	25	100	200	2
7	25	100	300	2
9	25	100	400	2
11	25	100	500	3
13	100	400	900	2
15	100	400	1300	2
17	100	400	1700	2

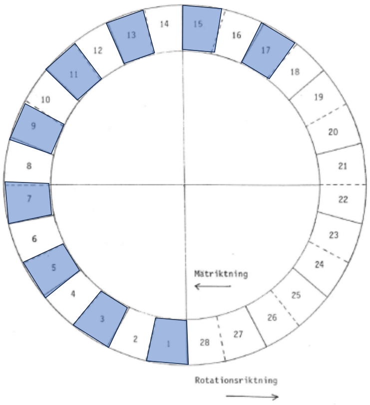

Figure 37. Pavement ring in road simulator and the used slabs in blue.

Analyses was made through drying and weighing the sample followed by wet sieving. The <0.5 mm fraction from the sieving was further analysed using laser granulometry (Malvern Mastersizer 3000) to get a particles size distribution also of finer fractions relevant from an air quality perspective.

During the measurements, particle concentrations and size distributions were measured using TEOM (1400a, Ruprecht & Pataschnik), Aerosol Particle Sizer (APS, TSI Inc), Scanning Mobility Particle Sizer (SMPS, TSI Inc) and AQ-Guard (Palas). For the APS, no PM10 inlet was used, to utilize the full-size range of the instrument. Also, ambient road surface and tyre surface temperatures were registered continuously.

Results and discussion

The low speed of the simulator in combination with the brush resulted in a low loss of material from the track. In Figure 38 the sampled amounts from each slab can be seen. On slab 1 the material was distributed and sampled without any wheel passages to validate the vacuum sweeper sampling method. In the following samplings there is a loss between a few up to 30 g corresponding to 7.5% mass loss. On the two last slabs a higher amount of material remained than was originally put out. The reason for this is not known but might reflect a contribution from road surface wear or along-track migration. Since these slabs are at the beginning of the sand applied slabs in relation to the simulator rotation (see Figure 37), they should rather be depleted on material as an edge effect, though.

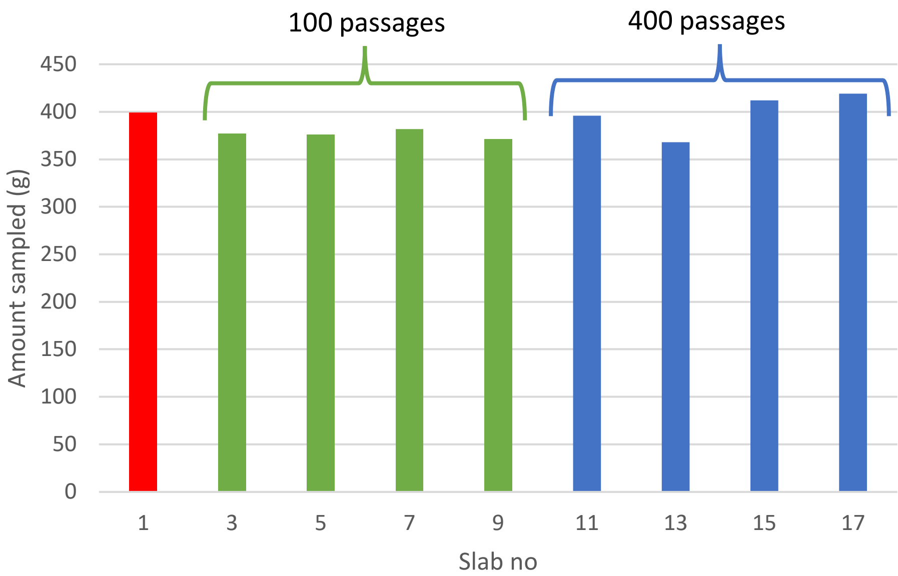

Figure 38. Amount sampled on each slab after tests.

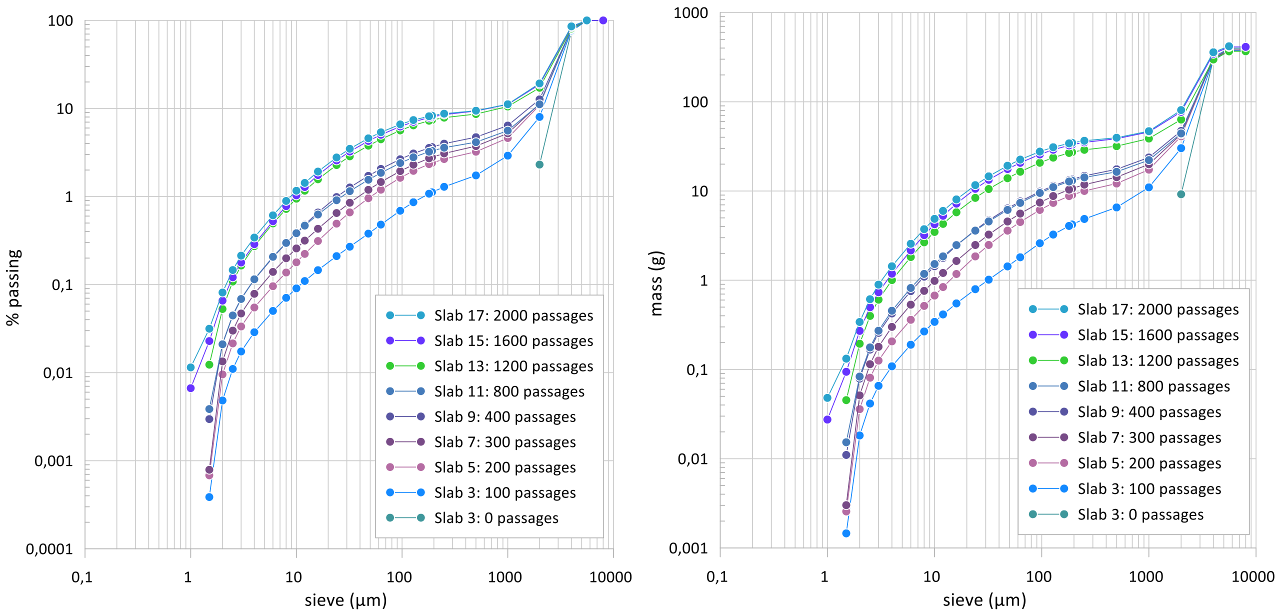

Figure 39. Combined size distributions from wet sieving and laser granulometry for all tests.

The crushing process affects mainly the coarser fractions, and it is probably more accurate to call the process abrasive wearing, i.e. the sharp edges of the coarser fractions are worn off to produce smaller fractions of all smaller sizes.

Each fraction below the coarsest will both lose material to the next finer fractions during wearing as well as gain material from the nearest coarser fraction. Material can also be abraded from coarser into fractions several steps smaller without passing all fractions in between.

In Figure 40, curve fits have been made on the fractions of interest for the NORTRIP model. Only the coarsest fractions are decreasing, while the finer fractions are increasing as abrasion continues.

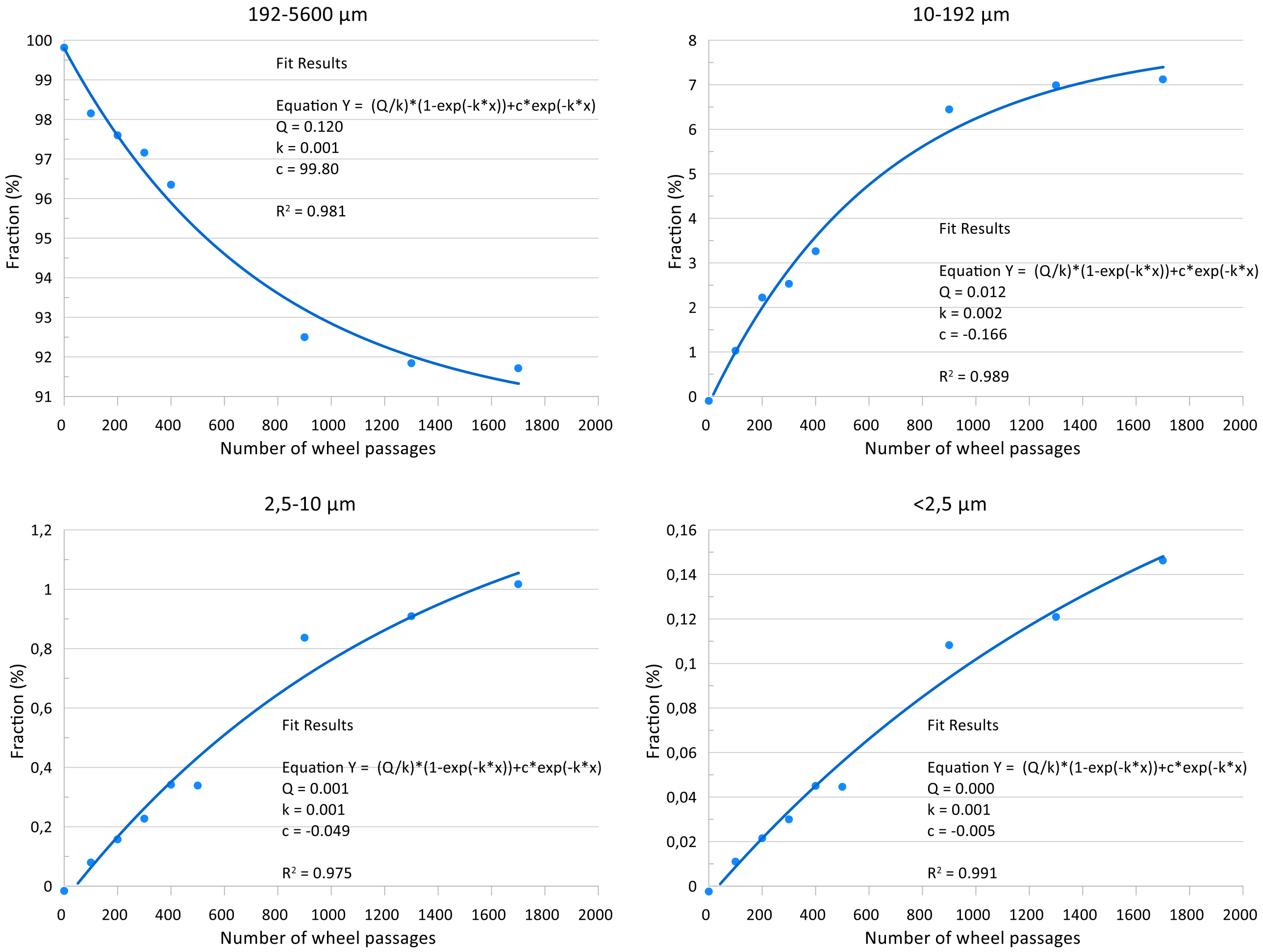

Figure 40. Development of percentages of four fractions used in the NORTRIP model for crushing with number of tyre passages.

After all tests, the remaining material on the track as well as the material that had left the track was collected. The amount sampled on the track (after each test plus remaining material) was very close to the original amount (11 177.5 g compared to distributed 11 200 g, Figure 41), i.e,. a 0.2% difference. But 320 g had left the track, creating a surplus in the mass balance of 297.5 g. This indicates a contribution from the pavement, which is also worn by the sand and tyre action during the tests, i.e., the so-called ”sand-paper effect” (Kupiainien et al, 2003). It was also observed that fine dust was stuck to the surfaces of the tyres, meaning that some fine material had to be excluded from the analyses.

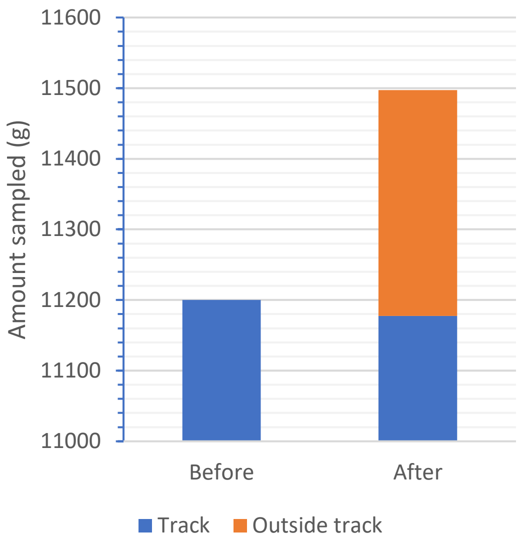

Figure 41. Mass balance of sand material used during the tests. Observe that the y-axis starts at 11 000 g.

Particulate matter

PM increases rapidly at simulator start (Figure 42). Except for a peak for the second measurement on plate 5, which might have been induced by a ventilation fan, the peaks at the same low speed 2 km/h tend to decrease after each round of 100 passages.

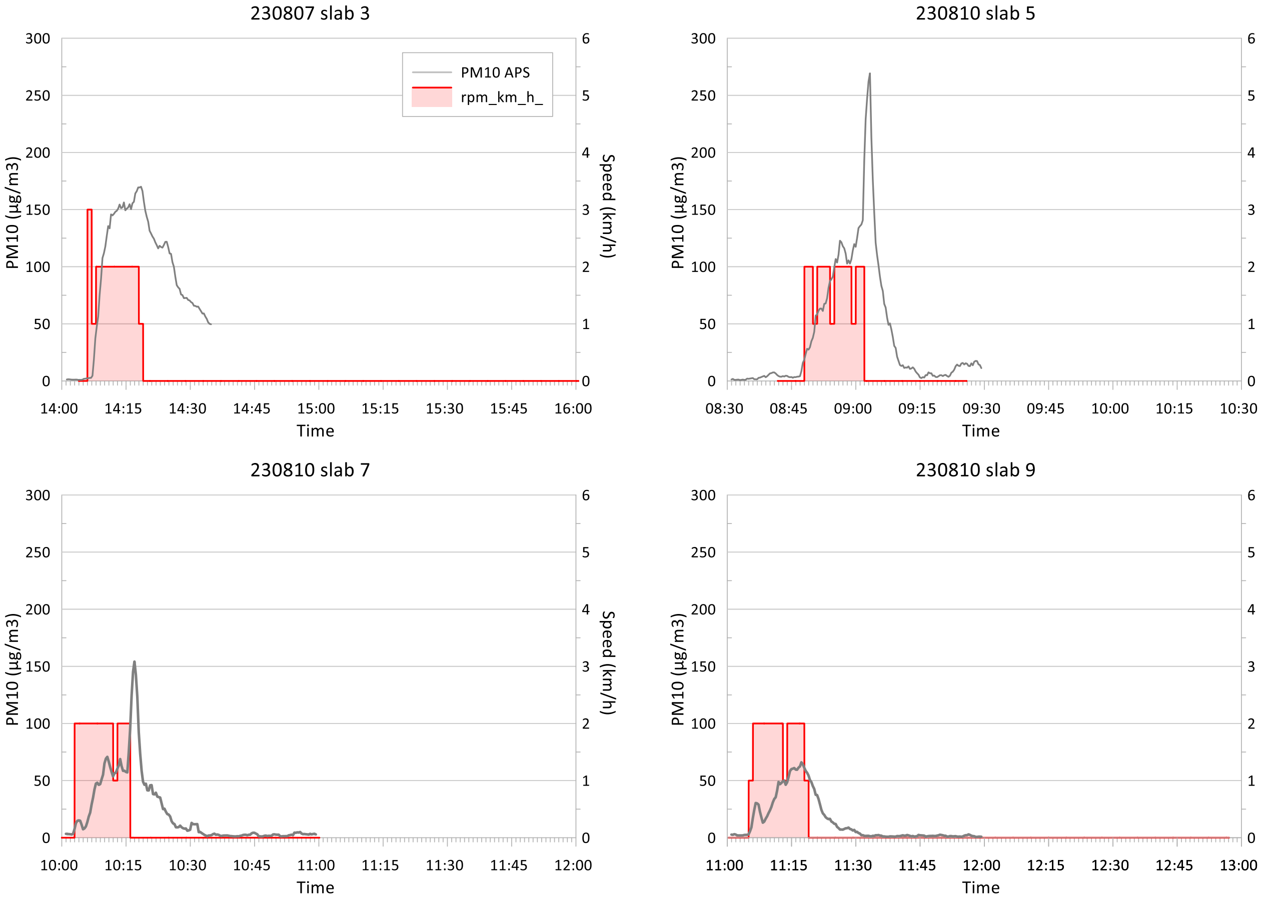

Figure 42. Speed and PM peaks at four first crushing tests at 2 km/h and 100 wheel passages.

The fifth test was made with a slightly higher speed (3 km/h), which resulted in a markedly higher PM peak (Figure 43).

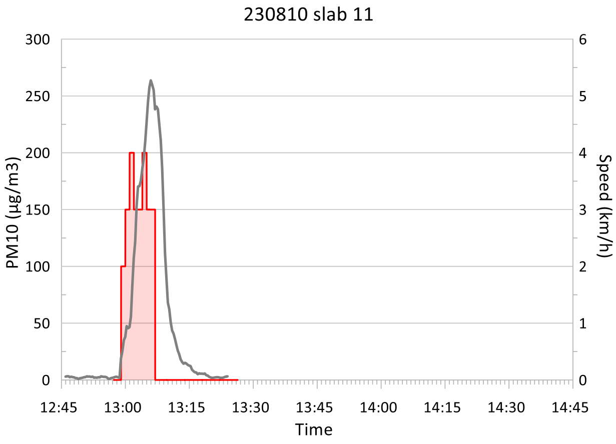

Figure 43. Speed and PM peak after test at 3 km/h and 100 wheel passages.

In the three final tests (Figure 44) which where prolonged to 400 passages at 2 km/h, the resulting mean PM10 concentrations are successively decreasing between successive tests in a similar manner as for the first four tests (Figure 42).

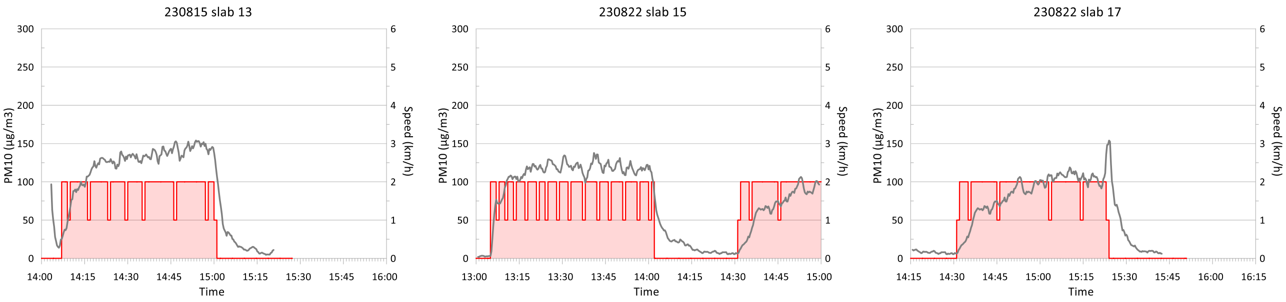

Figure 44. Speed and PM peaks at the three last crushing tests at 2 km/h and 400 wheel passages.

Since every slab only loses small amounts of sand at 2 km/h, the reasons for the decreasing trend could be several:

1. The coarser fractions can be assumed to wear off their edges first into finer fractions. As they are more and more worn, they are rounded and less fine fractions can be abraded.

2. The fine material produced might be transported down under the coarser fractions and hidden for suspension.

3. After each outtake of material from the pavement ring, a successively lower amount of sand is left on the track to contribute to PM concentrations in the air.

The particle mass size distributions (sampled without a PM10 inlet) peak at about 10 µm (Figure 45). This should still be regarded as an instrument or inlet cut-off effect. Particles larger than 10 µm will be airborne and contribute to the airborne mass concentration.

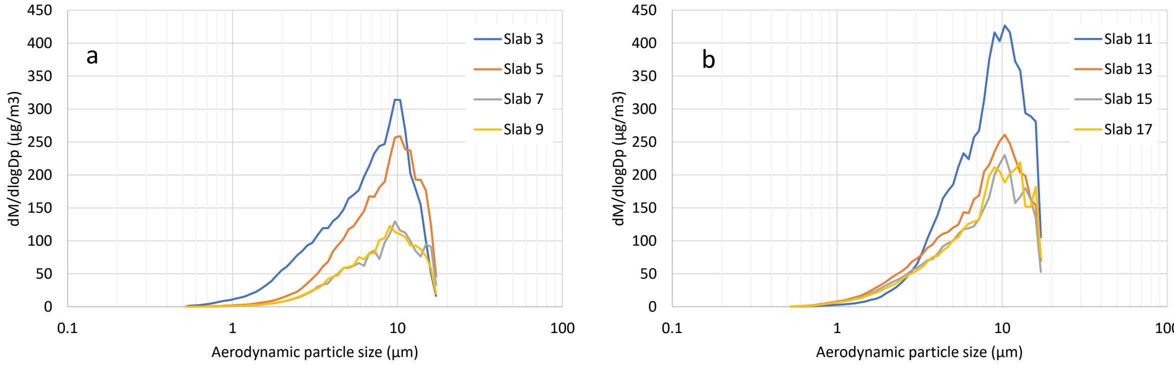

Figure 45. Particle mass size distributions from repeated tests with 100 passages at 2 km/h (A) and 100 passages at 3 km/h (slab 11) together with 400 passages at 2 km/h (B).

In Figure 46 the PM concentrations is plotted to the percentage of material smaller than 10 µm (DL10) sampled on each slab. For the first four tests at 2 km/h, the percentage of DL10 on the surface is increasing, while the concentration of PM in air decreases. This implies that even though more fine dust is produced in the track, successively less is emitted to the air. An interpretation is that, despite washing, the new, unabraded sand contains fine dust that is initially emitted, and the fine dust produced from abrasion falls down below coarser fractions and is hidden from the low suspension forces at 2 km/h. At 3 km/h, suspension increases to give rise to a higher PM peak. After the 400 passages at 2 km/h, the percentage of DL10 is increasing in the surface without giving obvious increase in PM, indicating that there is balance between PM generation and suspension.

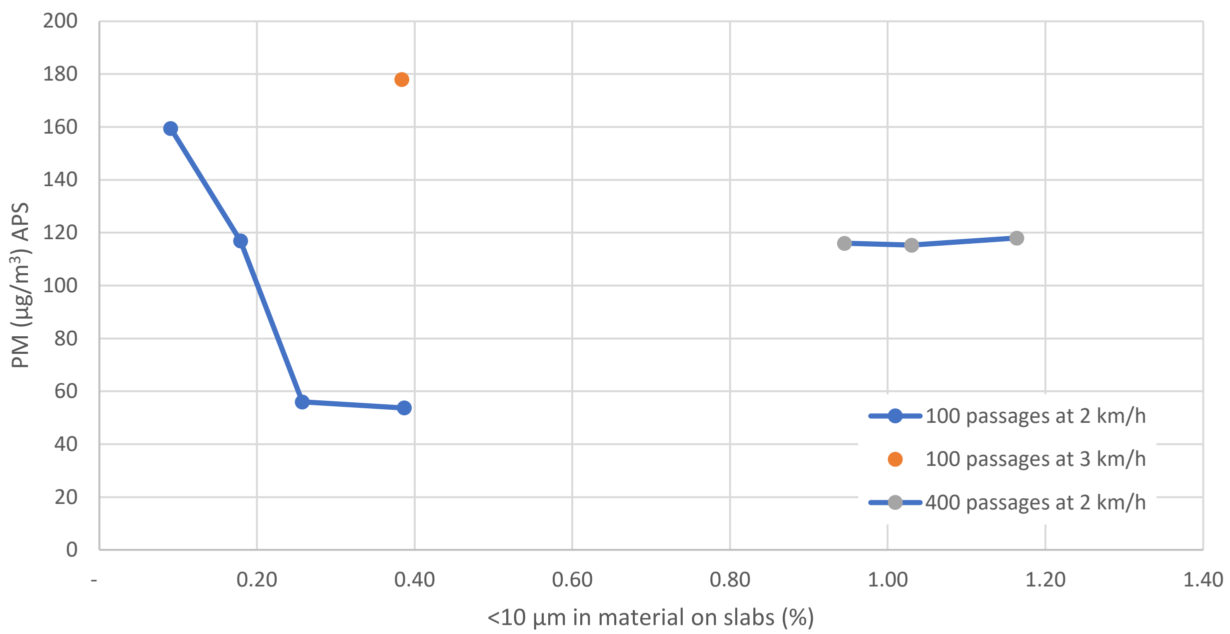

Figure 46. PM concentrations during each round of passages plotted to the percentage of material smaller than 10 µm (DL10) sampled on each slab after each round.

The results from this crushing test should be regarded as specific for the material chosen. Both fragmentation resistance of the rock material and original size distribution will affect the crushing process and the emission of PM10 from the crushing. Already in 2007, Kupiainen et al., showed that PM10 emission from a crushed rock material with poor fragmentation resistance were substantially higher than from higher quality aggregates.

Conclusions

From the sand crushing study it can be concluded that:

- The method developed for the purpose works in the sense that most material actually stays in the track and is crushed. The low speed needed is not representative for normal traffic, but the crushing process is expected to be as close to reality as possible in a laboratory set-up.
- A mass balance analysis showed that to total amount of material in the slabs sampled last was higher than originally applied, which is suggested to be a result of the sandpaper effect, i.e. that the sand also wears the pavement when run over by tyres.
- The volume of the coarsest fractions is reduced during the test, indicating that they abrade or are crushed into finer fractions. The coarse fraction reduction ceases with number of wheel passages, indicating that abrasion subsides.
- The volume of all finer fractions increases with increasing wheel passages, resulting from a net addition of particles from the coarser fractions. Since all fractions, except the coarsest and the finest, are likely to both receive abraded particles from any of the coarser fractions and lose particles to any of the finer fractions, it is not possible to determine a stepwise flow from coarse to finer fractions.
- PM10 concentrations in the air decreases with increasing number of wheel passages, which could be due to several processes, including reduced abrasion rate, hiding of suspendible particles and the successively lower amounts of material being abraded due to the sample outtakes.
- Particle size distribution (without PM10 inlet) peak at about 10 µm. The instrument size limitations and cutoff make the mass concentration decrease rapidly over 10 µm.
- The results should be regarded as specific for the material used. Other rock materials or other size distributions might generate differing results.

Removal of sand at different speeds

Methods

To analyse the removal rate and influence on material size distribution at increasing speed, 400 g of the material was spread out on two adjacent slabs in the road simulator (Figure 47). The brush sweeper was not used in these tests. The simulator was run in 2, 10, 20, and 30 km/h for approximately 100 rounds. For each test a new application of material was made. The remaining material in and outside the track was sampled separately also outside the original slabs since material was transported also along the track.

The same sieving routine as described for the crushing tests was used.

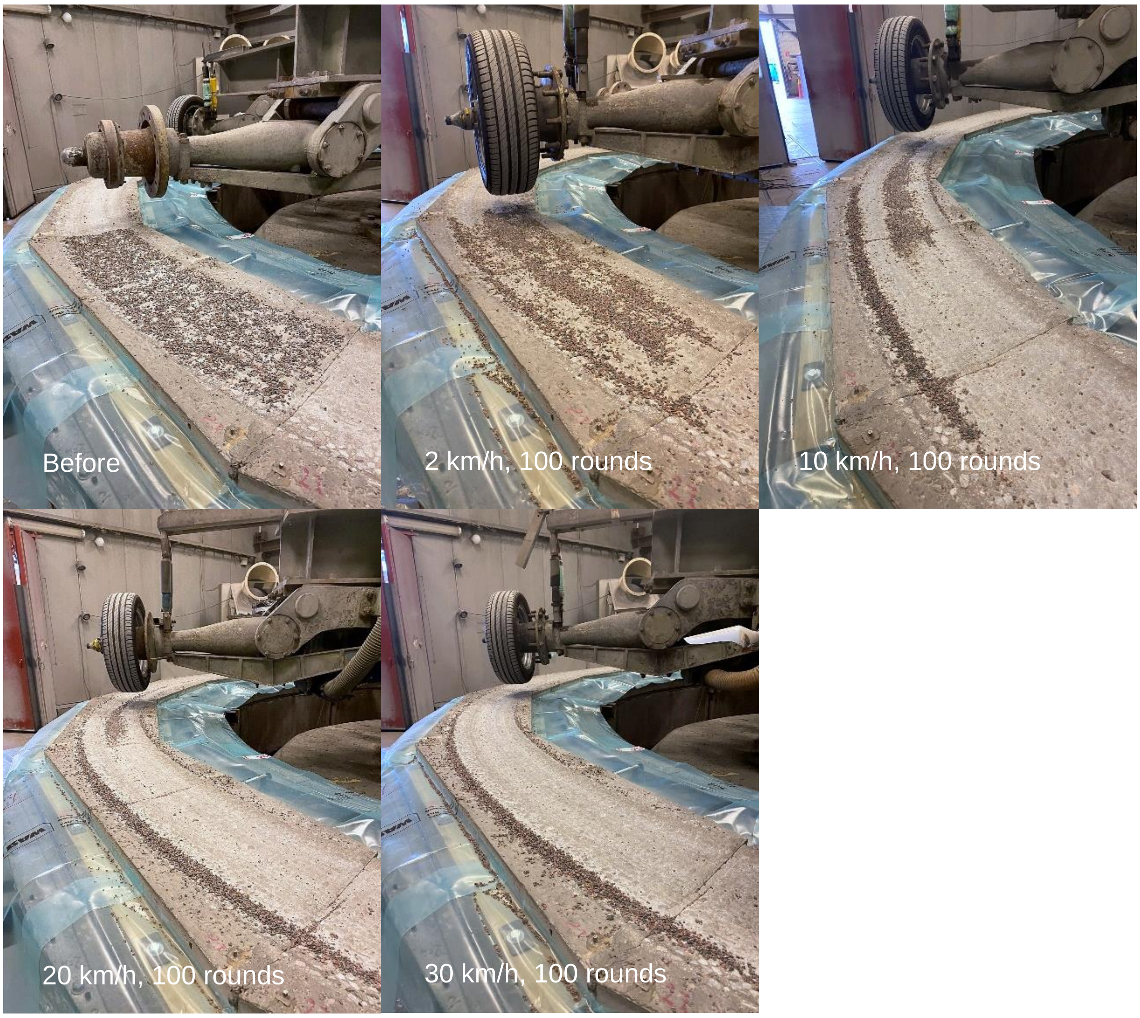

Figure 47. Applied sand on two slabs before test (left) and resulting sand distribution after test (right). Photo: Mats Gustafsson, VTI.

Results and discussion

Sand is effectively removed from the wheel track by the running tyre and removal is faster at higher speeds. The total amounts sampled in and outside the track is shown in Figure 48, together with the sum and what is lost from the sampled system. After an initially fast loss at 2 km/h, the loss is linear in wheel track. After 100 rounds (400 wheel passages) at 30 km/h only about 5% of the initially applied sand remain in wheel track.

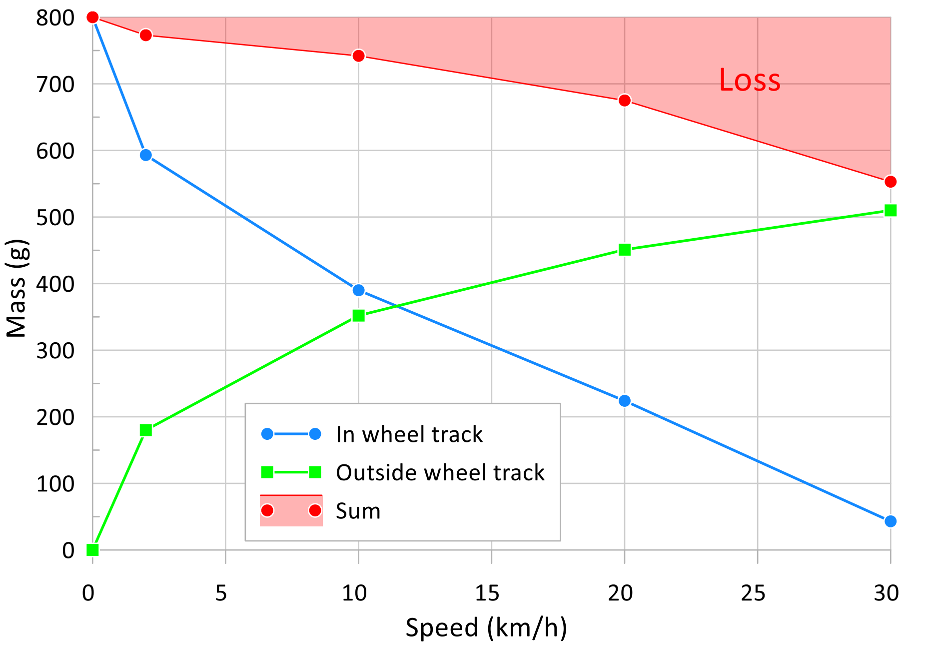

Figure 48. Amounts of sand sampled in and outside the wheel track and lost amount of sand after 400 wheel passages at different speeds.

The total mass loss linearity is described in Figure 49. For every 400 wheel passages (200 vehicles) mass loss increases with 2.4% / km/h.

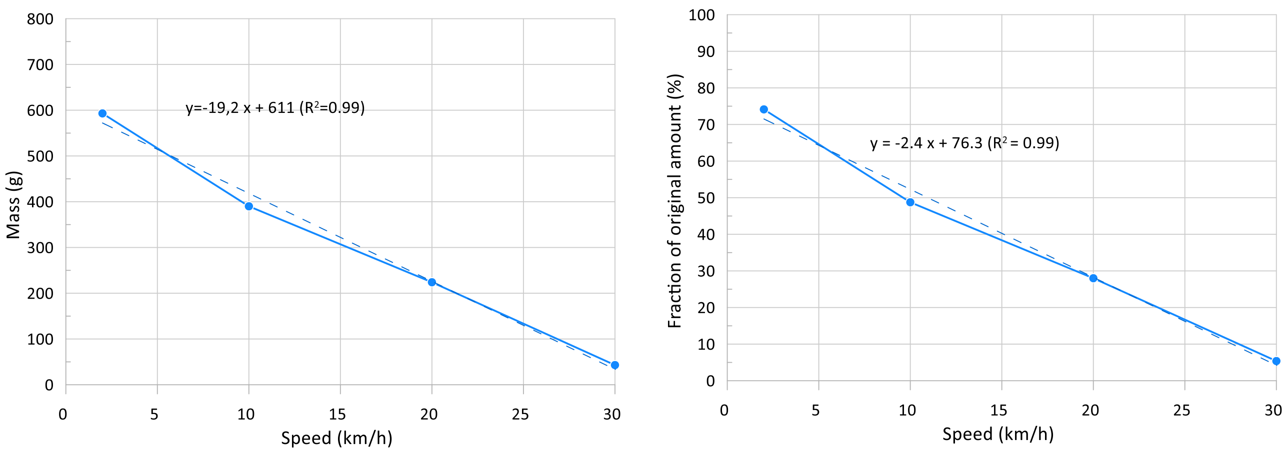

Figure 49. Absolute and relative sand mass loss in wheel track after 400 wheel passages as a function of speed.

The mass loss per wheel passage and per vehicle (four wheels) is described in Figure 50. It is likely that these figures are overestimated compared to straight driving due to the constant turning in the road simulator, which induces lateral removal forces. Nevertheless, they indicate values that can be assumed to be valid for cornering. Also, the figures might be material specific, so that another sand, with another original size distribution will result in other figures.

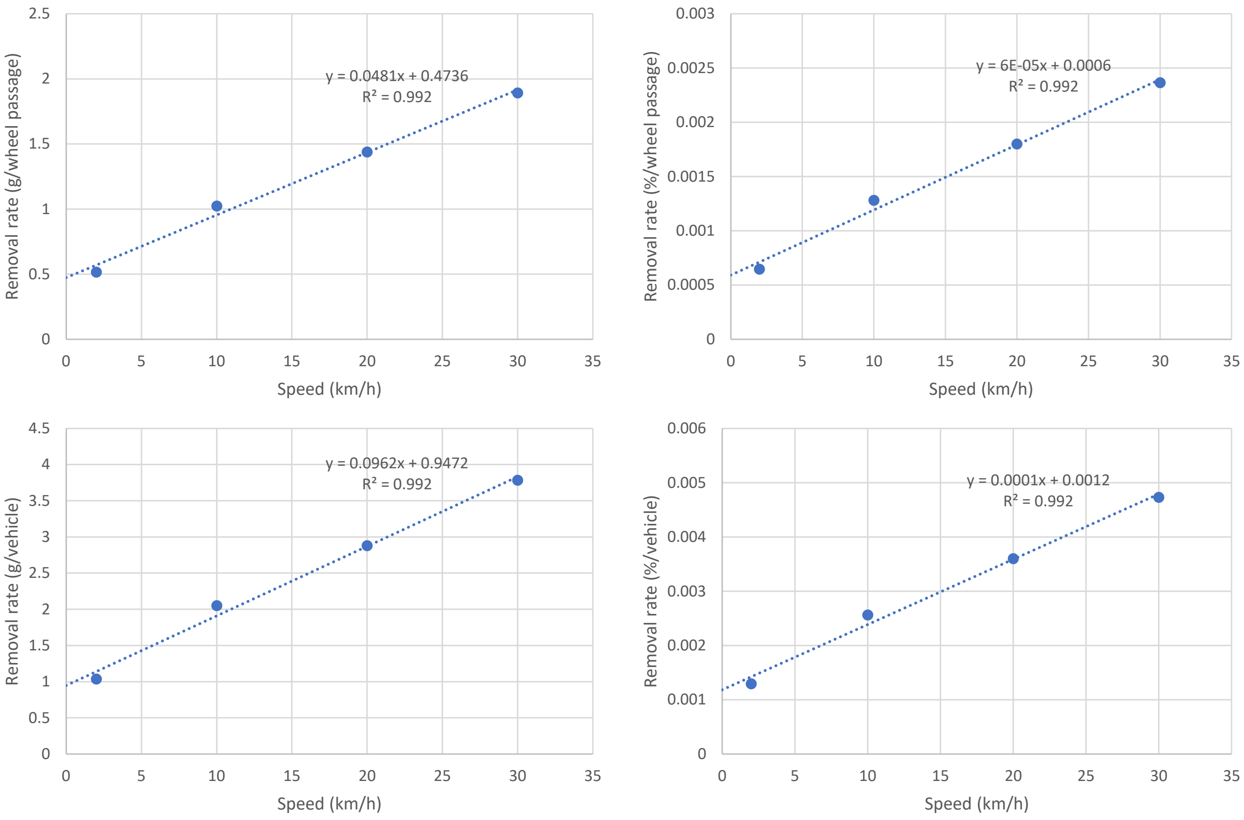

Figure 50. Absolute and relative removal rate per wheel passage and vehicle (two wheels).

The loss of sand from the wheel track is dominated by coarser fractions (Figure 51). Both the 1–192 µm and the 2.5–10 µm fractions peak in wheel track at 10 km/h, which might indicate that fragmentation into this fraction dominates over the removal forces, leading to a buildup. At 20 and 30 km/h in wheel track amounts are decreasing. Outside the wheel track the coarse fraction builds up at higher speed. The finer fractions follow this trend, but at 30 km/h the mass decreases. It is likely that the higher removal and suspension forces at 30 km/h result in these fractions being suspended into the air and deposited further away from the track, thus being lost in the sampling system.

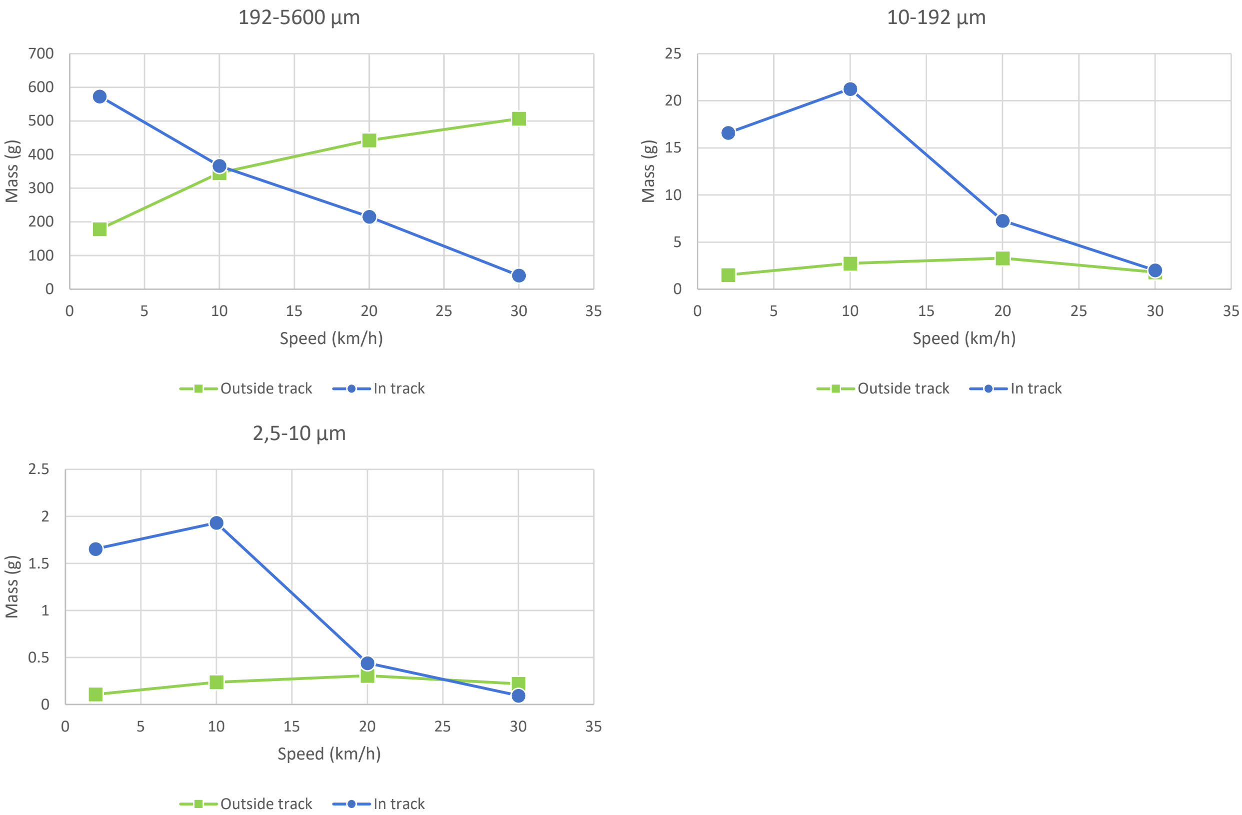

Figure 51. Mass of three fractions of sand in and outside wheel track at different speeds.

A detailed picture of the effects on different size fractions are seen in the size distributions in Figure 52. In the wheel track about 90% is larger than 1 mm, while only 1% outside the track. The percentage of fine fractions in wheel track grow from 2 to 10 km/h, but below 100 µm tend to be lower than the original percentage. Higher speeds than 10 km/h results in constantly reduced mass in all sizes. This could be attributed to increasing suspension of fine fractions. Outside the wheel track the distributions are very similar up to 30 km/h, when fine fractions are reduced, likely due to higher suspension and removal from the sampled system. Mass increases with speed in all sizes outside the track, except at 30 km/h, when finer fractions leave the sampled system.

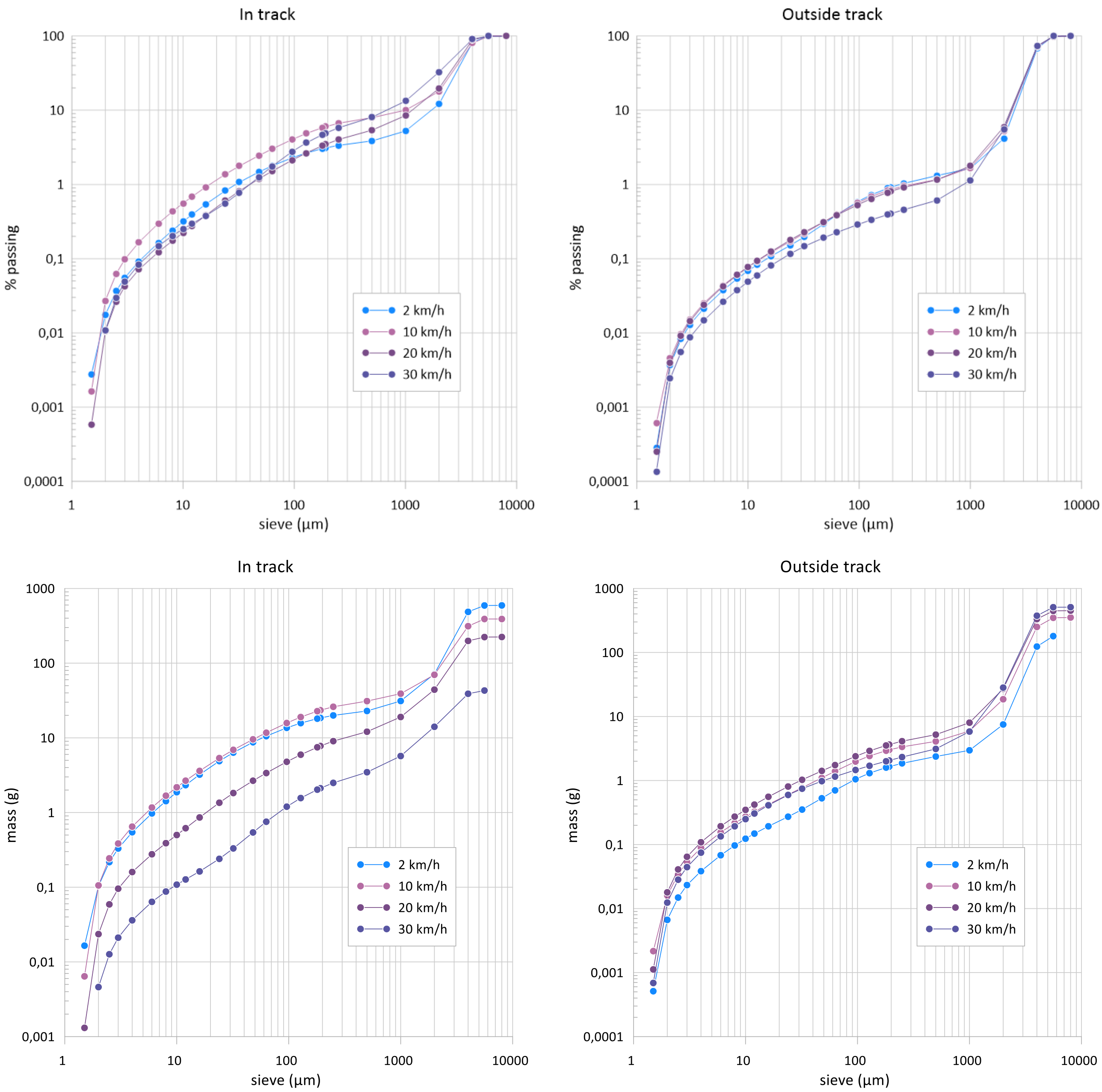

Figure 52. Relative and absolute size distributions in and outside the track at different speeds.

Particular matter

PM10 in the simulator hall rises quickly at start of the test sequence at all speeds (Figure 53). At 10 km/h, the concentration peak is lower and occurs later than at 20 and 30 km/h. The 20 km/h peak is lower than at 30 km/h but decreases very similarly. The initial amount of PM10 available in the applied sand is limited and can be assumed to be suspended rapidly. The higher resuspension forces at higher speeds causes a higher peak concentration. The deposition velocity in the room is higher with higher speed due to increased turbulence also after stopping the simulator, which is a probable reason for the faster decrease at higher speeds.

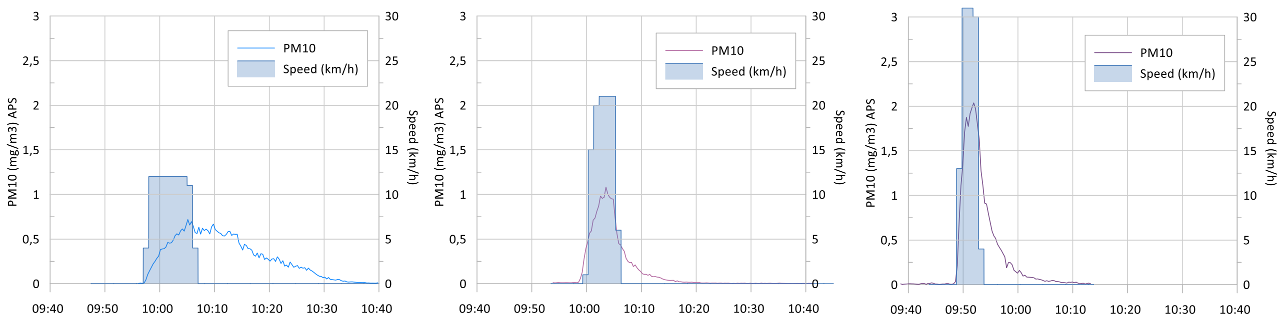

Figure 53. PM10 peaks and simulator speed at the three tests.

The particle mass size distributions during the peak concentrations can be seen in Figure 54. The distributions are very similar at 10 and 20 km/h, while at 30 km/h a considerably higher contribution to the coarser fractions within PM10 is obvious.

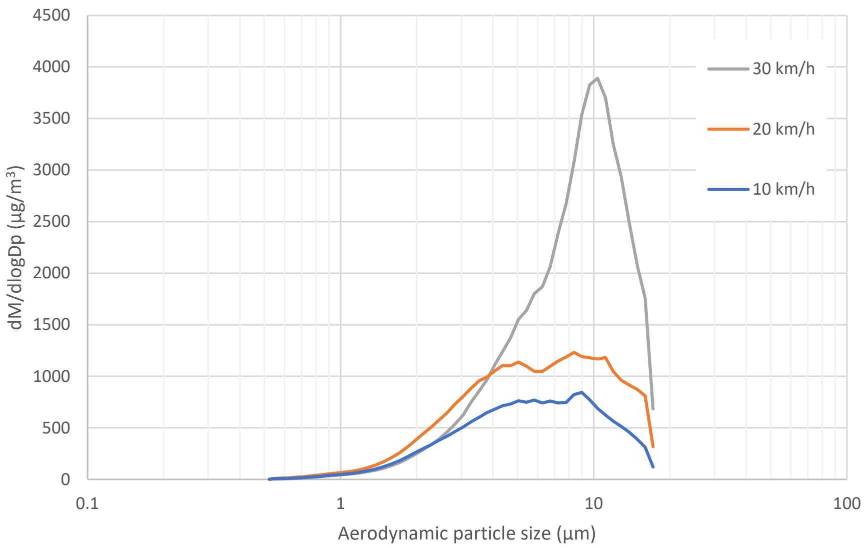

Figure 54. Particle mass size distributions at peak concentrations in Figure 53 (2-4 minute mean values).

Conclusions

From the sand removal study it can be concluded that:

- For the same number of wheel passages, the sand removal from the track is linearly depending on speed.
- At 30 km/h approximately 95% has been removed from the track after 400 wheel passages.
- The removal rate increases linearly with speed.
- The coarsest fraction 192-5600 µm is consistently removed with increasing speed. Finer fractions tend to accumulate at 10 km/h but is efficiently removed at 20 and 30 km/h, most likely due to suspension.
- Higher speed results in higher PM10 emissions. At 30 km/h, the coarser fractions in PM10 increases substantially indicating a markedly higher suspension compared to at 20 km/h.

CMA effect evaluation

Methods

CMA effect evaluation

Calcium magnesium acetate (CMA) is used as a dust binding agent in some cities in Sweden. It is, like other dust suppressant, an effective way to reduce suspension of dust from the road surface, making it suitable as a measure to reduce high PM10 concentrations caused by road dust suspension. The effect is commonly rather short-lived and depends on traffic and meteorological conditions. In autumn and winter, when air is often humid and insolation is low, the effect of dust binding is longer, while in springtime, with dryer air and higher insolation, the effect diminishes faster.

A key information to be able to model the dust binding effect in the NORTRIP model, is how the dust binding agent is removed and redistributed on the road by traffic. Also, better knowledge about the effect of dust binding is wanted in order to improve the parameterizing into the NORTRIP model regarding dust binding. This chapter describes a test where these questions were addressed.

Linköping municipality uses dust binding as a method to decrease levels of PM10. The dust binding is executed at around 04:00 AM on days where high levels of PM10 is expected, by applying 10 g/m^2 of a solution of 25% calcium magnesium acetate (CMA) on the road. In March 2022, Hamngatan, a street in Linköping, had measured concentrations of PM10 above the EU limits of 50 µg/m^3, as 24-hour average, 42 times (Linköpings kommun 2023; EU 2008). The analysis was carried out in two parts: determination of the effects of the dust binding, and determination if the dust binding was carried out on the right days, meaning days with high concentrations of PM10.

A challenge with this analysis, was that there is no location in Linköping where dust binding is not carried out, where PM10 concentrations are measured. This lack of a reference location makes it challenging to determine the effect of the dust binding. To be able to do the analysis, two different substitutes for the reference locations were used: (1) to do the analysis on dry days only, where there were high concentrations of PM10, and compare days where CMA was used with days where it was not used, and (2) to do the analysis with Norrköping as a reference location.

Data selection

The data provided from Linköping municipality consists of which dates in 2023 the dust binding was executed on Hamngatan. The measured concentrations of PM10 and NO_X were provided by SLB-analys, at Hamngatan 10 in Linköping (Figure 55, 58.4124°N, 15.6301°E) and at Kungsgatan 32 in Norrköping (Figure 55, 58.5915°N, 16.1779°E), with a time resolution of 15-minutes, from the 1st of March to the 30th of April. From these concentrations every 15 minutes, hourly averages and medians were used in the analysis. Both stations are shown in relation to each other in Figure 55. As for the assessment whether the dust binding was carried out on the wanted days, daily average concentrations from Hamngatan 10 were used, from the 1st of January to the 30th of April.

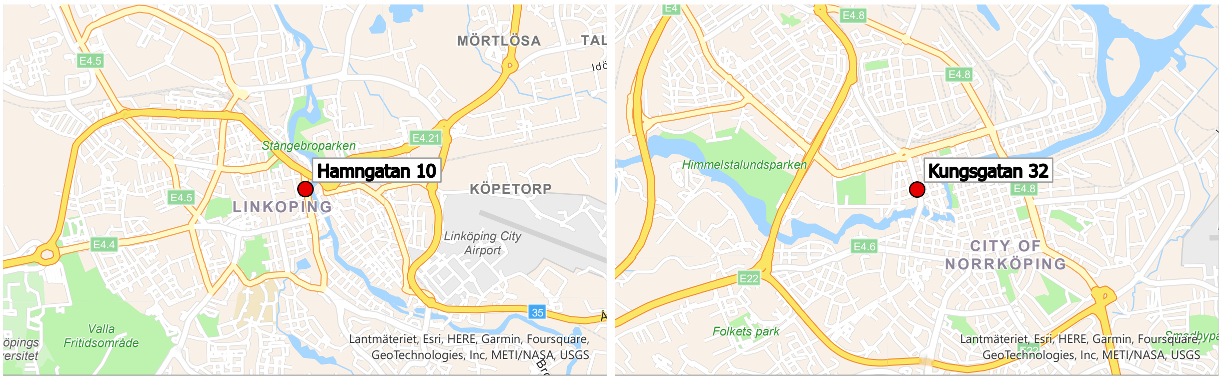

Figure 55. The location of the station in Linköping, Hamngatan 10, and in Norrköping, Kungsgatan 32, from which PM10 and NO_X concentrations were obtained.

Dust binding days vs no dust binding days

The first part of the analysis, to evaluate the effect of dust binding, was carried out by comparing the concentrations of PM10 on the days on which dust binding was done, with the concentrations on the days where dust binding was not done. Furthermore, only days with average concentrations of PM10 above 40 µg/m^3 between 04:00 AM and 11:00 AM were used in the analysis, since these dry days are those of largest interest.

Firstly, the concentrations of PM10 were divided by the concentrations of NO_X (Equation 1), to be able to minimize the differences in the amount of traffic each day and minimize the influence from meteorology. The

Is PM10/NOx ratio for each 15 minutes were then used to calculate hourly averages and medians. Then, the data was split in two parts: hourly values for days where CMA was used, and hourly values for days where CMA was not used. Lastly, the daily variations of the two data sets were compared using line diagrams.

Equation 1

$$Ratio\ Linköping = \frac{PM10_{Linköping}}{NOX_{Linköping}}$$

Linköping vs Norrköping

Norrköping is a city nearby Linköping; they are located around 37.5 km from each other. This should mean that the background concentrations of PM10 should be relatively similar. Norrköping also uses dust binding as a method to decrease the PM10 concentrations, similar to Linköping. This makes Norrköping a potential candidate to be a substitute for the lack of reference location in Linköping. In this part of the analysis, only days with their mornings (04:00 AM – 11:00 AM) having concentrations of PM10 over 40 µg/m^3 in Linköping and Norrköping were used, the same way as in the first part of the evaluation.

Firstly, the concentrations of PM10 and NO_X were divided for both Linköping and Norrköping (Equation 1 and Equation 2), to be able to disregard the differences in traffic between days and cities. From these values every 15 minutes, the hourly averages and medians were calculated, similar to the previous analysis. Then, the data was split into two parts: (a) data from Linköping and Norrköping on days where neither of the cities used CMA, and (b) data from Linköping and Norrköping on days where Linköping did use CMA while Norrköping did not. The daily variations of these two datasets were then analyzed using line diagrams. Further evaluation was done by dividing the PM10/NO_X ratios between Linköping and Norrköping (Equation 3 and Equation 4), and then dividing the new ratios between dataset a and b (Equation 5). Final ratios below 1 indicate an effect. To calculate the effect, the average of the final ratio was subtracted from 1, and multiplied by 100% (Equation 6).

Equation 2 $$Ratio\ Norrköping = \frac{PM10_{Norrköping}}{NOX_{Norrköping}}$$

Equation 3 $$Ratio\ dataset\ a = \frac{Ratio\ Linköping_{no\ dust\ binding}}{Ratio\ Norrköping_{no\ dust\ binding}}$$

Equation 4 $$Ratio\ dataset\ b = \frac{Ratio\ Linköping_{dust\ binding}}{Ratio\ Norrköping_{no\ dust\ binding}}$$

Equation 5 $$Final\ Ratio = \frac{Ratio\ dataset\ a}{Ratio\ dataset\ b}$$

Equation 6 $$Final\ effect = (1 - \bar{x}_{Final\ ratio})\ \times 100\%$$

Evaluation if the binding of dust was done the right days

To evaluate whether the binding of dust was carried out the days when it was needed, daily average concentrations of PM10 between the 1st of January and 30th of April was used, and analyzed in column diagrams.

Results and discussion

Dust binding days vs no dust binding days

As seen in Figure 56, the days when CMA was used show on average higher values of the PM10/NO_X ratio, compared to the days when CMA was not used. This is unexpected since a lower PM10 concentration, as a consequence of using CMA, would lead to a lower PM10/NO_X -ratio. However, since CMA is used on days when high levels of PM10 is expected, it is likely that these days show higher concentrations than days when CMA was not used. This does not mean that the CMA is not working, only that CMA was used on the right days. Doing the same analysis using medians instead of averages (Figure 57), however, shows a smaller gap between days when CMA was used and when it was not used, but the peak is still higher for the days where dust binding was executed. After the peak, the days when CMA was used show lower PM10/NO_X-ratios, indicating an effect. However, the effect should be much higher and noticeable during the morning than the afternoon. Furthermore, the PM10/NO_X-ratio were expected to have decreased significantly after CMA was spread on the streets, which can be seen in Figure 57, as the ratio decreases after 04:00 AM. This is not noticeable in Figure 56 showing the averages.

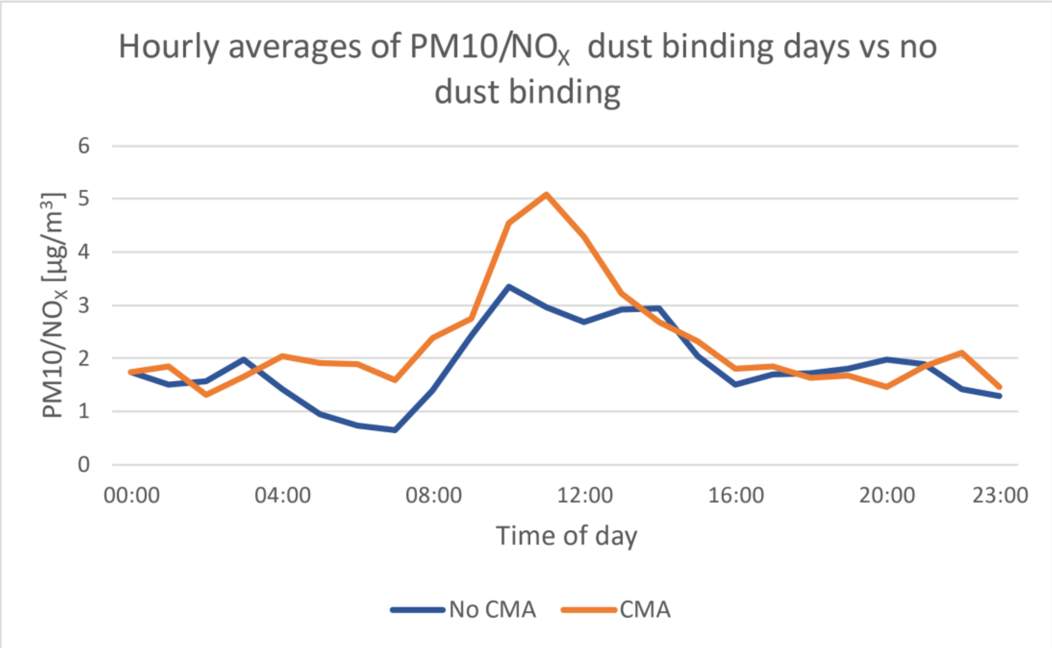

Figure 56. The hourly averages of the PM10/NO_X ratio. The days where dust binding was not executed are shown in blue, while the days when dust binding was done are shown in orange.

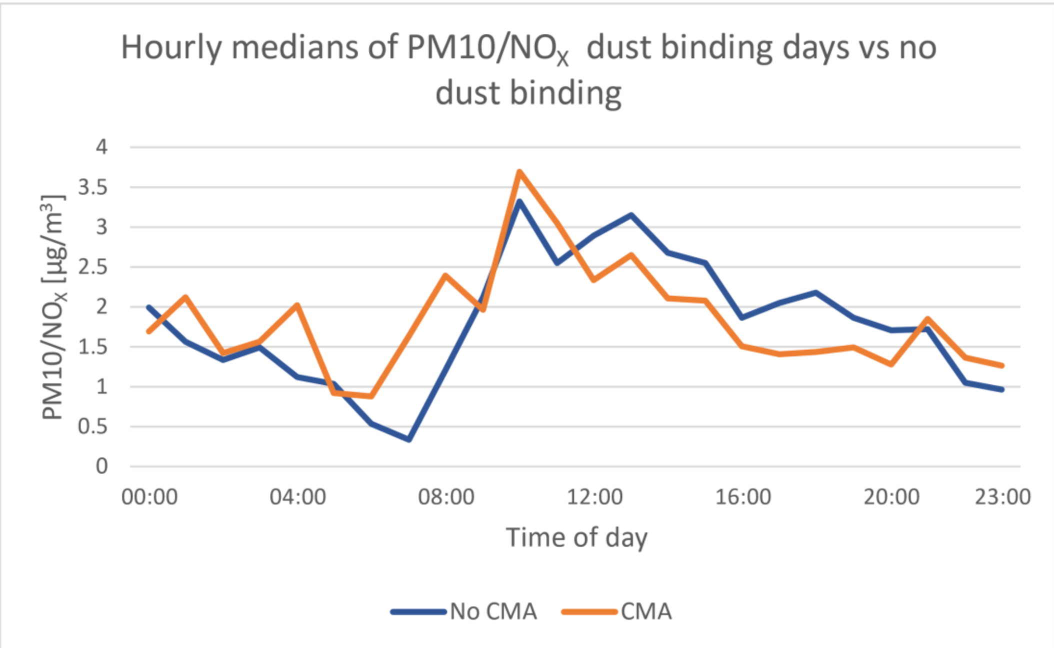

Figure 57. The hourly medians of the PM10/NO_X ratio. The days where dust binding was not executed are shown in blue, while the days when dust binding was done are shown in orange.

Linköping vs Norrköping

As seen in Figure 58, the PM10/NO_X ratio is higher in Linköping when CMA was used (orange line in (Figure 58A)), than when CMA was not used (orange line in (Figure 58B)). Again, this can be explained by that CMA is used on days when the concentrations of PM10 are expected to be high. An important aspect is that diagram A in the figure shows data from one day, while diagram B shows data from two days. Therefore, diagram A does not show an average daily variation, while diagram B shows the average daily variation of two days. This also causes an uncertainty in this part of the analysis.

Looking at the daily variation of the final ratio (Figure 59), it suggests that there is an effect in the morning, and during late afternoon. However, it does also show that there is an effect as early as 01:00, which is before CMA was used. There is no effect between 13:00 and 15:00. Looking at the average of the final ratio, it indicates an effect of around 16%. However, as noted before, the data selection is very small, causing an uncertainty.

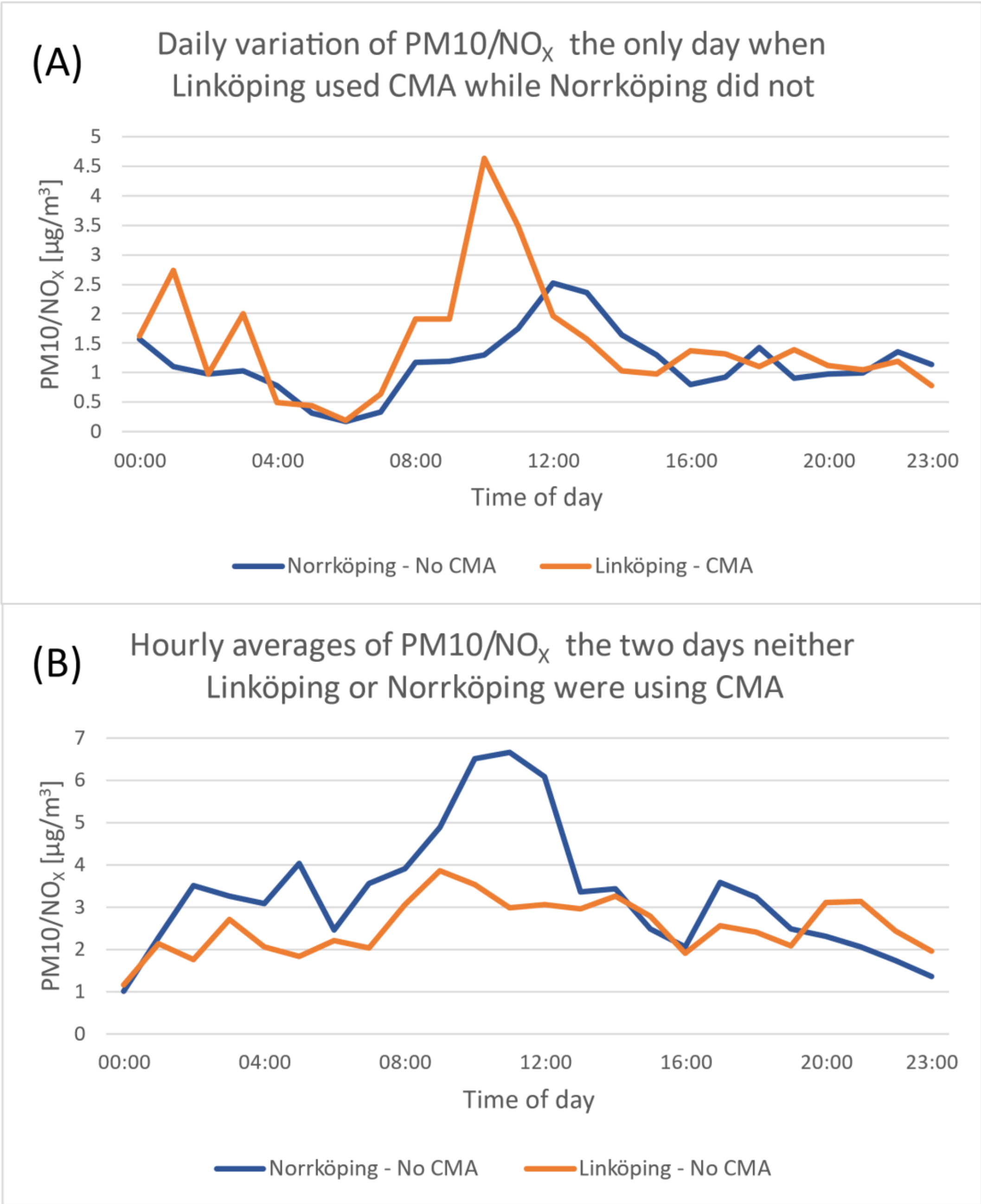

Figure 58. The hourly averages of PM10/NO$_X$ shown as a daily variation. Blue lines show Norrköping, while the orange lines show Linköping. (A) Shows data from days when Linköping used CMA, while Norrköping did not. (B) Shows data from days when neither Linköping of Norrköping executed dust binding.

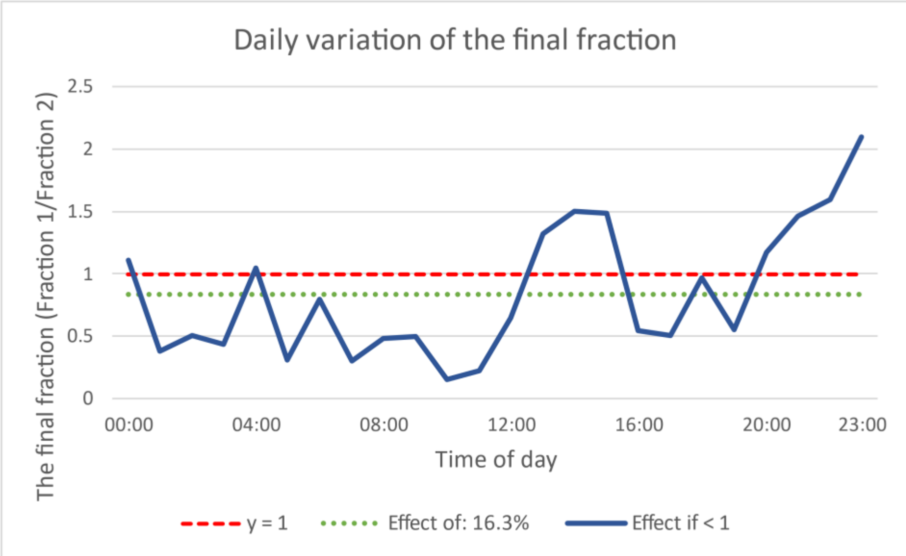

Figure 59. The hourly averages of the final ratio shown as a daily variation. The blue line shows the final ratio, and indicates an effect if its values are below 1 (the dashed red line). The dotted green line shows the overall average of the final ratio, which indicates an effect of roughly 16%.

Did Linköping use CMA on the right days?

The orange columns shown in Figure 60 are the days with CMA and the blue are days without dust binding. The orange columns shown in the figure, are mostly quite high, and often above the EQS (50 µg/m^3). There are, however, a couple of days where the PM10 concentrations would be well below the EQS, even if dust binding would not have been carried out; for example, the 6th and 19th of April. It is also visible that there are a few days with PM10 concentrations above the EQS, even though dust binding has been done that day, most notably in the first half of February. This period, no dust binding was carried out, which indicates that it might have been beneficial to start the dust binding earlier than was done.

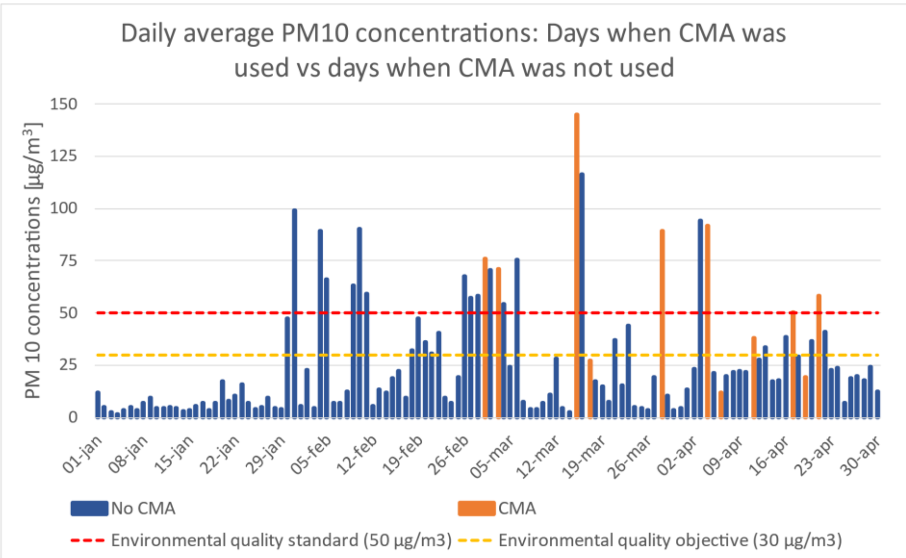

Figure 60. The daily average PM10 concentrations from the 1st of January to the 30th of April. Blue bars show PM10 concentrations on days where CMA was not used, while orange bars show PM10 concentrations on days when CMA was used. The dashed red line shows the environmental quality standard of 50 µg/m^3, and the dashed yellow line shows the Swedish environmental quality objective of 30 µg/m^3.

Conclusions

The effect of dust binding in Linköping was evaluated. Since there were no reference location (where PM10 are measured and where dust binding is not carried out), the effect was evaluated using two different methods: (1) To compare the PM10/NO_X-ratio on the same street, days when dust binding was carried out, with days when it was not; and (2) to compare the PM10/NO_X-ratio in Linköping and Norrköping, days when Linköping use dust binding while Norrköping did not, with days when neither of the two cities carried out dust binding.

The first method, could not detect a quantified effect. The second method however, suggests that there is an effect over the whole day of around 16%. An important note is that there were only one day when Linköping used CMA and Norrköping didn't, and two days when neither of the two cities used CMA. This is a large uncertainty.

This study shows the importance of designing the project so that there is a reference location that can be used. For example an additional measurement on the same or nearby street where no dust binding was done.

The dust binding was overall done on the right days, as it was mostly on days with high PM10-concentrations. However, there are multiple days with high concentrations in February, indicating that dust binding should be started earlier in the year – preferably in February.

Residual dust binder (CMA)

Methods

Site and CMA spreading

Field measurements were conducted on Hamngatan in Linköping, Sweden (Figure 61) from 2023-02-28 to 2023-03-01. The air temperature varied between -1,5ºC and 8ºC and the temperature on the road surface was approximately 0,5ºC during all measurements. Meteorological data was collected from the SMHI's open-source data base (station no. 85240). The weather was clear and dry with no precipitation during the test period (Figure 62).

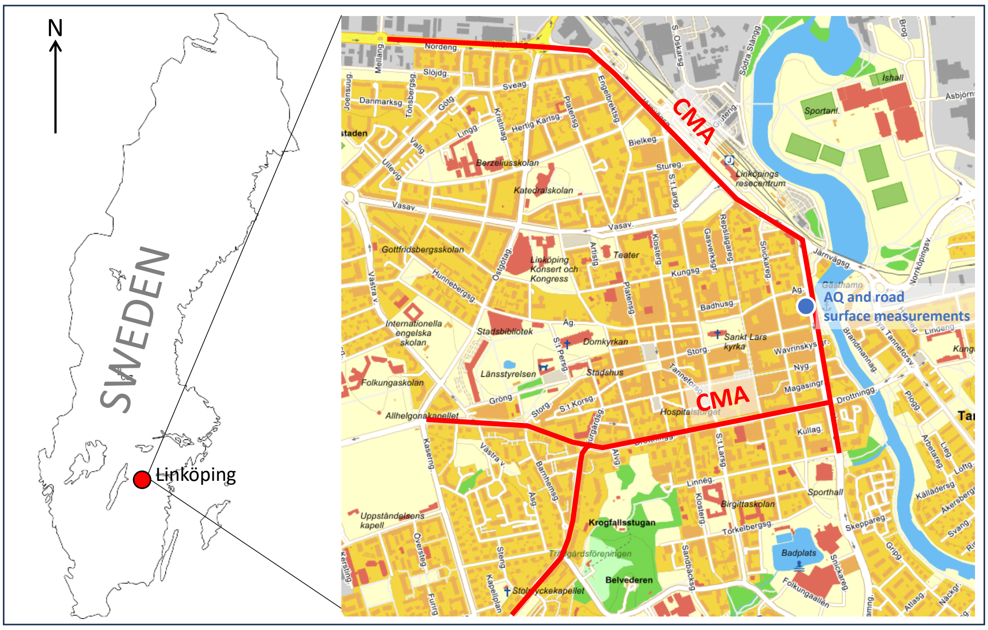

Figure 61. Map over street network treated with CMA (red streets) in the city of Linköping, Sweden. Measurements made for CMA follow-up was made on the street next to the air quality station on Hamngatan (blue dot). Map source: eniro.se

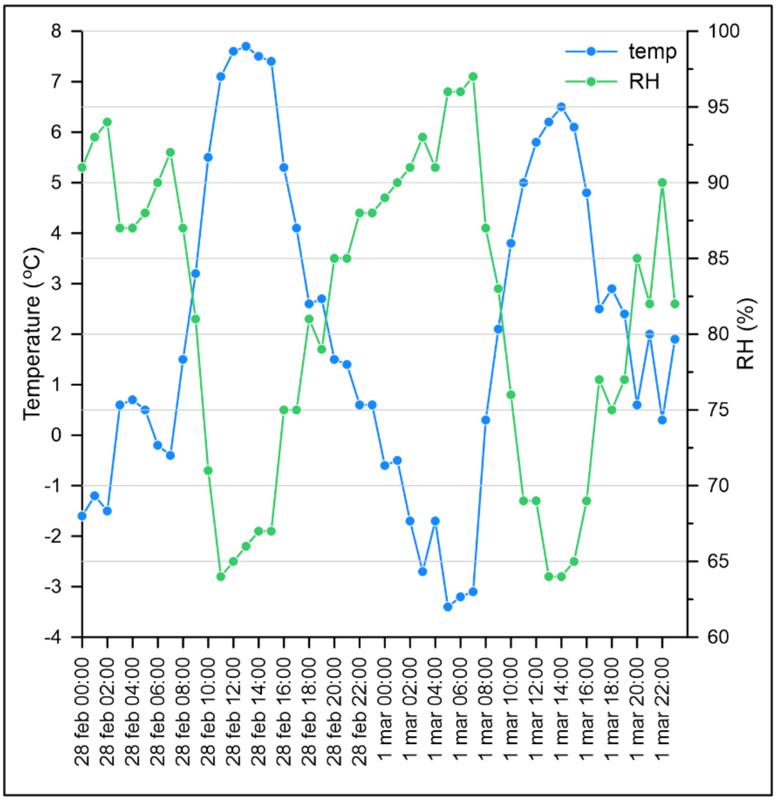

Figure 62. Air temparature and relative humidity during the field test.

The first measurement was made just before the CMA was applied and followed up by five measurements after the application. Thus, samples from six measurements were collected. The first five measurements took place every third hour with a start at 03.00 AM, while the last measurement was performed the morning the day after, i.e., 18 hours after the collection of the fifth measurement,

Table 9.
Samples were collected in profiles transverse the road surface with the Wet Dust Sampler (WDS II, see Figure 65), a device which washes a small circular surface of the road surface (20.42 cm^2) with a known amount of de-ionized water under high pressure and then pushes the sample into a sampling bottle for further analysis. Samples were collected every 20 cm, with one exception, for the second profile (collected directly after the application of CMA), samples were collected every 10 cm, Figure 64. Profiles were used to give a picture of the lateral distribution, and every profile consists of 18 samples (except for the second profile which contain 36 samples).

According to the contractors, the applied solution's concentration was 25% CMA and the dose was 10 g/m^2. The spreader was an Aebi Schmidt Traxos with a 430 litre liquid polyethylene tank with CMA and spinner disc as distributor (Figure 63).

Figure 63. Application of CMA using a tractor with a tank and spinner disc (A). Resulting CMA deposition pattern (B). The spinner spreading CMA at the sampling site (C) and the tractor while applying CMA (D). Photos: Mats Gustafsson and Göran Blomqvist, VTI.

Table 9. Time and date for WDS II measurements.

Date	Time	In relation to CMA application	Field observations
2023-02-28	03:00	Before CMA	Pre-CMA application
2023-02-28	04:30	Directly after CMA	Samples collected every 10 cm
2023-02-28	09:00	6h after CMA, after the morning rush	Moisture on the road surface
2023-02-28	12:00	9h after CMA	Moist in the wheel tracks, dried out in-between wheel tracks
2023-02-28	15:00	12h after CMA, prior the afternoon rush	Entire road surface was dry
2023-03-01	09:00	30h after CMA	No additional CMA or salt had been applied on the road surface during the night. The surface was dark, but dry.

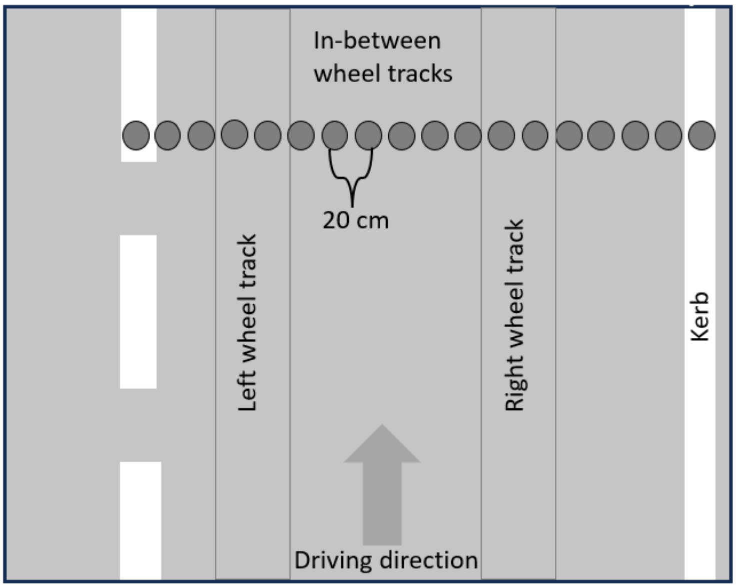

Figure 64. Schematic illustration of the sampling set-up.

Figure 65. Field sampling of road dust and CMA with the VTI Wet Dust Sampler, WDS. Photo: Göran Blomqvist, VTI.

Traffic data from 2018c, provided by the municipality, was used to relate the CMA concentration to traffic.

Analyses

Previous research has shown that turbidity can be used as a proxy for road dust in a WDS II-sample (Gustafsson et al., 2019). Turbidity was analysed in all samples since it is a fast and simple analytical method. The sampling bottle was shaken thoroughly whereafter approximately 10mL was transferred into a glass vial. The vial was placed into a Hanna Instrument Turbidity Meter (HI-88703-02) and the turbidity was analysed.

Electric conductivity was measured in all samples with a Hanna Instruments HI2030 Edge.

After the initial turbidity and conductivity measurements, a selection of samples were sent for standardized analyses at SGS Analytics. Four samples from each profile, kerb (20 cm), right wheel track (100cm), in-between wheel tracks (200 cm), and left wheel track (280cm) were sent for analysis. The analytical package contained the occurrence of acetate and ions (F, Cl, SO4, Al, Fe, Ca, K, Cu, Mg, Mn, and Na), and turbidity, conductivity, pH, color, alkalinity, hardness, COD-Mn, NH4-N, NO3-N, NO2-N, NO2, and Sum NO3/50+NO2/0,5.

Results and discussion

The annual average daily traffic (AADT) at Hamngatan, Linköping, is 5352 vehicles on weekdays and 4123 vehicles on weekends. Passenger cars stand for the majority of the passing vehicles (80–95%), and the traffic starts to increase around 06:00 AM. The traffic intensity peaks in the afternoon, between 15:00 and 18:00 o´clock before it starts to decrease again (Figure 66).

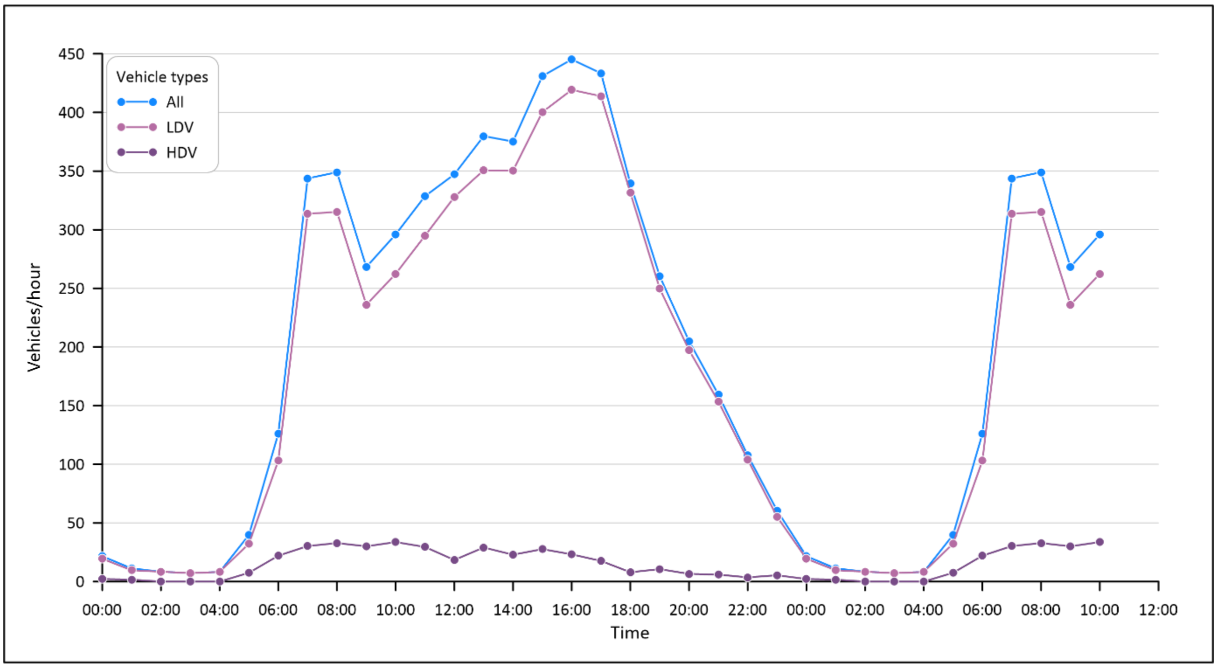

Figure 66. Traffic per hour on Hamngatan in Linköping, Sweden. (Traffic measurements from 2018).

Turbidity can be used as a proxy for the total amount of road dust on the road surface. The highest turbidity was detected adjacent to the kerb and close to the center line (Figure 67). The same pattern has been previously seen in Gustafsson et al., 2019 and Järlskog et al., 2020; 2021; 2022. It was complicated to detect a clear trend in turbidity that could be related to the application of CMA. The turbidity was at its lowest in the wheel tracks 8 h after CMA application. However, the turbidity had increased until the next measurement (12 h after CMA application) and reached its highest levels in the left wheel track 30 h after application of CMA. The turbidity in-between wheeltracks was higher than in the wheeltracks, and no significant reduction after CMA application could be seen. This pattern in time and space could likely be attributed to the dustbinding effect of the CMA; the increase of the turbidity reflects the amount of dust bound to the surface, instead of resuspending into the air, but even so, the dust is also redistributed within the road surface resulting in visible "wheel tracks" with lower amount of dust than outside the wheel tracks.

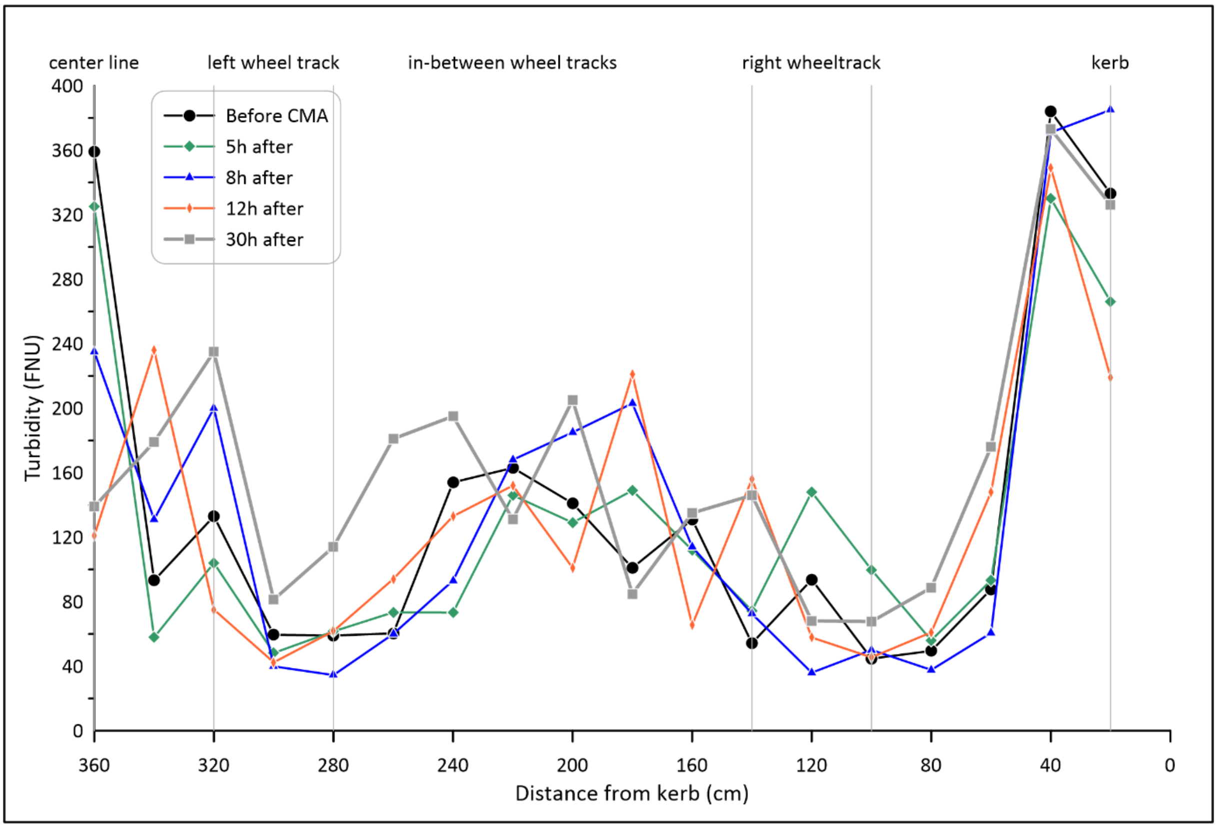

Figure 67. Turbidity (FNU) in samples collected transverse the road surface at Hamngatan, Linköping.

The electric conductivity increased after the CMA application, as expected due to the ions of the CMA (Figure 68). The highest conductivity was found adjacent to the kerb, just as for the turbidity. CMA solution collected from the contractor had a conductivity of 23800 µS/cm. The patterns for wheel tracks were not that obvious for conductivity as for turbidity, the conductivity decreased in the left wheel track in the samples collected 5 and 8 h after application, on the other hand, the conductivity had increased in the right wheel track during the same time. It should be noted that it is likely that some background conductivity could be related to remaining de-icing salt, especially on the kerb.

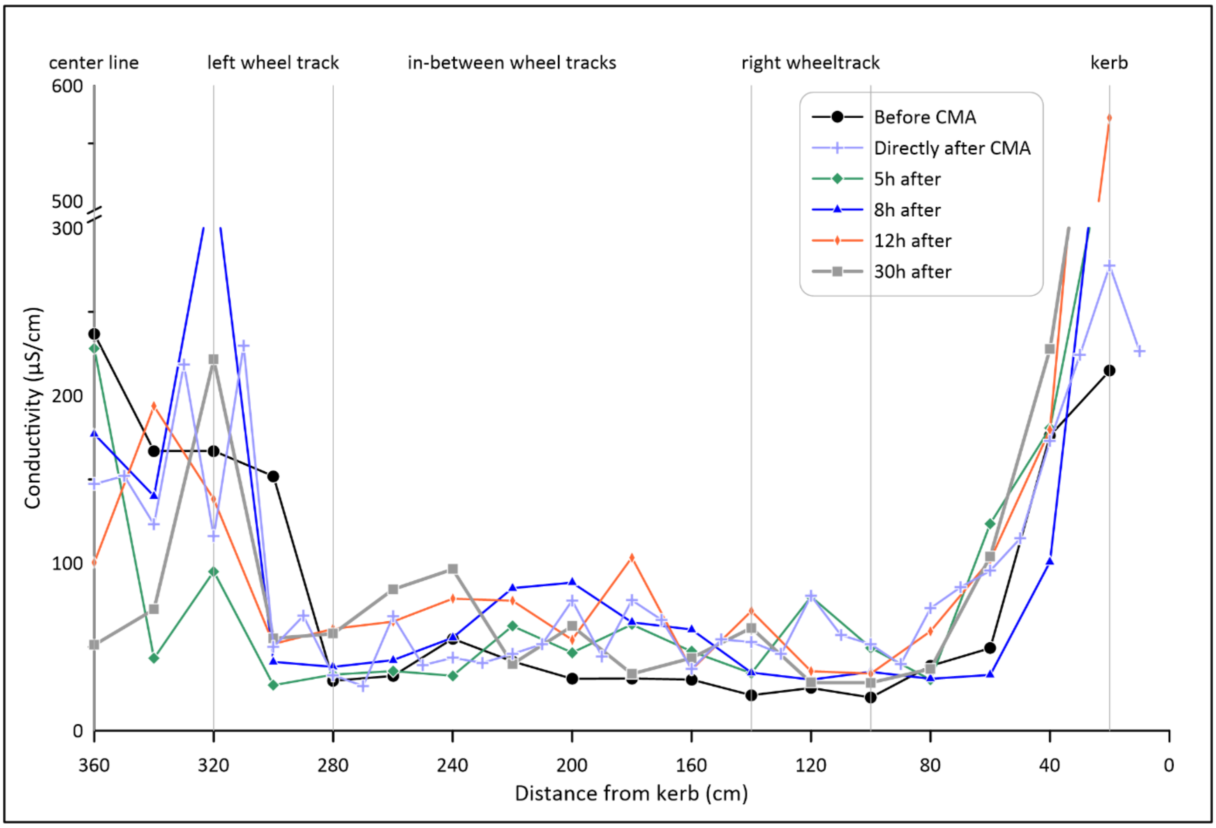

Figure 68. Conductivity (µS/cm).

Comparing the CMA amounts measured by time in the left wheel track (Figure 70), where almost no CMA was applied by the spreader, to the CMA amounts in the right wheel track (Figure 71), where ca 25 g/m^2 was added at the dust binding action, it is found that while the amounts in the right wheel track is decreasing, the amounts in the left wheel track is increasing. This type of redistribution of material on the road surface is well known from measurements of de-icing salts, which have showed that the salt amounts will be redistributed by both traffic (smearing and spraying) and road surface run-off (Eram et al., 2013). The CMA, under the circumstances studied here with non-wet road surfaces, may though be considered “stickier” than NaCl studied under the influence of melting snow.

The ion analyses shows diverging patterns of CMA related ions across the driving lane. The acetate ion is BDL before application. After application it is obvious that most of the CMA is spread over a width including the right wheel track and in-between wheel tracks, while the left wheel track receives low amounts and the kerb no CMA at all (Figure 69 A). The other CMA related ions, magnesium (Figure 69 B) and calcium (Figure 69 C), shows a different pattern with highest concentrations at the kerb and lowest in wheel tracks. This indicates that CMA is not the main source for these ions, but rather the mainly mineral dust accumulated on the street. Nevertheless, magnesium shows an apparent increase in all sampled areas right after CMA application. In contrast to acetate, magnesium increases also at the kerb, which is puzzling. Calcium shows only small variations over the test duration, especially in the driving lane.

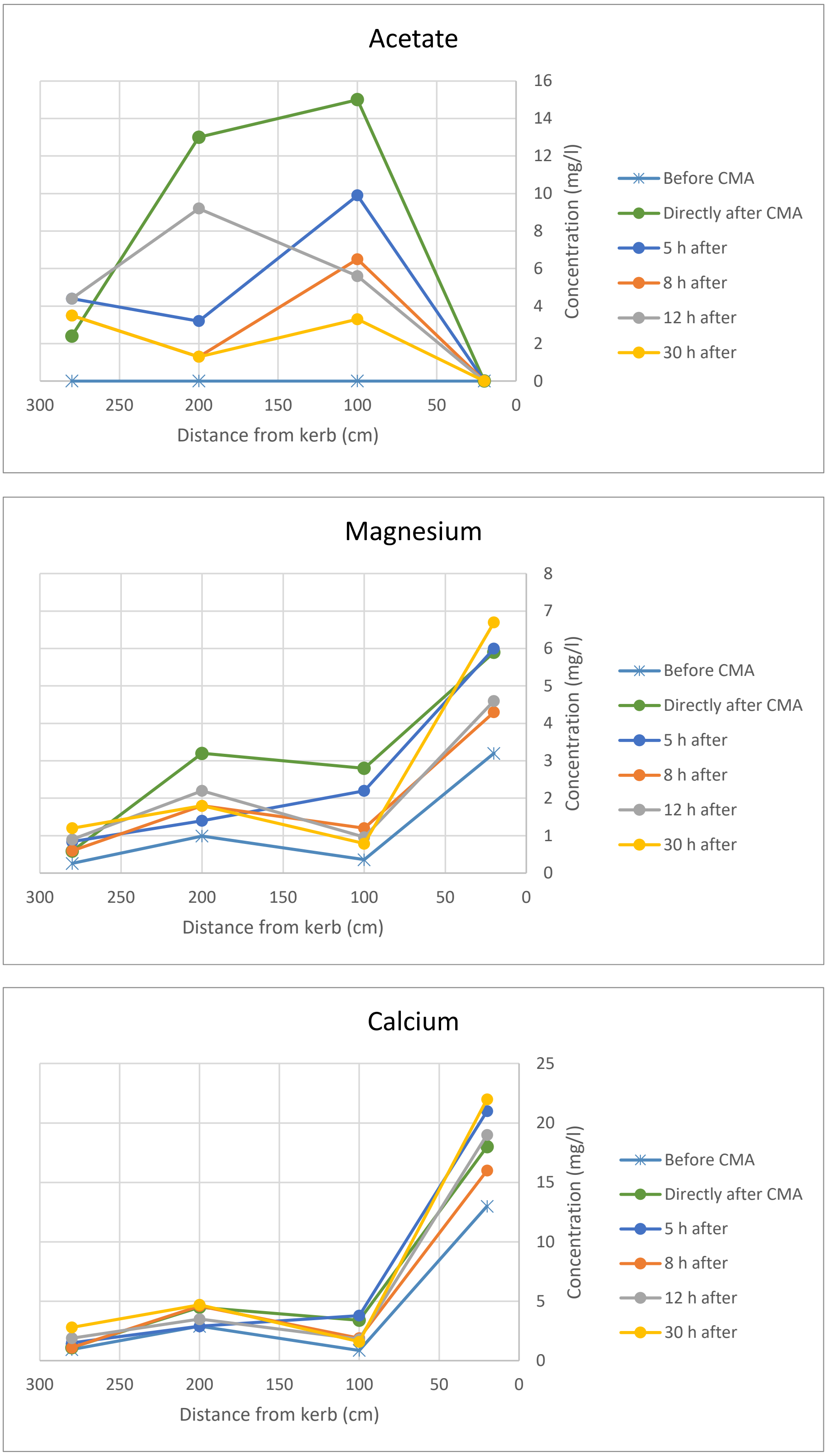

Figure 69. Spatial and temporal variation in main CMA ions at kerb, right wheel track (100 cm), between wheel tracks (200 cm) and left wheel track (270 cm).

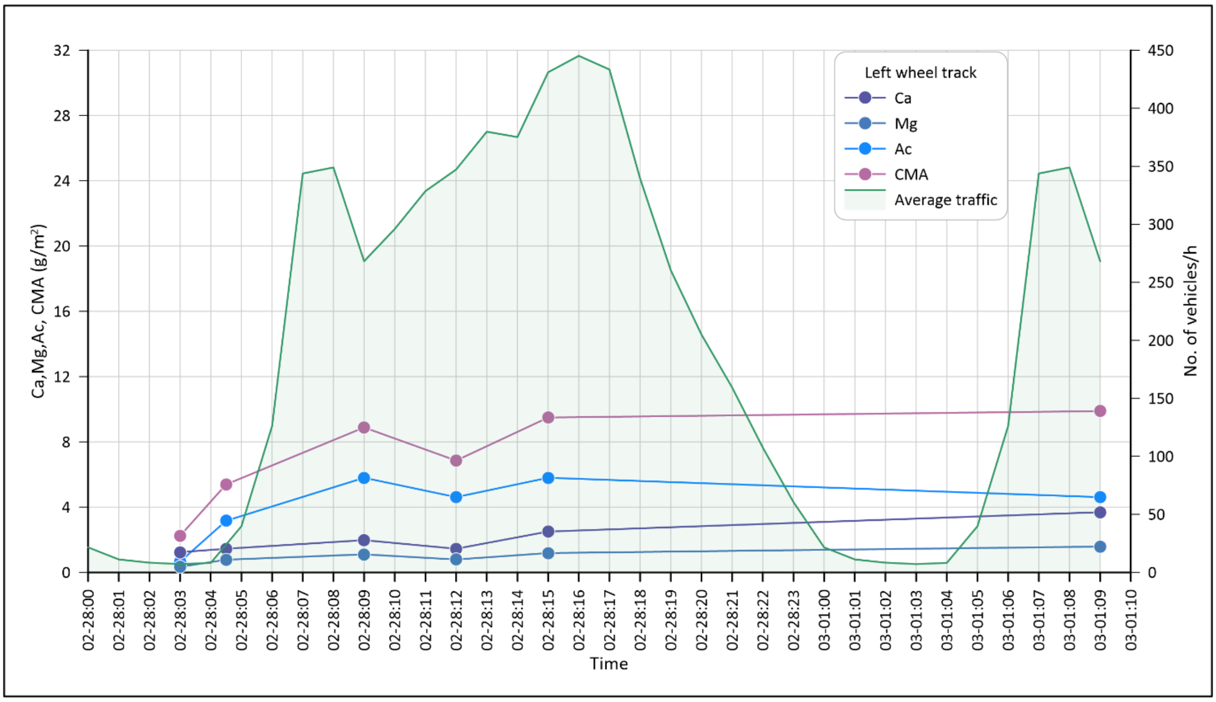

Figure 70. Surface load of Ca, Mg, Ac and CMA in left wheel track during tests.

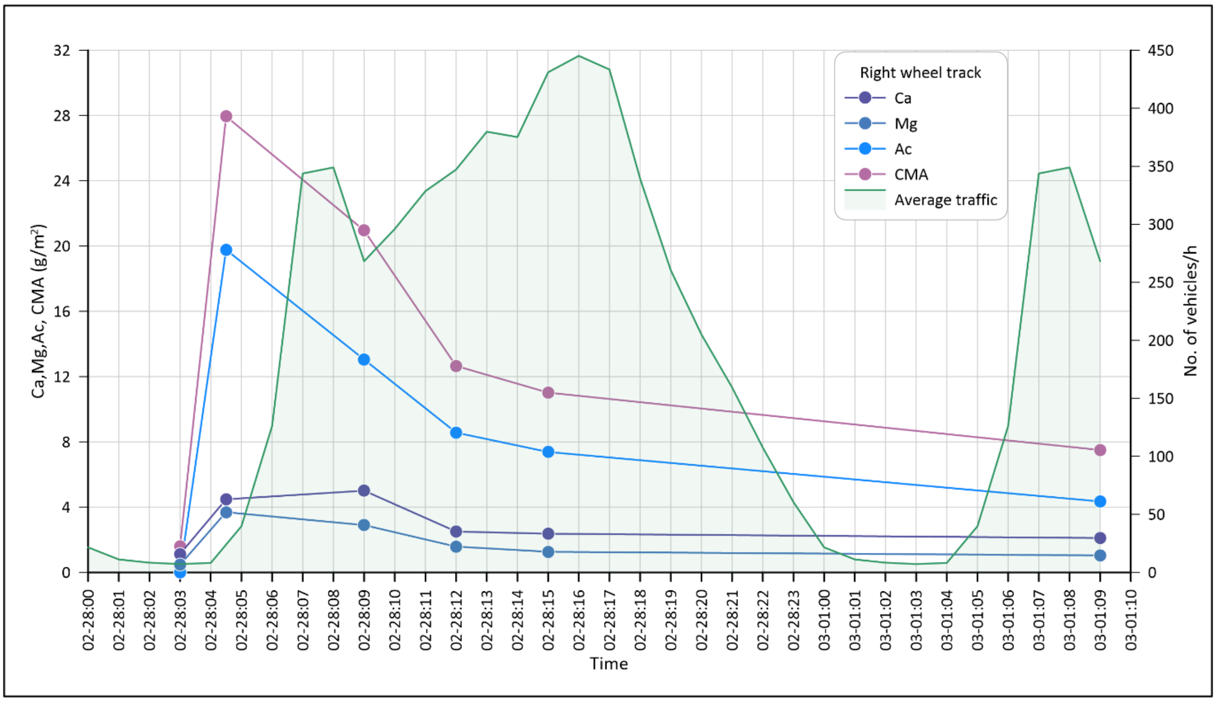

Figure 71. Surface load of Ca, Mg, Ac and CMA in right wheel track during tests.

In between wheel tracks (Figure 72), acetate increase after application, is reduced at 5 and 8 hours after application, but then increases after 12 hours. Calcium and magnesium do not follow the pattern, why it is hard to know if this is an actual effect or something related to the analysis. In the last sampling, acetate has been reduced to the same level as after 8 hours.

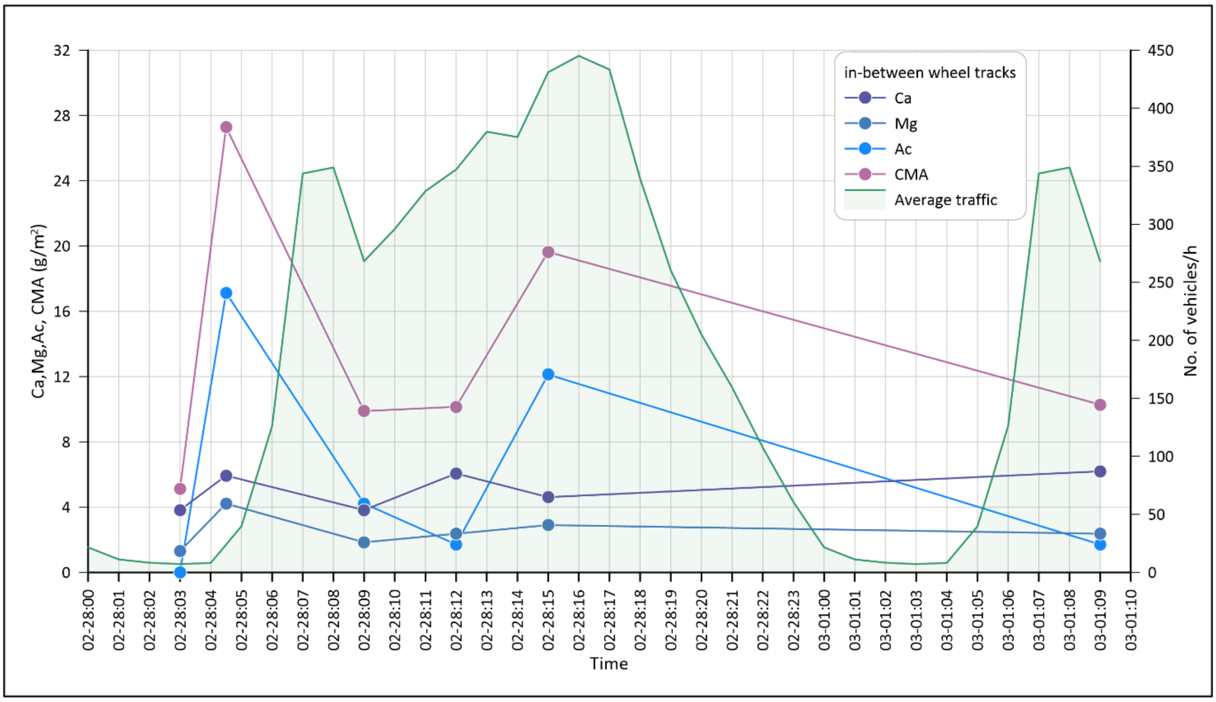

Figure 72. Surface load of Ca, Mg, Ac and CMA in-between wheel tracks during tests.

At the kerb, acetate was below the detection limit (BDL) in all samples, indicating that the CMA wasn't evenly spread on the road surface, and did not reach the kerb. This might be of concern since it is known that the majority of the road dust is located adjacent to the kerb. On the other hand, the kerbside is often less exposed to traffic (i.e., people normally drive in the wheel tracks and do not touch the kerbside area).

Plotting the accumulated traffic in the same plot as the change in acetate in the wheel tracks, shows a rapid decrease during high traffic hours and a slower decrease during night time (Figure 73).

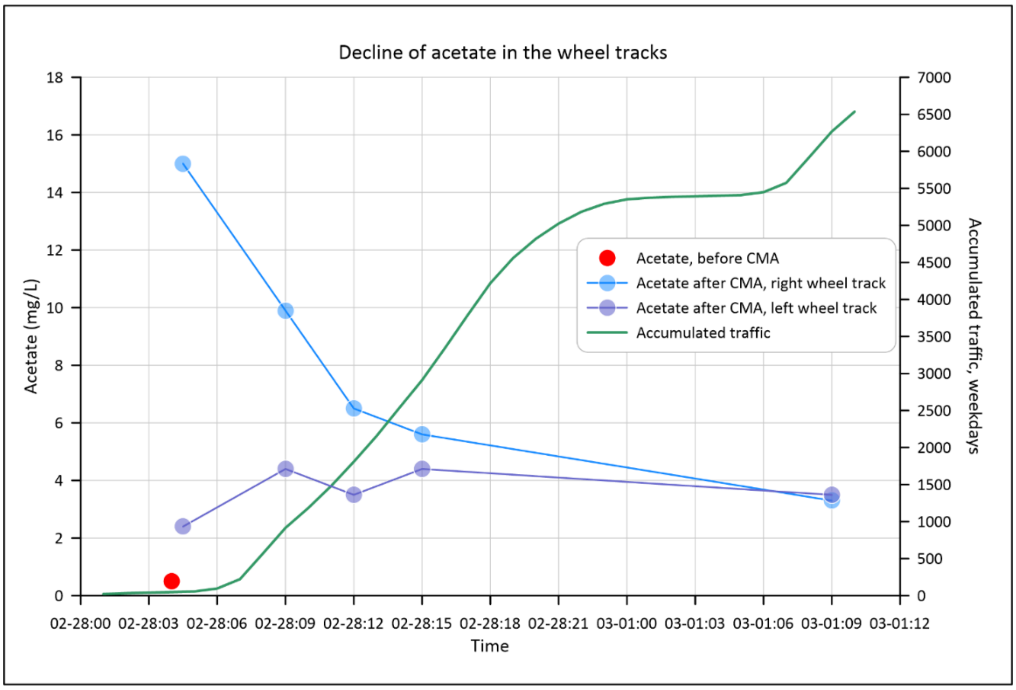

Figure 73. Decline of acetate in right and left wheel tracks in relation to accumulated traffic.

Conclusions

It was concluded that the CMA was not evenly spread throughout the road surface. As an example, the concentration of CMA was five times lower in the left wheel track compared to the right wheel track in the samples conducted directly after the CMA application. Further, the concentrations were several times lower in the left wheel track throughout all measurements, even if it was slowly increasing over time, probably due to redistribution by passing vehicles. It was also concluded that the measured dose was higher than the predicted applied concentration, 10 g/m^2, indicating that the spreader needs to be calibrated. CMA, mainly identified by the acetate ion, decreases continuously with time (and accumulating traffic) in right wheel track, while left wheel track and the area between wheel tracks shows alternating decrease and increase, likely to be due to redistribution and smearing of CMA both in lateral and longitudinal directions.

Overall WP2 Conclusions

Vehicle Weight and Speed

- Both lab and field tests show that particle mass emissions are positively and strongly correlated to vehicle weight and speed
- The study suggests that vehicle weight and speed are significant contributors to PM emissions, indicating potential areas for regulatory focus.

Tyre type Impact

- In spring, when road surface dust load is high, friction tyres emit PM10 at similar levels as studded tyres, due to resuspension overtaking direct wear emissions. Studded tyres contribute to the dust load, but resuspension is similar as for friction tyres.
- Studded tyres were found to contribute significantly more to PM emissions compared to studdless tyres.
- Tyre type plays a crucial role in the amount of PM emissions, with studded tyres showing notably higher emission factors.
- Studdless tyres might resuspend more dust than studded tyres when road surface dust load is high.
- When road surface dust load is low, studded tyres showcase direct wear emissions, whereas studless tyres showcase resuspension emissions, and in high dust load environments studded tyres show a combined effect (resuspension being dominant).

Emission Factors

- In field, emission factors increased linearly with vehicle weight. In campaigns B and C, they increased linearly with vehicle speed.
- Friction tyres generally emitted less PM compared to studded tyres, with summer tyres showing higher emission factors than friction tyres in some cases.

Particle Size Distributions

- Higher vehicle weights generates coarser particles within PM10.
- Lab tests show that also ultrafine particle number concentrations increase with vehicle weight and speed
- In field tests, three size peaks were observed in the mass size distributions around 1.2, 4.5, and 7.5 µm for each tyre type, with the highest concentrations around 4.5 µm.
- The PM2.5 share of PM10 decreased with increasing speed across all tyre types.

Crushing of winter sand

- Crushing of a winter sand material was described, showing that the coarsest fractions (192-5600 µm) are abraded and decrease in abondance while all finer fractions studied increase. The correlations between decline and increases to number of wheel passages were high.
- PM emissions decrease with continued crushing at constant speed, indicating abrasion and crushing of aggregates into airborne fractions decreases with time assumed to result from a decline in coarser fraction abrasion rate and finer fractions being less available for suspension.

Removal of winter sand

- Removal rate of winter sand from the wheel track was described as being linearly depending on speed. The mass removal was dominated by the coarsest fractions (192-5600 µm). Finer fractions could accumulate in the wheel track at 10 km/h, but was removed at higher speeds.

Residual dust binder

- CMA application was uneven across the treated street but a continuous decrease could be followed in the right wheel track.

Policy Implications

- The findings underscore the need for targeted strategies to reduce vehicular PM emissions by considering vehicle weight, speed, and tyre type.
- Suggests that regulatory measures, such as speed restrictions and promoting the use of lighter vehicles and less polluting tyre types, could mitigate PM emissions.

- The research provides a robust evidence base for formulating strategies to reduce vehicular PM emissions, emphasizing the need for a multifaceted approach that includes vehicle technology, urban planning, and public policy initiatives.

References

Aldrin, M., Hobaek Haff, I., Rosland, P., 2008. The effect of salting with magnesium chloride on the concentration of particular matter in a road tunnel. Atmospheric Environment 42, 1762-1776.

Beddows, D.C.S., Harrison, R.M., 2021. PM10 and PM2.5 emission factors for non-exhaust particles from road vehicles: Dependence upon vehicle mass and implications for battery electric vehicles. Atmospheric Environment 244, 10.1016/j.atmosenv.2020.117886.

Dahl, A., Gharibi, A., Swietlicki, E., Gudmundsson, A., Bohgard, M., Ljungman, A., Blomqvist, G., Gustafsson, M., 2006. Traffic-generated emissions of ultrafine particles from pavement-tyre interface. Atmospheric Environment 40, 1314-1323, 10.1016/j.atmosenv.2005.10.029.

Eram, M., Blomqvist, G., Thordarson, S., Lysbakken, K.R., 2013, Modelling Residual Salt -– MORS, NordFoU, http://urn.kb.se/resolve?urn=urn:nbn:se:vti:diva-5389

Fussell, J.C., Franklin, M., Green, D.C., Gustafsson, M., Harrison, R.M., Hicks, W., Kelly, F.J., Kishta, F., Miller, M.R., Mudway, I.S., Oroumiyeh, F., Selley, L., Wang, M., Zhu, Y., 2022. A Review of Road Traffic-Derived Non-Exhaust Particles: Emissions, Physicochemical Characteristics, Health Risks, and Mitigation Measures. Environmental Science & Technology, 10.1021/acs.est.2c01072.

Gertler, A., Kuhns, H., Abu-Allaban, M., Damm, C., Gillies, J., Etyemezian, V., Clayton, R., Proffitt, D., 2006. A case study of the impact of Winter road sand/salt and street sweeping on road dust re-entrainment. Atmospheric Environment 40, 5976-5985.

Gjerstad, K. I.., Gustafsson, M., Blomqvist, G., Denby, B., Elmgren, M., Grythe, H., Janhäll, S., Järlskog, I., Johansson, C., Kulovuori, S., Kupiainen, K., Lundberg, J., Malinen, A., Norman, M., Ritola, R., Silvergren, S., Stojiljkovic, A., Sundvor, I., Þorsteinsson, Þ., Stefani, M., Vogt, M., 2019, NORDUST : Nordic Road Dust Project, http://urn.kb.se/resolve?urn=urn:nbn:se:vti:diva-14950

Grigoratos, T., Gustafsson, M., Eriksson, O., Martini, G., 2018. Experimental investigation of tread wear and particle emission from tyres with different treadwear marking. Atmospheric Environment 182, 200-212, 10.1016/j.atmosenv.2018.03.049.

Gulia, S., Goyal, P., Goyal, S.K., Kumar, R., 2019. Re-suspension of road dust: contribution, assessment and control through dust suppressants—a review. Int. J. Environ. Sci. Technol. 16, 1717-1728, 10.1007/s13762-018-2001-7.

Gustafsson, M., Blomqvist, G., Jonsson, P., Ferm, M., 2010, Effekter av dammbindning av belagda vägar, 03476030 (ISSN), Statens väg- och transportforskningsinstitut, http://urn.kb.se/resolve?urn=urn:nbn:se:vti:diva-6527

Kupiainen, K., Ritola, R., Stojiljkovic, A., Pirjola, L., Malinen, A., Niemi, J., 2016. Contribution of mineral dust sources to street side ambient and suspension PM10 samples. Atmospheric Environment 147, 178-189, http://dx.doi.org/10.1016/j.atmosenv.2016.09.059.

Kupiainen, K., Tervahattu, H., Räisänen, M., 2003. Experimental studies about the impact of traction sand on urban road dust composition. Science of the Total Environment 308, 175-184.

Kupiainen, K., 2007. Road dust from pavement wear and traction sanding, Department of Biological and Environmental Sciences. University of Helsinki, Faculty of Biosciences, Helsinki, p. 50.

Norman, M., Johansson, C., 2006. Studies of some measures to reduce road dust emissions from paved roads in Scandinavia. Atmospheric Environment 40, 6154-6164, 10.1016/j.atmosenv.2006.05.022.

Pirjola, L., Parviainen, H., Hussein, T., Valli, A., Hämeri, K., Aaalto, P., Virtanen, A., Keskinen, J., Pakkanen, T. A., Mäkelä, T., & Hillamo, R. E. (2004). “Sniffer”—A novel tool for chasing vehicles and measuring traffic pollutants. Atmospheric Environment, 38(22), 3625–3635. https://doi.org/10.1016/j.atmosenv.2004.03.047

Pirjola, L., Kupiainen, K. J., Perhoniemi, P., Tervahattu, H., & Vesala, H. (2009). Non-exhaust emission measurement system of the mobile laboratory SNIFFER. Atmospheric Environment, 43(31), 4703–4713. https://doi.org/10.1016/j.atmosenv.2008.08.024

Timmers, V.R.J.H., Achten, P.A.J., 2016. Non-exhaust PM emissions from electric vehicles. Atmospheric Environment 134, 10-17, https://doi.org/10.1016/j.atmosenv.2016.03.017.

Work package 3: Microplastics from tyre wear in PM_{10}

Introduction

Exposure to particulate matter is a well-documented health concern (e.g., Kim et al. 2020). Emissions from road traffic significantly contribute to observed levels of particulate matter (PM), originating from both combustion and friction processes (Kukutschová and Filip 2018, Gustafsson et al., 2017). Combustion particles result from incomplete combustion of the fuel, whereas friction-generated particles are associated with wearing of tyre, brake, or road surface, collectively referred to as non-exhaust emissions (Vanherle et al., 2021).

The past decades have seen a significant reduction in combustion emissions across Europe, largely due to the implementation of stringent exhaust emission standards (Euro standards) for new vehicles. This includes incorporation of particulate filters for diesel exhaust (Samaras et al., 2022). With the renewal of the vehicle fleet, emissions of exhaust particles have decreased despite growing traffic volumes (Vanherle et al., 2021). Emissions of non-exhaust PM have not been subject to similar regulations, despite evidence of their growing significance (Piscitello et al., 2021). As a result, non-exhaust particles, which constituted approximately one third of total PM2.5, have, by 2020, exceeded exhaust particles in the context of overall road particle emissions across Europe (Vanherle et al., 2021).

Non-exhaust particles, while not always clearly distinguishable from each other, have a chemical signature characteristic of their sources. Tyre wear particles (TWP), as implied by the name, consists of tyre fragments, are comprised of natural and synthetic (from petroleum polymers) rubbers, along with numerous additives including oils, sulfur, zinc, silica, and black carbon (Kole et al., 2017).

Throughout its lifetime, a tyre from a light-duty vehicle can shed around 2–3 kg of mass, assuming typical driving conditions, resulting from the tyre's contact with the road. The tyre wear of a passenger car range approximately between 50 and 200 mg km^{-1} (Giechaskiel et al., 2024), which make TWP about one third of all non-exhaust particles. In Norway (8 000 tons) and Sweden (11 000 tons, Polukarova et al. (2024)) combined, an estimated 19 000 tons of TWP are generated. This makes it the largest single source of microplastic to the environment (e.g. Kole et al., 2017).

The size of particles is the single most important variable for their atmospheric lifetime. Large particles settle more quickly compared to smaller ones. Consequently, smaller particles have longer atmospheric residence times and can travel greater distances. This makes them a greater concern for air quality, both locally and regionally. Particles with an equivalent aerodynamic diameter (EAD) less than 2.5 µm are commonly referred to as fine particles (PM2.5), whereas coarse PM consists of particles between 2.5 µm and 10 µm (PM10-2.5). PM10 encompasses both PM2.5 and PM10-2.5. Evangeliou et al. (2020) highlighted that the fraction of TWP becoming airborne is the most important but also the most uncertain factor in understanding the dispersion of this class of aerosol. Estimates of TWP in PM10 vary widely (1–40%), as do estimates for PM2.5 (0% - 18%). Improving the precision of these numbers should be a priority.

Black particles are important in the context of climate considerations due to their capacity to absorb solar radiation. Hence, it is crucial to constrain the emissions of absorbing tyre wear particles (TWP). Notably, larger absorbing TWP can contribute substantially to the overall mass of absorbing particles. However, they are less efficient by mass at absorbing solar radiation as compared to smaller particles.

The present study seeks to establish a size-distribution of airborne TWP. This variable is crucial for understanding the environmental impact of this class of aerosol. In a controlled environment at the VTI road simulator facility, we utilized the high carbon content of car tyres to identify, isolate, and quantify TWP, minimizing and controlling the influence of carbonaceous aerosol from other sources than tyre wear. We also established size distributions of pyrolysis products of natural and synthetic rubbers present in tyres. Finally, emission factors for TWP were calculated using both carbonaceous aerosol data and rubber pyrolysis products.

Table 10. Abbreviations used in present study.

BAP	Background Aerosol Particles
CC	Carbonate Carbon
CC_{BAP}	Carbonate carbon (CC) content of Background Aerosol Particles
CC_{PAP}	Carbonate carbon (CC) Content of Pavement Abrasion Particles
CC_{TWP}	Carbonate carbon (CC) content of tyre wear particles
EC	Elemental Carbon
EC_{TWP}	Elemental carbon (EC) content of tyre wear particles (TWP)
ICP-MS	Inductive Coupled Plasma – Mass Spectrometry
$Mass_{TWP}$	Mass content of tyre wear particles (TWP)
NR	Natural Rubber
NY	Nylon
OC	Organic Carbon
OC_{TWP}	Organic carbon (OC) content of tyre wear particles (TWP)
PAP	Pavement Abrasion Particles
PC	Polycarbonate
PE	Polyethylene
PET	Polyethylene terephthalate
PMMA	Polymethylmetacrylat
PM10	Aerosol particles with and equivalent aerodynamic diameter (EAD) of 10 µm
PP	Polypropylene
PS	Polystyrene
PU	Polyuretane
PVC	Polyvenylchloride
RSP	Road Simulator Particles
SBR	Styrene Butadiene Rubber
TC	Total Carbon
TC_{TWP}	Total carbon (TC) content of tyre wear particles
TOA	Thermal-Optical Analysis
TRWP	Tyre and Road Wear Particles
TWP	Tyre Wear Particles

Methods

Test set-up

To generate TRWP the VTI road simulator was used (see Work package 2). The simulator used the same concrete pavement as in the tests for WP2 (Measurements for model parametrisations and processes) described earlier but was equipped with four summer tyres (Nokian Hakkapeliitta Blue). The inflation pressure was 2.5 bars and the axle load on each tyre was 450 kg. Ambient temperature in the simulator hall was set to 10°C before test start.

To generate and be able to sample as much TRWP as possible, a speed of 60 km/h constant speed during as long tests days as feasible were used. The resulting exposure times for the sampling equipment as well as distance run in the simulator is shown in Table 11.

Table 11. Test day data.

Day	*Speed*	*Number of laps*	*Distance (km)*	*Exposure time*
1	60	15 720	236	4 h 30 m
2	60	25 850	388	7 h 6 m
3	60	26 462	397	7 h 22 m
4	60	21 800	327	5 h 52 m
Total		89 832	1 347	24 h 50 m

During the measurements, particle concentrations and size distributions were measured using TEOM (1400a, Ruprecht & Pataschnik), Aerosol Particle Sizer (APS, TSI Inc), Scanning Mobility Particle Sizer (SMPS, TSI Inc) and AQ-Guard (Palas). Also, ambient, road surface and tyre surface temperatures were registered continuously.

The aim of the present study was to establish a size distribution of tyre wear particles (TWP) and emission factors of TWP for the size ranges 0.06 µm – 8 µm and for PM10. TWP emissions were isolated to the extent possible, performing the measurements in the hall housing the VTI (Swedish National Road and Transport Research Institute) road simulator. We assumed TWP and pavement abrasion particles (PAP) to be the primary particle sources in the hall. However, the presence of road simulator particles (RSP) and background air particles (BAP) must be considered (See eq. 1)

Identification and differentiation of TWP from PAP, RSP, and BAP relies on TWP being the major source of carbonaceous aerosol at the VTI test facility. Carbon is the major element in car tyres, accounting for up to 51% of the tyre mass (Evangeliou et al. 2020), which is consistent with the 43 – 48% for the car tyre examined in the present study (Table 12). To prevent generation of carbon-containing PAP, the tyres ran on a concrete surface, albeit concrete contains some carbonate. We find that carbonate carbon (CC) was mainly attributed to PAP (74%), then TWP (14%), and BAP (11%). To mitigate carbonaceous BAP impact, a filter sample was collected when the road simulator wasn't operational (Sample named RSOff;Table 13), and its level subtracted from that of the sample collected when the simulator was in use (Sample named RSOn;Table 13). Separate measurement of RSP was impracticable since the road simulator relies on tyres to run. However, we consider the road simulator a minor source of carbonaceous aerosol as it uses electrical engines. The possibility of carbonaceous aerosol originating from lubricants on moving parts of the road simulator cannot be excluded. Based on these assumptions, PM observed in the hall housing the VTI road simulator can be expressed as shown in (eq.1), providing an upper estimate TWP. Squared brackets in equations denote measured quantities. Parentheses denote emission ratios.

We calculated the carbonaceous mass of TWP (TCTWP) using (eq.2) and the CC concentration of PAP (CCPAP) according to (eq.3 and eq.4). We then converted TCWTWP (µg C m-3) to MassTWPs (µg m-3) using (eq. 5), allowing for solving (eq.1). The (CCTWP/TCTWP)Tyre ratio in (eq.4) was derived from the (CCTWP/MassTWP)Tyre and (TCTWPC/MassTWP)Tyre ratios, as shown in (Eq.6). The (TCTWP/MassTWP)Tyre ratio was determined by cutting a small piece of the tyre, weighing it, and establishing the TC carbon mass through TOA. The (CCTWP/MassTWP)Tyre ratio was similarly determined, only for the CC carbon mass. These ratios are found in Table 13.

$$[PM_{\text{Test facility}}] = TWP + [BAP] + \Sigma PAP,\ RSP \qquad \text{(eq.1)}$$

$$TC_{TWP} = [TC_{RS\text{ “On”}}] - [TC_{RS\text{”Off”}}] - PAP_{CC} \qquad \text{(eq.2)}$$

$$\text{Total CC} = CC_{TWP} + CC_{PAP} + CC_{BAP} \qquad \text{(eq.3)}$$

$$CC_{PAP} = [\text{Total CC}] - TC_{TWP} \times (CC/TC)_{Tyre} - [CC_{BAP}] \qquad \text{(eq.4)}$$

$$Mass_{TWP} = TC_{TWP} / (TC/Mass)_{Tyre} \qquad \text{(eq.5)}$$

$$(CC/TC)_{Tyre} = (CC/Mass)_{Tyre} \,/\, (TC/Mass)_{Tyre} \qquad \text{(eq.6)}$$

The CC_{TWP} level of the cascade impactor samples was not calculated as detailed in (eq.4). This is due to the low level, evident from the PM10 sample, and because it is distributed across seven samples. Hence, for each size bin we subtracted CC_{PAP} calculated for the PM10 sample, assuming a similar size distribution as for TC_{TWP}.

Cascade impactor samples provide data only for TCW_{TWP} thus EC_{TWP} and OC_{TWP} were derived by (eq.7) and (eq.8), respectively, including the EC_{TWP}/TC_{TWP} ratio (0.068) measured for the tyre. We base this assumption on the notion that the EC/TC ratio for TWP remains consistent irrespective of aerosol particle size, given their non-combustion origin.

$$EC_{TWP} = [TC_{TWP}] \times (EC/TC)_{Tyre} \qquad \text{(eq.7)}$$

$$OC_{TWP} = [TC_{TWP}] - EC_{TWP} \qquad \text{(eq.8)}$$

Carbonaceous aerosols are widespread and have numerous sources, making them unsuitable for tracing TWP in ambient air where emissions are mixed. Identifying, separating, and quantifying TWP in ambient air requires a unique tracer or a source-specific chemical fingerprint. In this study, we analyzed several organic species, including pyrolysis products of major constituents in tyres, such as styrene butadiene rubber (SBR). However, there are no methods considered entirely specific or quantitative for measuring TWP in air. Additionally, we analyzed pyrolysis products of the most used thermoplastic polymers (SeeTable 10). Analysis was performed on PM10 filter samples, size-segregated samples covering particle sizes from 0.06 – 8 µm, and tyre samples. We attempted to calculate concentrations of TWP based on observed concentrations of pyrolysis products of PVC, NY, and SBR, using (eq.9). This required information of the PVC, NY, and SBR content in the tested tyre (Table 15).

$$TC_{TWP} = [\text{Pyrolysis product}]_{TWP} / (\text{Pyrolysis product/Mass})_{Tyre} \qquad \text{(eq.9)}$$

Aerosol sampling

We collected size segregated aerosol particle samples using a Berner low-pressure cascade impactor, using prefired (850 °C, 3.5 h) quartz fibre filters (diameter = 70 mm, cut from 8” x 10” Whatman QM-A) as impaction plates. The cascade impactor collected aerosol particles in seven consecutive size bins, i.e., 8.0 - 4.0 µm, 4.0 - 2.0 µm, 2.0 – 1.0 µm 1.0 - 0.5 µm, 0.5 – 0.250 µm, 0.250 - 0.125 µm, and 0.125 - 0.060 µm, at a flow rate of 28 L min^{-1}. The sampling time was 24 h. The samples were stored in a freezer (-18 °C) prior to chemical analysis. One sample was collected while the VTI road simulator was in operation, and another when the road simulator was turned off.

We collected aerosol particles (PM10) on prefired (850 °C, 3.5 h) quartz fiber filters (8” x 10” Whatman QM-A) using a high-volume sampler (Sierra Anderson) operated at a flow rate of 1113 L min^{-1}. The sampling time was 24 hours. Filters were conditioned at 20 °C and 50% RH (relative humidity) for 48 h prior to and after exposure to determine the mass concentration by gravimetry. Filters were stored in a freezer (-18 °C) after gravimetry and prior to chemical analysis. One sample was collected while the VTI road simulator was in operation, and another when the road simulator was turned off.

Thermal-optical analysis

We used Thermal-optical analysis (TOA) for determination of TC, OC, EC, and CC (Eq.9), using the Sunset Lab OC/EC Aerosol Analyzer. We operated the instrument according to the EUSAAR-2 temperature program (Cavalli et al., 2010), using transmission for charring correction. For measurement of CC, we removed OC and EC using thermal-oxidative pre-treatment (Jankowski et al., 2008; Evangeliou et al., 2016). The instrument is regularly tested in the EMEP/ACTRIS quality assurance and quality control effort for OC/EC (e.g., Cavalli et al., 2016).

$$TC = OC + EC + CC \quad \text{(eq.9)}$$

Both the size segregated samples obtained by the cascade impactor and the filter samples collected by the PM10 sampler were analyzed by TOA. Additionally, aliquots of the tested tyre were subjected to TOA.

Pyrolytic GC-MS

We used pyrolysis-gas chromatography coupled with mass-spectrometry (Pyr-GC-MS) for analysis of selected organic molecules considered tracers of plastic and rubber. These were polymethyl-metacrylate (PMMA), styrene butadiene rubber (SBR), polypropylene (PP), polyvinylchloride (PVC), Nylon, Polyuretane (PU), polyethylene (PE), natural rubber (NR), polystyrene (PS), polyethylene terephtalate (PET) and polycarbonate (PC). The analysis followed the approach of Gossmann et al. (2023).

Both the size segregated samples obtained by the cascade impactor and the filter samples collected by the PM10 sampler were analyzed by Pyr-GC-MS. Additionally, aliquots of the tested tyre were subjected to Pyr-GC-MS analysis.

ICP/MS

Extraction of aerosol filter samples and analysis of Zn, Al, Ti, Fe, Mn, Cu, Co, Pb, Cd, and Ni were performed using ICP-MS (inductively coupled plasma mass spectrometry) (Agilent 7700x) following the procedure described in Zwaaftink et al. (2022). The selection of elements was consistent with elements previously documented in car tyres (Halsband et al., 2020).

The filter samples collected by the PM10 sampler were analyzed by ICP/MS, as were aliquots of the tested tyre.

Results and discussion

Pavement abrasion particles (PAP) and particles from the road simulator (RSP) combined, made up 53% of the observed PM10 concentration (16.1 µg m^{-3}) measured in the hall housing the road simulator. This was followed by tyre wear particles (TWP) at 33%, and background air particles (BAP) at 15% (Figure 74). TWP in PM10 measured 5.4 ± 0.3 µg m^{-3} (Mean ± SD) (Table 13, Table 12) which was higher than TWP (4.5 µg m^{-3}; not shown) derived from the 0.06 – 8.0 µm size range of the co-located cascade impactor.

The Zn content of the tyre was 6514 mg g^{-1}, while Al recorded 857 mg g^{-1}; Fe, Ti, Cu, Mn, Pb, Ni, Co, Cd, and Pb ranged from 86.1 to 0.066 mg g^{-1} (Table 14). The observations show great resemblance to the relative abundance of metals measured in 60 car tyres by O’Loughlin et al. (2023): Zn, Al, Fe, Mg, Ti, Cu, Ba, Pb, Ni, Sn, Sr, and Mn. The Zn to TC ratio matched well between the tyre (14.5) and the PM10 filter sample (11.7). However, for the remaining elements, the ratio was notably higher (100 - 1700) in the PM10 filter sample compared to the tyre. This discrepancy implies Zn's association with TWP, while PAP, RSP, and BAP accounted for the other elements.

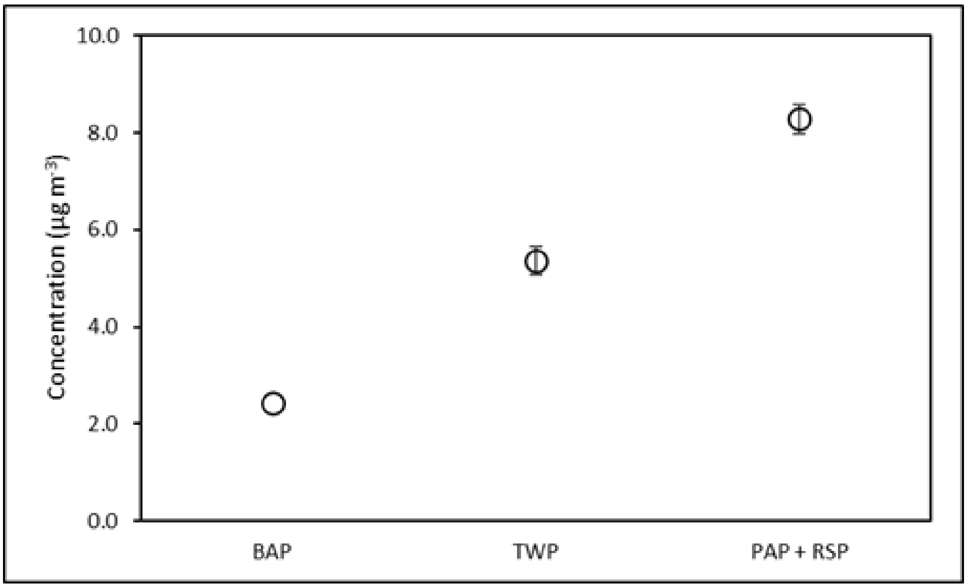

Figure 74. Apportioned mass of background aerosol particles (BAP), tyre wear particles (TWP), and pavement abrasion particles + road simulator particles (PAP + RSP) at the VTI road simulator facility.

The size distribution of TWP was unimodal peaking between 1 µm and 4 µm and with a tailing presence in the fine fraction (< $PM_{2.0}$) (Figure 75, left panel). 0.57 of TWP was present in the fine fraction, which was marginally higher than the 0.43 observed for the coarse fraction (2.0 µm < EAD < 8.0 µm). A minor fraction (0.04) of TWP was associated with the finest size fraction (0.06 < EAD < 0.125 µm), denoted ultrafine particles (UFP). The size distributions of EC_{TWP} and OC_{TWP} are identical to $Mass_{TWP}$ (Figure 75, right panel) as evident from (eq.7) and (eq.8), although levels are lower.

Nine out of the ten pyrolysis products of plastics and rubber that were analyzed were detected in the tyre sample. Only seven were detected in the PM10 filter sample, with concentrations ranging from 0.09 – 50.4 ng m^{-3}. For the cascade impactor samples, it was possible to obtain a full range size distribution (0.06 – 8.0 µm) for only PVC, NY, and SBR. For these three variables, levels were 3 – 6 times higher compared to the PM10 sample. Attempts to convert these tyre wear species to $Mass_{TWP}$ concentrations ranged from 0.6 µg m^{-3} to 184 µg m^{-3}.

The size distribution of PVC, Nylon, and SBR had a bimodal distribution, with a minor peak between 1 and 4 µm and a dominating one between 0.06 and 0.125 µm (Figure 76).

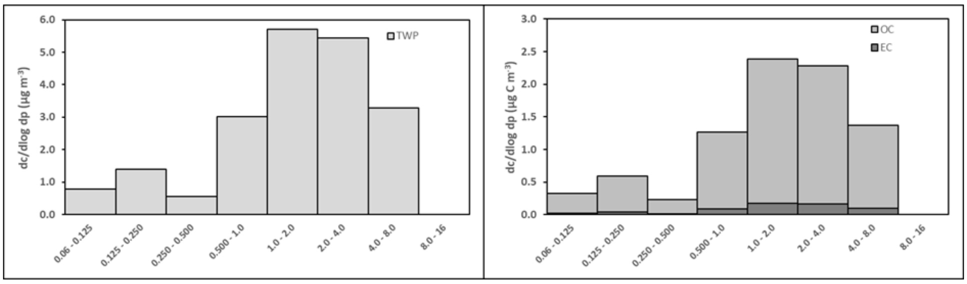

Figure 75. Size distribution of tyre wear particles (left panel) and of OC and EC associated with TWP (right panel).

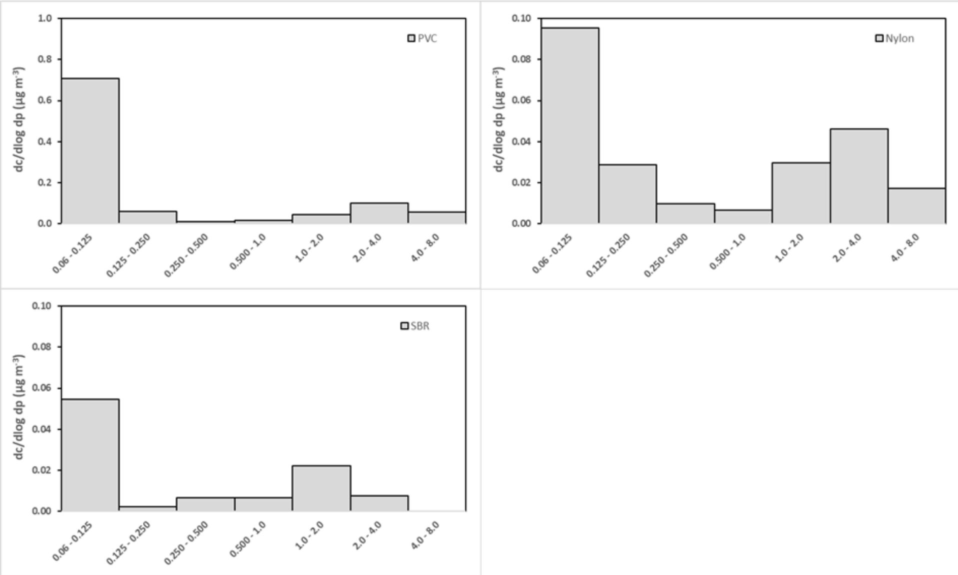

Figure 76. Size distribution of PVC (upper panel, left), Nylon (upper panel, right), and SBR (lower panel) pyrolysis products.

Our results suggest a successful separation of TWP from other sources. The Zn to TC_{TWP} ratio (11.7) calculated for PM10 was only 19% lower compared to the Zn to TC ratio of the tyre (14.5). This reaffirms our crucial presumption that TWP is the primary origin of carbonaceous aerosol at the test facility, validating TC as a reliable tracer for TWP both qualitatively and quantitatively. Likewise, the EC to TC ratio differed by no more than 22% between that calculated for PM10 (0.083) and for the tyre (0.068), supporting this conclusion.

Table 12. Ratios of TC, OC, EC, and CC to mass (Unit: µg C µg^{-1}), and OC, EC, and CC to TC (µg C µg C^{-1}) taken directly from the tyre sample (Nokian Hakka Blue) collected at the VTI road simulator facility. The notation uses subscript to harmonize with the text.

ID	$(TC/Mass)_{Tyre}$	$(OC/Mass)_{Tyre}$	$(EC/Mass)_{Tyre}$	$(CC/Mass)_{Tyre}$	$(OC/TC)_{TyreC}$	$(EC/TC)_{Tyre}$	$(CC/TC)_{Tyre}$
#1	0.430	0.402	0.028		0.934	0.066	
#2	0.443	0.412	0.031		0.930	0.070	
#3	0.479	0.447	0.033		0.932	0.068	
#4				0.003			0.011$^{1)}$
#5				0.007			

1) See (eq. 6)

Table 13. The two first rows show the mass concentration of PM10 (Unit: µg m^{-3}), TC, OC, EC, and CC (Unit: µg C m^{-3}) in the filter sample collected at when the road simulator was on (RS "On") and off (RS "Off"), the latter corresponding to BAP. Row three and four shows the calculated concentrations attributed to ΣPAP,RSP and TWP.

ID	PM10	TC	OC	EC	$TC_{CC}$$^{1)}$	OC_{CC}	EC_{CC}	CC
RS "On"	16.1	3.61	3.30	0.31	3.42	3.17	0.25	0.19
RS "Off" (BAP)	2.4	1.06	1.00	0.05	1.04	0.98	0.05	0.02
ΣPAP,RSP$^{2)}$	8.3 ± 0.3	0.14						0.14
TWP	5.4 ± 0.3	2.41	2.19	0.20				0.03

1) Subscript CC (e.g., OC_{CC}) demonstrates that co-evolving carbonate carbon (CC) has been subtracted; 2) ΣPAP,RSP contains only CC, no EC or OC, and all of it is attributed to PAP.

Table 14. Element concentrations in tyre and in air, and their relative contribution to TC in tyre and TC (TWP proxy) in air. Samples collected at the VTI road simulator facility.

Element	Tyre ($mg\ kg^{-1}$)	Element TC^{-1} ($ng\ \mu g\ C^{-1}$)	Air ($ng\ m^{-3}$)	Element TC^{-1} ($ng\ \mu g\ C^{-1}$)
Zn	6514	14.5	28.2	11.7
Al	857	1.90	538	223
Fe	86.1	0.191	229	94.8
Ti	12.5	0.028	17.8	7.37
Cu	2.85	0.0063	18.8	7.82
Mn	1.60	0.0036	5.51	2.29
Pb	0.909	0.0020	0.533	0.221
Ni	0.803	0.0018	< LOD	NA
Co	0.081	0.00018	0.720	0.299
Cd	0.066	0.00015	0.051	0.021

Table 15. Plastic and rubber pyrolysis products in tyre and in air, and their relative contribution to TC in tyre and TC (TWP proxy) in air. Samples collected at the VTI road simulator facility.

#	Tyre ($mg\ g^{-1}$)	# TC^{-1} ($ng\ \mu g\ C^{-1}$)	Air ($ng\ m^{-3}$)	# TC^{-1} ($ng\ \mu g\ C^{-1}$)
PMMA	ND	NA	7.87	3.27
PP	0.060	0.133	4.94	2.05
SBR	14.3	31.7	9.08	3.77
Nylon	0.390	0.867	14.5	6.03
PVC	53.9	120	50.4	20.9

A 20% difference in $Mass_{TWP}$ was observed between PM10 ($5.4 \pm 0.3\ \mu g\ m^{-3}$) and the 0.06 – 8.0 µm size range of the cascade impactor ($4.5\ \mu g\ m^{-3}$). Part of this discrepancy can be ascribed to the smaller size range covered by the cascade impactor. Other artefacts that can occur when collecting aerosol particles by impaction are particle bouncing, particle blow off, and particle wall loss. Chemical composition, particle loading, and collection substrate have an influence on the magnitude of these artefacts. Differences < 10% was observed when comparing total suspended particulate (TSP) matter obtained by cascade impactor and a filter sampler (Vaeck et al., 1979). Differences < 30% was observed for low volatility organic species and, but > 30% for high volatility organic species. A filter sampler is likely more prone to the positive sampling artifact caused by OC (McDow and Huntzicker, 1990) than a cascade impactor sample, overestimating particulate OC, and hence in our study, TWP. The PM10 concentration attributed to PAP and RSP ($8.3\ \mu g\ m^{-3}$) was approximately 1.5 times higher than that of TWP ($5.4 \pm 0.3\ \mu g\ m^{-3}$).

Studies (e.g., Kim and Lee, 2018; Hussain et al., 2008) have reported a unimodal size distribution of tyre wear particles (TWP) with a peak concentration between 1 µm and 5 µm. This is consistent with the unimodal size distribution shown in Figure 75. Size distribution of tyre wear particles (left panel) and of OC and EC associated with TWP (right panel). Figure 75, peaking between 1 µm and 4 µm. A substantial fraction of TWP (0.57) was associated with fine aerosol, which is notably higher than what is assumed in the NORTRIP model (0.1). Kim and Lee (2018) demonstrated that the relative contribution of PM2.5 to PM10 increased with higher speeds, rising from 0.24 at 50 km h^{-1} to 0.32 at 140 km h^{-1}. This ratio also increased with an increased lateral load. For instance, the PM2.5/PM10 ratio was significantly higher (0.77) at a load of 2500 N compared to 0.31 at 500 N. Formation of ultrafine TWP is linked to slip events and braking, but only braking seems to make a minor contribution to the mass concentration of TWP (Kim and Lee, 2018). During the test, no such events involving slip or deliberate braking were included, which aligns with the minor fraction (0.04) observed in the data. Conclusively, the size distribution of TWP derived by using carbonaceous aerosol as a proxy for TWP aligns with results from previous studies.

The presence of EC in the tested tyre was minimal, accounting for no more than 0.031 of the tyre's mass, and its aerosol size distribution identical to that of TWP. The small amount of EC efficiently boosts the mass of black TWP, making it relevant from a climate perspective, although larger particles are less efficient by mass at absorbing solar radiation compared to smaller particles. Additionally, their atmospheric lifetime is shorter.

The size distribution of pyrolysis products from PVC (Polyvinylchloride), Nylon (NY), and SBR (Styrene-butadiene rubber), closely resembled that of TWP based on carbonaceous aerosol (Table 14 and Table 16). Element concentrations in tyre and in air, and their relative contribution to TC in tyre and TC (TWP proxy) in air. Samples collected at the VTI road simulator facility. Plastic and rubber pyrolysis products in tyre and in air, and their relative contribution to TC in tyre and TC (TWP proxy) in air. Samples collected at the VTI road for the coarser particle sizes but not for the finest fractions. We speculate that this may result from higher efficiency of pyrolyzing smaller particles due to their higher surface area-to-volume ratio. Notably, the ratio of PVC, NY, and SBR to calculated TWP was highest in the finest aerosol size fraction, with a non-linear trend showing the lowest ratio in the accumulation mode (0.250 µm to 1.0 µm) and an increase in larger particles (>1.0 µm). This could also indicate that TWP's chemical composition varies with particle size, posing challenges for quantification that requires corresponding standards for different size fractions. Additionally, the documented variability in synthetic rubber mass in tyres further complicates quantification, as the composition of tyre samples and standards likely differ. Rauert et al. (2021) found that the styrene-butadiene and butadiene rubber content of tyres ranged from < 0.05% to 28%.

Consequently, our attempts to quantify TWP from PVC, NY, and SBR yielded highly variable and non-comparable results compared to TWP concentrations based on carbonaceous aerosol. A comprehensive analysis of the chemical content of commercially available tyres and a review of suitable pyrolysis products are necessary.

Conclusions

The importance of tyre wear particles (TWP) has grown due to the shift towards electric vehicles and reduced exhaust emissions. We examined the size distribution of TWP, a critical factor in comprehending their environmental implications and fate. We find a unimodal size distribution of TWP with the peak falling between 1 µm and 4 µm. Significantly, a predominant portion of the examined size fraction, ranging from 0.06 µm to 8 µm, corresponds to fine particles. Our findings align with contemporary studies that also distinguish TWP from road wear particles, confirming the consistency of our results. However, it deviates from the size distribution of TWP currently used in the NORTRIP model. Notably, only one tyre model was tested and on a road surface of concrete, different from most roads in Scandinavia. A higher number of tyres of various categories and from different manufacturers should be tested when considering a revision of the size distribution used in the NORTRIP model.

Size distributions of PVC, NY and SBR pyrolysis products, species derived from constituents present in the tyre, resembled that established for TWP for coarser particles, but deviated for the finest particles. The reason for this is unknown and should be explored further. Attempts to quantify TWP from pyrolysis products of PVC, NY and SBR provided variable and non-comparable results. Difference in polymer composition between the tyre tested and of the quantification standard, was speculated as one possible bias. There are no methods considered entirely specific or quantitative for measuring TWP in air. To explore the environmental effect of TWP, methods that are both specific and quantitative with respect to measuring TWP in air must be established. This is currently not available.

References

Evangeliou, N., Grythe, H., Klimont, Z. et al. Atmospheric transport is a major pathway of microplastics to remote regions. *Nat Commun* **11**, 3381 (2020). doi.org/10.1038/s41467-020-17201-9

Giechaskiel, B., Grigoratos, T., Mathissen, M., Quik, J., Tromp, P., Gustafsson, M., Franco, V., Dilara, P., 2024. Contribution of Road Vehicle Tyre Wear to Microplastics and Ambient Air Pollution. Sustainability 16, 10.3390/su16020522.

Gossmann, I., Herzke, D., Held, A., Schulz, J., Nikiforov, V., Georgi, C., Evangeliou, N., Eckhardt, S., Gerdts, G., Wurl, O. and Scholz-Botter, B. M. 2023. Occurrence and backtracking of microplastic mass loads including tyre wear particles in northern Atlantic air. Nat. Commun., 14, 3707.

Gustafsson, M., et. al., 2017, 'PM10 Emission Effects of New Studded Tyre Regulations'. Journal of Earth Sciences and Geotechnical Engineering, vol. 7, no.1, 2017, 1-9.

Halsband, C., Sørensen, L., Booth, A.M., Herzke, D.: Car tyre crumb rubber: does leaching produce a toxic chemical cocktail in coastal marine systems? Front. Environ. Sci., 8 (2020), p. 12.

Hussein, T.; Johansson, C.; Karlsson, H.; Hansson, H. C.Factors affecting non-tailpipe aerosol particle emissions from pavedroads: On-road measurements in Stockholm, Sweden.Atmos. Environ.2008,42(4), 688−702

Groot Zwaaftink, C. D., Aas, W., Eckhardt, S., Evangeliou, N., Hamer, P., Johnsrud, M., Kylling, A., Platt, S. M., Stebel, K., Uggerud, H., and Yttri, K. E.: What caused a record high PM10 episode in northern Europe in October 2020?, Atmos. Chem. Phys., 22, 3789–3810, https://doi.org/10.5194/acp-22-3789-2022, 2022.

Kim, H., Kim, W. H., Kim, Y. Y., & Park, H. Y. (2020). Air pollution and central nervous system disease: a review of the impact of fine particulate matter on neurological disorders. *Frontiers in Public Health*, *8*, 575330.

Kole, J. P., Löhr, A. J., Van Belleghem, F. G. A. J. & Ragas, A. M. J. Wear and tear of tyres: a stealthy source of microplastics in the environment. *Int. J. Environ. Res. Public Health* **14**, 1–4 (2017).

Kukutschová, J. and Filip P., 2018, 'Review of Brake Wear Emissions: A Review of Brake Emission Measurement Studies: Identification of Gaps and Future Needs'. In Amato F (Ed.) Non-Exhaust Emissions. An Urban Air Quality Problem for Public Health; Impact and Mitigation Measures. Elsevier Inc.

McDow, S. R., Huntzicker, J. J., 1990. Vapor adsorption artifact in the sampling of organic aerosol: face velocity effects. Atmospheric Environment 24, 2563–2571.

O'Loughlin, D., Haugen, M., Day, J., Brown, A., Braysher, E., Molden, N., Willis, A. E., MacFarlane, M., Boies, A. M. 2023. Multi-element analysis of tyre rubber for metal tracers. Environment International, 178, 2023, 108047.

Piscitello, A., Bianco, C., Casasso, A., & Sethi, R. (2021). Non-exhaust traffic emissions: Sources, characterization, and mitigation measures. *Science of the Total Environment*, *766*, 144440.

Polukarova, M., Hjort, M., Gustafsson, M., 2024. Comprehensive approach to national tyre wear emissions: Challenges and implications. Science of The Total Environment, 171391, https://doi.org/10.1016/j.scitotenv.2024.171391.

Samaras, Z. C., Kontses, A., Dimaratos, A., Kontses, D., Balazs, A., Hausberger, S., ... & Dilara, P. (2022). A European regulatory perspective towards a euro 7 proposal. *SAE International Journal of Advances and Current Practices in Mobility*, *5*(2022-37-0032), 998-1011.

Vanherle, K., Lopez-Aparicio, S., Grythe, H., Lükewille, A., Unterstaller, A., & Mayeres, I. (2021). Transport Non-exhaust PM-emissions. *An Overview of Emission Estimates, Relevance, Trends and Policies*.

Work package 4: Mitigation policies and health effects

Aims

The overall aim of WP4 is to investigate mitigation policies impacts on non-exhaust emissions and health utilizing the NORTRIP model. The planned mitigation scenarios to be analysed are impacts on exposures and health of the electrification of the vehicle fleet (considering effects of brake wear, tyre wear, road wear – weight + exhaust) and associated changes in studded tyre use.

Motivation

Road traffic is the most important source of exposure and associated adverse health outcomes of people living in most urban areas in Europe. Electrification of the transport sector is underway to varying degrees in Europe. In Norway, Iceland, Sweden, Finland and Denmark the share of new battery electric vehicles registered in 2023 (Jan-Sep) was 83%, 42 %, 39%, 33% and 33% respectively[2].

Scenarios

Table 16 summarises the assumptions made for the calculations of the impacts of the electrified fleet in Stockholm, Trondheim and Helsinki. The different shares of electric cars are based on official governmental national forecasts. The shares of studded tyres are based on observed shares in the cities and extrapolations for future years. The weight of electric vehicles is based on Swedish statistics and the impact of weight on road wear is assumed linear as discussed later in this report.

[2] https://www.acea.auto/pc-registrations/new-car-registrations-9-2-in-september-battery-electric-14-8-market-share/

Table 16. Scenarios for calculations of the impacts of electrification of vehicle fleets in Stockholm, Trondheim and Helsinki.

Parameter	**Stockholm**		**Trondheim**		**Helsinki**	
Share of electric vehicles in traffic	2022: 14% 2030: 34% 2040: 75% 2050: 95%		2021: 13% 2030: 60% 2040: 90% 2050: 95%		2021: 1% 2030: 14% 2040: 39% 2050: 63%	
Share of studded tyres	Fossil 2022: 47% 2030: 47% 2040: 47% 2050: 47%	Electric For all years: 47%, 23% and 16%	Fossil 2021: 18%, 18% 2030: 18%, 13% 2040: 18%, 9% 2050: 18%, 6%	Electric 2021: 9%, 18%, 9% 2030: 9%, 18%, 6% 2040: 9%, 18%, 4% 2050: 9%, 18%, 3%	Fossil 2021: 70%, 70% 2030: 70%, 49% 2040: 70%, 34% 2050: 70%, 24%	Electric 2021: 18%, 70%, 18% 2030: 18%, 70%, 13% 2040: 18%, 70%, 9% 2050: 18%, 70%, 6%
	With spatial variation		Scenarios: Current electric and fossil share -30% per decade Current fossil fuel share No spatial variation			
Weight of electric compared to conventional	Variable: From same up to 3 times fossil		Constant ratio 1.5		Constant ratio 1.5	
Studded tyre season	Same for all years.		-20% per decade		-20% per decade	
Exhaust	HBEFA, but not considered in scenarios		HBEFA: -5% per year		HBEFA: -5% per year	
Share PM2.5	20% of PM10 based on observations at five sites		From NORTRIP: 15% to 18%		From NORTRIP: 13% to 15%	
Vehicle km's driven	Same all years		+9% per decade		+12% per decade	

Stockholm

Methods Stockholm

The health impacts of PM exposure with an increased share of electric vehicles is compared with a present situation (2022) with 14% of all passenger cars being electric.

Of specific interest is the to assess the importance of the

- share of studded winter tyres by conventional and electric vehicles
- reduction in emissions from electric vehicles of wear particles from brakes
- electric vehicles on road and tyre wear due to their higher weight compared to conventional cars.

The model domain for Stockholm is the “Greater Stockholm metropolitan area” (35 km x 35 km, Figure 77) with horizontal resolution 500 m including 1.86 million inhabitants in 2020. All modelling of emissions and dispersion are done using the same meteorology, i e year 2022, with hourly time resolution.

Separate model runs were made with the NORTRIP model to determine the contributions both to the emissions and concentrations from all vehicles, only passenger cars and only electric passenger cars. In addition, for each vehicle category the contributions from road wear, brake wear, tyre wear and suspension were determined separately. Three separate emission inventories with different shares of studded winter tyres were constructed in order to assess the importance of studded tyres for the road wear. By combining different vehicle and wear contributions it was then possible to assess the importance of electric vehicles and associated road, tyre and brake wear depending on studded tyre shares to the total PM10 and PM2.5 population exposure.

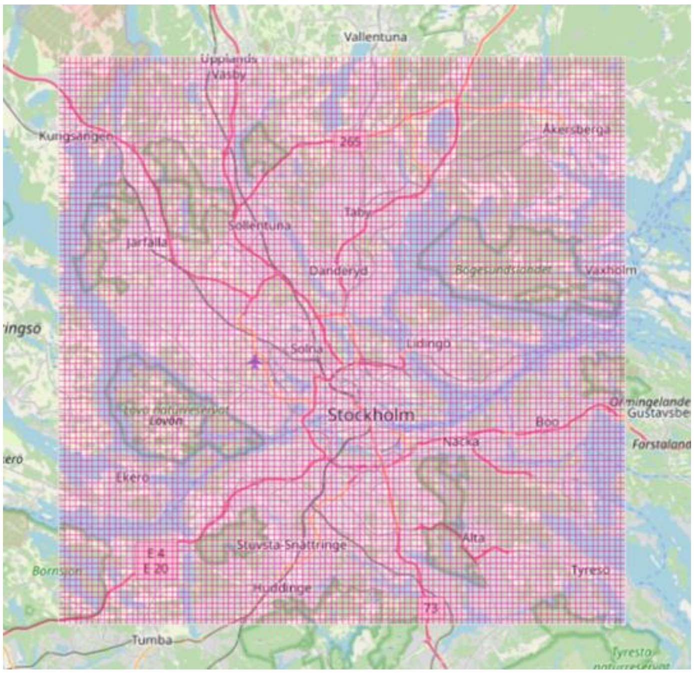

Figure 77. Greater Stockholm, 35 km x 35 km.

Emissions

The NORTRIP emission model has been implemented in the Airviro system (https://www.airviro.com/airviro/) and used in several projects to obtain population exposure to PM2.5 and PM10 (e g Yu et al., 2022 and 2023; Svensson et al. 2023). The emission inventory includes local emissions from road traffic (exhaust and non-exhaust), residential wood combustion, energy production, industrial processes, and other sources (eg, off-road machinery, agriculture and shipping). In this region, road traffic is the dominant source of PM2.5 and PM10. Road traffic exhaust emissions were described with emission factors for different vehicle and road types according to the European emission model HBEFA (Handbook Emission Factors for Road Transport), version 4.1.26 Emissions of wear particles were calculated using the NORTRIP model. Settings for all roads:

- No sanding
- No dustbinding
- Salting, cleaning, ploughing were active through the built in weather dependent rules

The total number of vehicles on all roads are the same in all scenarios and it is based on the vehicle emission database of the Eastern Sweden Air Quality Association (Säll, 2021) with traffic data 2022. The emission data base contains information of the average diurnal, weekly and seasonal traffic variation, the share of light and heavy vehicles, speed and tyre type based on measurements and estimations (see also Svensson et al., 2023). Only roads with more than 4000 vehicles were included in the emissions. Then the total number of kilometres driven by all vehicles in this area 2022 is 7128 million vehicle kilometres and the total emission of PM10 is 1767 tons per year giving an overall emission factor of 248 mg PM10/km.

Vehicle fleet and share electric 2022, 2030, 2040, 2050

The default vehicle fleet composition in the emission database 2022 (based on registered cars in traffic) and forecasted for 2030 according to the Swedish Transport Administration is shown in Figure 78. In 2022 and 2030 14% and 34%, respectively, of all vehicles are electric passenger cars according to this database. The Swedish Government Official Reports SOU 2021:48[3] present three scenarios of the share of electric cars 2030, 2040 and 2050 - low, middle and high (Figure 79).

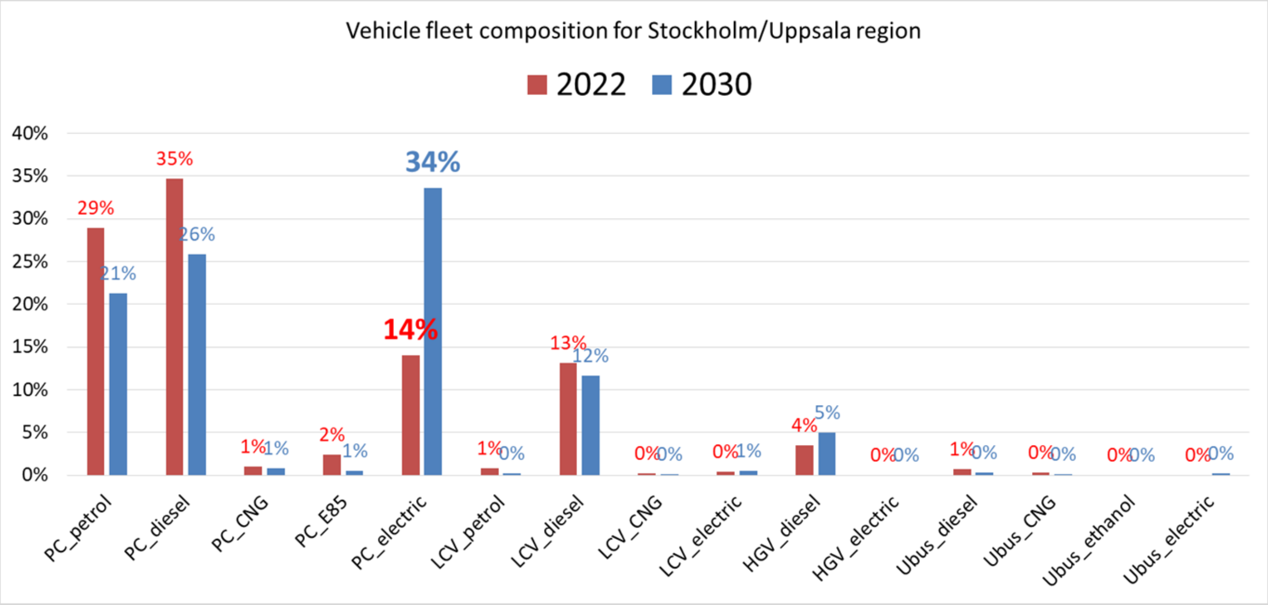

Figure 78. Vehicle fleet composition in the emission database for the modelling in Greater Stockholm. PC = passenger cars, LCV = light commersial vehicles, HGV = heavy goods vehicles, Ubus = urban buses, CNG = compressed natural gas, E85 = ethanol with 15% gasoline.

3

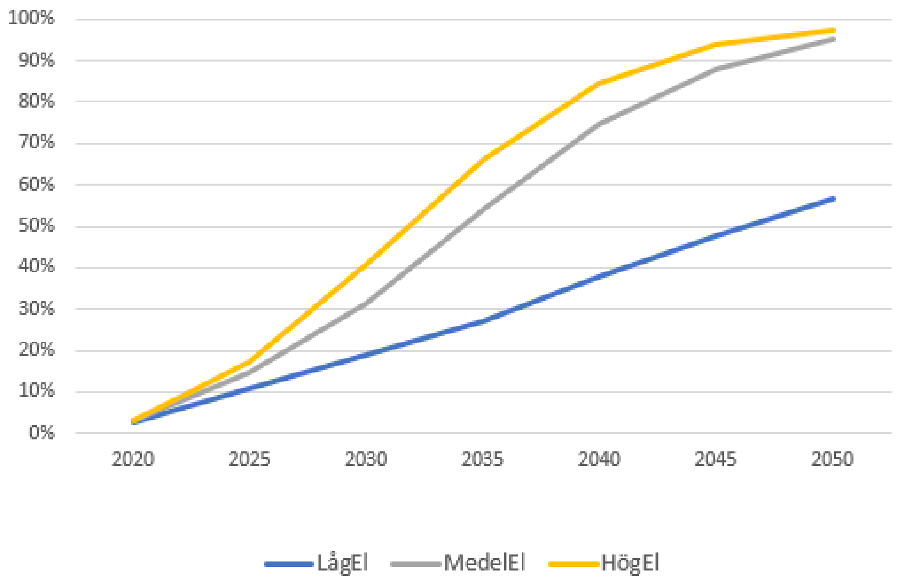

Figure 79. Prognoses of the share of electric cars according to the Swedish Government Official Reports SOU 2021:48. "LågEl", "MedelEl" and "HögEl" refers to three scenarios, low, middle and high, respectively

In this report we have adopted the middle scenario, i.e. 34%, 75% and 95% for the years 2030, 2040 and 2050 respectively. We assume that the total driven km's is the same for all years. As a whole for Sweden transports is expected to increase by around 10%, 20% and 30% by 2030, 2040 and 2050, respectively, compared to 2022 (according to the same report SOU 2021). But the situation in the Greater Stockholm area is different. Since 2002 the traffic in and out of central Stockholm has decreased as can be seen in Figure 80. The political goal is that traffic should have decreased by 30% by 2030 compared to 2017.

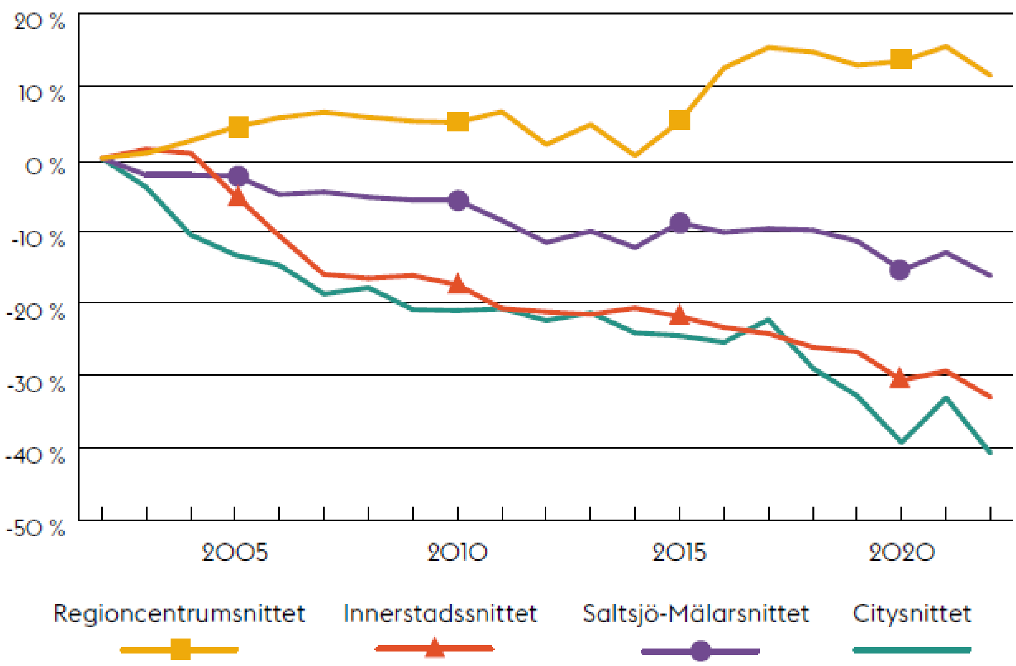

Figure 80. Change in traffic across different parts of Greater Stockholm 2002 – 2022. "Regioncentrumsnittet" = regional parts outside metropolitan area; "Innerstadssnittet" = inner city of Stockholm; "Saltsjö-Mälarsnittet" = across city from south to north or north to south; "Citysnittet" = central metropolitan area.

Share of studded tyres

The most important factor affecting the emissions of PM10 is the share of studded winter tyres. The shares of studded tyres vary in the model domain as shown in Figure 81. The data for the present case is based on manual counting along some key roads in the inner city and along larger roads outside the city. The counting is based on the difference in the sound of around 100 individual vehicles passing by with or without studded tyres.

The share of studded tyres on electric vehicles is not regularly checked in Sweden. According to one manual counting in February 2023 along one inner city road (Sveavägen) the share of studded tyres on electric cars is 16% compared to 30% for conventional cars.

The shares of studded tyres on parked cars in Trondheim were 10% and 23% for electric and conventional cars, respectively in 2021 (Tore Berg, personal communication). For 2022 Trondheim recorded 9% and 25% respectively. In Helsinki a survey for Helsinki residents in spring 2023 showed 18% studded tyres on electric compared to 69% and 65% on petrol and diesel vehicles respectively (Anna Stojiljkovic, SYKE, personal communication). It could also be that the lower share on electric vehicles is connected with the fact that these cars are new, and that all new cars have lower shares of studded winter tyres.

Anyway, it seems clear that studded tyres are not used as frequently on electric vehicles as on the present conventional car fleet. The domain weighed mean shares are 47% and 23% for the present case 2022 and a case with half the share is shown in Figure 81. In addition, a case with one third of present share of studded tyres is applied and this case correspond to 16% as a domain weighted share.

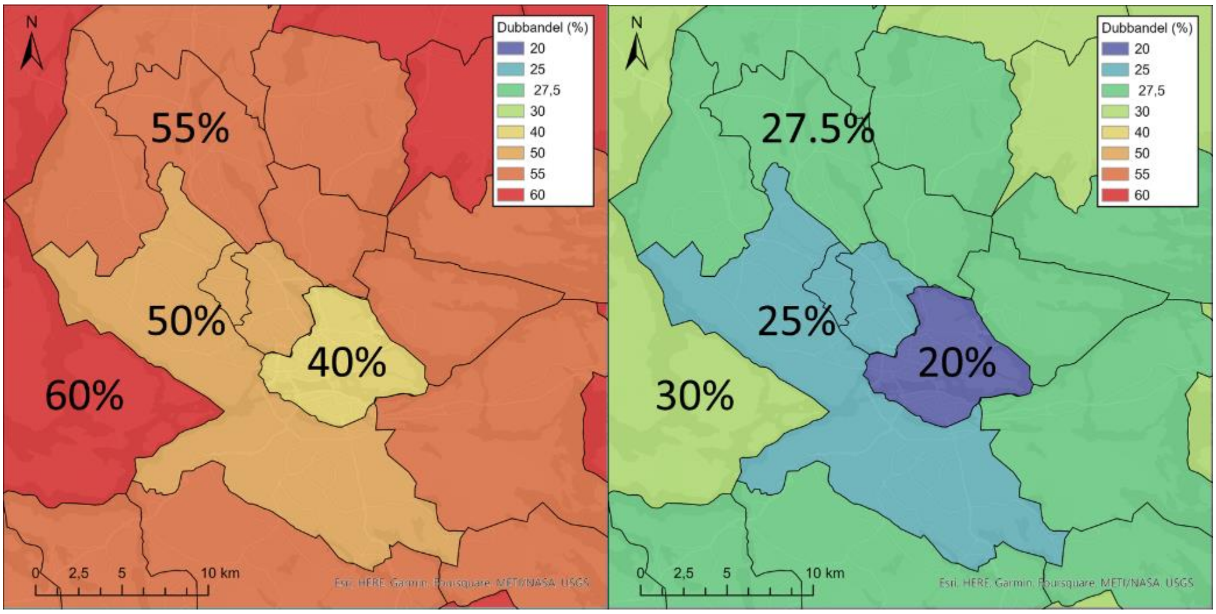

Figure 81. Share of Studded tyre among passenger cars for present case (left), for a case with half of the share in the present case (right) as implemented in the emission database and used for calculating the contribution of studded tyres from the road wear of passenger cars.

Tyre and road wear

According to a survey and interview study by VTI (Mirzanamadi and Gustafsson, 2022) approximately 33% of private users and 12.5% of professional users experienced faster tyre wear in their electric vehicles (EVs/HEVs/PHEVs), compared with tyre wear in conventional (ICEVs) vehicles. Most professional users (taxi, bus transport and car rental companies) experience similar tyre wear as for ICEVs. Vehicle acceleration and weight are the two most commonly mentioned reasons for faster tyre wear, while driving behaviour is the most commonly answered reason for slower tyre wear, compared to tyre wear in ICEVs.

Studies have shown that non-exhaust emissions from electric vehicles are similar to or higher than conventional non-studded vehicles despite lower brake wear (Soret et al., 2014; Timmers and Achten, 2016). Non-exhaust emissions due to both tyre and road wear increase with weight of the vehicle as shown by Liu et al. (2021) for non-studded tyre vehicles on urban, rural and motorways in the UK. Higher PM2.5 non-exhaust emissions were found for EVs compared to corresponding ICE passenger cars if regenerative braking was not taken into account. But when accounting for the lower emissions from brake wear associated with 50% and 100% regenerative braking they concluded that PM2.5 emissions from EVs were lower than corresponding ICEs for all roads and weight classes ("small", "medium" and "large").

To our knowledge are there no published studies comparing road wear as a function of weight of the vehicles when studded tyres are used. Extrapolating data from the road simulator at VTI (See WP2) shows that 50% higher load (from 350 kg to 525 kg) on the axes of the 4 wheels with studded tyres increases the emission by approximately 60% if the speed of the wheels is 60 km/h. At 40 km/h the emission to increase by approximately 20% when the load increases by 50%. As part of WP2 there are also data on the relation between emissions behind the rear wheel and speed and weight of the vehicle during periods with heavy and low dust (see WP2).

For the modelling presented in the results below it was assumed that the road and tyre wear increase linearly and proportionally with the weight of the cars.

Brake wear

Regenerative braking of electric cars can effectively reduce brake wear emissions. But the effect on the emissions will be depends on many factors. Liu et al. (2021) evaluated the effects on emissions using 0%, 50% and 100% less brake wear. In this study default has been 50% less brake wear from electric vehicles but the sensitivity of this assumptions is also assessed.

Weight of cars

As pointed out above the weight of vehicles influences the emissions associated with tyre and road wear. The average weight of plug-in electric and conventional (mean of diesel and gasoline weighted by the number of diesel and gasoline cars in traffic) cars in Sweden during 2017 to 2022 is shown in Figure 82. The difference in weight between the electric and conventional vehicles has increased from 274 kg in 2017 to 417 kg in 2022 (or from 18% to 27% heavier electric vehicles compared to conventional). Making a simple linear extrapolation shows that the electric vehicles would be 47% heavier than conventional by 2030 (739 kg heavier), but this may of course not be true since there are tendencies that the batteries are becoming lighter.

Figure 83 shows more information of the weights of several different passenger car types. The heaviest car is the plug-in hybrid electric car. It should be noted that in 2021 new diesel cars sold were heavier than new electric cars. Mean weight of diesel cars was 2100 kg and mean weight of electric plug-in was 1960 kg. Weight of all cars sold in 2021 was 1800 kg. This means that as the fleet is exchanged, the relative difference in mean weight of electric and diesel cars will decrease, but at the same time less cars sold will be diesel and gasoline, and more be electric. Prognoses of share of electric cars used here is shown in Figure 79.

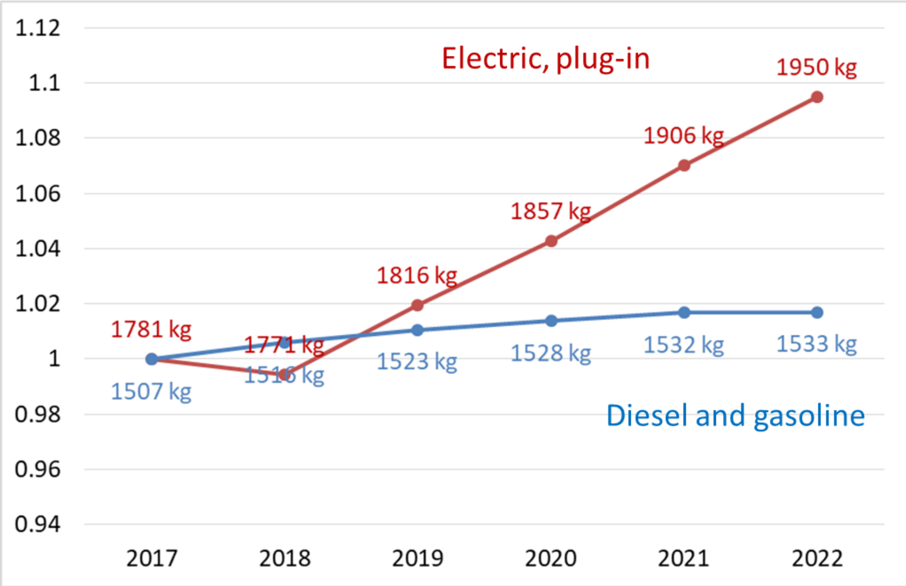

Figure 82. Weight of EVs in Sweden compared to gasoline & diesel passenger cars. (data from Transport Analysis, https://www.trafa.se/en/tags/statistics/).

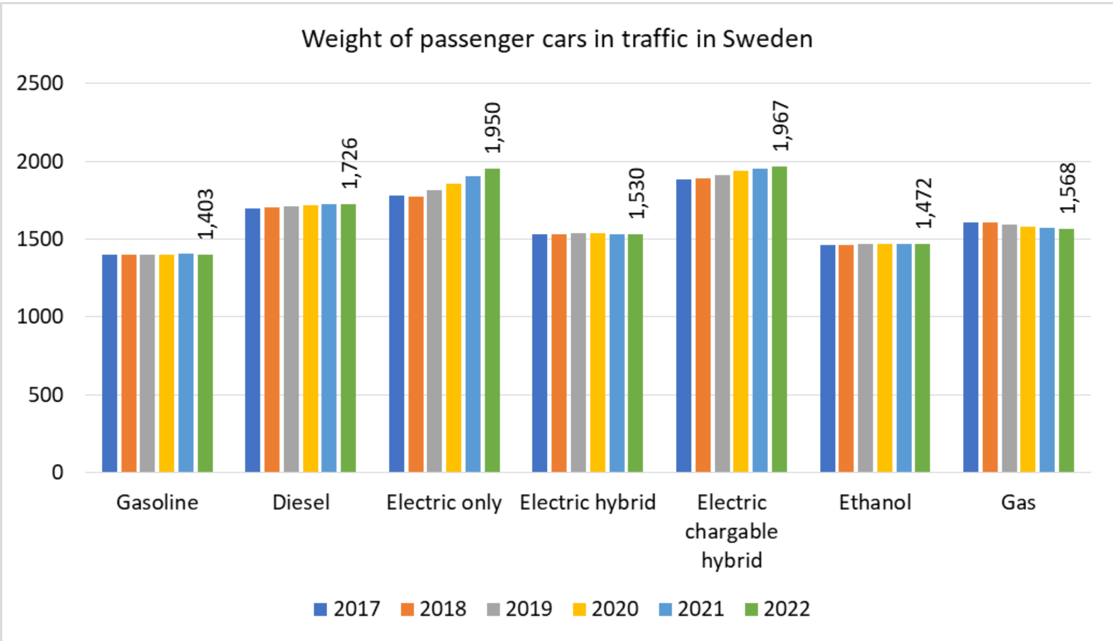

Figure 83. Weight of several vehicle types in Sweden 2017 to 2022 (data from Transport Analysis, https://www.trafa.se/en/tags/statistics/).

Dispersion modelling and population exposure

A Gaussian air quality dispersion model and a wind model, both part of the Airviro air quality management system described elsewhere (e g Segersson et al., 2017) has been used to obtain ambient concentrations across the model domain at 500 m horizontal resolution. Meteorological data for the wind model were taken from a 50-m mast in Högdalen in southern Stockholm. The diagnostic wind model produces a wind field over the model domain considering the effects on the wind and stability of different land use and topography. Concentrations represents 2 m above ground or roof-top where buildings are present. Street canyon effects are not considered.

A population weighted annual average concentration is obtained based on the annual average concentrations in the grid cells times the number of inhabitants in the cells and dividing by the total number of inhabitants in the domain. Population data (residential address) were from 2020 and the resolution was 100 m x 100 m.

Health impacts

The change in health impact is estimated as (Marteneis et al., 2015):

$$\Delta Y = Y_o \cdot (1 - e^{-\beta \Delta x}) \qquad (7)$$

Where

ΔY = change in health outcome

Y_o = baseline incidence

β = dose-response function (logarithm of relative risk)

Δx = change in population weighted exposure concentration.

The baseline mortality for Stockholm is 1329 per 100 000 inhabitants. The relative risk is taken from the epidemiological study of Turner et al. (2016), i e 1.26 (95% CI: 1.19 – 1-34) for PM2.5 per 10 µg/m^3. This is the value recommended to be used to quantify impacts of road traffic emissions on chronic mortality in Sweden (Forsberg et al., 2022). Other health outcomes that are recommended to be assessed are daily mortality, myocardial infarction, stroke, lung cancer, dementia, diabetes, COPLD, asthma and premature birth.

PM2.5 share of PM10

Since the relative risks are expressed per µg/m^3 PM2.5 we need to estimate the annual mean share PM2.5 of PM10. Mean values from observations of the net ratio (i e only local road traffic emissions included without background) of PM2.5 to PM10 at 5 different sites in Stockholm (using different types of instruments) shows that PM2.5 is around 20% of PM10 (Figure 84). This includes all non-exhaust and exhaust emissions from the road traffic.

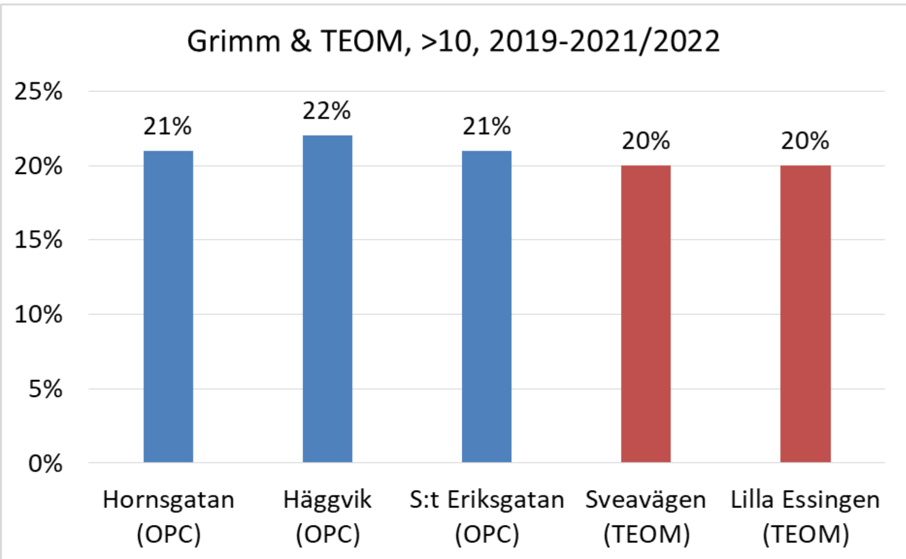

Figure 84. Share of PM2.5 of PM10 from observed net concentrations at 5 different locations in Stockholm.

The NORTRIP model was run on data from Hornsgatan in Stockholm for the years 2016 – 2019 and average contributions to PM10, PM2.5 and coarse particles are shown in Figure 85. It can be seen that 15% of PM10 in suspended dust is PM2.5. Corresponding shares in road wear, tyre wear, brake wear, road salt, CMA and exhaust are 8%, 10%, 62%, 8%, 8% and 100% respectively.

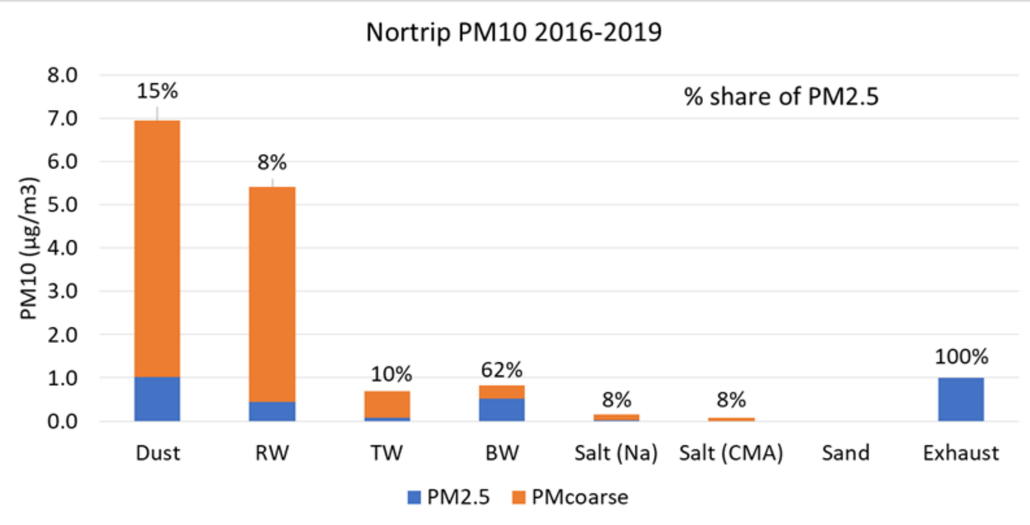

Figure 85. Average contributions to PM10 (divided in fractions that are 2.5 and 10 – 2.5 µm) and percent that is PM2.5 for the different emissions. Calculations according to the NORTRIP model for Hornsgatan 2016 to 2019. Dust = suspended road dust, RW = road wear, TW = tyre wear, BW = brake wear, Salt (Na) = sodium chloride from salting, Salt (CMA) = calcium magneium acetate and Exhaust = vehicle exhaust PM (from HBEFA).

A comparison of the modelled share of PM2.5 and observed based on the ratio of the incremental concentrations of PM2.5 and PM10 at Hornsgatan and urban background, i e:

$$Observed\ \frac{PM2.5}{PM10} = \frac{PM2.5_{Hornsgatan} - PM2.5_{urban\ background}}{PM10_{Hornsgatan} - PM10_{urban\ background}}$$

The share varies from a few percent, with low ratios (below 20%) during periods with high PM10 emissions associated with large road dust emissions and high ratios during periods when exhaust emissions dominate the local PM10 concentration. Generally, the agreement is good but there are systematic deviations as can be seen in Figure 86 and Figure 87.

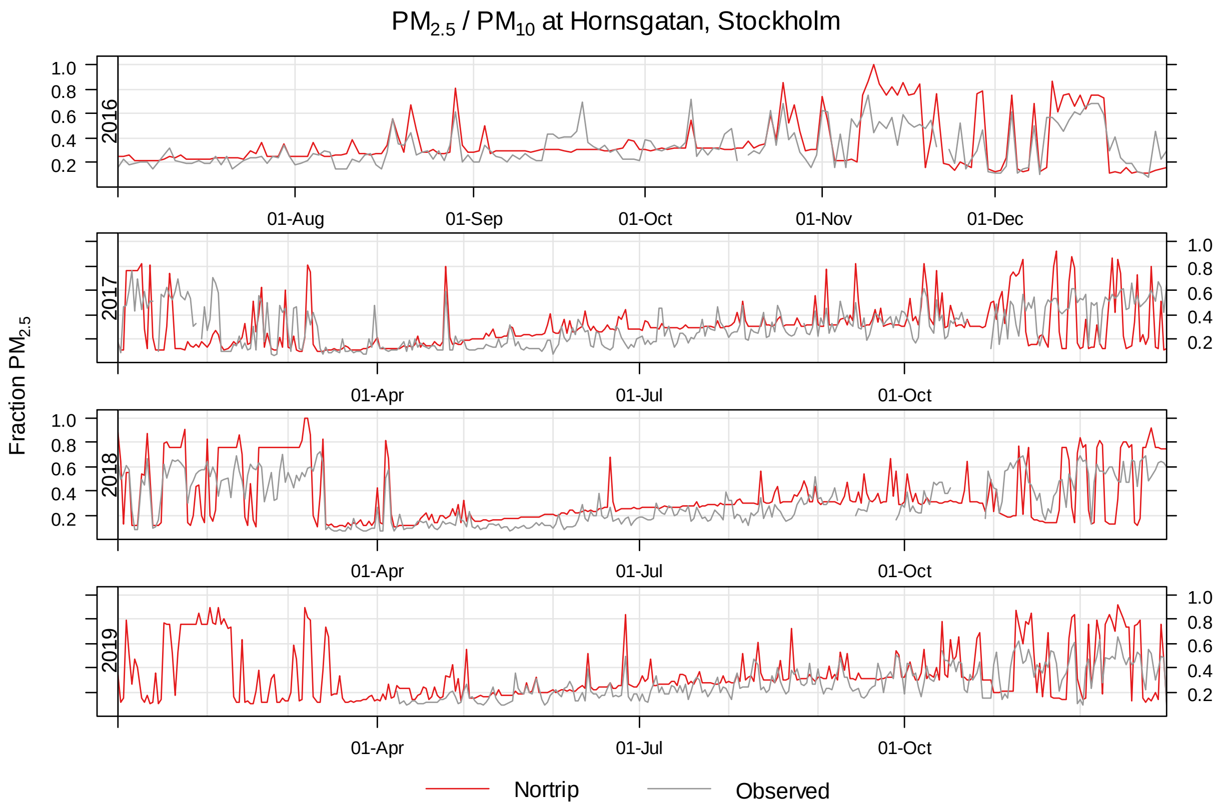

Figure 86. Variation of the share of PM2.5 of PM10 during 2016, 2017, 2018 and 2019 on Hornsgatan in Stockholm according to the NORTRIP model (red) and according to the measured ratio of incremental concentrations of PM10 and PM2.5 in the street canyon (grey). Daily mean values.

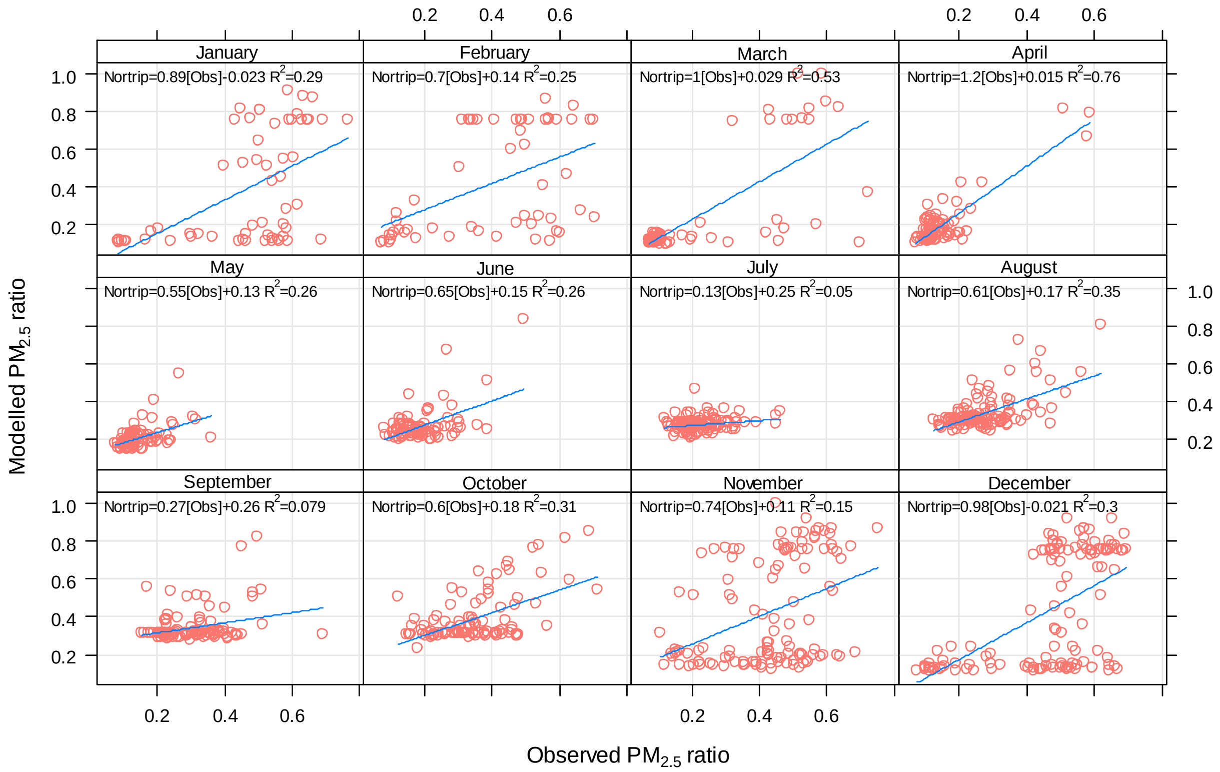

Figure 87. Scatterplots of modelled versus observed PM2.5 / PM10 ratio (based on daily mean concentrations) for all data 2016-2019 at Hornsgatan.

Results Stockholm

The spatial variations in the annual mean (for the year 2021) contributions to PM10 from road traffic emissions based on the NORTRIP model is shown in Figure 88. When all local and non-local sources are included comparison of the calculated levels with measurements of daily mean values at a traffic monitoring site and 2 urban background sites have shown R2 values of 0.90 for PM10 and 0.97 for PM2.5 (Yu et al., 2022).

It is important to note that all concentrations in the figures below are due to local road traffic emissions only – relative effects on total PM10 concentrations will be smaller.

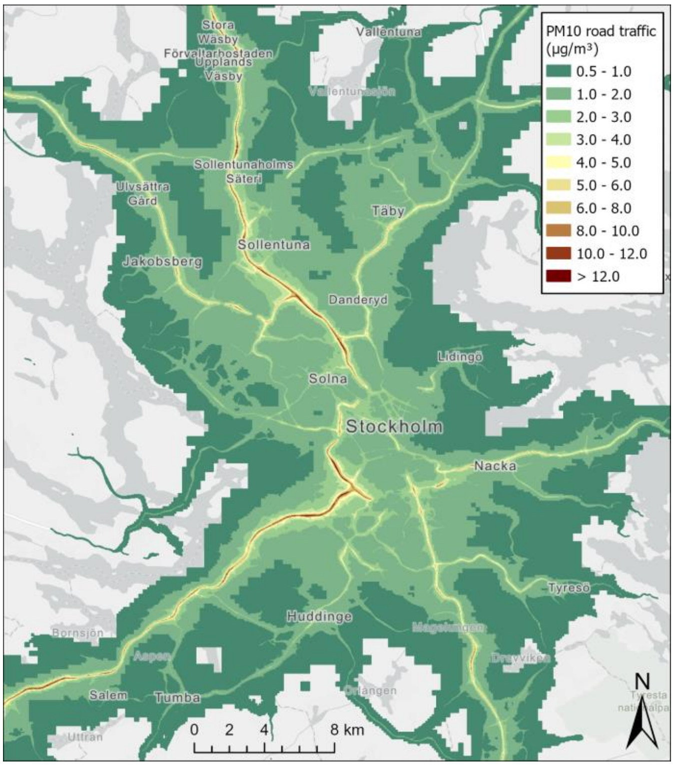

Figure 88. Annual mean concentrations of PM10 due to road traffic emissions 2021 in the Greater Stockholm area.

Contributions from road, tyre and brake wear

As can be seen in Figure 89 road wear is the most important source of PM10, irrespective of vehicle type. This is based on the emissions 2022 with a studded tyre share of 47% (Figure 81) and 17% of all passenger cars being electric. Around 10% of the wear comes from the electric vehicles. For all passenger cars the contributions to PM10 are 90%, 6% and 4% from road wear, tyre wear and brake wear respectively. For other vehicles road, tyre and brake wear contribute with 80%, 12% and 8% to PM10, respectively. Exhaust emission is only 2% of all PM10 emissions from passenger cars in 2022.

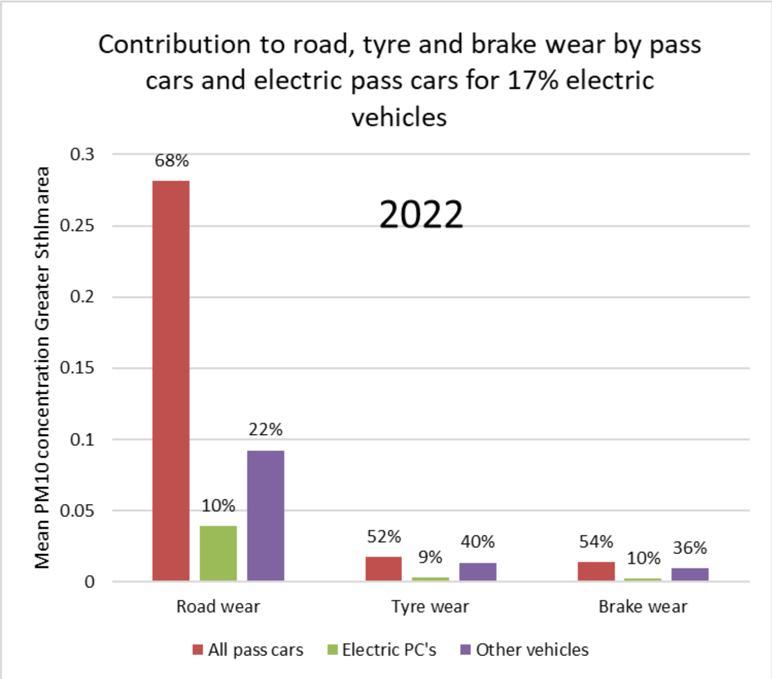

Figure 89. Contributions to the annual mean PM10 concentration in the Greater Stockholm area from different vehicle types road wear, tyre wear and brake wear based on the emission database 2022.

Figure 90 shows the change in PM2.5 concentrations with increased share of electric cars 2022, 2030, 2040 and 2050 (assuming 14%, 34%, 75% and 95% electric cars) if

road and brake wear increase in proportion to the weight and (i e 50% higher wear by electric cars) and there is 50% less brake wear emissions from electric vehicles and the domain weighted studded tyre share is 47%, 23% or 16% with the spatial variation as shown in Figure 81.

In the cases with the same studded tyre share on electric cars as on conventional cars the concentrations increase with 4%, 10%, 23% and 29% for 14%, 34%, 75% and 95% electric cars, respectively (Figure 90). The exposure concentrations will decrease with increasing electric vehicle share if the share of studded tyres on electric vehicles is lower than on conventional. With a share on electric cars that is one third of that on conventional the concentrations are 3% to 20% lower for electric car shares of 14% to 95%. This is mainly due to the decreased influence of road wear (due to less studded tyres) despite the effect on road wear of the higher weight of electric vehicles. Right panel in Figure 90 shows changes in PM2.5 exposure if the RW and TW by electric cars is the same as diesel/gasoline cars. If in this case the amount of studded tyres is only one third on electric cars the exposure will be 5%, 12%, 26% and 33% lower with 14%, 34%, 75% and 95% electric cars, respectively.

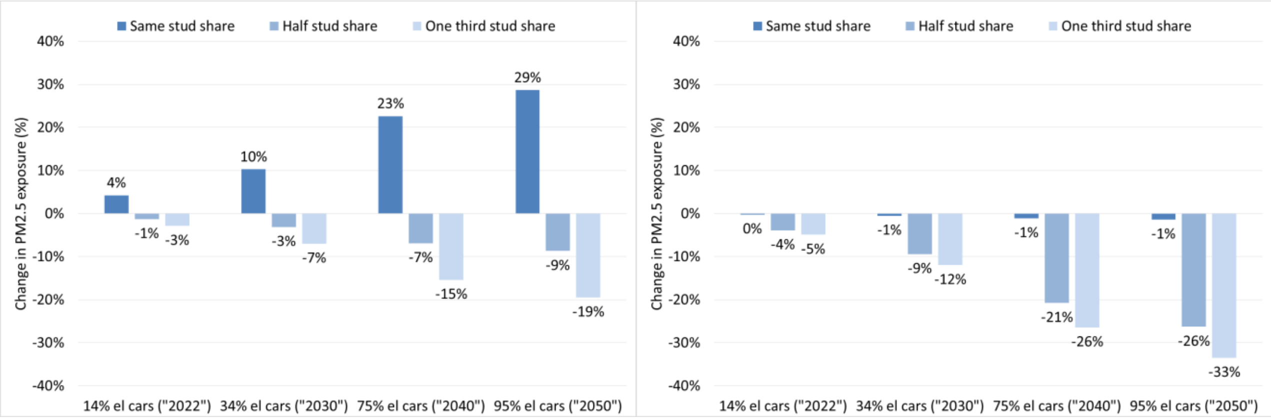

Figure 90. Change in population weighted PM2.5 concentrations for different shares of electric passenger cars depending on corrections of higher wear and/or lower studded tyre share by electric cars. Left panel shows changes assuming 50% higher RW and TW by electric cars as diesel/gasoline cars. Right panel shows changes assuming the same RW and TW by electric cars as diesel/gasoline cars.

Other factors that influence the trend in total PM2.5 and PM10 concentrations

Other factors that influence the future total concentrations are trends in the:

- number of vehicles on different roads
- exhaust emissions
- other local emissions, e g residential wood burning
- contribution from non-local sources

The number of vehicle kilometres driven may increase by 30% until 2050 compared to 2020 according to linear extrapolations made by The Swedish Government Official Reports SOU 2021:48. But for Greater Stockholm the trend may be different in different parts of the region due to the congestion tax and the new environmental zone (see Figure 80). Exhaust emissions is expected to decrease with less diesel vehicles. But this will also depend on the amount of biofuel in diesel. Sweden's policy is to cut its biofuel mandate – less biofuel might increase exhaust particle emissions per kilometre from diesel vehicles. Trends in emissions from residential biomass burning are very uncertain. Non-local sources might decrease due to the decrease in emissions of exhaust particles and precursor emissions (NOx and hydrocarbons) when electric vehicles replace diesel and gasoline vehicles in Europe.

The importance of the correction for larger road wear associated with heavier electric vehicles is also illustrated in Figure 91, where the share of studded tyres on electric passenger cars is half of the share on conventional cars. It can be seen that if the road wear by electric vehicles is less than 50% larger compared to conventional vehicles the PM10 concentration will be creasing with increasing share of electric vehicles.

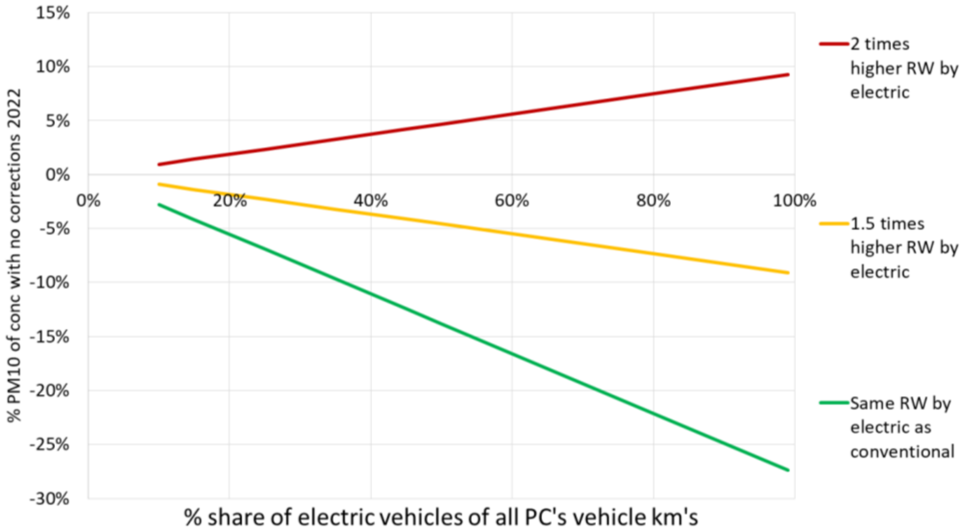

Figure 91. Percent change in PM10 concentration depending on road wear correction and share of electric cars.

As was indicated in Figure 90 the 50% less brake wear did not compensate for the increased emissions due to increased road wear. Figure 92 shows that reduced brake wear has relatively small effect on PM10 concentrations. With 100% electric vehicles that has 50% less brake wear compared to conventional vehicles concentrations are reduced by less than 3%.

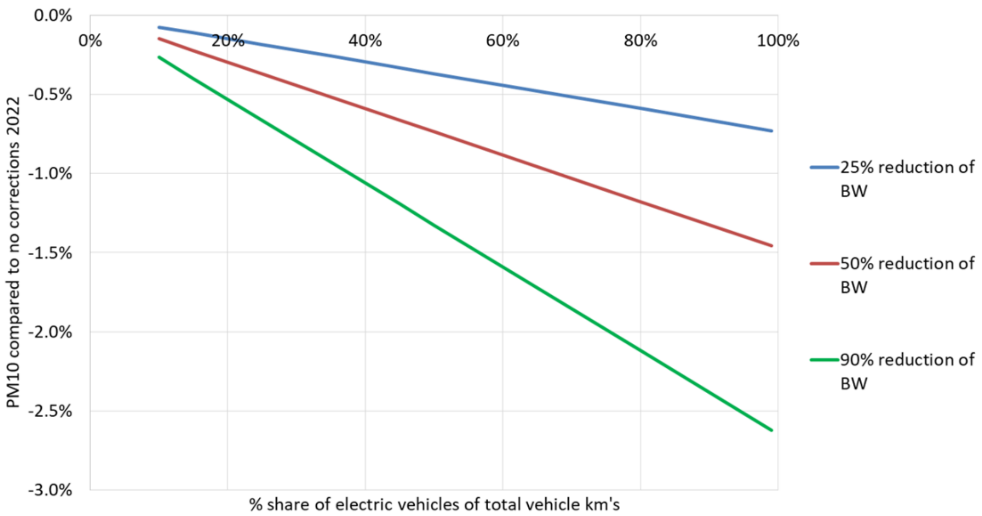

Figure 92. Change in PM10 concentration depending on the share of electric vehicles and reduction in brake wear emissions from electric vehicles.

Impacts on premture mortality

Assuming that 20% of the population weighted PM10 concentrations (Figure 90) is PM2.5 the premature mortalities are calculated according to equation (7). As shown in Figure 93 the number of premature deaths per year could increase by 4, 9, 21 and 26 with 14%, 34%, 75% and 95% electric cars, respectively. This is assuming that the share of studded tyres is the same on electric vehicles as it is on conventional vehicles and with 50% higher road and tyre wear due to the heavier weight of the electric vehicles. But this scenario is not very likely since measurements indicate that the share of studded tyres is much less on electric vehicles compared to conventional. So more likely is that there will be a decrease in the mortality with increasing shares of electric vehicles – in this case there may be 1, 3, 6 and 8 fewer premature deaths per year with only half amount of studded tyres on electric vehicles compared to conventional for 14%, 34%, 75% and 95% electric cars respectively. Or with only one third studded tyre share on electric there would be 3, 6, 14 and 18 fewer premature deaths per year for 14%, 34%, 75% and 95% electric cars.

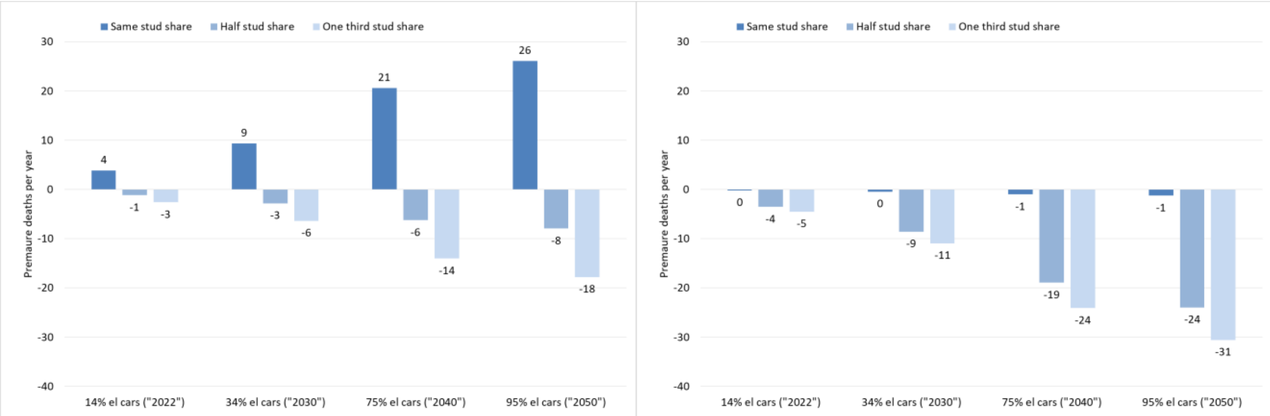

Figure 93. Total number of premature deaths due local road traffic emissions depending on the share of electric vehicles and the share of studded tyres on electric vehicles (see text and Figure 90 for more detailed explanation of the bars).

It can be noted that there will be an break-even point, i e net zero effect on mortality, depending on the larger road and tyre wear by electric cars as illustrated in Figure 94. Independent on the share of electric cars, there will be no extra premature deaths associated with road and tyre wear by electric cars if the wear is 1.75 times higher than conventional cars and assuming that the studded tyre share of electric cars is only one third of that of the conventional cars. In other words, the increased road and tyre wear with studded tyres due to the heavier electric cars is outweighed by the lower share of studded tyres on electric cars compared to fossil fuel cars.

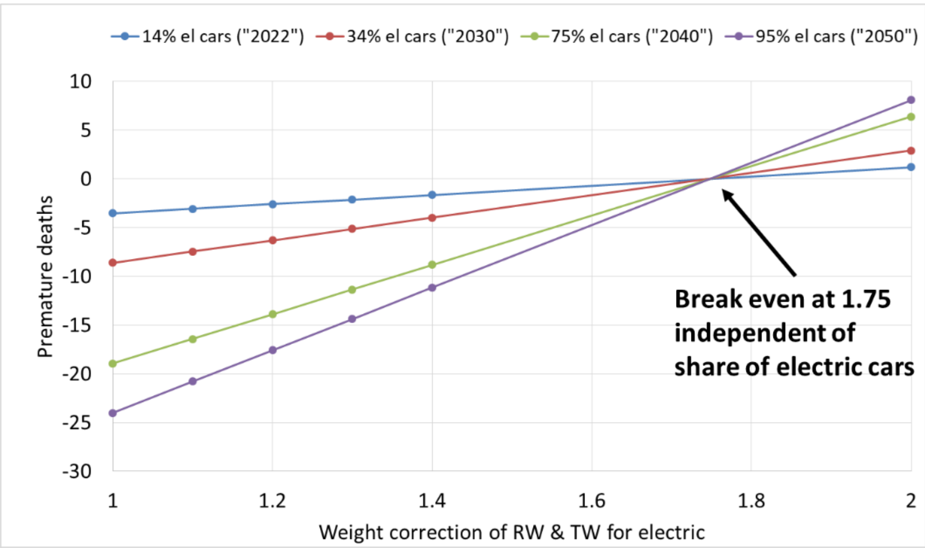

Figure 94. Calculated number of premature deaths depending on weight correction and share of electric cars for the case that the ectric cars have half the share of studded tyres as fossill cars.

Impacts on health related costs/benefits

According to the Swedish REVSEK report (Forsberg et al., 2021) the health costs associated with PM2.5 emission varies for different areas depending on population density etc. The cost of emissions in rural areas was estimated at 392 SEK per kg PM2.5 whereas for large densely populated city centres like Stockholm the cost was estimated to be 33 820 SEK per kg PM2.5 emitted. This cost refers to the year 2017 and includes not only mortality but also daily mortality, myocardial infarction, stroke, lung cancer, dementia, diabetes, COPD, asthma and premature birth associated with exposure to PM.

The cost for large suburban area (“Storstadsförort”) may be representative for the exposure in Greater Stockholm, i e 11 967 SEK per kg PM2.5 or expressed in terms of an exposure concentration 13 500 SEK per µg/m^3 per person. If this value is applied to the Greater Stockholm population weighted PM2.5 concentrations (i e 20% of the PM10 concentration in Figure 90) the health cost will increase by 170, 412, 910 and 1152 million SEK with 14% (2022), 34% (achieved by e g 2030), 75% (2040) and 95% (2050) electric cars respectively, due to increased road and tyre wear and decreased brake wear (Figure 95). But if the share of studded tyres on electric cars is assumed to be only half of that on conventional cars the costs would decrease by 52, 125, 276, 350 million SEK for the different shares of electric cars. And if the share of studded tyres on electric cars is assumed to be one third of that on conventional cars the costs would decrease by 117, 283, 625, 791 million SEK for the different shares of electric cars.

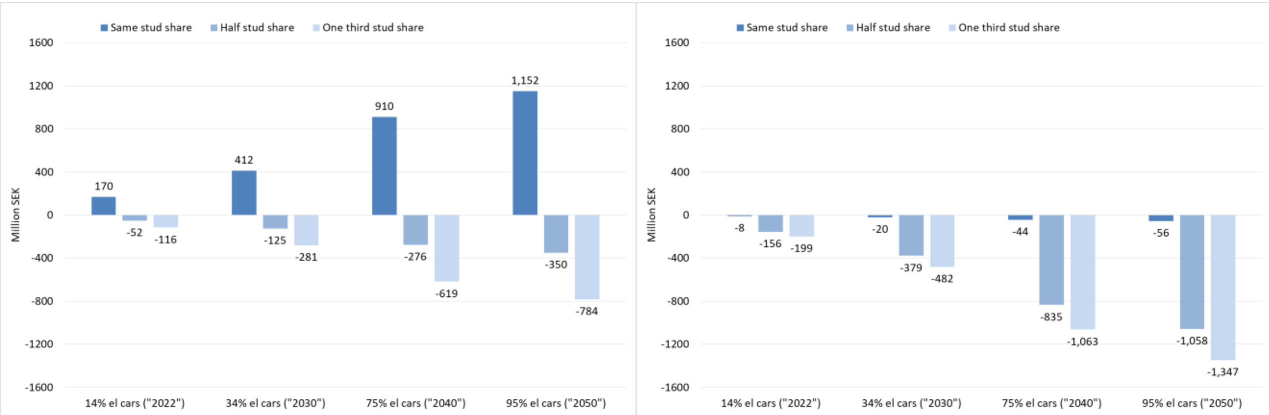

Figure 95. Increase/decrease of health costs with 14%, 25%, 75% or 100% electric cars when RW, TW and BW are corrected (four bars to the left) and also adjusting studded tyre share of electric to half of the conventional cars (four bars to the right).

Conclusions Stockholm

Since most wear comes from road wear (90% for passenger cars) the impact of electric fleet depends mainly on the share of studded tyres on electric cars compared to conventional vehicles and the weight correction for road wear with studded tyres.

Tyre wear and brake wear caused by electric cars has only minor effect on PM10 compared to the effects due to road wear.

With 100% electric cars PM10 can increase if the studded tyre share is the same as on conventional vehicles and road wear is higher due to the heavier weight of electric cars. Decreased brake wear will likely not compensate for the increased road wear.

But more likely is that PM10 will decrease since observations indicate that the studded tyre share on electric vehicles is less than on conventional vehicles. But the decrease depends on the correction of road wear due to the heavier weight of electric cars compared to conventional cars.

In summary more knowledge is needed regarding effects of the heavier weight of electric cars. It is also very important to keep track of the share of studded tyres on electric cars.

The trend in the total PM10 and PM2.5 concentration is uncertain due to several factors, i) total number kilometres driven, which in turn depend on the congestion tax and environmental zone in Stockholm, ii) exhaust emissions, which depend on the biofuel blend in diesel and replacement of diesel vehicles (cars, trucks, buses); iii) trend in other local sources such residential biomass burning, iv) trend in long-range transported particles.

Trondheim

Methods Trondheim

A similar approach as described for Stockholm is also applied to Trondheim. Precalculated emissions and source contributions from 2021 calculations in Trondheim (https://www.miljodirektoratet.no/tjenester/fagbrukertjeneste-for-luftkvalitet) are used as the basis. In these calculations source contributions from within the city are derived for PM10 and PM2.5. The traffic source contributions are then rescaled based on the different emission scenarios.

Scenarios

We investigate the following scenarios for the years 2021, 2022, 2025, 2030, 2040 and 2050:

1. **Reference calculation:** Predicted changes in traffic volumes retaining the current day studded tyre share for fossil and electric vehicles but including the change in fleet makeup.
2. **Studded tyre reduction:** In this case the existing 2021 studded tyre shares are reduced by 30% per decade.
3. **Constant studded tyre share:** In this scenario all personal vehicle types (fossil, hybrid and electric) are allocated studded tyre shares equivalent to the 2021 fossil fuel vehicles.
4. **Reduced studded tyre season:** As an alternative scenario we reduce the studded tyre season by 20% per decade.

Heavy duty vehicles are included in the calculations but no changes are made to these in the scenario runs, with the exception of the reduced studded tyre season that will also impact the heavy duty studded tyre use.

Emissions

Road traffic emissions in Trondheim are modelled using the NORTRIP model. Emissions from other major sources are also included. For this report only the residential combustion emissions are included in the source allocation as these are the only other major source contributor to local PM emissions. A description of the emission sources generally in Norway can be found in Denby et al. (2020).

Share of studded tyres

Studded tyre counting and surveys in Trondheim indicate varying numbers. For the regular modelling in Trondheim studded tyre counts at petrol stations and parking houses in 2019-2020 indicate a studded tyre share for all personal vehicles of 18% and for heavy duty vehicles 10%. Independent counts in 2021 (personal communication Trondheim municipality) indicate a studded tyre share for fossil fuel vehicles of 25% and for electric vehicles 9%. For the current assessment, based on previous modelling, we use a studded tyre share for fossil fuel vehicles, electric vehicles and heavy duty vehicles of 18%, 9% and 10% respectively.

Tyre and road wear

Road wear is determined by the NORTRIP model for the 2021 reference year. Road wear is then adjusted in future years according to the relative changes in vehicle weight. This is assumed to be a linear function of weight. For tyre wear it is assumed in this study that tyre wear for electric vehicles is twice as high as for fossil fuel vehicles, due to both weight differences and differing accelerations. This is slightly different to the approach used for Stockholm where the tyre wear was also linearly dependent on weight, as with road wear.

Brake wear

We assume throughout that brake wear for electric vehicles is 50% of the NORTRIP specified wear factor for fossil fuel vehicles. Similar assumption have been made for Stockholm.

Weight of cars

Weights of fossil and electric vehicles are based on the results provided for Stockholm (Figure 82) and adapted for Trondheim (Figure 96). Hybrids are assumed to have the same weights as electric vehicles. The relative weight of vehicles is assumed to be the same for 2040 and 2050 as for 2030. Relative weights of heavy duty vehicles are unchanged.

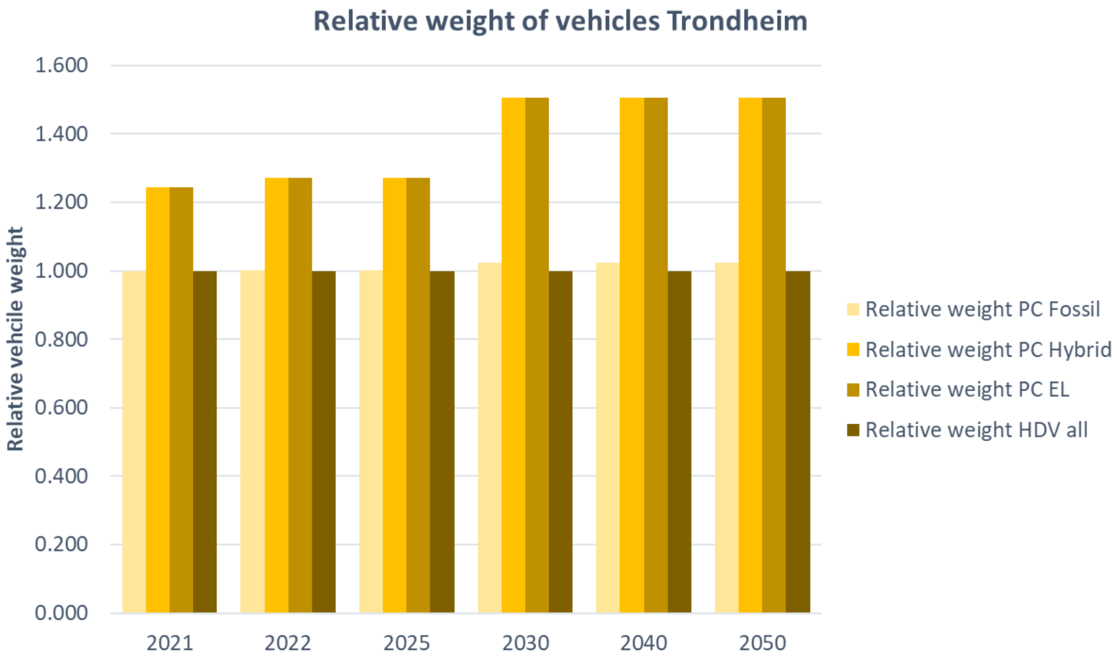

Figure 96. Relative weights of vehicles in Trondheim used in all the emission scenarios for the different years

Vehicle traffic volumes

Predictions for the change in traffic volumes (km driven per vehicle class) are based on the national prognosis from the 2018-2029 National Transport Plan for Norway extended to 2050 (Fridstrøm, 2019). This prognosis is rescaled to the traffic volumes in the municipality of Trondheim. This prognosis indicates an ambitions plan for a 95% electrification of the personal vehicle fleet by 2050, Figure 97. This traffic prognosis is used throughout all scenarios.

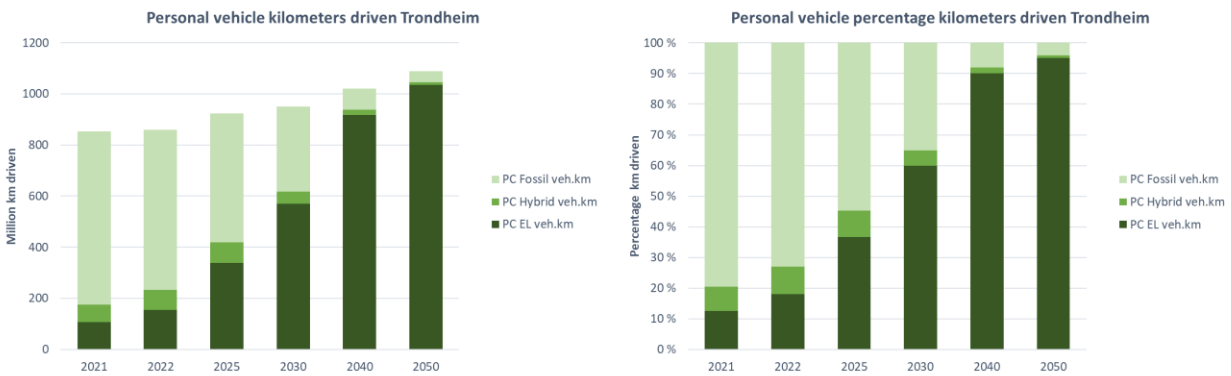

Figure 97. Vehicle kilometres driven by fossil, electric and hybrid vehicles used in the different emission scenarios for the municipality of Trondheim. Left are the total kilometres driven and right the relative, in percent, kilometres driven.

Dispersion modelling and population exposure

Air quality modelling has been carried out using the EMEP/uEMEP modelling suite. This is described in detail in Denby et al. (2020). Calculations for Trondheim can be found at https://www.miljodirektoratet.no/tjenester/fagbrukertjeneste-for-luftkvalitet. Population density is based on home address data aggregated to 100 m, the same resolution as the calculated concentrations.

Results Trondheim

Spatial distribution

Calculated PM10 and PM2.5 maps for Trondheim for 2021 are shown in Figure 98 and Figure 99. These are the same maps that can also be found at https://www.miljodirektoratet.no/tjenester/fagbrukertjeneste-for-luftkvalitet.

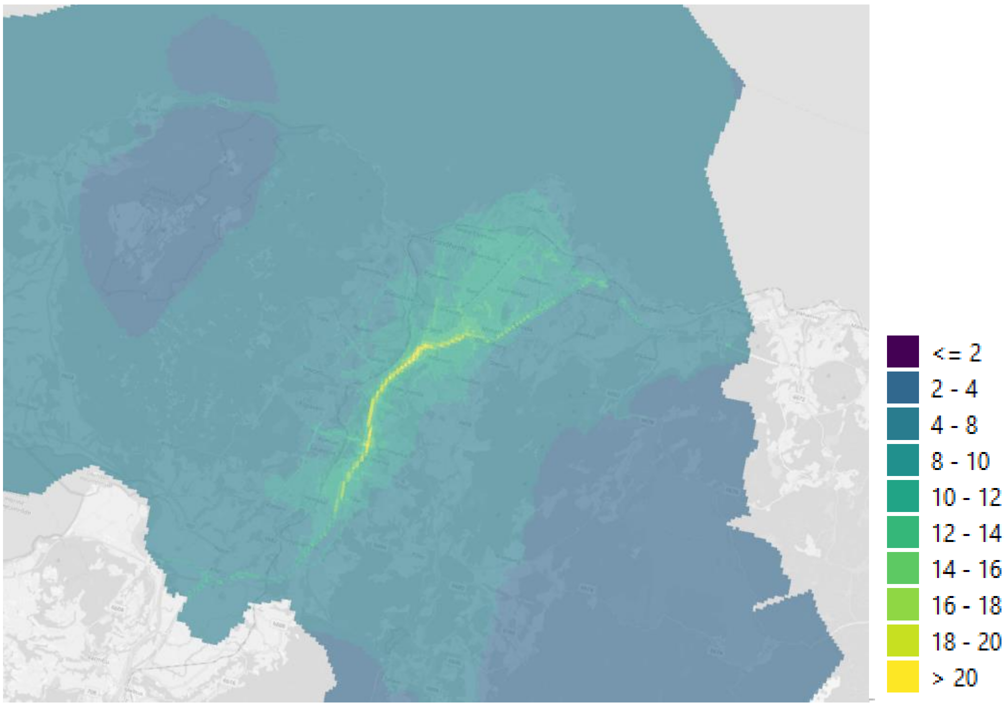

Figure 98. Calculated PM10 concentrations for the Municipality of Trondheim, 2021 annual mean.

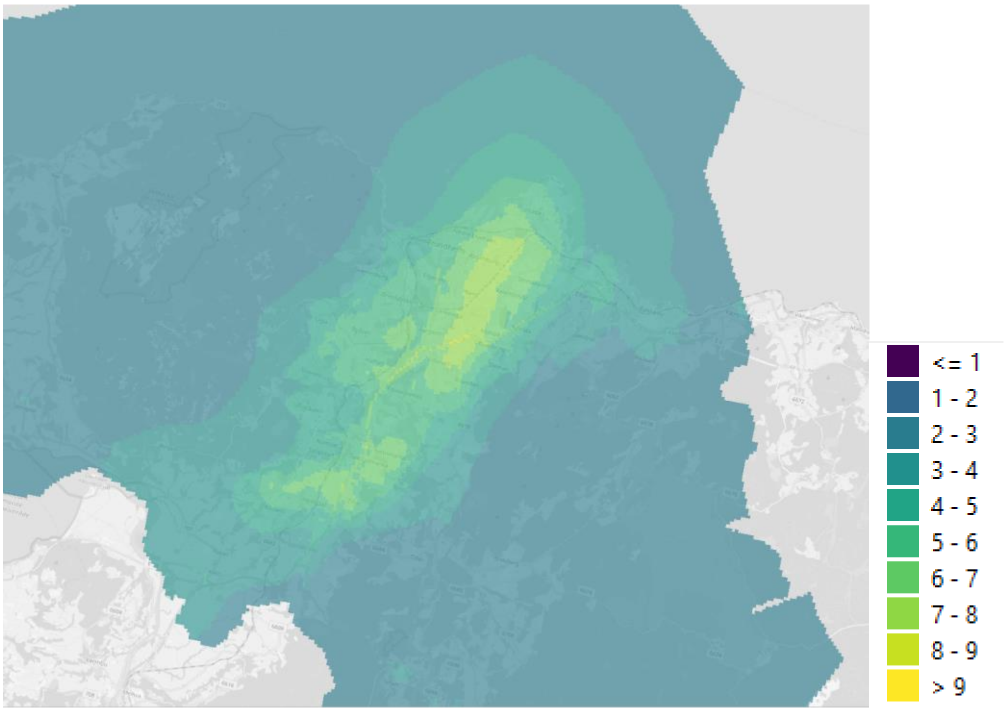

Figure 99. Calculated PM2.5 concentrations for the Municipality of Trondheim, 2021 annual mean.

Scenario 1: Reference scenario

In Figure 100 the complete set of input and output data is shown for the reference scenario. This scenario uses the predicted changes in traffic volumes, retaining the current day studded tyre share for fossil and electric vehicles but including the change in fleet makeup.

Figure 100. Input data and results for the reference scenario (1) for the different years

Scenario 2: Studded tyre reduction scenario

In Figure 101 the complete set of input and output data is shown for the studded tyre reduction scenario. This is the same as the reference scenario but in this case the existing 2021 studded tyre shares are reduced by 30% per decade. This leaves a relatively small share in 2050, 6% for fossil vehicles and 3% for electric.

Figure 101. Input data and results for the studded tyre reduction scenario (2) for the different years

Scenario 3: Constant studded tyre share scenario

In Figure 102 the complete set of input and output data is shown for the constant studded tyre share scenario. This is the same as the reference scenario but in this case all personal vehicle types (fossil, hybrid and electric) are allocated studded tyre shares equivalent to the 2021 fossil fuel vehicles (18%).

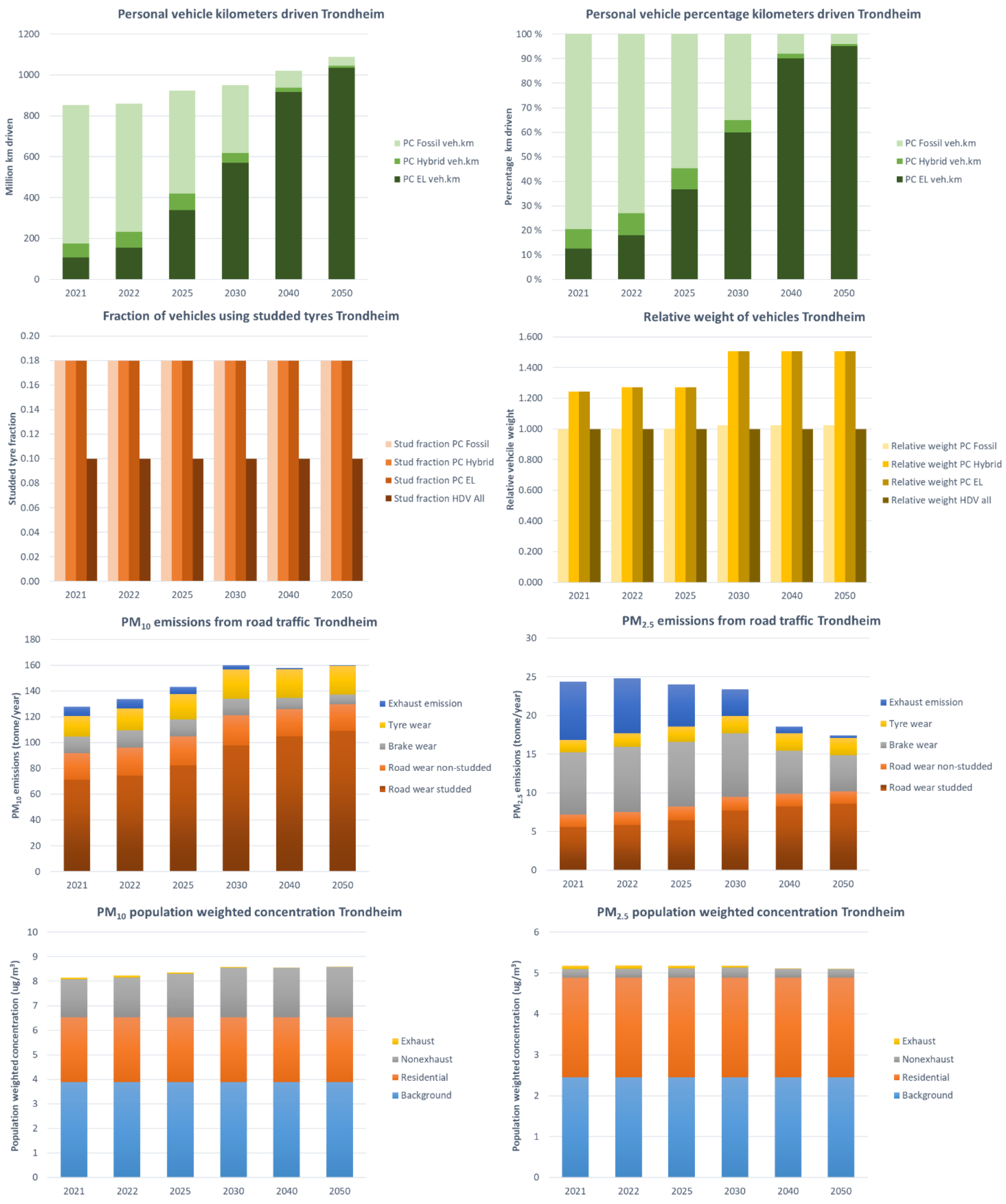

Figure 102. Input data and results for the constant studded tyre share scenario (3) for the different years

Scenario 4: Reduced studded tyre season

In Figure 103 the complete set of input and output data is shown for the reduced studded tyre season scenario. This is the same as the reference scenario, but the studded tyre season is reduced by 20% per decade.

Figure 103. Input data and results for the reduced studded tyre season scenario (4) for the different years

Health impacts

The health impact, in terms of premature deaths per year (see Section on Health impacts) due to PM2.5 non-exhaust emissions, for each scenario and each year is presented in Figure 104. The total population in the municipality of Trondheim is 212 000 inhabitants and the baseline incidence of mortality in Norway is 780 per 100 000 (World Bank, 2021).

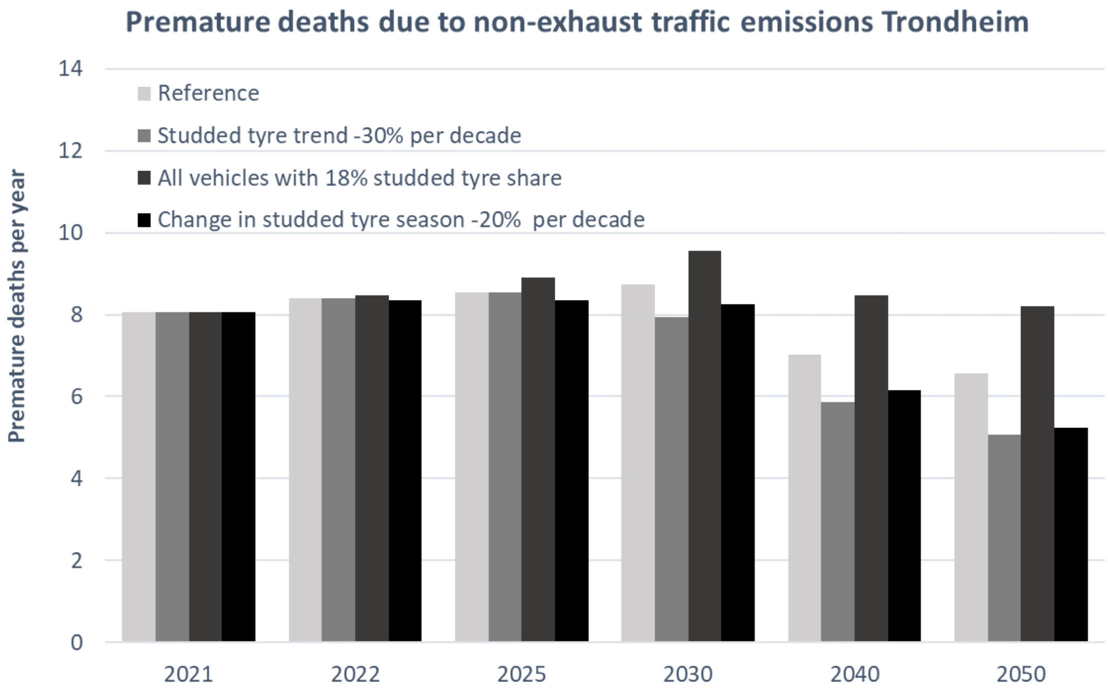

Figure 104. Health impact in terms of premature deaths per year for the 4 scenarios and all years in the municipality of Trondheim.

Helsinki

Methods Helsinki

The same approach as described for Trondheim is applied in Helsinki. However, for Helsinki the NORTRIP and EMEP/uEMEP models have been implemented for the first time. Details concerning this new application are contained in the Modelling work package 7 section of this report. As in the Trondheim calculations, model calculations for emissions and source contributions from 2021 are used as the basis. In these calculations source contributions from within the city are derived for PM10 and PM2.5. The traffic source contributions are then rescaled based on the different emission scenarios.

Scenarios

The scenarios for Helsinki are the same as for Trondheim. In this case the years 2021, 2022, 2023, 2030, 2040 and 2050 are modelled. As in Trondheim the heavy duty vehicles are included in the calculations but in Helsinki these do not use studded tyres.

Emissions

Road traffic emissions in Helsinki are modelled using the NORTRIP model. Emissions from other major sources are also included. For this report only the residential combustion emissions are included in the source allocation as these are the only other major source contributor to local PM emissions.

Share of studded tyres

Studded tyre counting and surveys in Helsinki from 2023 (Anna Stojiljkovic, SYKE, personal communication) provide studded tyre shares for fossil (70%), electric (18%) and hybrid vehicles (48%).

Tyre and road wear

The same assumptions are made in Helsinki as for Trondheim.

Brake wear

The same assumptions are made in Helsinki as for Trondheim.

Weight of cars

The same assumptions are made in Helsinki as for Trondheim. Weights of fossil and electric vehicles are based on the results provided for Stockholm (Figure 82) and adapted for Helsinki (Figure 105). Hybrids are assumed to have the same weights as electric vehicles. The relative weight of vehicles is assumed to be the same for 2040 and 2050 as for 2030. Relative weights of heavy duty vehicles are unchanged.

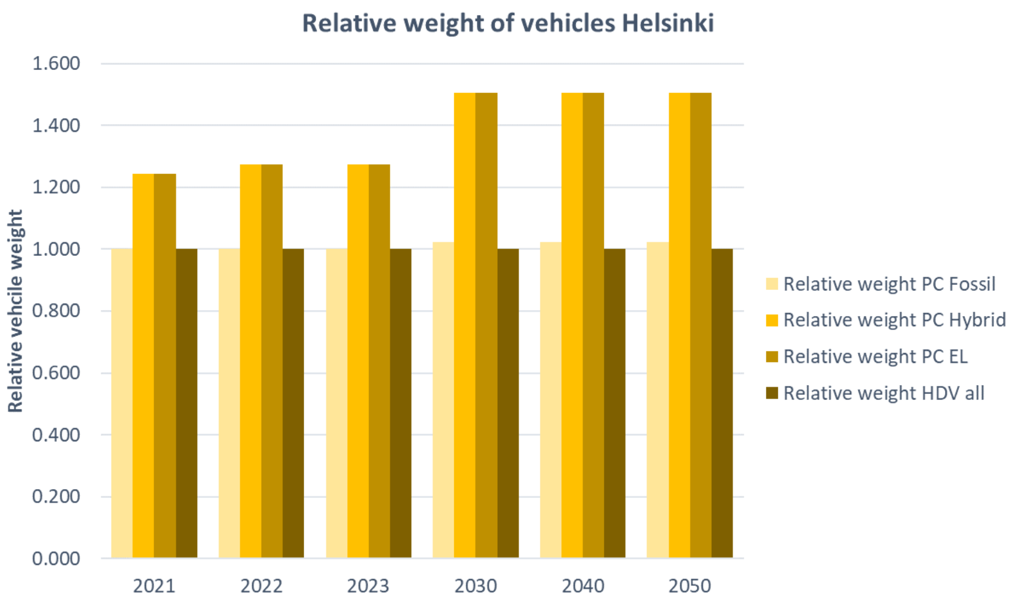

Figure 105. Relative weights of vehicles in Helsinki used in all the emission scenarios for the different years

Vehicle traffic volumes
Predictions for the change in traffic volumes (km driven per vehicle class) are based on the national based prognosis (VTT, 2021; Traficom, 2021). This prognosis is rescaled to the traffic volumes in Helsinki. This prognosis indicates a 63% electrification of the personal vehicle fleet by 2050, Figure 106. This traffic prognosis is used throughout all scenarios.

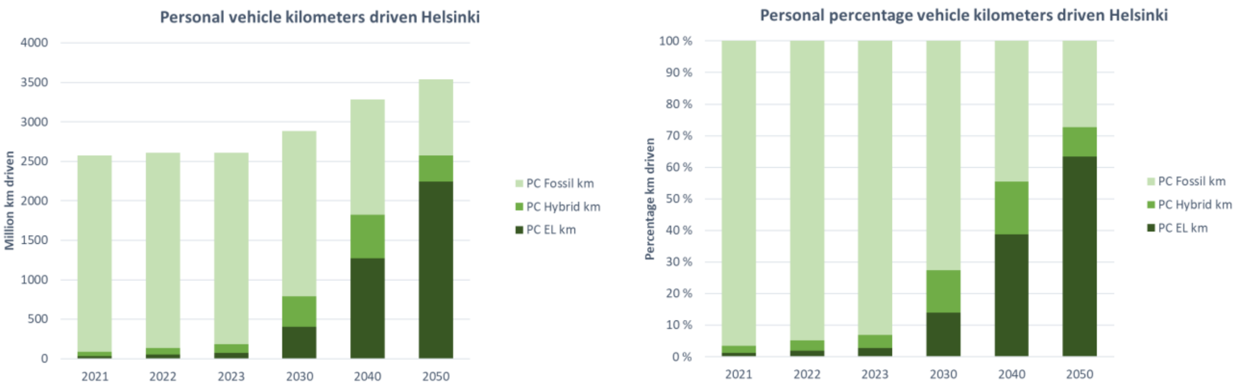

Figure 106. Vehicle kilometers driven by fossil, electric and hybrid vehicles used in the different emission scenarios for Helsinki Left are the total kilometers driven and right the relative, in percent, kilometers driven.

Dispersion modelling and population exposure
Air quality modelling has been carried out using the EMEP/uEMEP modelling suite. The model is described in detail in Denby et al. (2021) and the calculations for Helsinki are described in Work package 7 in this report. Population density is based on home address data aggregated to 100 m, the same resolution as the calculated concentrations.

Results Helsinki

Spatial distribution

Calculated PM10 and PM2.5 maps for Helsinki for 2021 are shown in Figure 107 and Figure 108. These are also presented and discussed in Work package 7 in this report.

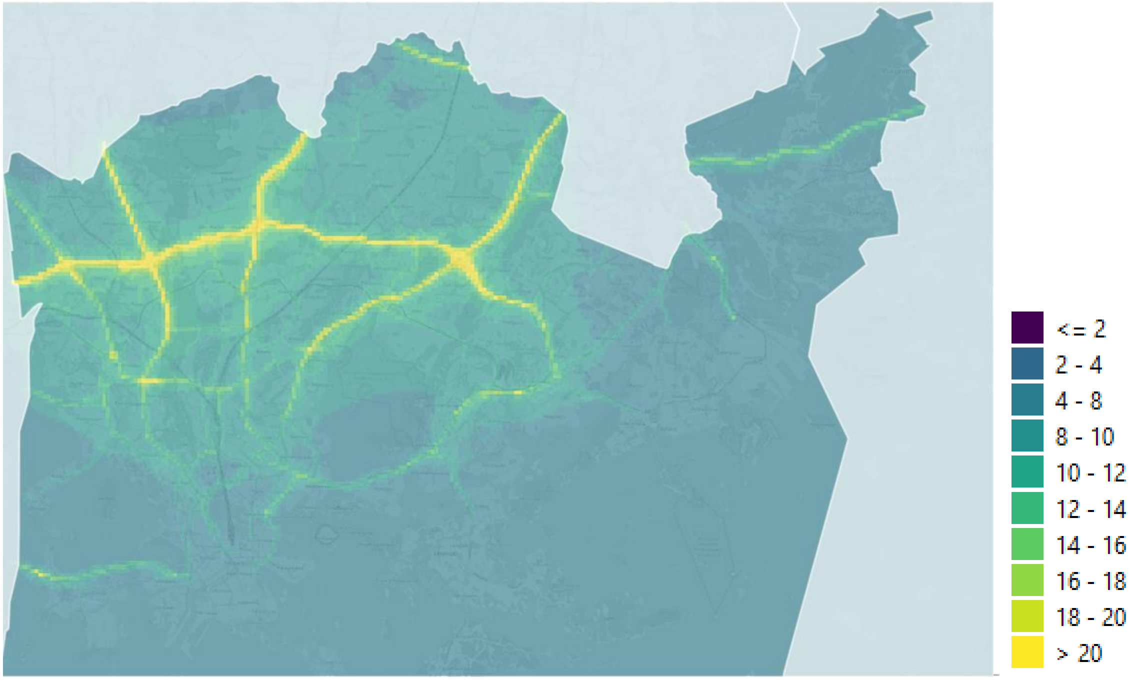

Figure 107.Calculated PM10 concentrations for the Helsinki, 2021 annual mean.

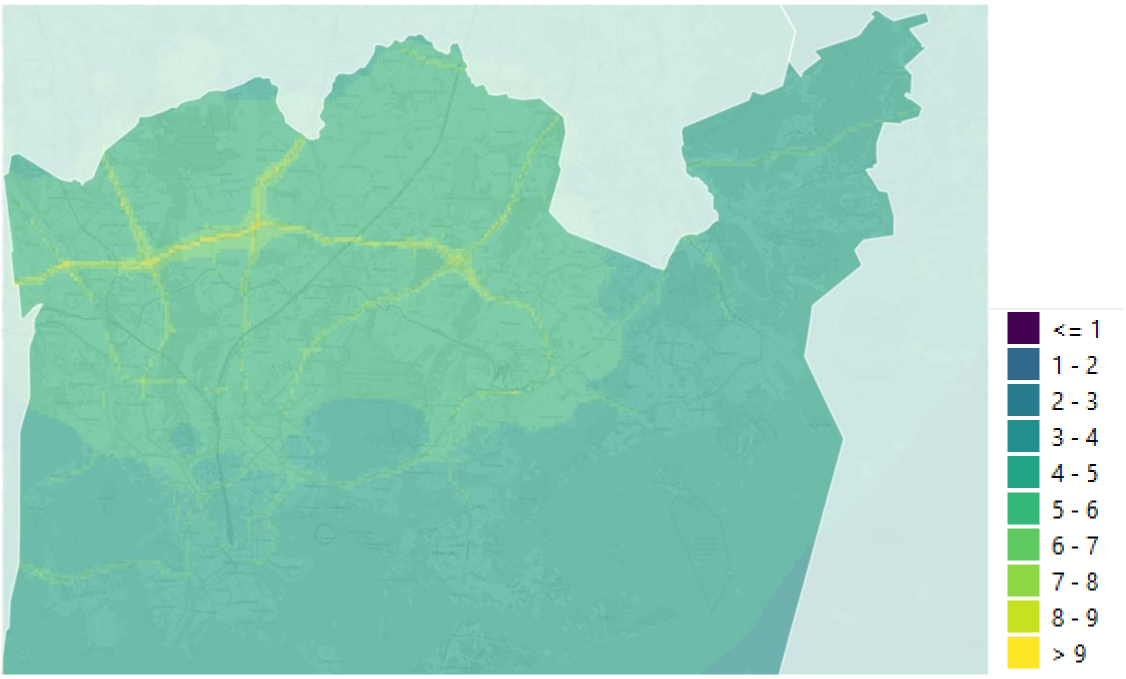

Figure 108. Calculated PM2.5 concentrations for the Helsinki, 2021 annual mean.

Scenario 1: Reference scenario

In Figure 109 the complete set of input and output data is shown for the reference scenario. This scenario uses the predicted changes in traffic volumes, retaining the current day studded tyre share for fossil, hybrid and electric vehicles but including the change in fleet makeup.

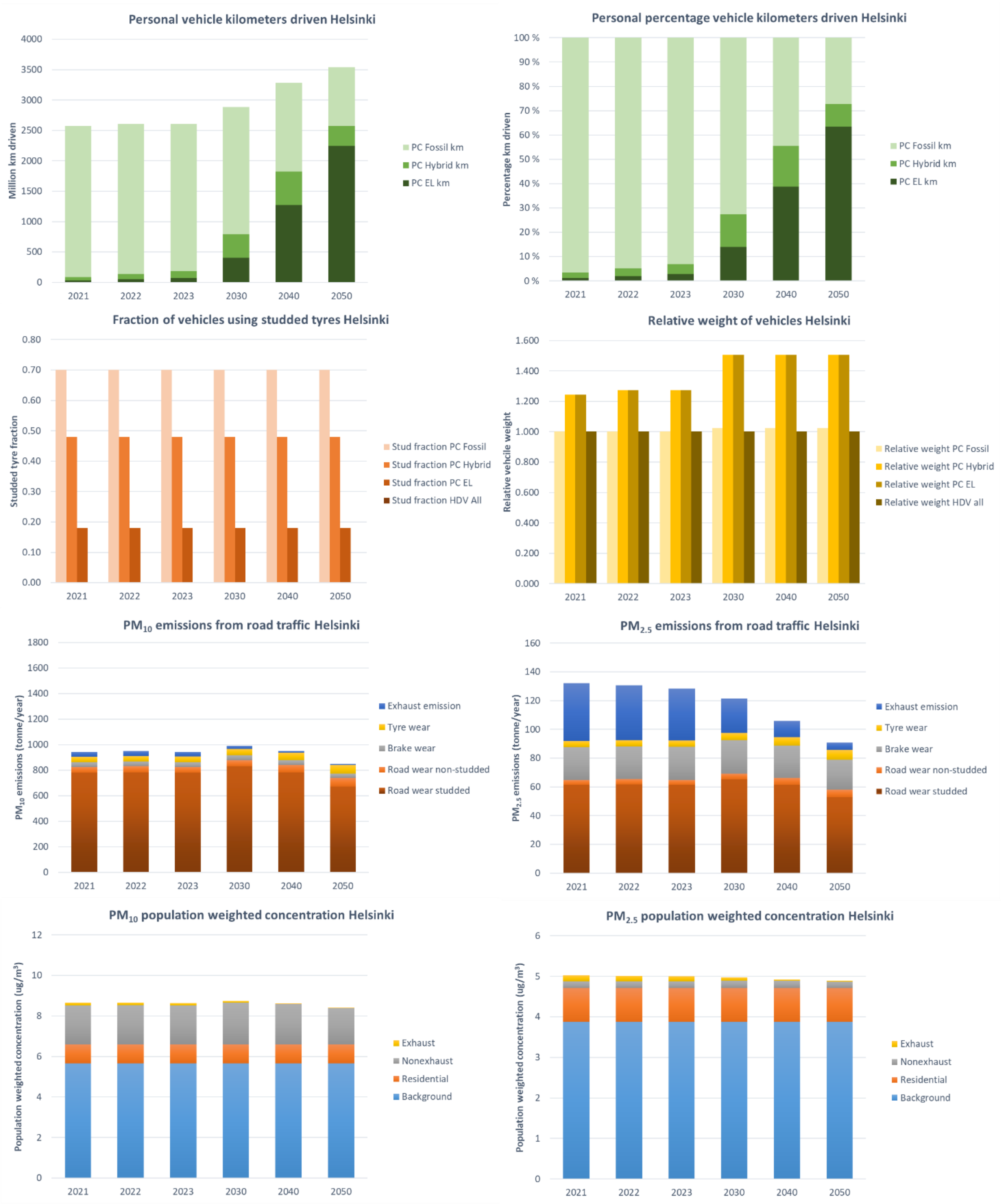

Figure 109. Input data and results for the reference scenario (1) for the different years

Scenario 2: Studded tyre reduction scenario

In Figure 110 the complete set of input and output data is shown for the studded tyre reduction scenario. This is the same as the reference scenario but in this case the existing 2021 studded tyre shares are reduced by 30% per decade. This leaves a share in 2050 of 24% for fossil vehicles, 16% for hybrids and 5% for electric.

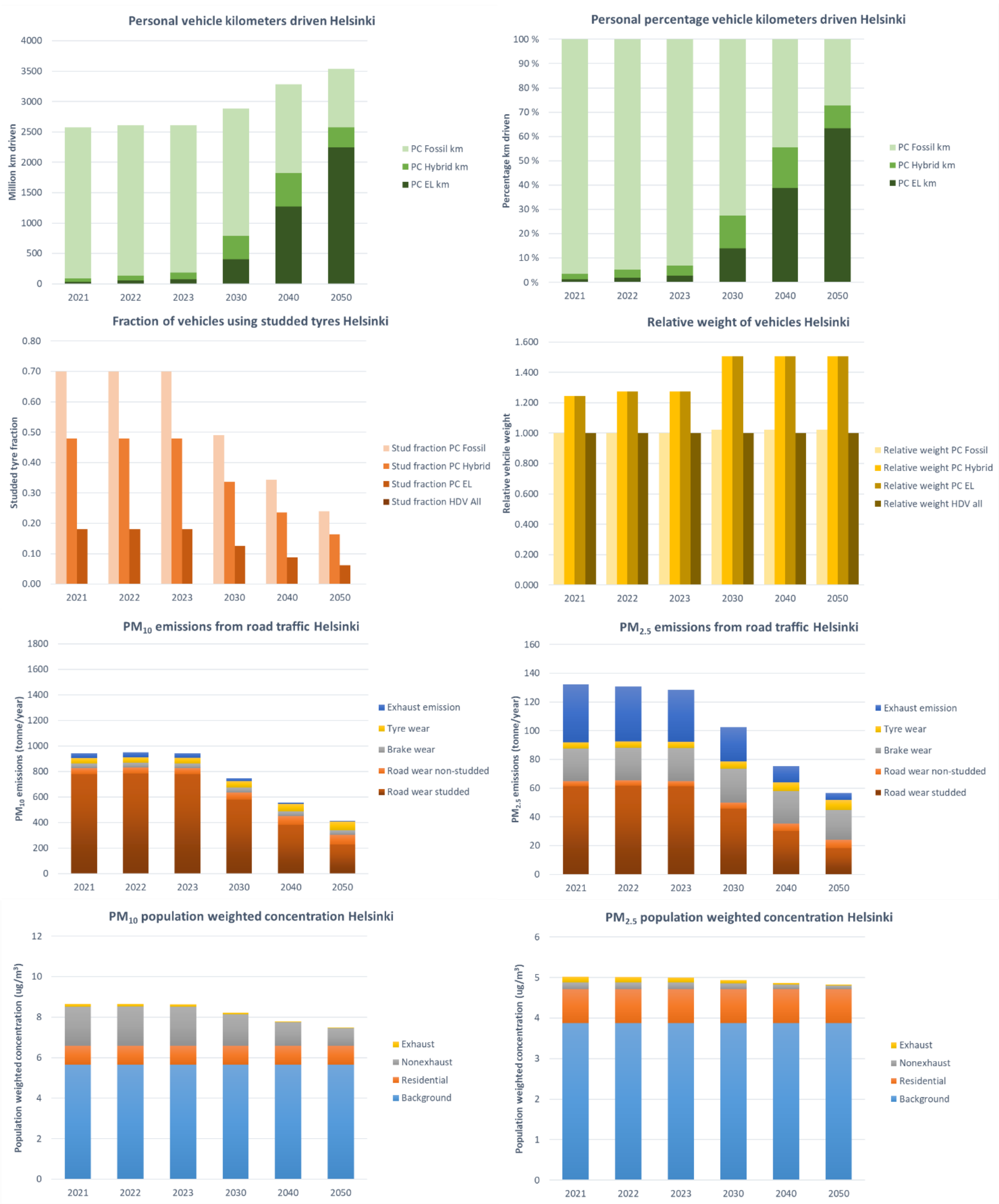

Figure 110. Input data and results for the studded tyre reduction scenario (2) for the different years

Scenario 3: Constant studded tyre share scenario

In Figure 111 the complete set of input and output data is shown for the constant studded tyre share scenario. This is the same as the reference scenario but in this case all personal vehicle types (fossil, hybrid and electric) are allocated studded tyre shares equivalent to the 2021 fossil fuel vehicles (70%).

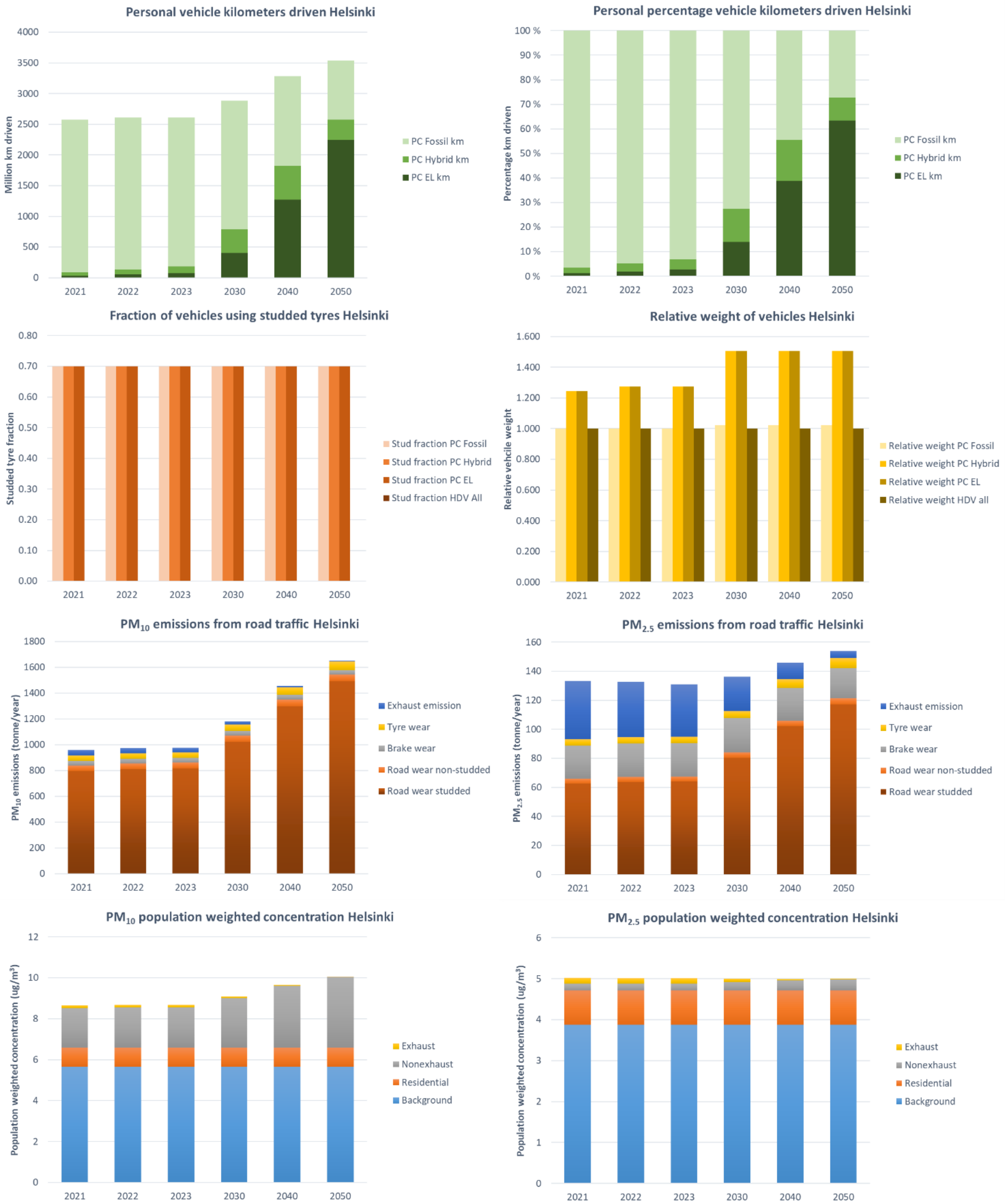

Figure 111. Input data and results for the constant studded tyre share scenario (3) for the different years

Scenario 4: Reduced studded tyre season

In Figure 112 the complete set of input and output data is shown for the reduced studded tyre season scenario. This is the same as the reference scenario, but the studded tyre season is reduced by 20% per decade.

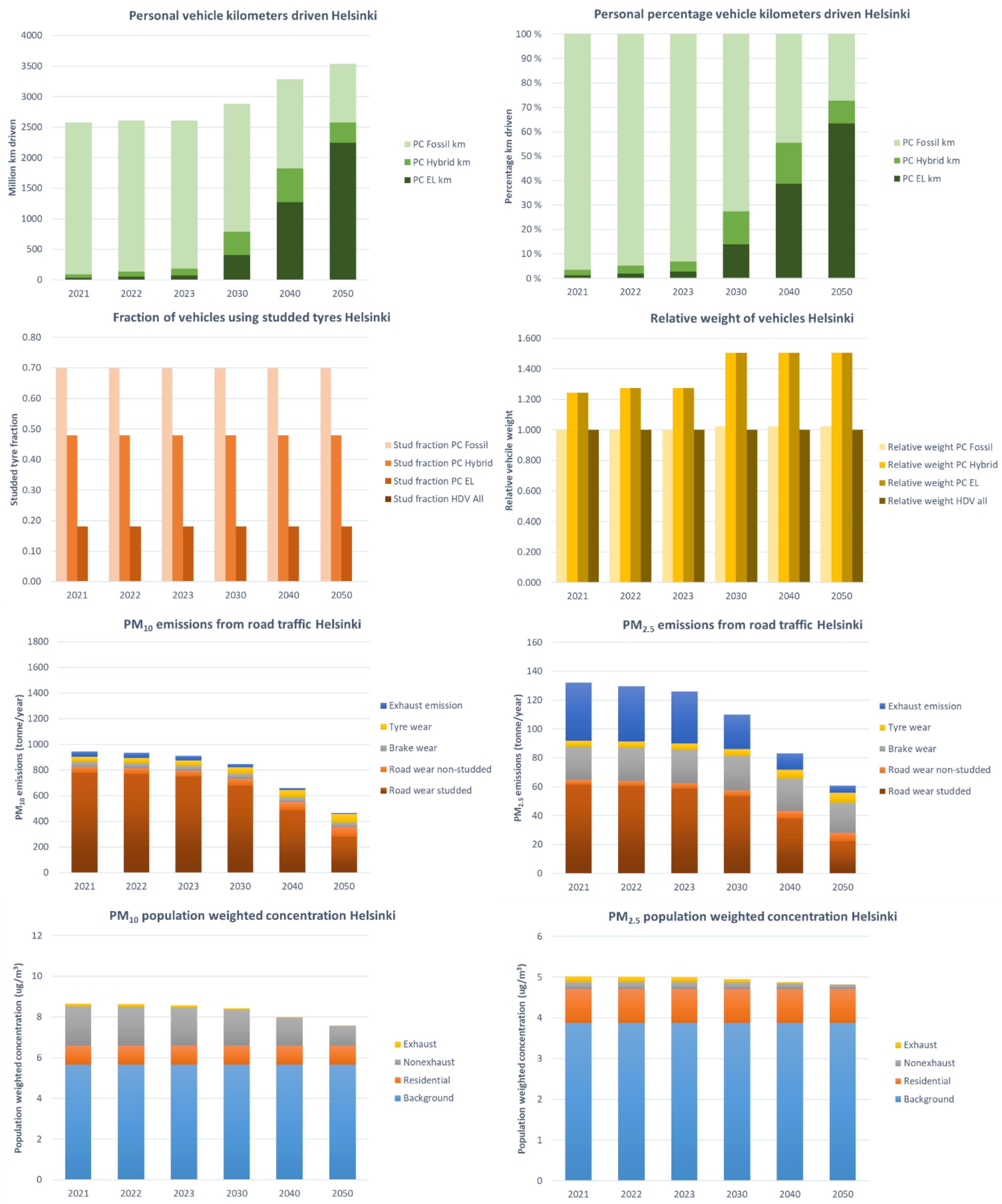

Figure 112. Input data and results for the reduced studded tyre season scenario (4) for the different years

Health impacts
The health impact, in terms of premature deaths per year (see Section on Health impacts) due to PM2.5 non-exhaust emissions, for each scenario and each year is presented in Figure 113. The total population in the modelled Helsinki region is 673 000 inhabitants and the baseline incidence of mortality in Finland is 1040 per 100 000 (World Bank, 2021) .

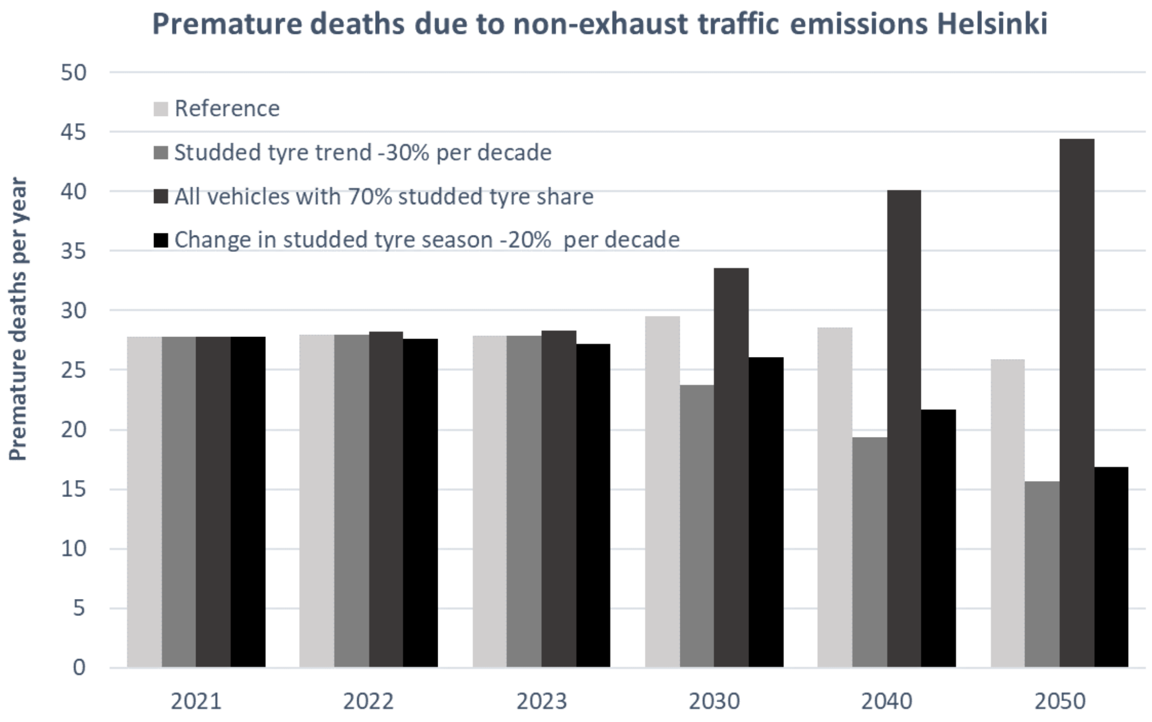

Figure 113. Health impact in terms of premature deaths per year for the 4 scenarios and all years Helsinki.

Conclusions for Trondheim and Helsinki

In the baseline reference scenario for both Trondheim and Helsinki non-exhaust emissions will only decrease slightly in the coming decades. This scenario assumes a constant studded tyre share over the next three decades. The shift from fossil to electric vehicles, that currently have roughly half the studded tyre share in Trondheim and a quarter in Helsinki, is offset by the enhanced weight of the electric vehicles leading only to a slight reduction in road wear and non-exhaust emissions. However, we do see a significant reduction in exhaust emissions.

Effective measures for reducing non-exhaust emissions are a reduction in studded tyre share (scenario 2) and a reduction in the length of the studded tyre season (scenario 4). In scenario 4 we see that the increased use of studded tyres on electric vehicles, to current levels used by fossil fuel vehicles, will lead to an increase in non-exhaust emissions over the coming decades.

Trondheim and Helsinki differ from each other:

- Population and traffic volume are 3 times higher in the Helsinki city region than in Trondheim
- Studded tyre share is 4 times higher in Helsinki than in Trondheim
- The ambition for electric vehicles (2050) is lower in Helsinki (63%) than in Trondheim (95%)
- The population distribution relative to traffic sources is different

Despite these differences the resulting health impact of non-exhaust emissions is quite similar. For the current situation, around 4 premature deaths/year per 100 000 inhabitants is calculated for both Helsinki and Trondheim, while the figure in Stockholm is 4.7 premature deaths/year per 100 000 inhabitants. These numbers are quite low but are based on current health impact knowledge for PM2.5, whilst the bulk of the emissions from studded tyres are in the coarse fraction of PM10.

By 2050 exhaust emissions will account for only 2% of the total traffic related PM2.5 emissions in Trondheim and for 5% in Helsinki. This study reiterates the importance of non-exhaust emissions as the major emission source for traffic, both now and in the coming decades.

References

Denby, B.R., Gauss, M., Wind, P., Mu, Q., Grøtting Wærsted, E., Fagerli, H., Valdebenito, A., Klein, H., 2020. Description of the uEMEP_v5 downscaling approach for the EMEP MSC-W chemistry transport model. Geoscientific Model Dev. 13, 6303–6323. URL: https://gmd. copernicus.org/articles/13/6303/2020/, doi:10.5194/gmd-13-6303-2020.

Forsberg, B., Lövenheim, B., Sommar, J., Kriit, H., Strömgren, M., Johansson, C. (only in Swedish) Bättre metoder att beskriva hälsovinster av minskad luftföroreningsexponering från vägtrafik. Trafikverket, Borlänge; 2021:253. https://www.diva-portal.org/smash/record.jsf?pid=diva2%3A1674008&dswid=302.

Fridstrøm, L. (2019). *Framskriving av kjøretøyparken i samsvar med nasjonalbudsjettet 2019*. Report 1689/2019. Norwegian Institute of Transport Economics (TØI). ISBN 978-82-480-2222-0. URL: https://www.vegvesen.no/globalassets/fag/fokusomrader/nasjonal-transportplan-ntp/transportanalyser/prognoser/toi-rapport-1689-2019-framskriving-av-kjoretoyparken.pdf

Martenies, S., Wilkins, D., Batterman, S. Health impact metrics for air pollution management strategies Author links open overlay panel. Environment international 2015.

Segersson D, Eneroth K, Gidhagen L, et al. Health impact of PM10, PM2.5 and black carbon exposure due to different source sectors in Stockholm, Gothenburg and Umea, Sweden. Int J Environ Res Public Health. 2017;14 (7):E742. doi:10.3390/ijerph14070742.

Soret, A., Guevara, M., Baldasano, J., 2014. The potential impacts of electric vehicles on air quality in the urban areas of Barcelona and Madrid (Spain). Atmos. Environ. 99, 51–63.

SOU 2021:48. ”I en värld som ställer om Sverige utan fossila drivmedel 2040”, https://edokmeetings.stockholm.se/welcome-sv/namnder-styrelser/hagersten-alvsjo-stadsdelsnamnd/mote-2021-08-26/agenda/remissunderlag-del-1-betankandet-utfasningsutredningen-pdf?downloadMode=open#page149

Svensson, N., Engardt, M., Gustafsson, M. and Andersson-Sköld, Y. Modelled atmospheric concentration of tyre wear in an urban environment. Atmospheric Environment: X, Volume 20, December 2023, 100225. https://www.sciencedirect.com/science/article/pii/S2590162123000254#undfig1

Säll, B., 2021. Luftföroreningar i Östra Sveriges Luftvårdsförbund - utsläppsdata för ABCDX-län år 2018. SLB Analys 7, 2021. https://www.slbanalys.se/slb/rapporter/pdf8/slb2021_007.pdf

Timmers, V.R.J.H., Achten, P.A.J., 2016. Non-exhaust PM emissions from electric vehicles. Atmos. Environ. 134, 10–17.

Traficom, 2021. Nationwide road traffic forecast (Tieliikenteen valtakunnallinen ennuste, in Finnish). URL: https://api.hankeikkuna.fi/asiakirjat/d99a3ae3-b7f9-49df-afd2-c8f2efd3dc1d/5d4db40f-4cf4-4ad5-9e42-99031175f27e/MUISTIO_20210920060527.pdf

Turner, M. C., M. Jerrett, C. A. Pope III, D. Krewski, S. M. Gapstur, W. R. Diver, B. S. Beckerman, J. D. Marshall, J. Su and D. L. Crouse (2016). "Long-term ozone exposure and mortality in a large prospective study.". American journal of respiratory and critical care medicine 193(10): 1134-1142.

VTT, 2021. Forecast for greenhouse gas emissions from transport 2020-2045 (Liikenteen kasvihuonekaasupäästöjen perusennuste 2020-2045, in Finnish)

https://api.hankeikkuna.fi/asiakirjat/d99a3ae3-b7f9-49df-afd2-c8f2efd3dc1d/1a483d38-ee85-418e-9086-fd5ef6ea40d0/MUISTIO_20210920060401.docx

World Bank, 2021. Death rate, crude (per 1,000 people) - European Union. URL: https://data.worldbank.org/indicator/SP.DYN.CDRT.IN?end=2021&locations=EU&most_recent_year_desc=false&start=1960&view=map&year=2021

Yu, Z., Bellander, T., Bergström, A. et al. Association of Short-term Air Pollution Exposure With SARS-CoV-2 Infection. Among Young Adults in Sweden. JAMA Network Open. 2022;5(4):e228109. doi:10.1001/jamanetworkopen.2022.8109.

Yu, Z., Ekström, S., Bellander, T. et al. Ambient air pollution exposure linked to long COVID among young adults: a nested survey in a population-based cohort in Sweden. The Lancet Regional Health - Europe, 28, 2023, https://doi.org/10.1016/j.lanepe.2023.100608.

Work package 5: Sampling and measurement techniques for road dust

Introduction

The WDS (Wet Dust Samples) equipment is a tool to measure the dust load on a surface. It has been described in Jonsson et al. (2009), Gustafsson et al., (2019a) and Lundberg et al (2019?) and used in many research projects (e.g. Gjerstad et al., 2019, Gustafsson et al. 2019b, Järlskog et al., 2022). The WDS cleans a small, sealed surface, with a known area (20,4 cm^2) using a known amount of de-ionized water at high pressure. The dust on the surface is thus removed from the surface macrotexture and the mixture of water and dust is collected in a bottle, which can later be analysed. The standard analysis involves filtering of the sample which is labour intensive since it includes sieving, filtering, weighing, and drying of the sample, annealing of the sample to remove the organic content and then measuring the weight to calculate the minerogenic part. Previous measurements have shown good correlation between road dust concentration, calculated by gravimetric analysis and annealing of the WDS samples, and turbidity (Svensson et al. 2020), why turbidity has successively been more commonly used and completed with filter analyses of choses samples to assure the correlation is valid. A direct reading and data storing of turbidity when sampling with WDS would be a very useful addition. It would also be valuable for adjusting and planning sampling patterns in field.

As part of the OptiDrift project a direct measurement module (DMM) was therefore added to the WDS in order to be able to get direct measurements of the turbidity in the water, and in that way an estimate of the dust amount (Figure 114, Figure 115).

Figure 114. The WDS II designed in CAD with the direct measurement module, DMM, mounted.

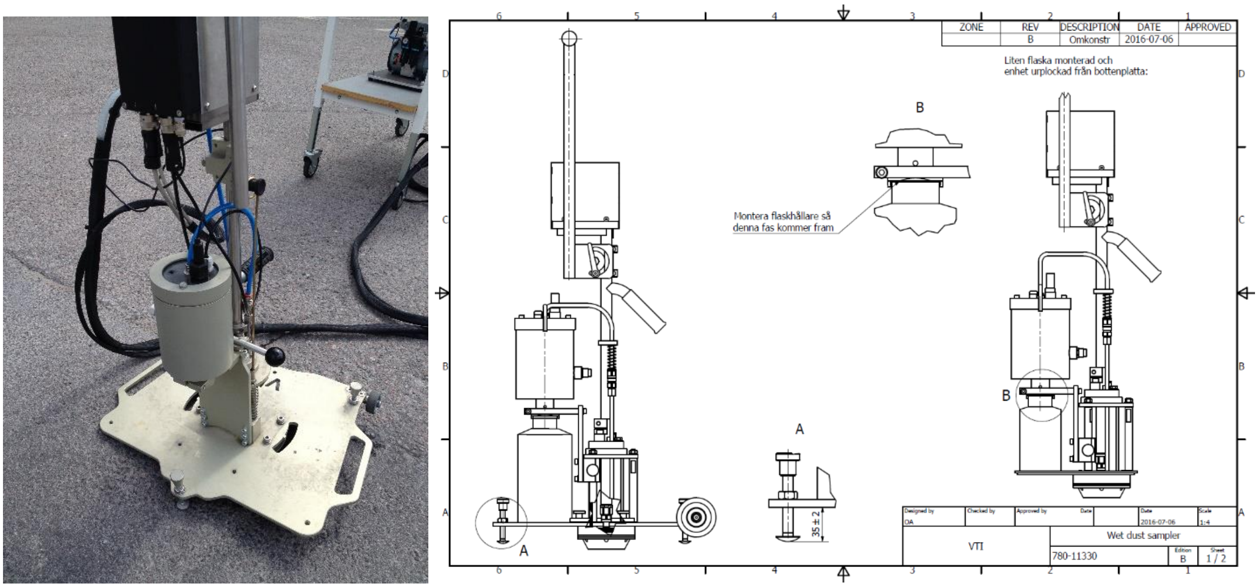

Figure 115. Left: photo of the WDS II with the DMM. Photo: Jakob Kristofers. Right: construction drawing of DMM. Photo: Mats Gustafsson, VTI.

The DMM consists of a container with a turbidity sensor which is fastened to the WDS. The water-dust mixture goes through this container before it is collected in a sample bottle for further analysis. The DMM is connected to a computer for direct readings in the field.

Suspension of dust from the road surface is a main contributor to PM10 during dry periods in winter and spring in the Nordic countries. Important factors influencing the suspension is dust load, which can be measured using the Wet Dust Sampler, road surface humidity and suspension forces implied by traffic and wind. To measure the suspension in a repeatable way is complicated. Instrumented cars are an option, but suffers from measurement difficulties behind tyres, high dependency on road surface conditions and high lateral variability in road surface dust load, which affects repeatability and representativeness of the results. A method, based on the PI-SWERL equipment (Etyemezian et al., 2007), was developed to accomplish this. The original PI-SWERL, was used for soils and the VTI method, DUSTER II, was used on gravel roads in Blomqvist et al. (2012).

Figure 116. The original DUSTER II during measurements in Stockholm. Photo from Gustafsson et al., (2012).

The rotating flat ring used for suspending the dust worked less efficiently on paved surfaces (Gustafsson et al., 2012), why a further development was needed.

This chapter describes both the testing of a turbidity meter in the DMM and further development and testing of the DUSTER II.

Methods

Evaluation of the WDS direct measurement module

Choosing a turbidity sensor small enough for fitting in the DMM and being suitable for field work is challenging, since most commercial turbidity meters are used for controls in large pipes or in rivers. There was also a criterium that the meter must be able to deliver an analogue signal to be able to incorporate the data into our WDS dedicated software. The turbidity sensor purchased is a 90-degree scatter nephelometer (WQ730 from Xylem), which measures the intensity of scattered light from particles. There were two measurement ranges of the WDS DMM, one low (0-50 NTU) and one high (0-1000 NTU).

The direct measurement module installed on the WDS was evaluated in a short test sequence. A known amount of dust (in grams) was laid out on a smooth surface for each WDS shot.

The Duster equipment

The rotating flat ring was exchanged for a fan propeller, expected to result in a considerably higher suspension force directed to the surface (Figure 117). Except for the original DustTrak, a Palas AQguard was connected to the suspension chamber, to be able to analyse the particle size distribution of the suspended dust.

Figure 117. Duster II with wagon and computer (eft), with connected AQguard (right). Photo: Mats Gustafsson, VTI

The Duster equipment was tested on different surfaces and during the process of drying of a surface. The goal was to see how the suspension and size distribution varied with the speed of the fan and with different types of surfaces and the effect of moisture.

After some initial tests it was decided that the Duster should be run in a sequence starting from 800 rpm and increasing with 200 rpm in each step until 1800 rpm. Each step was 2 minutes long. After the 1800, the fan speed was zero for 2 minutes. Thereafter it increased and the Duster was lifted from the ground to allow all the dust inside the box to be ejected.

During the first set of experiments the measurement limit in the Duster program was set to 10 mg/m^3, which meant that in case of high concentrations, the maximum was sometimes exceeded. The time resolution was 1 second.

To see the effect of surface characteristics, three different surfaces were chosen, where the macrotexture was different, which likely affects the dust load and perhaps also the suspendible dust load. Figure 118 shows photos of the three surfaces. The first surface (Figure 118a) was a worn, rough surface on a parking lot, where a lot of dust was expected to be stored in the texture. Some dust was also visible on the surface. The second surface (Figure 118b) was a newer, smoother asphalt surface on a parking lot, with less visible dust. The third surface (Figure 118c) was a concrete surface in a garage. It looked very smooth, without any visible texture or dust and thus the dust load was expected to be low. There were, however, some small holes/cracks in certain places of the floor which can be seen in the photo. On each surface, the Duster runs were performed in 2-4 spots close to each other. (The reason for not placing it in exactly the same spot was that it might then affect the following measurements.). All road surfaces were dry, with no rain the preceding day.

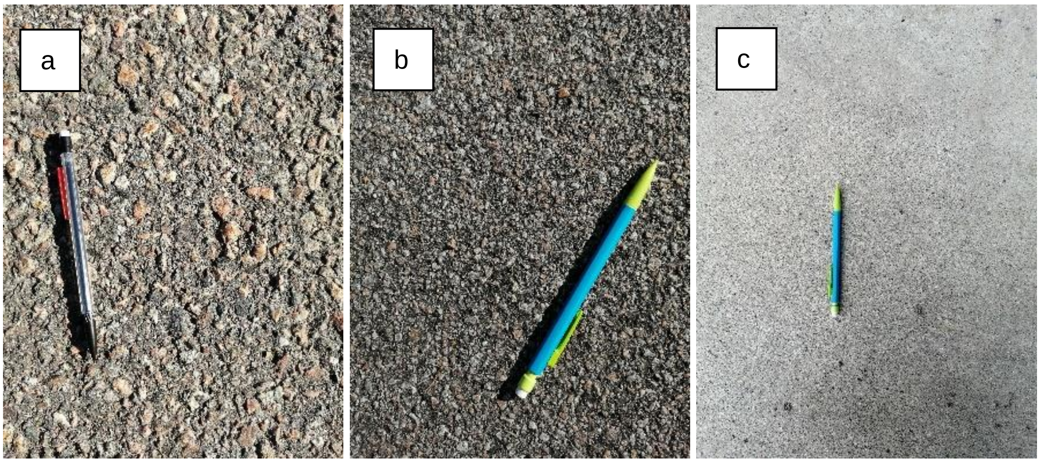

Figure 118. Photos of the three different surfaces where the Duster was tested. A) rough asphalt surface, b) less rough asphalt surface, c) smooth concrete surface. Photo: Nina Svensson, VTI.

To study the effect of moisture on resuspension, two series of experiments were performed, where an asphalt surface was wetted and thereafter allowed to dry. The Duster was placed several times on the same location on the wetted surface while it dried. The surface was a rough asphalt, similar to Figure 118a. In the first experiment, 140 g/m^2 was sprayed on to the surface and in the second experiment 57 g/m^2. The weather conditions were dry, with no rain on this or on four of the preceding days.

Results and discussion

Duster equipment

Figure 119 shows an example of how the concentrations changed over time during the sequence of increasing fan speed. There were large variations in concentration, but the average value for each rpm seemed to be relatively constant. This was also confirmed by running a longer experiment on the rough surface. There was one exception, however, on the concrete surface.

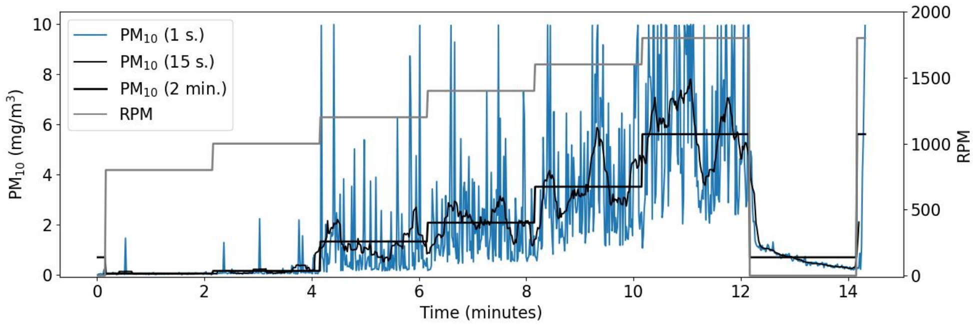

Figure 119. Example of time series of PM10 concentration and fan speed (rpm). The example is from the rough asphalt surface.

Figure 120 shows a summary of all the experiments on the three different surfaces and during the drying of a surface. Each marker symbolizes the 2-minute average concentration. Note, that during the first set of experiments (the different surfaces), the measurements close to or above 10 mg/m^3 where not correctly measured. The occasions where this is believed to have a more pronounced effect are marked empty circles. The increasing concentration on the dry surfaces seem to follow either a linear or exponential trend, while the trend looks more exponential in the case of a moist surface.

During the drying sequence there is first no/very low suspension for the first 1.5 hours. 2 hours after the wetting, there was a sudden increase in concentration, but mainly during high fan speed, while the low fan speeds did not manage to suspend almost any dust. After this initial suspension, the following Duster runs caused lower concentrations. A speculation is that the Duster managed to remove much of the available dust, which decreased the concentration in the following runs.

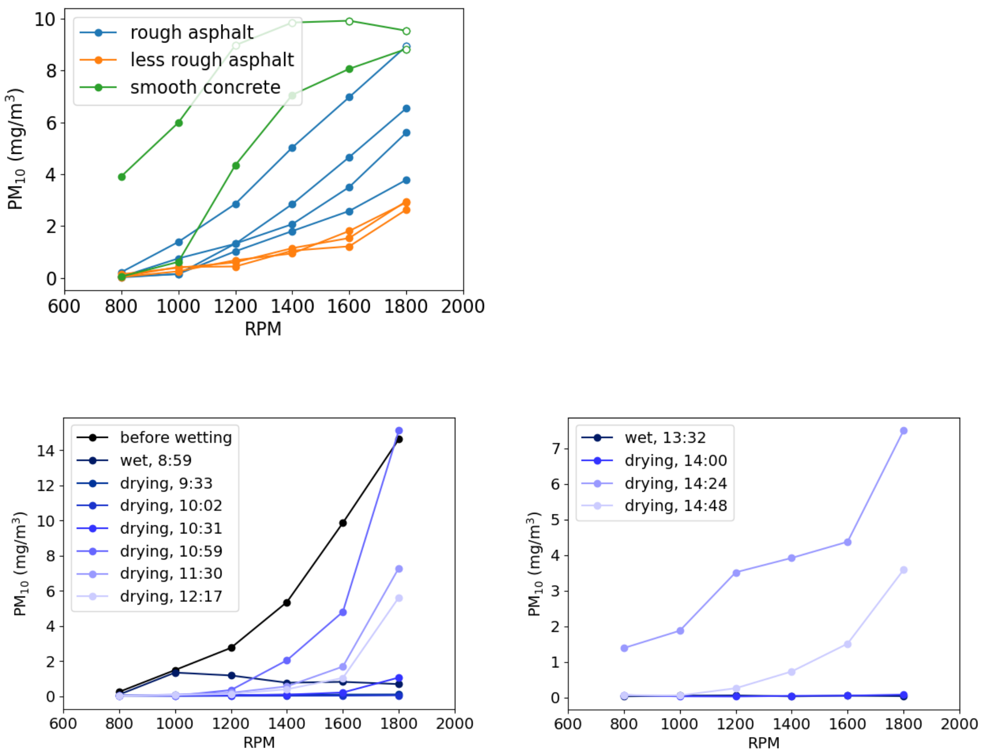

Figure 120: PM10 concentration as a function of the fan speed for three different surfaces and for drying of one surface. The empty circles denote when the values are underestimated due to that the measurement range of the instrument was set to too low.

Figure 121 shows the PM measurements from the two instruments. There are some clear differences. The AQguard shows higher values for PM10 and much less variation than the DustTrak. The concentrations also decrease very slowly after the propeller has stopped at around 8:53-8:54. This may be related to the way it is mounted, sucking in air through a tube at the top of the Duster box, while the DustTrak sucks in air from a pipe which is mounted inside the box.

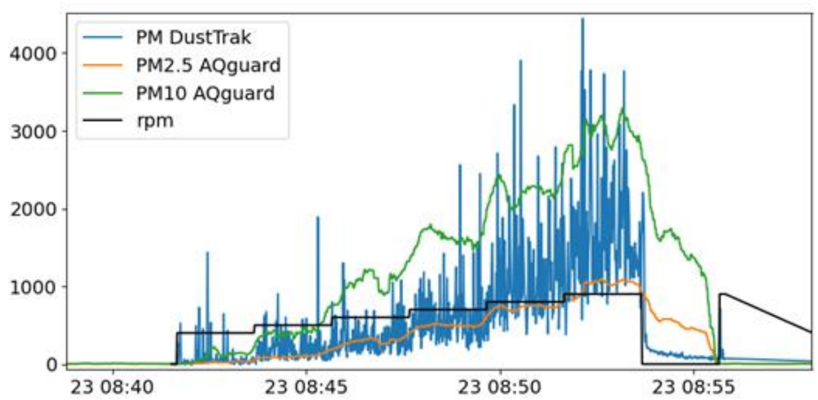

Figure 121. PM10 for DustTrak and AQguard and PM2.5 for AQguard together with rpm.

Figure 122 shows an example of the number size distributions of particles from the drying sequence. Figure 122a shows the size distributions before wetting and Figure 122b during the first burst of suspension after the surface has started drying (10:59 in Figure 120). It can be seen that most particle sizes (0.3-2 µm) increase with increasing rpm at approximately the same rate. The size distribution from the moist is different. It is clear that it is mainly the higher rpm:s that cause suspension.

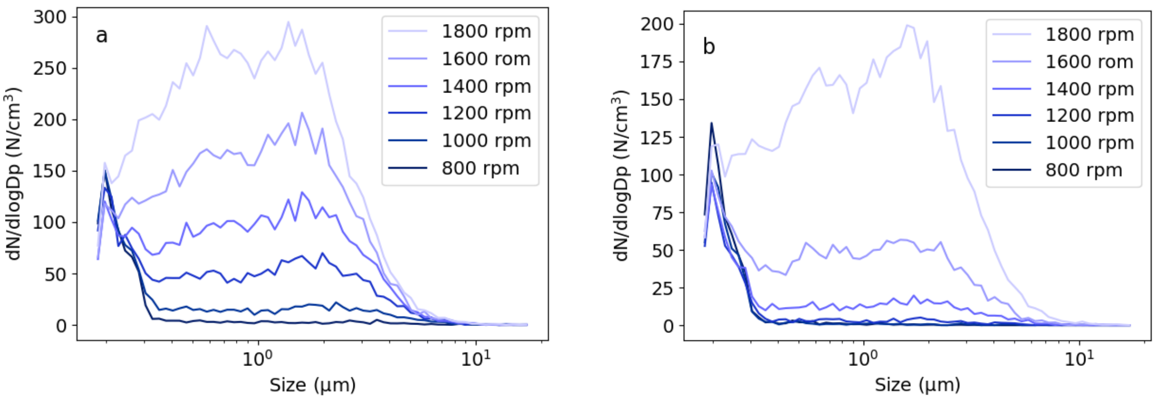

Figure 122 Number size distributions of particles for different fan speeds. a) before wetting and b) during the drying sequence.

The drying sequence is visualized in Figure 123. The drying is, of course strongly influenced by the prevailing weather. At the time for this test, weather was sunny and a bit windy, which calls for a rapid drying. From the photos is it obvious that the DUSTER itself affects the drying of the wetted square. During measurement it protects the enclosed surface from drying, why the sirface outside the encloser dries up faster. Within the inclosure, a circle between the middle and the outer part of the dries up faster, which might be an affect of the air movement pattern being higher in this area. Since the propeller blades are not covering the full width of the inclosure, it is likely the area where the propeller is most efficient. This is valuable input for future design improvement of the equipment.

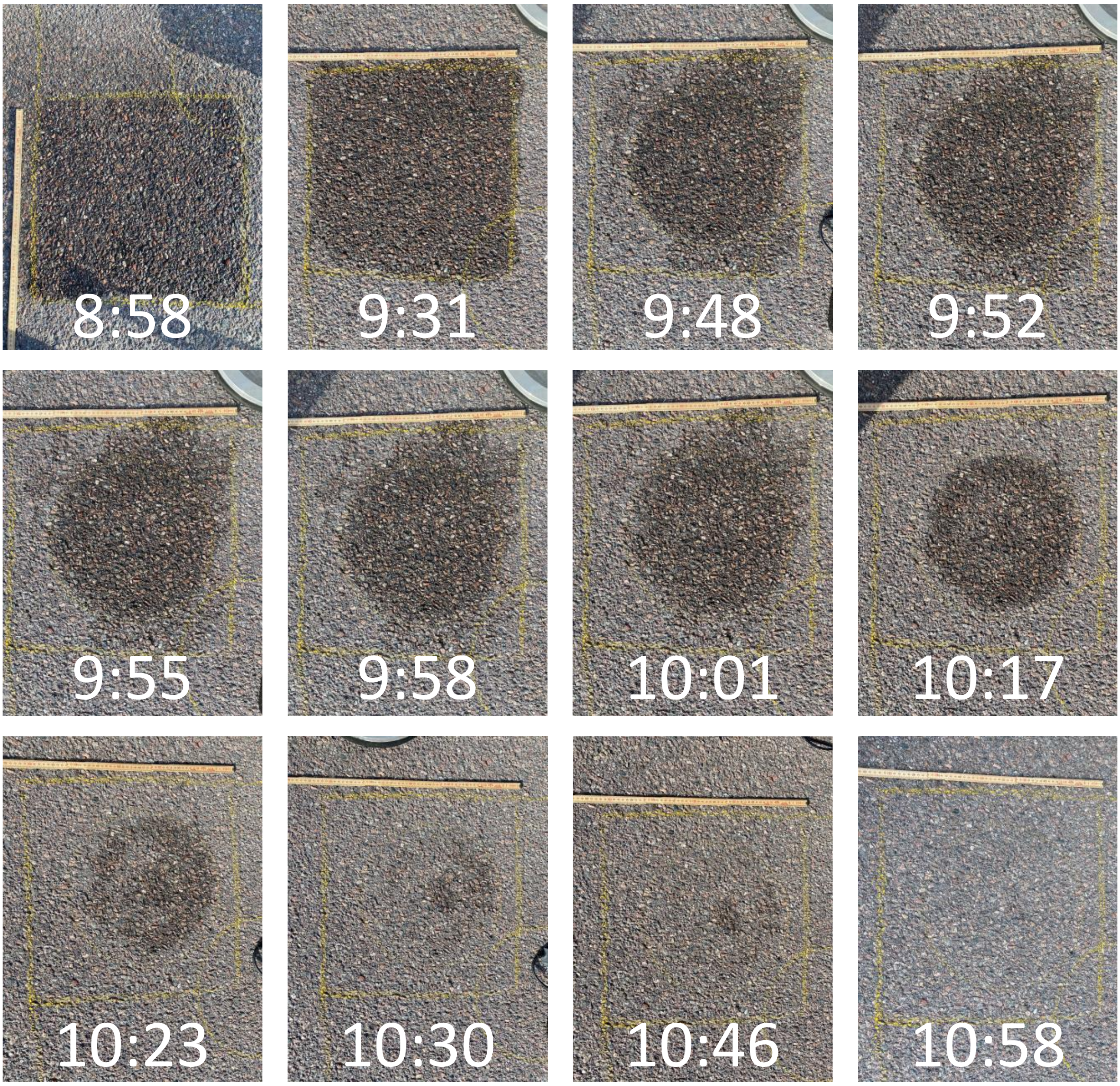

Figure 123. Photographs of the drying sequence (Photo: Mats Gustafsson, VTI)

WDS DMM equipment

Figure 124 shows a time series of WDS DMM measurements, with markers approximately at each shot in both measurement ranges (low and high). The water was allowed to flow through the WDS and out again without any obstruction (as opposed to later, where the drainage pipe was blocked for a while after the shot).

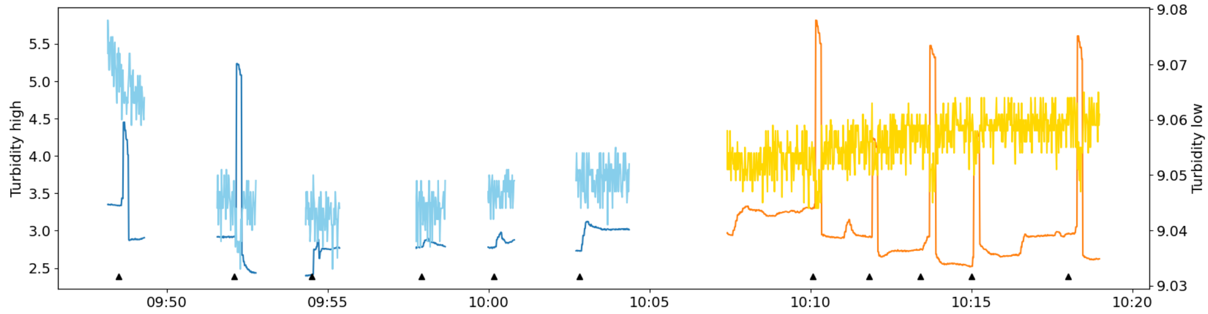

Figure 124: Time series of turbidity measurements. The black markers show the approximate time of each shot. For the blue colours, the dust amount was 2 grams for each shot. For the orange/yellow colours, the dust amount was 4 grams per shot.

Figure 125 shows a similar time series, but where the flow from the output tube was closed off for a while after each shot. Both the high and low range react at the same time. The low range values decrease during the shot and the high range values increase. However, there does not seem to be any clear correlation between the amount of dust on the floor and the turbidity. One reason for this may be that air bubbles are produced, which cause an increase in the turbidity levels. It is interesting to note that disrupting the flow by blocking the output tube sometimes causes an increase in turbidity for a very long time and sometimes not.

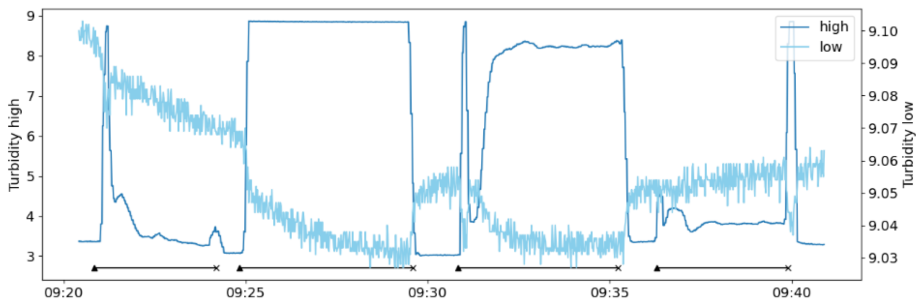

Figure 125: Time series of turbidity measurements, where the outward flow is obstructed for a while after each shot. The black triangles show the approximate time of each shot and the x marks the time when the outward flow is released. The amount of dust in each shot is 1 grams.

Conclusions

Duster

- From these test sequences it seems that the Duster can, to some extent, be used to compare the dust load on different surfaces. The experiments showed that the dust load on cement>rough asphalt>less rough asphalt. However, the variations on the same type of surface were large. Some more studies on the scale of the variations are needed.
- The concrete surface, which looked very smooth, gave rise to the highest concentrations. One speculation is that the dust on this surface was much more easily suspendible than in the dust in the macrotexture on the two asphalt surfaces. More experiments on different types of surfaces are needed.
- The Duster can also be useful for studying the effect of moisture on suspension, e.g. by estimating how long particles are bound by moisture on different surfaces. Here it was seen that the effect of surface moisture on suspension lasted for at least 3 hours after wetting (possibly longer, but no more tests were performed after this)
- For future studies, it would be interesting to find out what fan speed corresponds to which wind speed.

WDS

- The DMM on the WDS did not produce reproducible results when tested with known amounts of dust on a smooth floor. One reason could be that air bubbles are produced in the water container causing errors in the measurements.
- Air bubbles or dust that settles on the sensors glass openings, where the light is emitted and received will disturb the measurements. The conditions within the DMM is probably not good enough for using this type of precise instrument. Maybe a simpler turbidity sensor that is designed to be in these types of harsh environments would be a better choice, that at least would give an indication on the dirt concentration.

References

Blomqvist, G., Edvardsson, K., Gustafsson, M., Wik, O., 2012, Damning från flygaskstabiliserade grusvägar, 16531248 (ISSN), Värmeforsk, http://urn.kb.se/resolve?urn=urn:nbn:se:vti:diva-20163

Etyemezian, V., Nikolich, G., Ahonen, S., Pitchford, M., Sweeney, M., Purcell, R., Gillies, J., Kuhns, H., 2007. The Portable In Situ Wind Erosion Laboratory (PI-SWERL): A new method to measure PM10 potential for windblown dust properties and emissions. Atmospheric Environment 41, 3789-3796, 10.1016/j.atmosenv.2007.01.018.

Gjerstad, K. I., Gustafsson, M., Blomqvist, G., Denby, B., Elmgren, M., Grythe, H., Janhäll, S., Järlskog, I., Johansson, C., Kulovuori, S., Kupiainen, K., Lundberg, J., Malinen, A., Norman, M., Ritola, R., Silvergren, S., Stojiljkovic, A., Sundvor, I., Þorsteinsson, Þ., Stefani, M., Vogt, M., 2019, NORDUST : Nordic Road Dust Project, http://urn.kb.se/resolve?urn=urn:nbn:se:vti:diva-14950

Gustafsson, M., Blomqvist, G., Johansson, C., Norman, M., 2012, Driftåtgärder mot PM10 på Hornsgatan och Sveavägen i Stockholm : utvärdering av vintersäsongen 2011-2012, 03476030 (ISSN), VTI, http://urn.kb.se/resolve?urn=urn:nbn:se:vti:diva-1847

Gustafsson, M., Blomqvist, G., Järlskog, I., Lundberg, J., Janhäll, S., Elmgren, M., Johansson, C., Norman, M., Silvergren, S., 2019. Road dust load dynamics and influencing factors for six winter seasons in Stockholm, Sweden. Atmos. Environ. X 2, 10.1016/j.aeaoa.2019.100014.

Gustafsson, M., Blomqvist, G., Järlskog, I., Lundberg, J., Niska, A., Janhäll, S., Norman, M., Eneroth, K., Johansson, C., 2019, Optidrift : optimerad vinter- och barmarksdrift för bättre luftkvalitet, 1004, Statens väg- och transportforskningsinstitut, http://vti.diva-portal.org/smash/get/diva2:1296413/FULLTEXT02.pdf

Jarlskog, I., Jaramillo-Vogel, D., Rausch, J., Gustafsson, M., Stromvall, A.M., Andersson-Skold, Y., 2022. Concentrations of tire wear microplastics and other traffic-derived non-exhaust particles in the road environment. Environ Int 170, 107618, 10.1016/j.envint.2022.107618.

Jonsson, P., Blomqvist, G., Gustafsson, M., 2008. Wet dust sampler : technological innovation for sampling particles and salt on road surface, Fourth National Conference on Surface Transportation Weather and Seventh International Symposium on Snow Removal and Ice Control Technology June 16–19, 2008 Indianapolis, Indiana. Transportation Research Board, TRB, Washington DC, pp. 102-111.

Lundberg, J., Blomqvist, G., Gustafsson, M., Janhäll, S., Järlskog, I., 2019. Wet Dust Sampler—a Sampling Method for Road Dust Quantification and Analyses. Water, Air, & Soil Pollution 230, 180, 10.1007/s11270-019-4226-6.

Work package 6: Road dust, PM_{10} and NORTRIP implementation in Iceland

Introduction

Pollution in cities due to traffic is of great concern globally. It is known that such pollution, for instance particulate matter (PM10 and PM2.5), causes various illnesses and deaths (Krzyzanowski and Cohen 2008; OECD 2020).

Car ownership in Iceland is very high, with 749 passenger cars per 1000 inhabitants in 2022 (Figure 126). That is almost 60% higher than in Sweden and Denmark, and more than in Norway (35% more) and Finland (13%). With 63% of the population living in the greater capital area (~243 thousand on 1 January 2023; Statistics Iceland, 2023), the traffic density can be very high in the capital area.

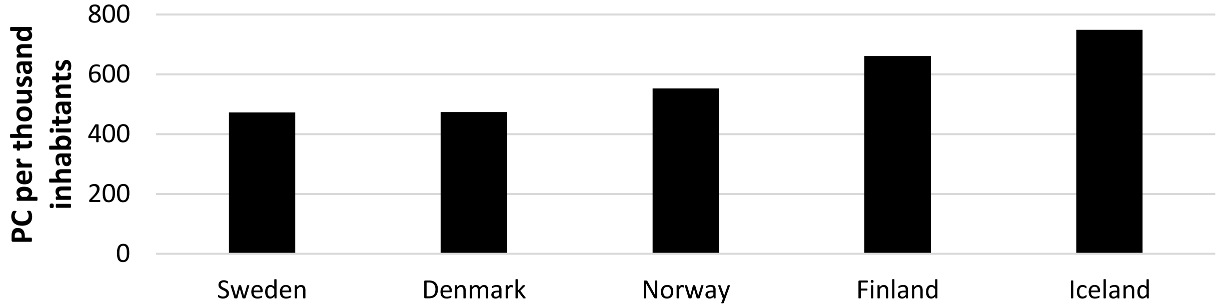

Figure 126. Passenger cars (PC) per thousand inhabitants in 2022 (Eurostat data).

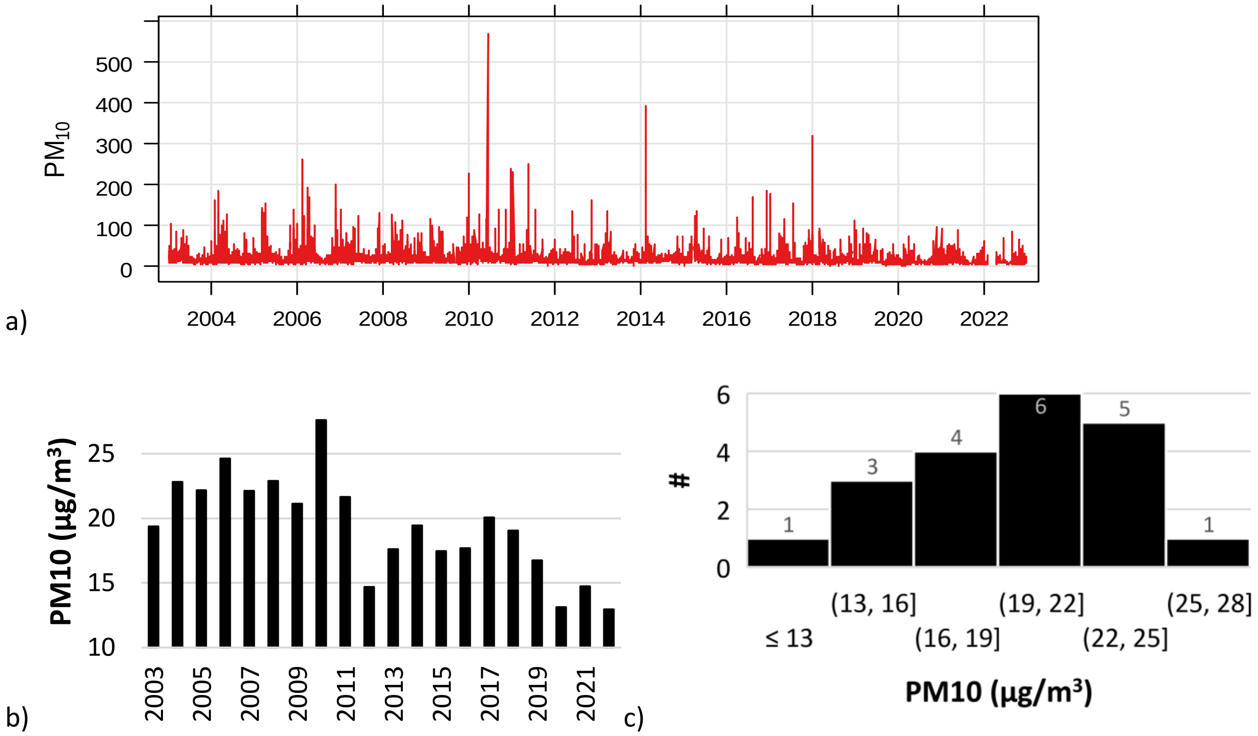

Figure 127. PM10 concentration at GRE-station, Reykjavik, for the years 2003 - 2022. a) Daily values, b) annual values, and c) histogram of the annual values.

Particulate matter (PM10) is the most common pollutant in the greater capital area that exceeds the given health limit (50 µg/m^3 for a 24-hour average). The concentration is measured at several locations within the greater capital area, but here the focus is on traffic related pollution. An example of a traffic station is the GRE-station, located near one of the busiest intersections in the capital area. Regular monitoring of the particulate matter concentration started in Reykjavik in 1986, and the Grensasvegur air quality station has been operating since 1994 (Einarsson et al., 2013). Monitoring data show that the capital area has problems with particulate matter, where daily averages exceeded set health limits several times a year, mostly during winter and early spring due to traffic; spring to summer often due to dust storms (Thorsteinsson et al., 2011). The PM10 concentration at the GRE-station (Figure 127) quite often records high values, where the 24-h averages go over 100 µg/m^3. The annual averages are usually between 13 – 25 µg/m^3 (Figure 127 b, c).

Over the past 20 years, the concentration at GRE-station has gone over the health limit (OHL) of 50 µg/m^3 as 24-hours average for 4 to 29 times a year (Figure 128).

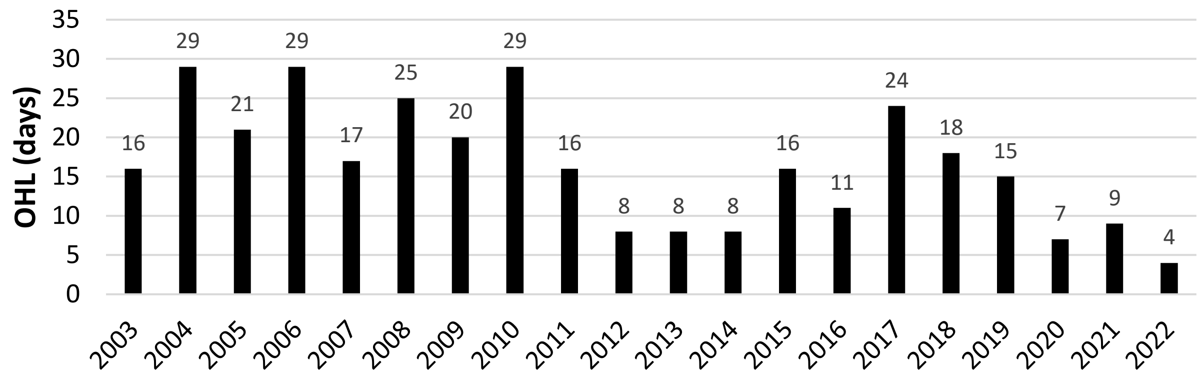

Figure 128. Number of times the concentration at GRE-station has been over the health limit (OHL) in the past 20 years.

The monthly mean values vary a lot, as can be seen by the range of values between the 25th and 75th percentile (Figure 129).

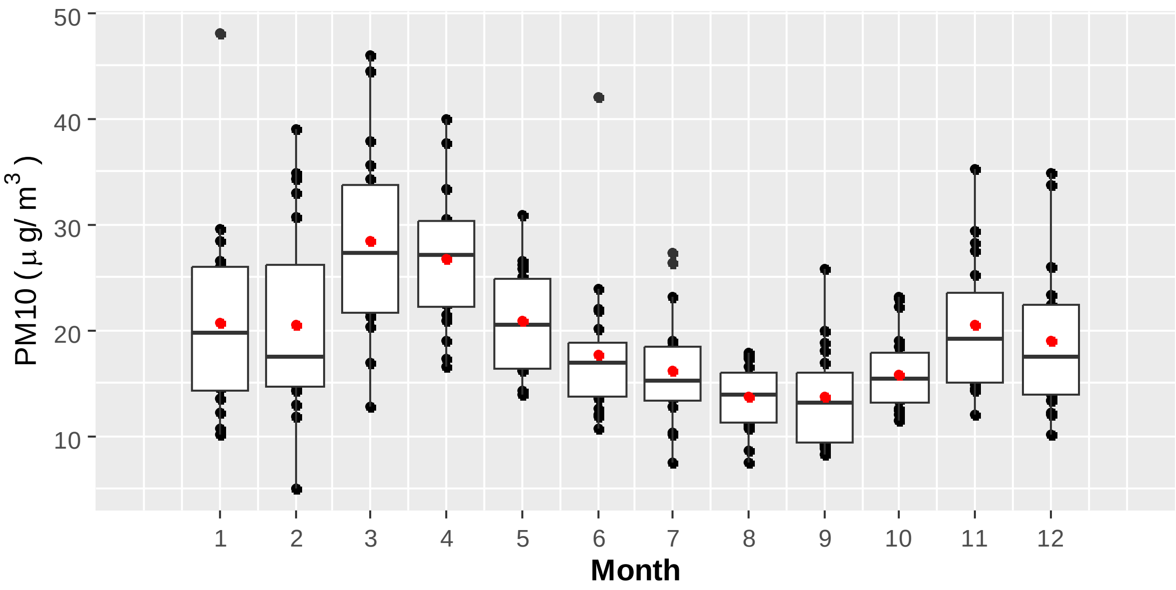

Figure 129. Box plot of monthly average PM10 concentration at GRE-station (2003 – 2022), Reykjavik. Red dot are average values, line the median values and box the 25th and 75th percentile.

The variation in daily median values is very large (Figure 130). The large variation in concentration indicates that identifying the effects of mitigation effort might be difficult to do, statistically.

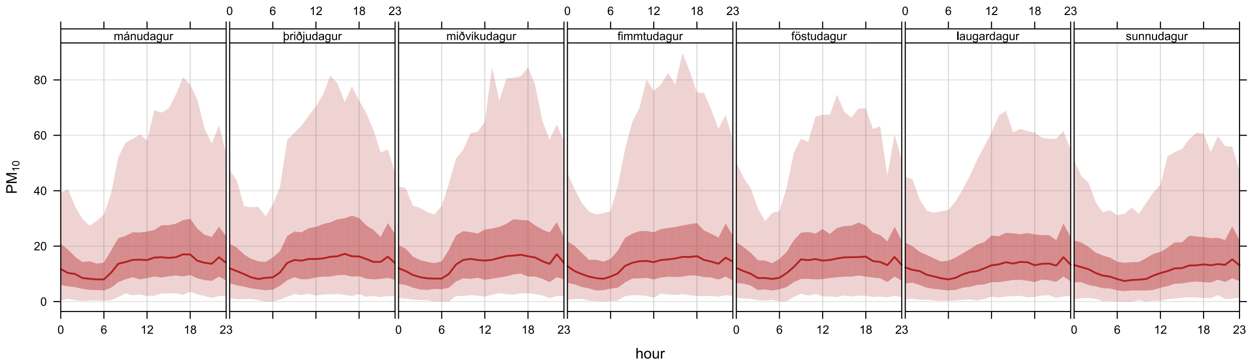

Figure 130. The hourly median PM10 concentration for each day of the week at GRE-station shown with the 25/75th and 5/95th quantile values.

However, there is perhaps a chance to see the effect of mitigation efforts by focusing on calm (wind speed less than 5 m/s) days (Figure 131). On those days dust storms, resuspension and other sources are generally not contributing to the particulate matter pollution, and traffic is the main source, as the smaller variation in concentration values on calm days indicates.

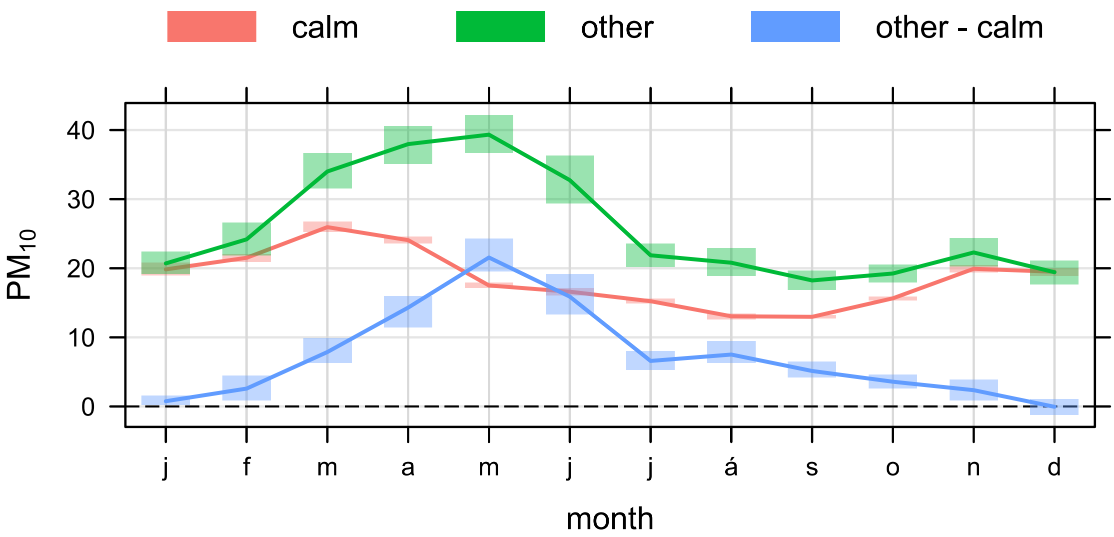

Figure 131. PM10 values at GRE-station when winds are calm (<5 m/s; red) and above (green), and the difference (blue).

Modelling can be used to calculate the expected effects of mitigation measures and those can then be compared to measurements. The advantage of modelling is that the effects of weather are included and therefore should include those effects on the daily, monthly, and annual means, when simulations are run for a given year.

As mentioned above the sources of particulate matter emissions in Iceland are both natural and anthropogenic. The anthropogenic sources are mostly related to traffic, such as exhaust and, especially, non-exhaust emissions from vehicles. During the last 15 years periodic studies analysed the composition of the measured PM in Reykjavík. According to a study carried out to find a standard in measuring PM10 emissions in Iceland (Skúladóttir et al., 2003) the PM10 measured in Iceland and in particular in the capital area consists in 55% of asphalt, 25% of soil, 7% soot, 11% of salt and around 2% of brake lining. When the PM10 concentrations are above the normative limits the composition changes and asphalt prevail with 60% (Skúladóttir et al., 2003). A study carried out for the Road Administration in 2013 by the Engineering Company EFLA, shows a change in composition with 30% soot, 18% of soil, 18% ash, 17% of asphalt, 14% of brake lining, and 3% of salt (Höskuldsson, 2013). The latest report, published in June 2017 and referring to measurements carried out during the winter 2015 shows the following composition: 48.8% of asphalt, 31,2% of soot, 7,7% of soil, 1,6% of brake lining and 3,9% of salt (Höskuldsson & Thorlacius, 2017), but with a lot of variation (Figure 132). Ash and soil can be referred to natural particulate matter, all the other categories are directly referable to road traffic both exhaust and non-exhaust related.

Road dust in Iceland typically causes over 70% of the exceedances of the health limit (50 µg/m^3, 24-h average) for PM10 every year in the capital, Reykjavik. That is based on work done by looking at the wind speed, wind direction and concentration of NOx.

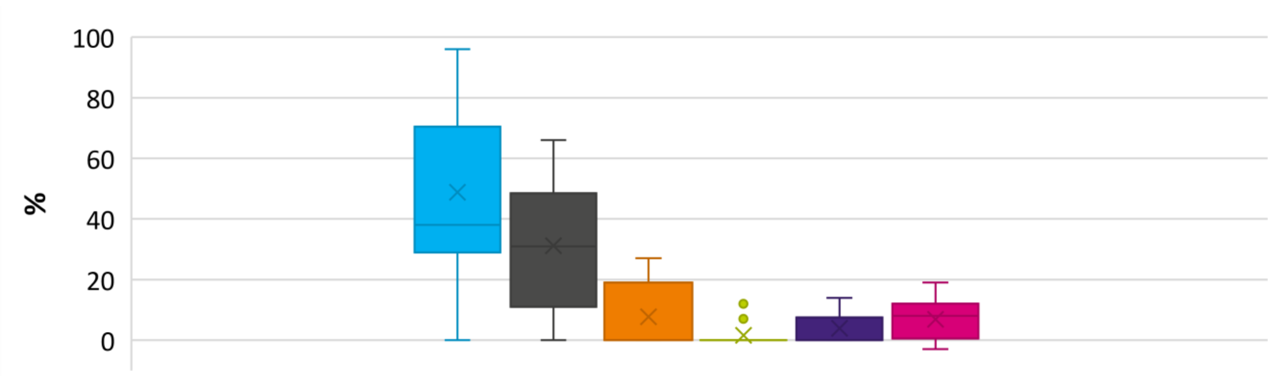

Figure 132. Source of PM10 (Höskuldsson and Thorlacius, 2017); road wear (blue), soot (gray), soil (orange), brake wear (green), salt (purple) and undefined (pink).

The use of studded tyres is allowed from 1 November to 15 April each year and contributes greatly to the dust load; along with at times weak surface material. Road services in winter, where temperatures fluctuations around 0°C are common, include salting and snow removal, which means that snow cover and ice is very uncommon on the main roads in Reykjavik. Street cleaning is generally done a couple of times a year.

The problem with non-exhaust pollution is not likely to go away any time soon in the greater capital area. In recent years traffic has been increasing. As an example, is the sum of three profiles in the capital area (Hafnarfjarðarvegur south of Kópavogslæk, Reykjanesbraut by Dalveg in Kópavogur and Vesturlandsvegur above Ártúnsbrekka), where the number of cars has increased, on average, by about 3100 cars each year since 2005 (Figure 133).

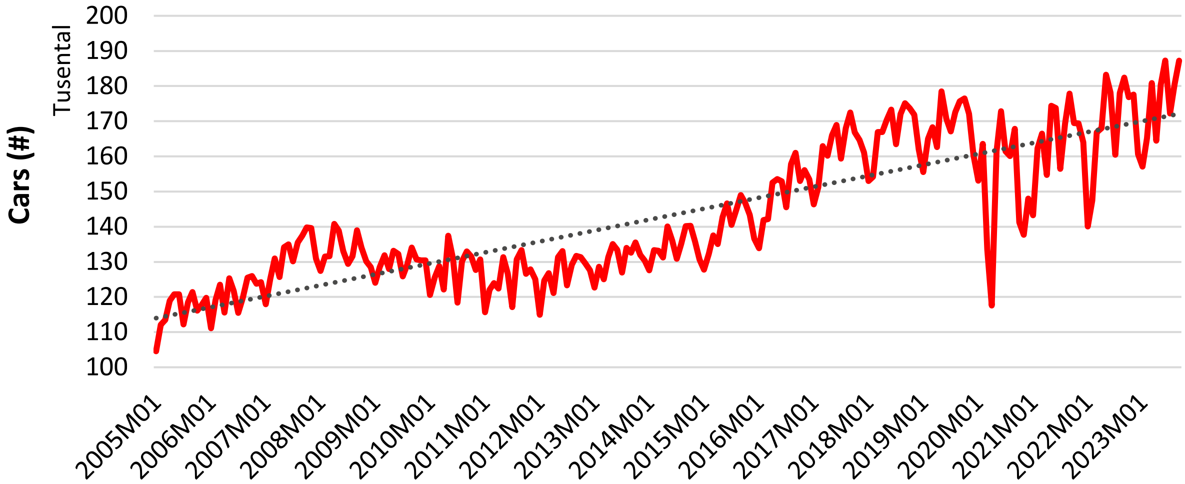

Figure 133. Average daily traffic over three cross sections in the capital area (data SAM31002 from Hagstofa.is).

And although the composition of the car fleet is slowly changing, with electric cars (e-cars) especially becoming more prominent (Figure 134), it alone is not likely to reduce the non-exhaust pollution. E-cars advantage is that there are no direct exhaust emissions, however, tyres, bakes and road wear will still be present. And there is even concern that the electric cars might be heavier and thus lead to more wear (Simons 2016; Timmers and Achten 2018).

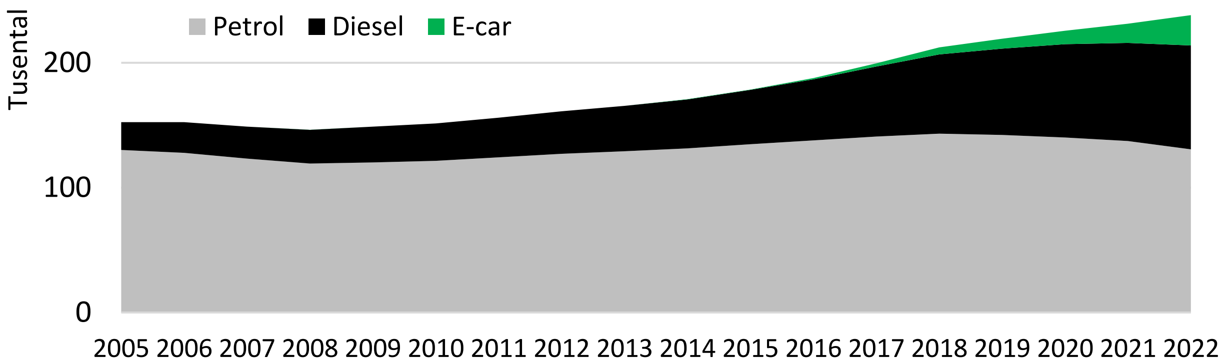

Figure 134. Number of petrol (gray), diesel (black) and electric (green) passanger cars.

And studded tyre use is not decreasing (recent years have been around 45%) (Figure 135). There is no information about whether the same ratio applies to electric vehicles, but that is an interesting aspect to research further.

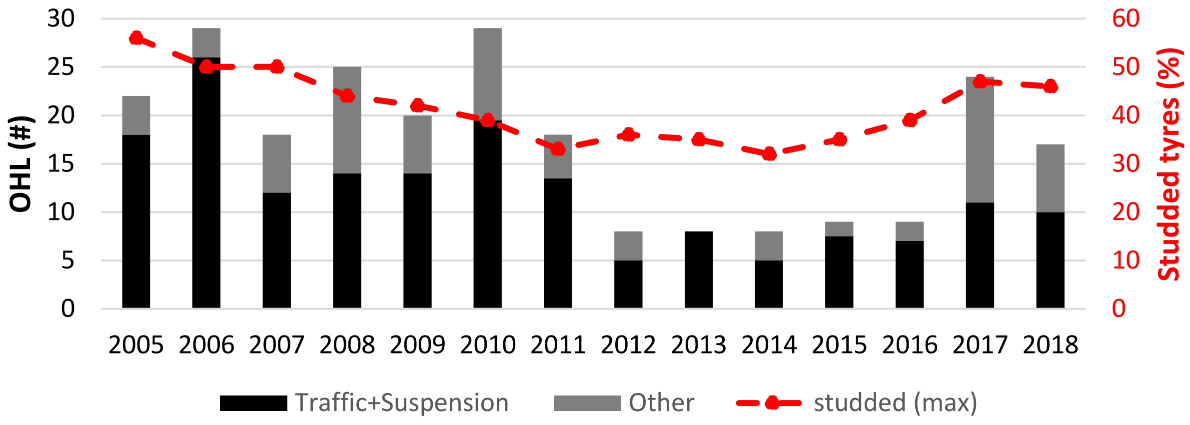

Figure 135. Studded tyre use (red) and times over the health limit (OHL) due to traffic (black bars) and other (gray bars).

Dust loading is thus likely to just increase in the near future. The NorDust II project aimed to measure the dust load on roads with Wet Dust Sampler (WDS), to see how much there is and how it evolves through the seasons. Although those measurements have not, so far, been done over a whole season, a first experiment has been conducted.

To understand the contribution of non-exhaust emissions to the urban particulate matter pollution in Reykjavik, the NORTRIP model (NOn-exhaust Road Traffic Induced Particle Emissions), developed by the Nordic Institute for Air Research, and to explore the effects of mitigation measures (Barr et al., 2021).

And finally, multiroad NORTRIP model was included in AirViro calculations at the Environmental Agency of Iceland. Results from that model are used to calculate the average exposure of individuals in the capital area and can be further utilized to calculate the health burden and cost of pollution.

Methods

Following is a brief description of the methods used in the project. There is extensive literature about the development and use of WDS measurements (e.g., Gustafsson et al. (2019) and references therein).

WDS

A WDS instrument was borrowed from VTI, Sweden as a part of the project. It is a first version WDS 1, which worked fine in a trial run that was made in October 2022. Throstur Thorsteinsson (University of Iceland), Þorsteinn Jóhannsson (Environmental Agency of Iceland), Gísli Guðmundsson (Mannvit) and Páll V. K. Jónsson (the Icelandic Road and Coastal Administration) participated in the measurements.

A turbidity meter from Hanna Instruments (www.hannainst.com), HI88713 ISO Turbidity Meter, was used to measure the turbidity.

NORTRIP model

Single road model was used for a road segment that had good data on traffic density and weather conditions; Kauptún. For model setup and parameters please see Barr et al. (2021).

The multilane version of the NORTRIP model was used to model the pollution due to traffic in the greater Reykjavik area. It was implemented by UST (the Environment Agency of Iceland) in the AirViro system (www.airviro.com), with assistance from Apertum (Lars Gidhagen, pers. comm.).

Results and discussion

WDS trial run

The trial run using WDS 1 was made at Hofsvallagata on 20 October 2022 (Figure 136). This is a relatively quiet street, chosen for easy access and relatively safe environment to gain experience in using the WDS.

Figure 136. WDS measurements at Hofsvallagata on 20 October 2022.

The samples collected were measured for turbidity, according to guidelines from VTI. The results showed relatively low concentrations, but consistent with previous studies the load was less in the wheel tracks and higher between and near the centreline (Gustafsson et al., 2019) (Figure 137).

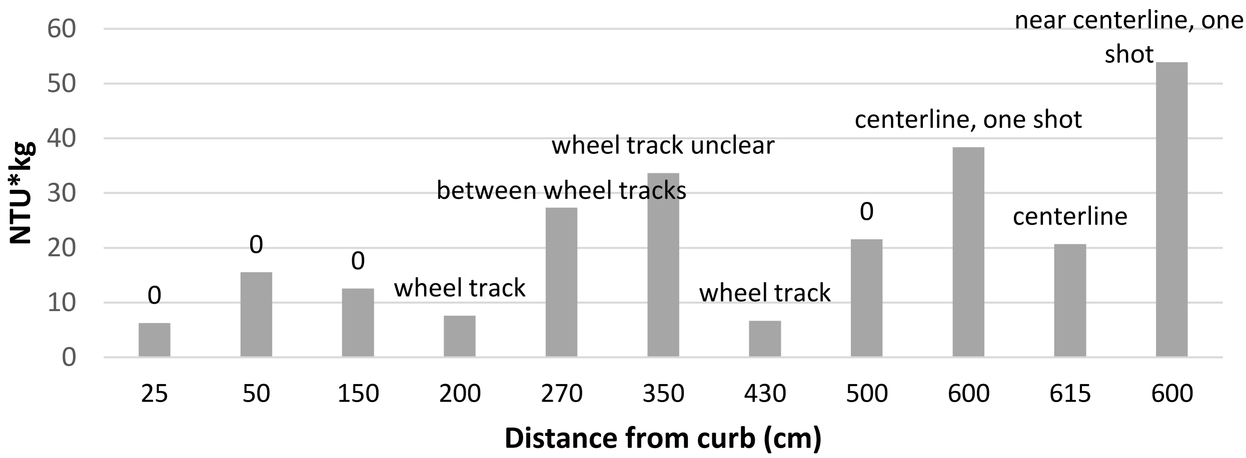

Figure 137. Results of the turbidity measurements (NTU; adjusted for size of sample) of the WDS samples.

The next step for WDS measurements is to measure repeatedly on a busy road, near the GRE-station in Reykjavik. This will give the time variation over season(s), autumn-winter-spring, and comparison to other Nordic cities in terms of dust load. The measurements will also be compared to model results using NORTRIP for the same location.

NORTRIP modelling of mitigation measures

The NORTRIP model was used to explore the effects of weather, changes due to climate change for instance, and a number of mitigation efforts (Barr et al., 2021).

Effect of weather

Although not a mitigation measure, as outlined in the introduction, weather, has a large effect on the atmospheric concentration of particulate matter. It also affects the load buildup on roads, since spraying is a function of the road wetness (Denby and Sundvor, 2012; Denby et al., 2013).

The sensitivity to precipitation and relative humidity (RH) was modelled with the NORTRIP model (Table 17). As a rough summary, wetter means less PM10. Weather does explain a lot of daily and seasonal variations. More details about the calculations and scenarios can be found in Barr et al. (2021).

Table 17. Sensitivity to changes in precipitation frequency, phase, and relative humidity (RH) compared to baseline model run (Barr et al., 2021).

Category	Scenario	Δ Maximum daily PM_{10} ($\mu g/m^3$)	Δ Average PM_{10} ($\mu g/m^3$)	Δ HSL exceedances (days)	Δ% Wet roads	Δ Days with road ice > 0.1 mm
Baseline Simulation	507 mm total precipitation; 57% of days; mean temp = 1°C; mean RH = 82%	104	21	20	53%	38
Precipitation Frequency	No Precipitation, no plowing or salting (P = 0 mm/hr) (RH unchanged)	0	6	7	-15%	-36
	Less Freq. Precipitation (455 mm total) (No precip if RH ≤ 95%)	-2	1	0	-3%	-7
	More Freq. Precipitation (1,248 mm total) (0.1 mm/hr if P = 0 & RH > 80%)	-33	-13	-16	29%	+54
	Constant Precipitation (475 mm total) (P = 0.1 mm/hr) (RH unchanged)	-102	-20	-20	+47%	+80
	Constant Precipitation (950 mm total) (P = 0.2 mm/hr) (RH unchanged)	-102	-20	-20	+47%	+92
Precipitation Phase	Rain Only, no plowing or salting (T_{air} < 4°C increased to 4°C)	-3	-3	-7	+3%	-38
	Snow Only (T_{air} > 0°C decreased to 0°C)	-26	-6	-4	+14%	+85
Relative Humidity	RH +20% (max 100%)	-36	-7	-8	+17%	+27
	RH +10% (max 100%)	-16	-4	-5	+10%	+16
	RH -10%	-1	1	4	-5%	+3
	RH -20%	-1	3	6	-9%	+7

Mitigation

NORTRIP, single lane model, was used to assess the effects of mitigation policies. A further goal is to quantify the impact of mitigation policies on health and related health cost. Several scenarios were modelled, the ones discussed here are changes in studded tyre use and speed controls; the effects of weather have already been discussed.

Further scenarios, when data is available, would include electrification of the vehicle fleet and more on dust binding and other road maintenance measures. The results of a baseline run, using observations of meteorology, traffic density and road conditions indicate that the NORTRIP model does a very good job of modelling the atmospheric concentration of PM10 (Figure 138). The observations are from the nearby GRE-station, no measurements are made on-site.

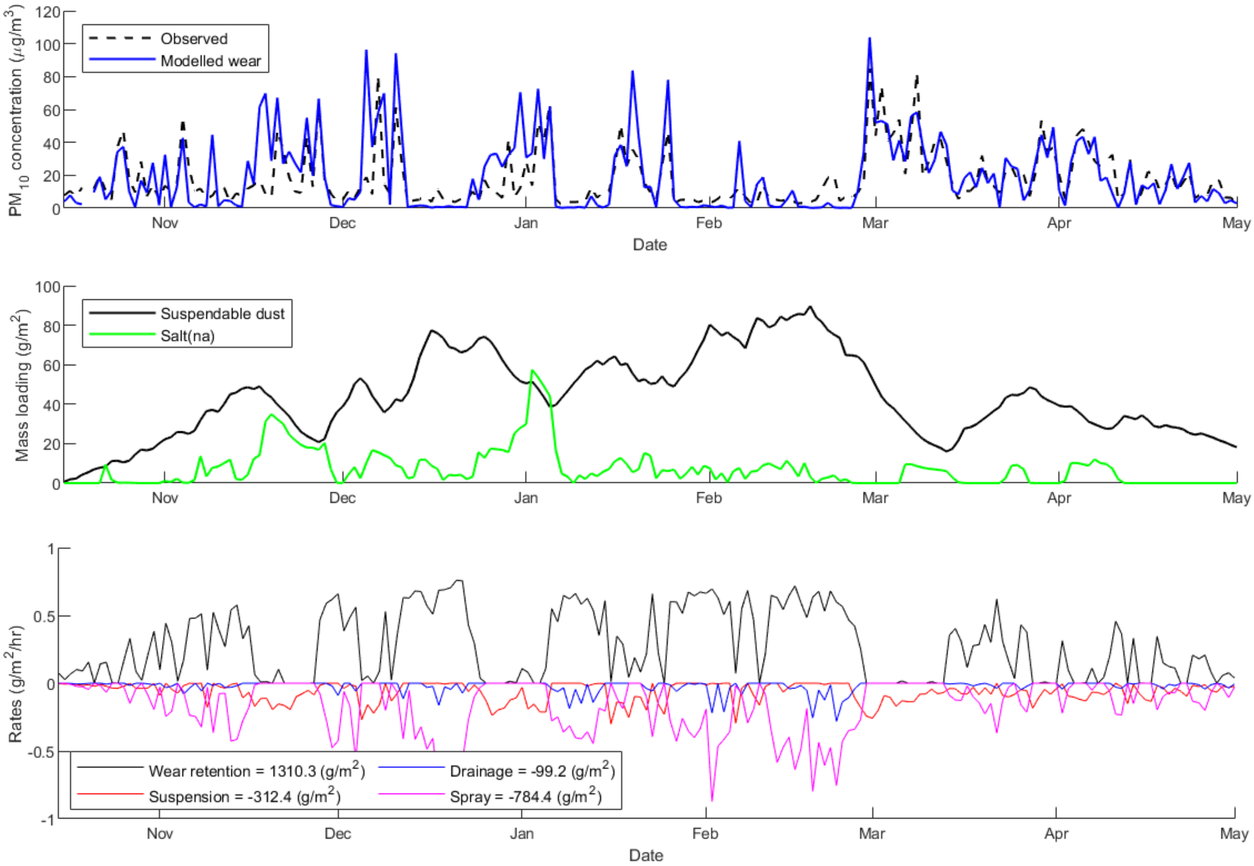

Figure 138. Results from NORTRIP calculations for Kauptún. The modelled atmospheric concentration of PM10 (blue line; top) and the measured concentration (black dashed line; top), dust load (middle) and fluxes of material (bottom).

The mass loading (middle panel in Figure 138) is what we want to measure with the WDS. It shows build up during winter, from the beginning of the studded tyre season (1 November) till early spring. The fluxes of material (Figure 138; bottom) show the importance of spray in reducing the mass load.

Based on the baseline scenario, changes in atmospheric concentration of PM10 were modelled for changes in studded tyre use, changes in velocity and traffic volume (Table 18).

Table 18. Changes from baseline scenario for various mitigation measures (modified from Barr (2020)).

Category	Scenario	∆ Maximum daily PM10 (µg/m^3)	∆ Average PM10 (µg/m^3)	∆ HSL exceedances (days)
Baseline Simulation	Unchanged*	104	21	20
Studded Tyres	40% Max	-11	-2	-4
	30% Max	-30	-6	-10
	20% Max	-48	-9	-17
	0% (studded tyres banned)	-80	-16	-20
Traffic Volume	-5%	-4	-1	-2
	-10%	-7	-2	-3
	-20%	-15	-4	-6
Traffic Speed	-5%	-2	-1	-1
	-10%	-4	-2	-2
	-20%	-9	-4	-6
Traffic Composition	HE vehicles excluded	0	-2	-2

* 46% max studded tyres; ~18.9 million vehicles; ~82 km/h

As expected, the reduction in both maximum daily PM10 concentration, as well as annual average concentration and the number of times over the health limit (OHL) is linear. This is, for instance, the case for the number of cars using studded tyres (Figure 139).

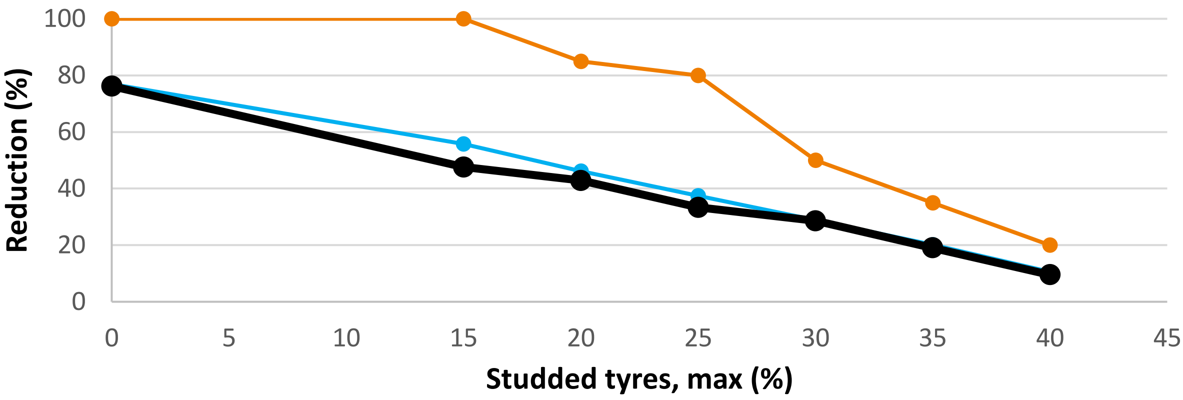

Figure 139. Reduction in average PM10 concentration (black), maximum 24-h concentration (blue) and times OHL (orange) as a function of number of cars using studded tyres.

It will be difficult to get a quick estimate of the success of any mitigation measures that don’t lead to extreme changes. We can see that the annual average values are reduced by 2 – 4 µg/m3 for a 10% change in the number of cars using studded tyres, 10% reduction in velocity or volume. Since the variability of PM10 pollution is very high (Figure 128, Figure 129, Figure 130), this might be very difficult to verify with measurement unless those measures are sustained over long time. There is though, perhaps, as pointed out before (Figure 131) a possibility to see effect on peak concentration (Table 17) during days with calm weather conditions.

If we take a closer look at the effects of velocity, and especially for cars using studded tyres, we find that there is a big opportunity for reduction in road wear. For a passenger car using studded tyres reducing the velocity from 50 km/h to 30 km/h would lead to a 47% reduction in PM10 material generated (

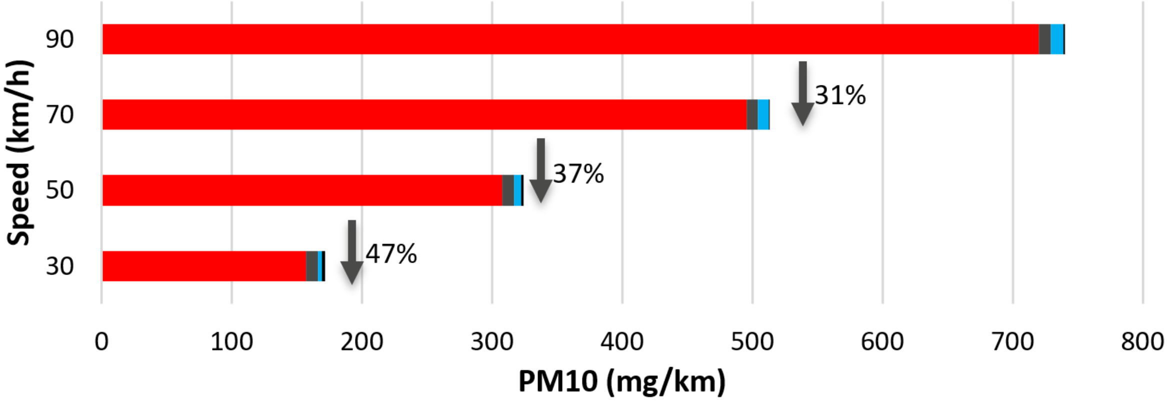

Figure 140). It is important to note that this is road dust generated, not the concentration in the atmosphere. Part of the dust load is removed by spray and other processes (Figure 138) and hence does not contribute to the atmospheric concentration. However, the relation between resuspension and vehicle speed is linear, for instance in NORTRIP (Denby et al., 2013), so all other variables being equal the concentration in the atmosphere should change in a similar manner.

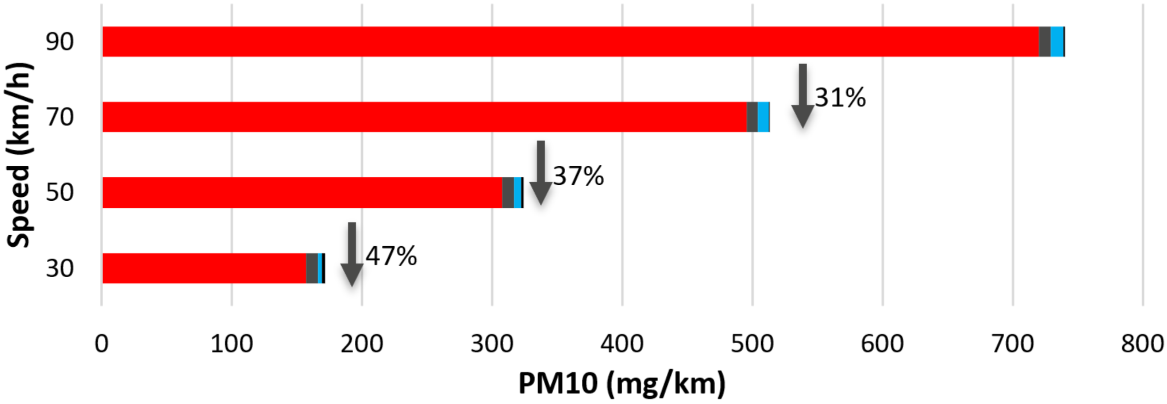

Figure 140. Road wear (red), brake wear (gray), tyre wear (blue) and exhaust (black) as a function of speed for a passenger car using studded tyres.

Although well known, it is interesting to compare the source (amount) of PM10 generated in a year by a car using studded tyres during winter and one that does not (Figure 141). Exhaust and brake wear are the same, the difference is in the road wear during winter. Here, an average driving distance of 12600 km per year in Iceland is equally split over the year and variations between months in road moisture not consideredfor simplicity.

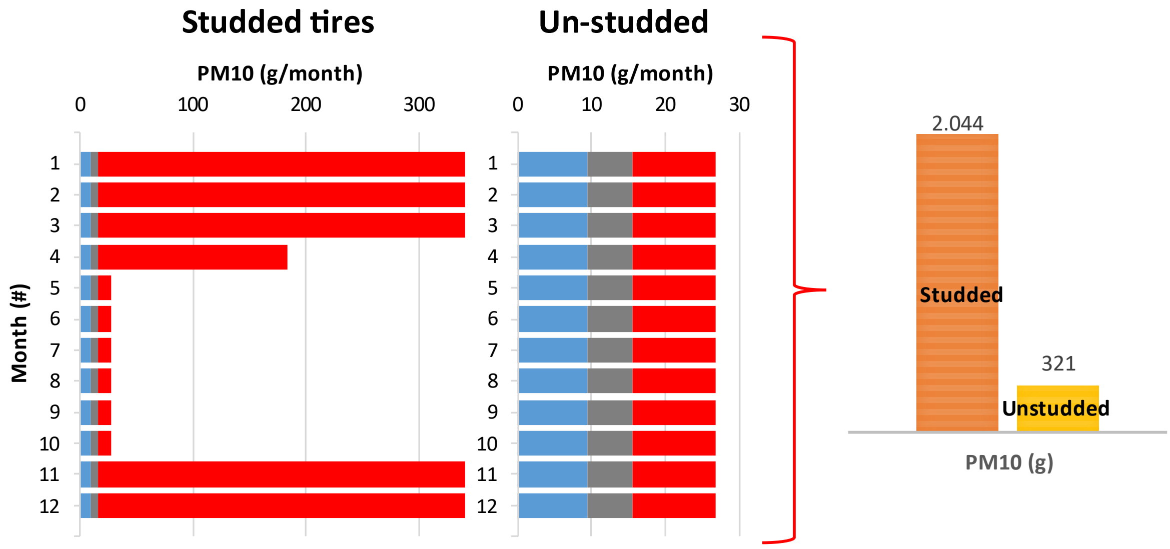

Figure 141. The difference in PM10 material generated depending on whether a car uses studded tyres or not. Tyre wear (blue), brake wear (gray) and road wear (red) are shown as a function of month (left), and the annual sum for the studded tyres and unstudded car (right).

Based on recent trends (Figure 133) there is little reason to believe traffic volume will be reduced in the near future. The opposite is probably much more likely. Therefore, mitigation efforts must target studded tyre use and velocity. This is necessary because of the negative health effects of pollution, in this case, particulate matter pollution. With the implementation of NORTRIP in AirViro modelling package at the Environmental Agency of Iceland we can soon both get high resolution concentration maps (based on the model) and model different scenarios on large scale. This will be very important when considering the effects of mitigation measures and the improvements to health.

Pollution and health

The effects of particulate matter pollution on health are well known (e.g., WHO, 2021; EEA, 2022). It is important to know the exposure of residents, to identify areas of high concentrations and how serious the pollution is by knowing the contribution of different sources for instance.

Large scale efforts often produce results on rather coarse grids (1 km by 1 km), as for instance the concentration of PM2.5 from UBM model for the year 2011 made in the NordicWelfAir project (Figure 142) (NWA, 2020). This makes it difficult to say much about local effects due to proximity to busy roads and such.

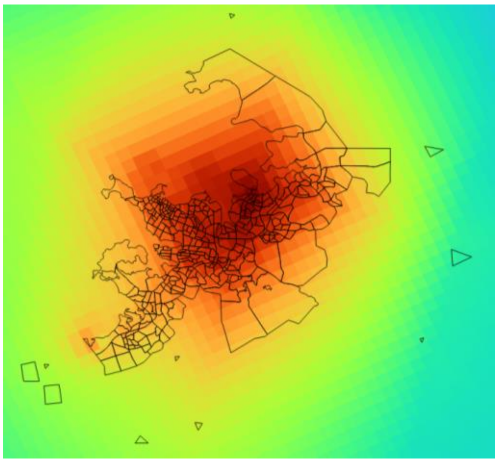

Figure 142. Modelled concentration of PM2.5 on a 1 km by 1 km grid using the UBM model; color scale from 3 μg/m^3 (green) to 6.2 μg/m^3 (dark red) (NWA, 2020).

Traffic volume is known from counts at several cross sections and then modelling (VSO, 2007). An example is shown in Figure 143 for the capital area. With that information and all the other variable needed for NORTRIP and AirViro the atmospheric concentration of pollutants related to traffic (and other sources, although not important within the capital area) can be modelled (Figure 144).

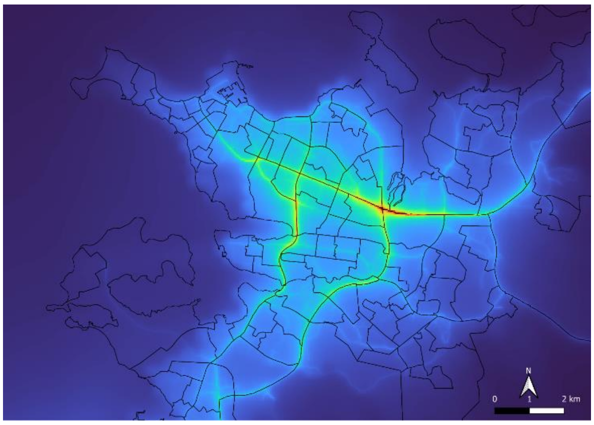

Figure 143: Traffic density; red color about 90 thousand cars per day (VSO, 2007).

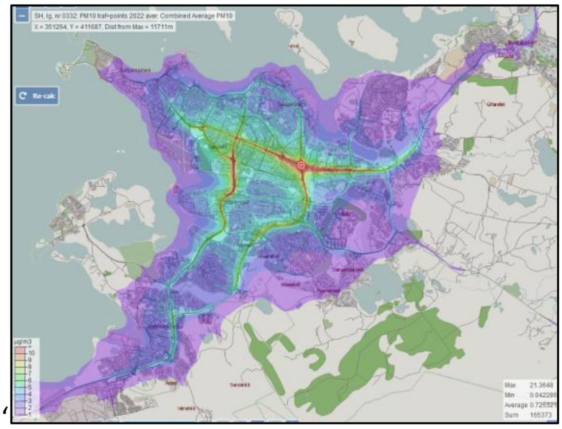

Figure 144: Example of AirViro results for PM10 based on NORTRIP model (preliminary results; Lars Gidhagen, Apertum).

Modelling, analysis of sources, shows that contributions to particulate matter from sources other than traffic are minor (there is a little effect near harbours and aluminium smelters). The high-resolution modelling allows for calculations of exposure in smaller areas within the capital area (Figure 145).

From that kind of map, and with information about the population (Figure 146), we can calculate how many people live in areas with the highest concentration of various pollutants and, as appropriate, focus mitigation efforts accordingly. Some preliminary results, for instance, give the population weighted average PM2.5 exposure of 3.4 µg/m^3 in the capital area.

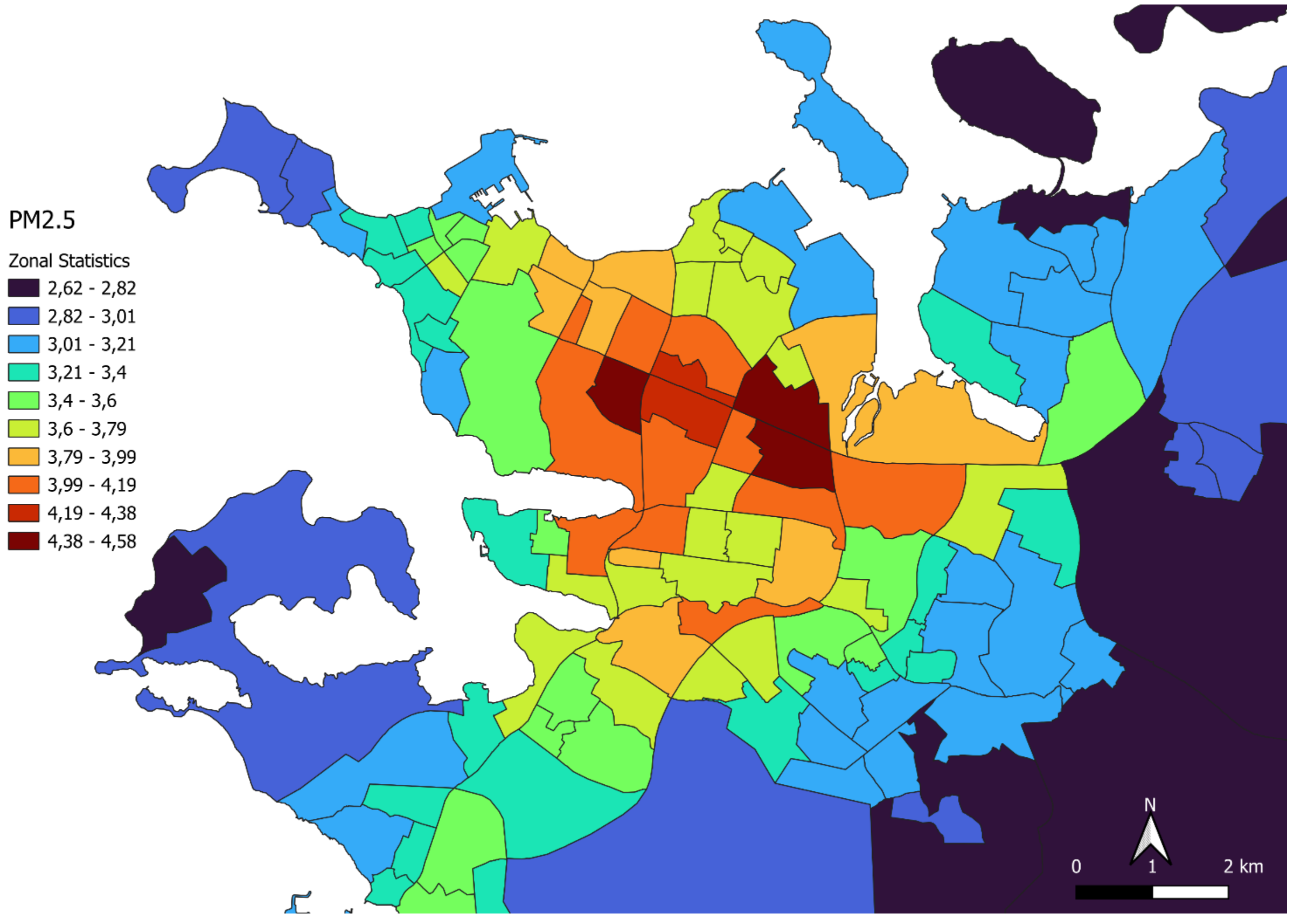

Figure 145. Average PM2.5 concentration in areas within the capital region based on model in Figure 144 (for PM2.5).

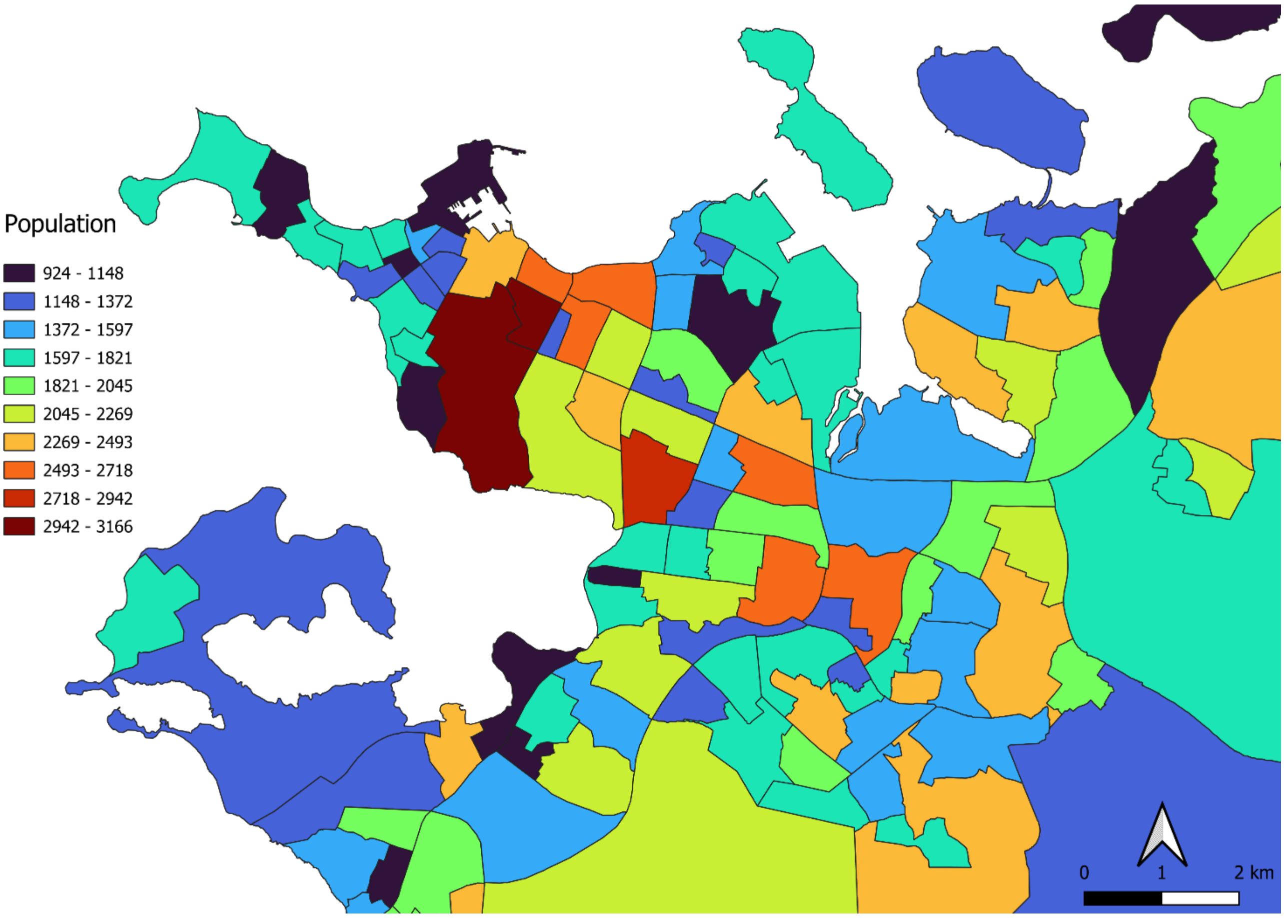

Figure 146. Population in each sub-area within the greater capital area.

Conclusions

In Iceland, as many other countries in the world, traffic is a major source of pollution, especially in the capital area. Unlike some other countries, wood burning, industry and other local effects don't contribute much. With the electrification of the vehicle fleet, although the time scale is very uncertain, we can hope to eliminate much of the exhaust pollution. The non-exhaust pollution will remain a problem to mitigate. We mostly know the solutions, reducing the source by limiting the use of studded tyres and reducing the velocity. Where to focus those mitigation measures can be answered with modelling.

Measuring the effect of mitigation measures can prove difficult, given the large range of values on different time scales for PM10 concentrations. However, there may be opportunities in focusing on calm days where traffic is expected to be the only important variable.

NORTRIP is a very valuable tool for modelling and predicting the pollution levels due to traffic and modelling future scenarios. That further allows us to estimate the health impacts of the pollution and associated cost.

References

Barr, B.C. 2020. Processes and Modelling of Non-Exhaust Vehicular Emissions in the Icelandic Capital Region. MS Thesis, University of Iceland, http://hdl.handle.net/1946/36857

Barr, B.C., Hrund Ólöf Andradóttir, Throstur Thorsteinsson, & Sigurður Erlingsson. 2021. Mitigation of Suspendable Road Dust in a Subpolar, Oceanic Climate. Sustainability, 13(9607), 1 – 16. https://doi.org/10.3390/su13179607

Denby, B. R., and I. Sundvor. 2012. NORTRIP Model Development and Documentation Emission Modelling. NILU, Scientific Report, 2012.

Denby, B. R., I Sundvor, C. Johansson, L. Pirjola, M. Ketzel, M. Norman, K. Kupiainen, M. Gustafsson, G. Blomqvist, M. Kauhaniemi, and G. Omstedt. 2013. A Coupled Road Dust and Surface Moisture Model to Predict Non-Exhaust Road Traffic Induced Particle Emissions (NORTRIP). Part 2: Surface Moisture and Salt Impact Modelling. Atmospheric Environment 81:485–503.

European Environment Agency [EEA]. 2022. Air quality in Europe 2022. https://www.eea.europa.eu//publications/air-quality-in-europe-2022

Einarsson, S., V. Gunnarsdóttir, Á. Sigurðardóttir, G. Pétursdóttir, H. V. Jensson, L. S. Jónsdóttir, S. Þ. Sigurðarson, & Þ. Jóhannsson. 2013. Hreint Loft, Betri Heilsa/Clean Air, Better Health. Umhverfis- og auðlindaráðuneytið / velferðarráðuneytið. doi:ISBN 978-9979-799-64-1.

Gustafsson, M., G Blomqvist, I. Järlskog, J. Lundberg, S. Janhäll, M. Elmgren, C. Johansson, M. Norman, S. Silvergren. 2019. Road Dust Load Dynamics and Influencing Factors for Six Winter Seasons in Stockholm, Sweden. Atmospheric Environment: X, vol. 2, no. September 2018, p. 100014, doi:10.1016/j.aeaoa.2019.100014.

Höskuldsson, P. (2013). Samsetning svifryks í Reykjavík [Chemical composition of particulate matter in Reykjavik]. Report to the Icelandic Road and Coastal Administration, Samsetning svifryks í Reykjavík (vegagerdin.is)

Höskuldsson, P. & A. Thorlacius. 2017. Uppruni svifryks í Reykjavík [Sources of particulate matter in Reykjavik]. Report to the Icelandic Road and Coastal Administration, Uppruni svifryks í Reykjavík.pdf (vegagerdin.is)

Krzyzanowski, M. and A. Cohen. 2008. "Update of WHO Air Quality Guidelines." Air Quality, Atmosphere and Health 1(1):7–13.

NordicWelfAir [NWA] project. 2020. https://projects.au.dk/nordicwelfair/

OECD. 2020. Non-exhaust Particulate Emissions from Road Transport: An Ignored Environmental Policy Challenge. Paris.

Simons, A. 2016. "Road Transport: New Life Cycle Inventories for Fossil-Fueled Passenger Cars and Non-Exhaust Emissions in Ecoinvent V3." International Journal of Life Cycle Assessment 21(9):1299–1313.

Skúladóttir, B., Thorlacius, A., Larssen, S., Bjarnason, G. G., & Thórdarson, H. (2003). Method for determining the composition of airborne particle pollution. Nordtest technical report 544.

Statistics Iceland. 2023, March 9. *Mesta fjölgun íbúa frá upphafi*. Hagstofa.is. Retrieved December 8, 2023, from https://hagstofa.is/utgafur/frettasafn/mannfjoldi/mannfjoldinn-1-januar-2023/

Throstur Thorsteinsson, Guðrún Gísladóttir, Joanna Bullard and Grant McTainsh. 2011. Dust storm contributions to airborne particulate matter in Reykjavík, Iceland. Atmospheric Environment, 45: 5924 – 5933.

Thorsteinsson, Throstur & Hrund O Andradottir. 2021. Using modelling to map out ways to mitigate traffic related particulate matter in Iceland. Nordic Road & Transport Research, 28 May 2021.

Timmers, Victor R. J. H. and Peter A. J. Achten. 2018. Non-Exhaust PM Emissions From Battery Electric Vehicles. Elsevier Inc.

VSO, 2007. Nýtt umferðarlíkan Höfuðborgarsvæðisins [New traffic model for the capital area]. Report to the Icelandic Road and Coastal Administration.

World Health Organization [WHO]. 2021, November 17. How air pollution is destroying our health. https://www.who.int/news-room/spotlight/how-air-pollution-is-destroying-our-health

Þröstur Þorsteinsson. 2021. Áhrif hraða á mengun vegna umferðar. Skýrsla til Vegagerðarinnar, mars 2021.

Höskuldsson, Páll, and Arngrimur Thorlacius. 2017. Uppruni Svifryks í Reykjavík. Report to the Icelandic Road and Costal Administration.

Work package 7: NORTRIP model devel-opments

Aims

The overall aim of WP7 is to improve NORTRIP model parameterisations using field campaign and laboratory data collected during the project. Improvements based on existing observational datasets are also part of WP7.

Motivation

The NORTRIP model has been developed to represent non-exhaust emissions from traffic. This can be a complex process since non-exhaust emissions are very dependent on road surface conditions as well as winter road maintenance activities. In this project a number of processes were selected where NORTRIP currently lacks observational evidence for the further development of model parameterisations. In addition, NORTRIP has been applied in new regions, Iceland (see WP 6) and Helsinki (WP 4). The following processes have been addressed in the model development.

- Development of a tunnel module (application to dust binding migration)
- Wet removal processes and their parameterisations (sensitivity tests using existing data)
- Speed dependence of wear (field campaigns and sensitivity tests)
- Evaluation of dust binding (field campaigns and existing data)
- Parameterisation of sanding and crushing of sand (laboratory experiments)
- Implementation of NORTRIP in Helsinki (model implementation for health impacts)
- Impact of vehicle weight on wear (field and laboratory campaigns)

Migration module in NORTRIP and its application to the dust binding field campaign

As part of the model development to implement a tunnel model in NORTRIP a migration module has been developed. This module describes the migration of water and/or chemicals/salt/dust along the road surface. For tunnels this module is intended to predict the migration of water into the tunnels from outside of the tunnel, in order to predict road surface wetness along the tunnel, which in turn controls the road dust emissions in the tunnel.

The case we will describe here is for the application of dust binder to the road surface, but the model formulation is the same for water, except for additional source and sink terms such as dripping from vehicles and evaporation/condensation. Dust binder is usually applied over a limited street length so the dust binder can be transported from the treated road area to the non-treated part of the road. At the same time dust-binder is reduced in the treated area. This process is dependent on several processes including:

- Vehicle speed
- Vehicle volume
- Driving patterns
- The rate of uptake of the chemical on the vehicle tyres
- The rate of deposition from the vehicle tyres
- Tyre width and size
- The wetness of the road surface

Migration module description

The tyre and road water/salt interaction can be described as an advection process where water/salt on tyres is transported into the tunnel or along the road from wet/salted regions to dry/unsalted regions. In addition to the advection an exchange process also takes place where water/salt is deposited on the road and/or tyre by direct physical contact. The overarching differential equations that govern this process where the production (*P*) and sinks (*S*) provide the tendency for each prognostic variable can be written as

$$\frac{\partial g_t}{\partial t} + V_{veh}\frac{\partial g_t}{\partial x} = P_{wt-t} - S_{t-wt} + P_{bwt-t} - S_{t-bwt} \qquad (1)$$

$$\frac{\partial g_{wt}}{\partial t} = P_{t-wt} - S_{wt-t} \qquad (2)$$

$$\frac{\partial g_{bwt}}{\partial t} = P_{t-bwt} - S_{bwt-t} \qquad (3)$$

where g_{wt}, g_{bwt} and g_t are the mass of water and/or salt on the road wheel tracks, between wheel tracks and on the tyres respectively, at time t and position x along one lane of the road. These are given with units mm or kg/m^2 for water and g/m^2 for chemicals. V_{veh} is the vehicle speed. In these equations it is assumed that the interaction between the wheel track and the between wheel track mass is via production and sink terms from the tyres. i.e. that there is a form of lateral transfer, via the tyres, between the wheel tracks and the between wheel tracks due to meandering of the traffic.

The production of road water/salt onto the tyre, P_{wt-t} and P_{bwt-t} (g/m^2/veh), is dependent on the rate of uptake and deposition to and from the tyre as well as on the eventual surface mass balance of the tyre, i.e. how much water/salt is on the tyre, in relation to the road surface water/salt, under steady state conditions. We prescribe then a length scale L_{tyre} that reflects the length over which this transfer occurs. Visually this is represented by the wheel track left behind on a dry road surface after driving over a wet road surface. We write this as being dependent on the tyre circumference C_{tyre} and a characteristic number of revolutions of the tyre n_{tyre} as:

$$L_{tyre} = n_{tyre}\, C_{tyre} \qquad (4)$$

For water, observed length scales are of the order of 5 to 50 m, which for C_{tyre} =1.5 m would give n_{tyre} of between 5 and 35 revolutions. For salt this may be quite different. Based on this length scale the related time scale is then specified by dividing by the vehicle speed V_{veh} in Equation 1.

In addition, the uptake from the road surface to the tyre will be limited, e.g. if the road surface has 1 mm of water it is not expected that the tyre, in equilibrium with the road water, will also be covered by 1 mm of water. The same for surface salt. This is given as an equilibrium balance factor b_{tyre} which indicates the fraction of the road surface water/salt that is in balance with the tyre surface. The production of water/salt on the tyre, and corresponding sink term from the tyre to the road, can then be written as:

$$P_{(b)wt-t} = \frac{V_{veh}}{L_{tyre}}\, b_{tyre}\, g_{(b)wt} \qquad (5)$$

$$S_{t-(b)wt} = \frac{V_{veh}}{L_{tyre}}\, g_t \qquad (6)$$

Note that the sink term from the tyre to the road does not include the factor b_{tyre} as this is not a limiting factor when depositing from the tyre to the road. The factor b_{tyre} is not measured, though this should be possible. In cases with migration of other substances, such as salt and dust binder, this factor may be quite different to that for water.

Since a tyre only covers a fraction of the road surface an additional parameter a_{tyre} is used that provides the fraction of the road width, per lane, covered by the passing vehicles tyres. This will depend on whether we are modelling the wheel tracks or between wheel tracks.

$$a_{tyre} = \frac{2\, w_{tyre}}{w_{lane}}$$

$$a_{wt} = \frac{w_{tyre}}{w_{wt}}$$

$$a_{bwt} = \frac{w_{tyre}}{w_{bwt}}$$

$$w_{lane} = w_{bwt} + w_{wt} \quad (7)$$

In these equations, w_{tyre} and w_{lane} are the width (in meters) of a tyre and of a lane, respectively, and w_{wt} and w_{bwt} are the width of a lane covered by wheel tracks and between wheel tracks, respectively. Formulated in this way the modelling area for the wheel tracks does not need to be the same as the width of the tyres, but for simplicity we do so here so that $a_{wt} = 1$ and $a_{bwt} = 1 - a_{tyre}$

This parameter will be around a_{tyre} ~ 0.1 - 0.2 and will be vehicle type dependent. Similarly, in the along road direction, the vehicle density or specifically the density of tyre surface along the road, must be taken into account. This is specified as the length of tyre per km road and is given by

$$d_{tyre} = 2\ C_{tyre} \frac{N_{veh}}{V_{veh}} \quad (8)$$

where N_{veh} is the number of vehicles per lane per hour. The factor 2 occurs because each car is assumed to have 2 wheels per wheel track. The production and sink terms for tyre to road will be balanced by the same terms as in Equations 5 and 6, but take into account the crossroad tyre $a_{(b)wt}$ fraction and the along road tyre fraction d_{tyre} as follows:

$$P_{t-(b)wt} = \frac{V_{veh}}{L_{tyre}}\, d_{tyre}\, a_{(b)wt}\ g_t \quad (9)$$

$$S_{(b)wt-t} = \frac{V_{veh}}{L_{tyre}}\, d_{tyre}\, a_{(b)wt}\, b_{tyre}\, g_{(b)wt} \quad (10)$$

It is useful to rewrite these two equations using an effective speed such that

$$P_{t-(b)wt} = \frac{V_{eff}}{L_{tyre}}\ g_t \quad (11)$$

$$S_{(b)wt-t} = \frac{V_{eff}}{L_{tyre}}\ b_{tyre}\, g_{(b)wt} \quad (12)$$

where

$$V_{eff}^{(b)wt} = 2\ C_{tyre}\, N_{veh}\ a_{(b)wt} \quad (13)$$

This effective speed represents the rate of advance of the advected water/salt and is significantly less than the vehicle speed, for example for N_{veh} = 1000 veh/h, V_{eff} is just 3 km/h when $a_{(b)wt}$ = 1 and C_{tyre} = 1.5 m.

The last parameter required is the amount of time, or distance, the tyres are in the wheel tracks or between the wheel tracks. This factor f_{bwt} ~ 0.01 – 0.1 reflects the meandering and lane changing of the traffic and is the fraction of time spent inbetween the wheel tracks.

The final equations are then given as:

$$\frac{\partial g_t(x,t)}{\partial t} + V_{veh}\frac{\partial g_t(x,t)}{\partial x} = -\frac{V_{veh}}{L_{tyre}}\left[g_t(x,t) - b_{tyre}\big((1-f_{bwt})\, g_{wt}(x,t) + f_{bwt}\, g_{bwt}(x,t)\big)\right] \quad (14)$$

$$\frac{\partial g_{wt}(x,t)}{\partial t} = \frac{V_{eff}^{wt}}{L_{tyre}}(1-f_{bwt})\big(g_t(x,t) - b_{tyre}\, g_{wt}(x,t)\big) \quad (15)$$

$$\frac{\partial g_{bwt}(x,t)}{\partial t} = \frac{V_{eff}^{bwt}}{L_{tyre}} f_{bwt}\left(g_t(x,t) - b_{tyre}\, g_{bwt}(x,t)\right) \quad (16)$$

It can be shown that the tyres quickly adapt to the surface conditions, when L_{tyre} is short. In this case Equation 14 quickly reaches an equilibrium between advection and tyre uptake and deposition. A quasi-steady state solution then neglects the first term in Equation 14 and then the whole set of Equations become independent of vehicle speed, making it easier to solve both analytically and numerically. Equation 14 can then be written:

$$\frac{\partial g_t(x,t)}{\partial x} = -\frac{1}{L_{tyre}}\left[g_t(x,t) - b_{tyre}\left((1-f_{bwt})\, g_{wt}(x,t) + f_{bwt}\, g_{bwt}(x,t)\right)\right] \quad (17)$$

There can be physical limits to how much water/salt a tyre can accumulate, e.g. this formulation will not be valid when passing over deep puddles of water. However, since we always limit the accumulated water on the road surface to a threshold in NORTRIP, through drainage, we do not enforce any limit to the uptake of the vehicle tyre in the migration model.

In addition, there are possible other processes that will affect the mass balance. For water this includes precipitation, evaporation, condensation, drainage and vehicle spray. For salt, drainage and spray may affect the balance but under dry conditions, when dust binding is applied, vehicle spray, or suspension, may lead to a loss of surface salt. In NORTRIP spray is parameterised as a sink from the road surface, rather than a loss from the tyre which would be more appropriate here. We can include this spray loss term in the tyre mass balance using

$$S_{spray} = f_{spray} \frac{V_{veh}}{L_{tyre}}\, g_t \quad (18)$$

where f_{spray} is a fraction of water/salt on the tyre that is lost to spray. This fraction is not known and is also likely speed dependent. The spray rate, though perhaps small compared to the road interaction, is dependent directly on the mass on the tyre rather than the difference between the road and tyre mass. It can therefore be an important process and may also lead to an increase in mass between the wheel tracks, in addition to a loss from the wheel tracks.

Steady state homogenous solutions are achieved with these formulations when the amount of water/salt deposited on the road is the same as the uptake of the tyres and there are no horizontal gradients for advection, giving

$$b_{tyre}\, g_{(b)wt} = g_t \quad and \quad g_{wt} = g_{bwt} \quad (19)$$

Equations 14 to 16 are solved numerically using a simple first order implicit upwind advection scheme. The grid length is 10 m and the time step is 0.1 seconds. The time step is limited by stability criteria of the advection scheme.

Application to the Linköping CMA field campaign

During the CMA field campaign in Linköping, Chapter Residual dust binder (CMA, measurements of on road CMA have been made. We concentrate on the acetate measurements as these give the best representation of the CMA concentration. The main characteristics of the experiment and dataset are:

- CMA was placed on the road surface up to 1.2 km upstream of the measurement point at 3 am in the morning. CMA was also applied downstream and on other roads, but this was not included in the calculations.
- Measurements of acetate were made 0.5, 6, 9, 12 and 30 hours after the application.
- The right wheel track showed acetate concentrations of 20 g/m^2 immediately after application but the left wheel track showed only 3 g/m^2 due to inhomogeneity of the distribution. 17 g/m^2 was

measured between the wheel tracks with the first measurement, but the wheel track measurements also showed a large variability, likely the result of the inhomogeneous distribution of the CMA.

- Traffic volume past the measurement site is 7200 veh/day (ADT) in the Southern direction and an hourly traffic temporal profile is available from 2018 counts.
- Several intersections occur along the upstream dust bound region and estimates of traffic leaving or coming onto the dust bound region were made.
- The number of lanes is set to 2.

The model was set up with the following inputs and parameters:

- A 2.5 km stretch of road was set up in the model. Acetate was distributed 1.2 km upstream of the measurement point with a loading of 20 g/m^2 and nothing downstream of this point.
- The model was sampled at 1.19 km to show the change in loading at the end, but within, the binding area, representing the right wheel track. Another point at 1.3 km, 100 m beyond the binding area, was also sampled. This is intended to simulate the left wheel track, since the left wheel track did not appear to be treated with much CMA at the measurement site. It is not known how far upstream this inhomogeneity exists.
- Calculations were made with the realistic traffic temporal profile.
- Traffic speed is taken to be the signed speed of 40 km/h
- Incoming and leaving traffic to the dust bound part of the road were included at 4 points along the dust bound road. These are shown in Figure 147.
- Plots of loading are made along the model road trajectory at various times, out to 30 hours, as well as temporal plots at particular points along the road, particularly the two points at 1.19 and 1.3 km representing the right and left wheel tracks.
- The fraction of the lane width covered by tyres is set to a_{tyre} = 0.15.
- The length scale chosen is L_{tyre} = 7.5 m, or 5 tyre revolutions.
- The factor b_{tyre} , that determines the relative fraction of dust binder on the tyre, compared to the road, is given a value of b_{tyre} = 0.2.
- The fraction of time spent not in the wheel tracks, f_{bwt}, is set to 0.05
- Two spray loss terms were assessed, no loss f_{spray} = 0 and f_{spray} = 0.02 (2%) is included in the model results.

Figure 147. Map of Linköping showing the CMA application area. The model follows the bound road from the surface measurement site back to roughly the end of the dust binding track in the North. Blue arrows, with traffic numbers, indicate where the model took in traffic without dust binder on the tyres. Only at 1 point, 200 m north of the measurement site, are 3400 vehicles allowed to leave the dust binding transect.

In Figure 148 the results of the model calculations, for the specified parameters, is shown using two different values for the spray loss parameter. The model output at 1.19 km and 1.3 km are intended to represent the right and left wheel tracks respectively. The parameters in the model have been chosen to give similar results to the observations, though it was not possible to tune the model to exactly fit the observations. Better results are achieved with a 2% loss rate.

Given all the uncertainties in the input data and in the spreading of the CMA on the road surface, the results in Figure 148 show that given the appropriate model parameters the model can largely reproduce the impact of traffic migration on the observed acetate concentrations. Many more experiments would be required to better specify these parameters.

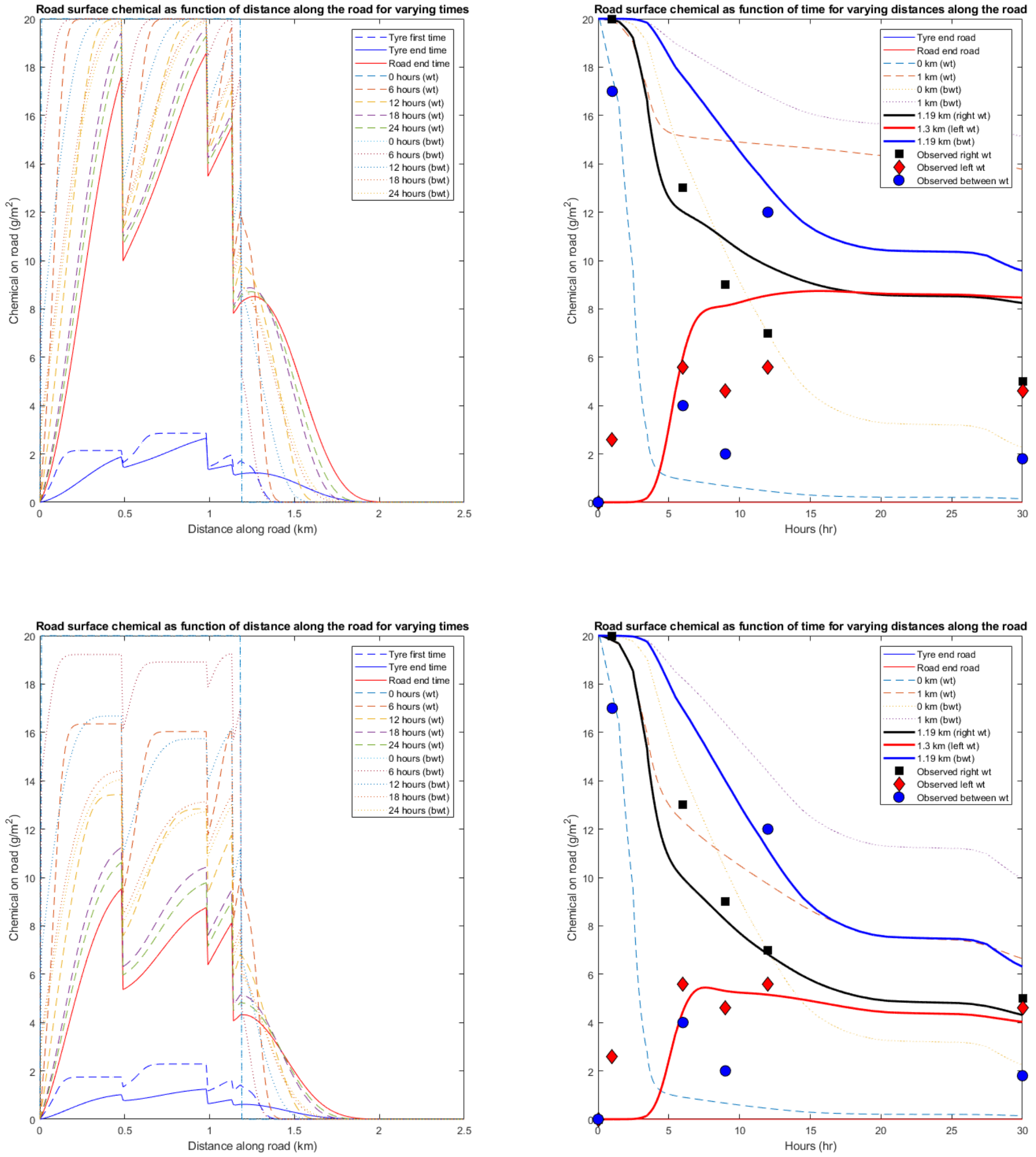

Figure 148. Results of the migration model calculations including observed road surface Acetate. Top is with no spray loss from the tyres and the bottom plot shows calculations with a loss rate of 2%. See text for details.

As a model experiment, we extended the calculations to cover 1 week (168 hours), both with and without a spray loss rate of 2%. The results are shown in Figure 149. After one week most of the dust bound road had a coverage of < 1 g/m^2 acetate with 2% spray loss and < 5 g/m^2 acetate without spray loss. If an acetate level of 5 g/m^2 is required for effective dust binding then, in the case with 2% spray loss, this implies that dust binding should be applied perhaps every 72 hours.

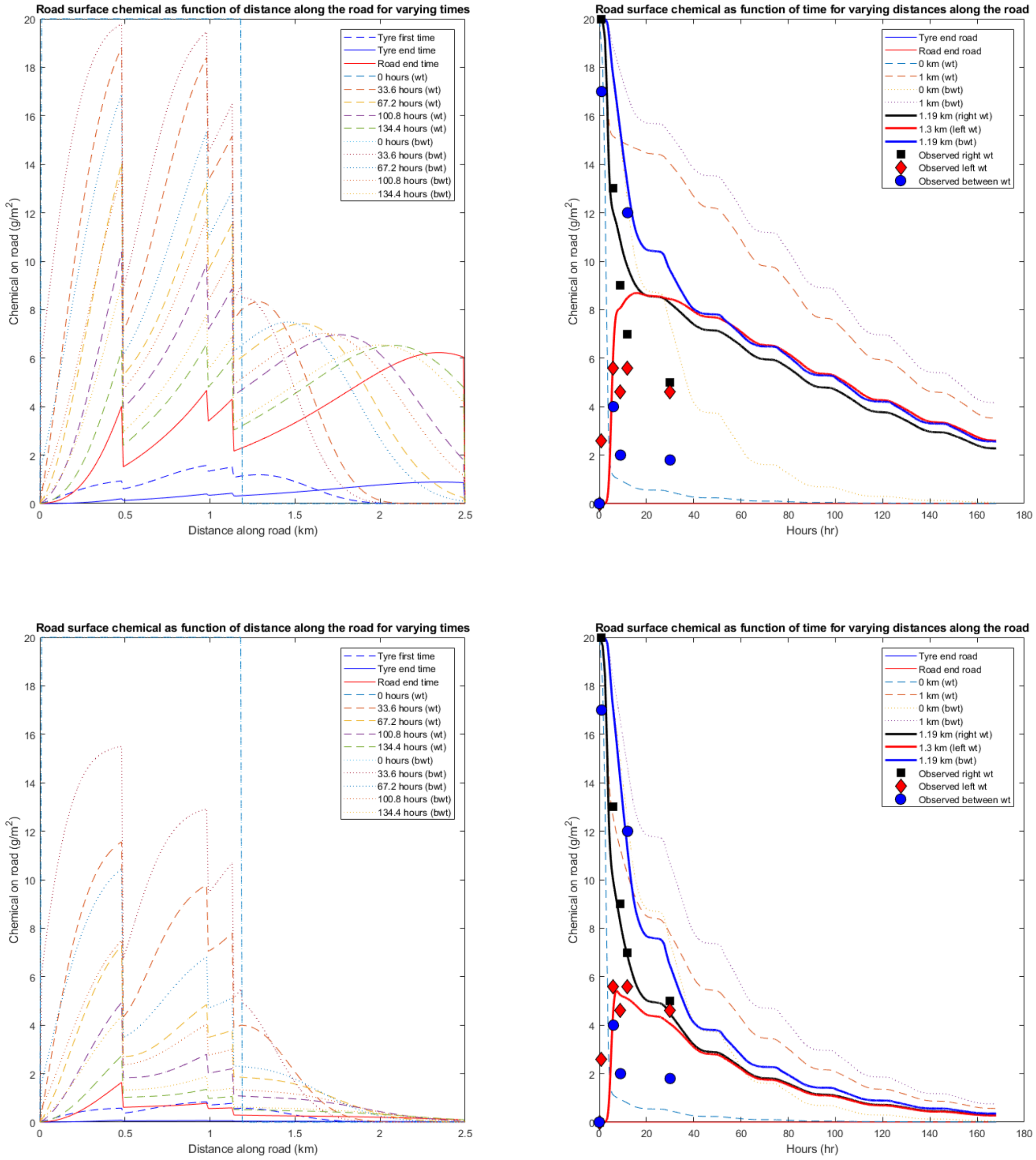

Figure 149. As in Figure 147 but for a 168-hour period.

Conclusions, migration modelling

A simple model for traffic migration of road surface water and chemicals, originally developed for tunnel modelling, has been applied to model the migration of CMA dust binding in Linköping. Measurements of road surface acetate have been used to assess the model. Despite the uncertainties in much of the input data and in the spreading of the CMA on the road surface, the results show that given the appropriate model parameters the model can largely reproduce the impact of traffic migration on the observed acetate concentrations. Interestingly, the model provides a quantification for the decay rate of dust binder on the road surface, based on the area where dust binder is applied and the traffic flow in and out of the applied area. This then becomes a tool for managing effective dust binding. Many more specific experiments would be required to better specify the model parameters used including measurements of acetate on the tyres and more downstream measurements of acetate. The methodology is also applicable for the migration of water, which is an easier substance to measure.

Assessment of model parameters through sensitivity analysis using existing data in Norway

A number of model parameters have been assessed through sensitivity analysis. Model runs were implemented for the year 2021 where NORTRIP calculations were made for all roads in Norway. These emissions and the resulting concentrations were then compared to the 58 stations in Norway where PM10 measurements are available using the dispersion model uEMEP. The processes addressed were:

- Drainage of water and road dust
- Vehicle spray of water and road dust
- Retention of road dust under dry conditions
- Suspension rates for light and heavy duty vehicles
- Speed dependence of wear
- Modelled PM2.5/PM10 ratio

The sensitivity analysis targeted what was seen as general problems with road dust emission calculations, namely:

- There was generally too little dust available at the end of the studded tyre season, resulting in underestimates in late spring.
- The modelled daily cycle of PM10 follows closely the traffic volume, with peaks in the rush hours and with a dip in concentrations in between, similar to NO_X concentrations. Observations show a flattening between the peaks or even a peak in the middle of the day for PM10. The hypothesis is that the daily cycle of PM10 should follow more closely the heavy duty vehicle daily cycle, than the light duty daily cycle.
- The current model concept that all wear under dry conditions is directly emitted to the air and not accumulated at all on the surface seems unphysical.
- The model is generally too dry, allowing emissions when none occurs in reality.

The results of the sensitivity analysis are summarised as follows:

- Road wear particles during dry conditions are now 50% emitted directly and 50% retained on the surface. Before all road wear was emitted under dry conditions. This increases the amount of dust loading on the surface which also leads to greater loss, through wet removal processes, leading to lower concentrations.
- Drainage removal of dust in the model has been reduced by a factor of 5, increasing the road dust emissions.
- Spray removal of water and dust has been reduced by a factor of 5, increasing the road dust emissions and increasing the time when the road was wet.
- Suspension rates for heavy duty vehicles has been 10 times higher than for light duty. This difference has been increased. Suspension rates for light duty vehicles have been decreased by a factor of 2 and increased by a factor of 2 for heavy duty vehicles. This results in a shift in the daily cycle for suspended emissions towards the heavy duty traffic profile. The increase in dust loading from the previous points made more dust available for suspension by heavy duty vehicles.
- An assessment of modelled verses measured annual mean concentrations at 58 stations in Norway was carried out in regard to speed dependence of road wear. Results when road wear was prescribed as independent of vehicle speed show significantly poorer correlation between stations indicating that vehicle speed is a factor influencing road dust emissions. Vehicle speed dependence on road wear has been retained in the model.

The end results of these changes are shown in Figure 150 to Figure 153, where the improved model parameters have been implemented in the 2022 model calculations for all stations in Norway. Though there can be significant deviations at individual stations, the average daily means and daily cycles, particularly for the coarse mode of PM, are very well captured.

In regard to the daily cycles, Figure 153 also shows the daily cycle for NO_X and NO_2. In this case the concentrations follow more the traffic variation, with a dip in the middle of the day. Note that PM concentrations seem to be shifted slightly, by roughly an hour, compared to the observations. This is less obvious in the NO_X concentrations.

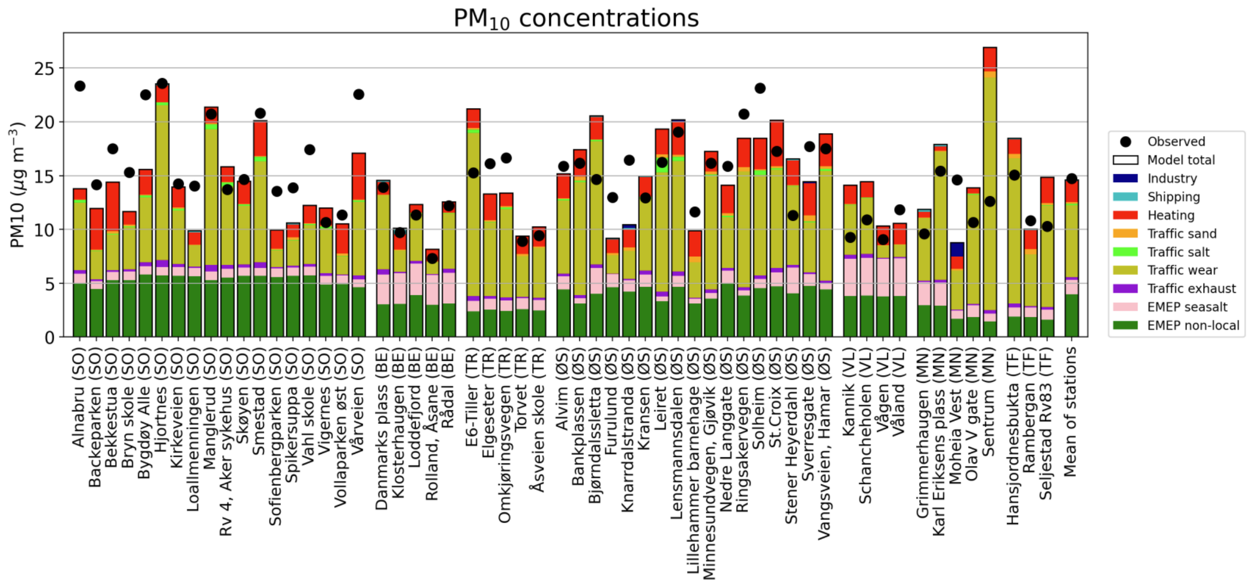

Figure 150. Annual mean PM10 concentrations for 58 station sites in Norway, 2022.

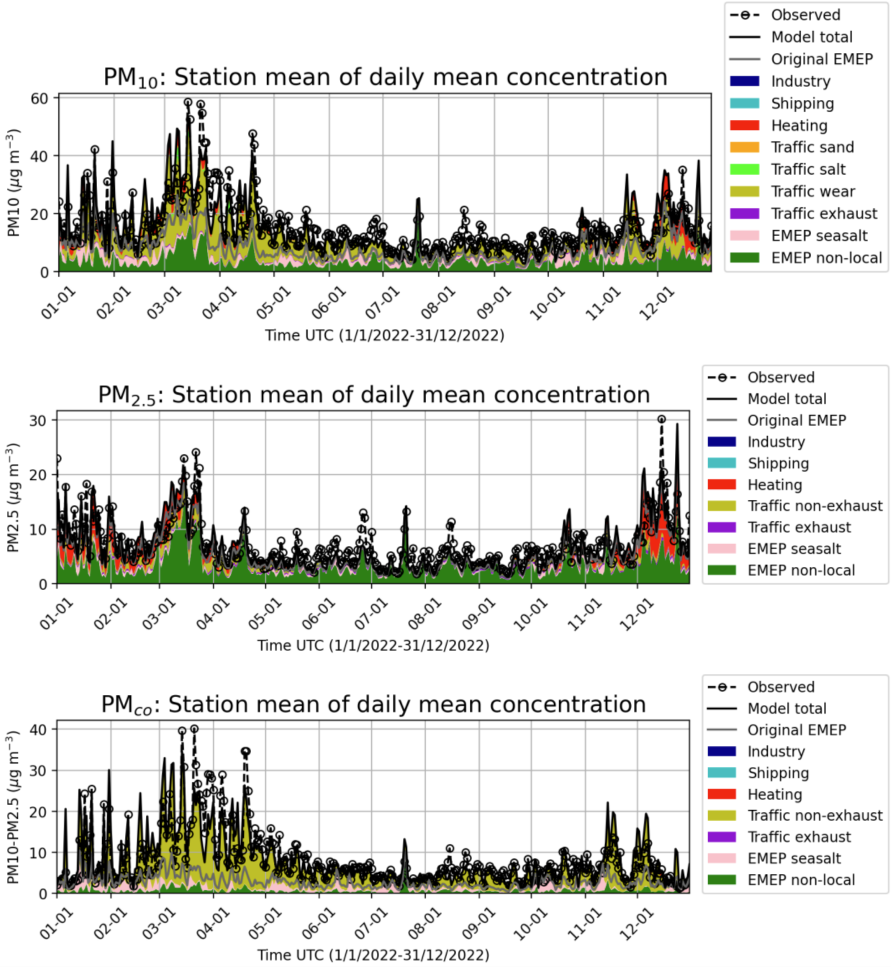

Figure 151. Daily mean concentrations of PM10, PM2.5 and PM_{co} (10 – 2.5 µg/m^3) averaged over 58 station sites in Norway, 2022.

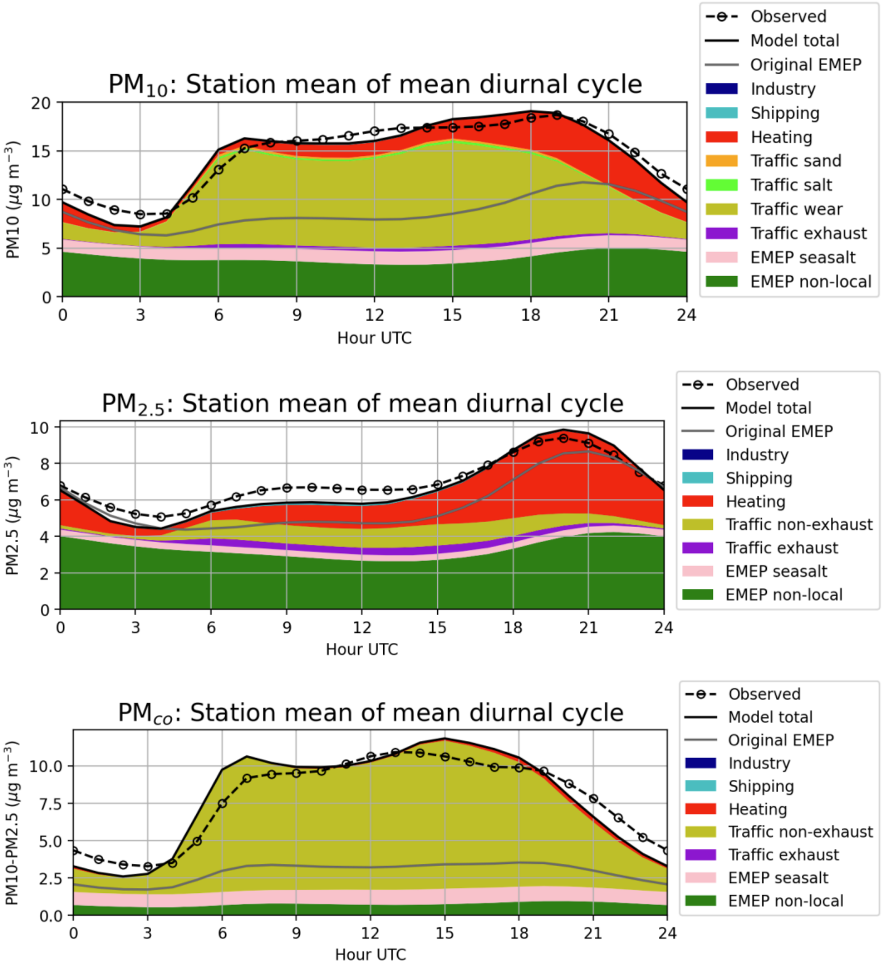

Figure 152. Daily cycle concentrations of PM10, PM2.5 and PM_{co} (10 – 2.5 µg/m^3) averaged over 58 station sites in Norway, 2022.

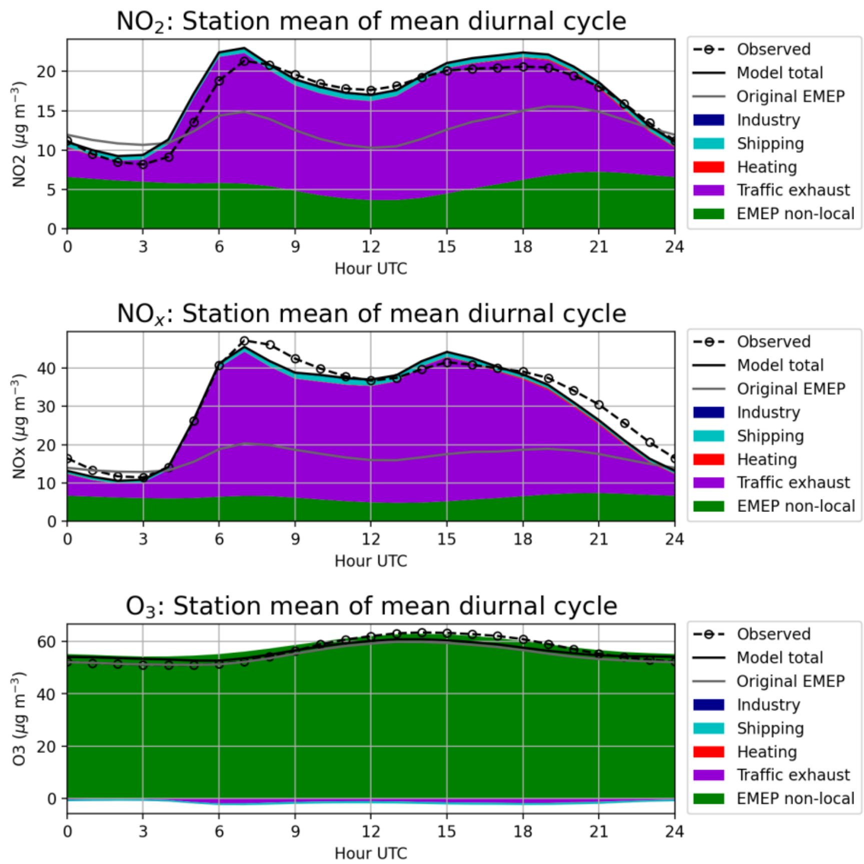

Figure 153. Daily cycle concentrations of NO_2, NO_X and O_3 averaged over 44 station sites for NO_X and 10 station sites for O_3 in Norway, 2022.

In Chapter WP4 - Stockholm, the ratio of PM2.5/PM10 for non-exhaust emissions was assessed for Stockholm. Calculating this ratio requires accounting for all background contributions as well as exhaust. To simplify this, we simply assess the total modelled and observed ratio for the 58 stations in Norway. In Figure 154 this is plotted as an average daily cycle for the year 2001. We see that the model well represents the ratio with just a slight overestimation during the evening. The traffic non-exhaust has a ratio of around 15%. We conclude that the NORTRIP model fairly well estimates the non-exhaust emission ratio, with the possibility that the current 8% ratio for road dust could be slightly higher.

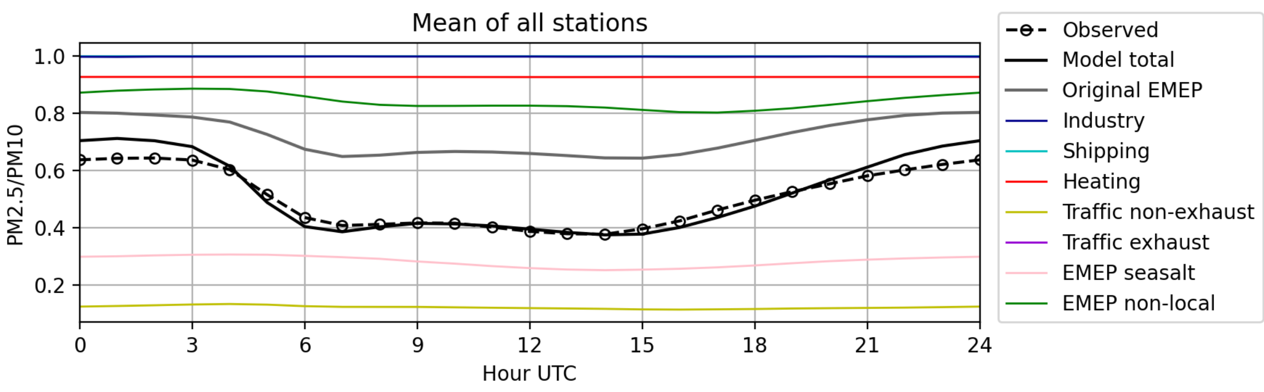

Figure 154. Calculated daily cycle PM2.5/PM10 concentrations for 58 measurement stations in Norway compared to the modelled ratio, 2021.

Conclusions, sensitivity analysis

Sensitivity analysis of model calculations in Norway have been used to assess the model dependencies on vehicle spray, drainage, suspension, direct or suspended emissions and on speed dependence. As a result, a number of changes have been implemented. Removal processes via spray and drainage have been reduced. Road wear under dry conditions has been split 50/50 so half of the road wear is emitted directly into the air and the other half is deposited on the surface. Suspension rates for heavy duty vehicles have been doubled and suspension rates for light duty vehicles have been halved. The net result of the increased accumulation of road dust on the surface combined with the enhanced suspension by heavy duty vehicles leads to a better representation of the daily profiles of non-exhaust emissions. Modelled sensitivity to speed indicates better model performance when including the speed dependence of wear and this has been retained. The new model parameters, based on 2021 calculations, were implemented in the 2022 calculations with improved results.

Evaluation of dust binding in Trondheim

Dust binding is part of the NORTRIP model. Hygroscopic properties of dust binding chemicals such as CMA, $MgCl_2$ and $CaCl_2$ are described in the model by water vapour deficit curves and freezing temperature curves that are dependent on chemical solution concentrations. In this way the effective surface vapour pressure is reduced in the model allowing condensation of atmospheric humidity to occur when the atmospheric specific humidity is greater than the specific humidity of the surface. In the presence of dust binding chemicals this means that the surface will remain wet as long as the atmospheric humidity is higher than the surface, which for dust binders can be between 30% and 50% humidity. The amount of water condensed on the surface will be dependent on the amount of dust binder available.

A dedicated field experiment was implemented to assess dust binding, see Chapter 2.

CMA effect evaluation, however results of this campaign came too late in the project for additional modelling to be carried out. At an earlier stage of the project dust binding assessments were carried out for the winter season 2020-2021 in Trondheim. Trondheim was used since real world dust binding and road salting activities were available through Zeekit, a Norwegian company that collects winter road maintenance activity data in real time by attaching sensors to the maintenance vehicles and reporting on position, time, activity and volume/mass. These data were then implemented in NORTRIP and a comparison made between calculations made with and without dust binding to see how this impacted on the model concentrations and how well this compared to observed PM10 concentrations.

Road activity data

Road activity data was provided in real time via an api from Zeekit. In Figure 155 the yearly total of NaCl and $MgCl_2$ are shown for the road network in Trondheim.

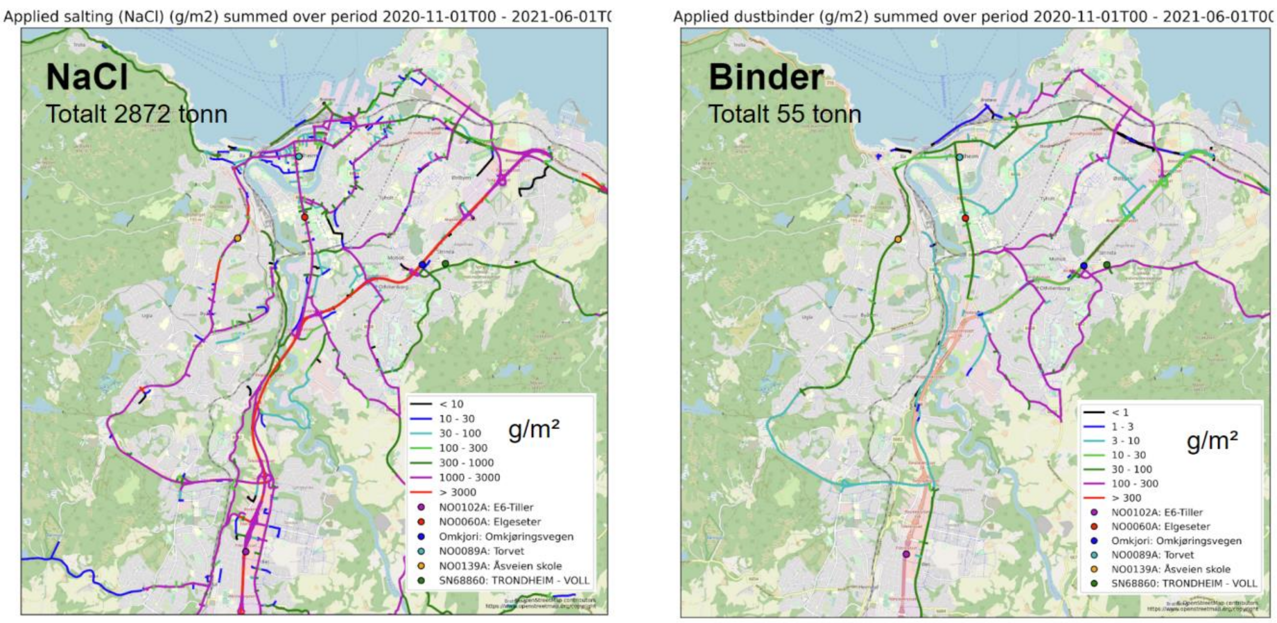

Figure 155. Total amount of dry salt (NaCl) and dust binder (MgCl2) applied on the road network in Trondheim, November 2020 to May 2021.

Model setup

The modelling was carried out over the entire winter period. In this season only 8 dust binding events in total occurred near 3 of the measurement stations. For the example presented here we show a two week period with 2 dust binding events at the station Elgeseter (24 Dec 2020 - 07 Jan 2021). The NORTRIP model was run with and without dust binding using the Zeekit road maintenance data for the simulation, including salting and snow removal. Concentrations of PM10 were calculated with the uEMEP dispersion model. In these calculations all the other PM sources are also included. Apart from road dust the two other major contributors to PM10 concentrations were the background concentrations and residential heating emissions. Binding occurred in this period on the mornings of the 28'th of December and the 4'th of January.

Results

Two calculations are shown, one with binding and one without binding for this period, Figure 156. For the first binding episode, 28'th December, there is a clear reduction in the modelled road dust contribution and an improvement compared to observed concentrations. This shows very clearly the impact of dust binding, where it's application on this occasion avoided a PM10 exceedance day (daily mean PM10 > 50 µg/m^3). Even so, the model still slightly overestimates the road dust contribution. The impact of the dust binding in the model persists several days until the 1’st January. For the second binding episode, 4’th January, there is no difference between the two model calculations and there is no indication that there is significant road dust contribution in either the model or the observations. During this period the model predicted generally wet road conditions, so the application of binding chemicals did not seem necessary.

The model bias is reduced by 24% in this period, from 54% without binding to 30% with binding, and the temporal correlation improves significantly, from r^2=0.09 to r^2=0.27. In this case the model performed well in describing the impact of dust binding.

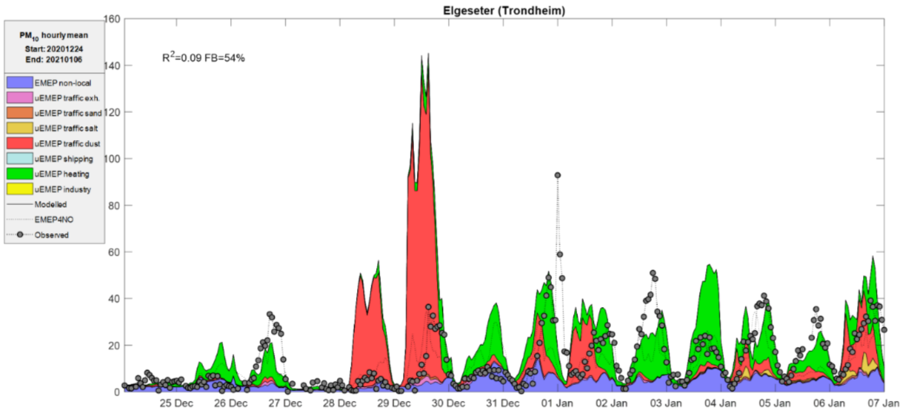

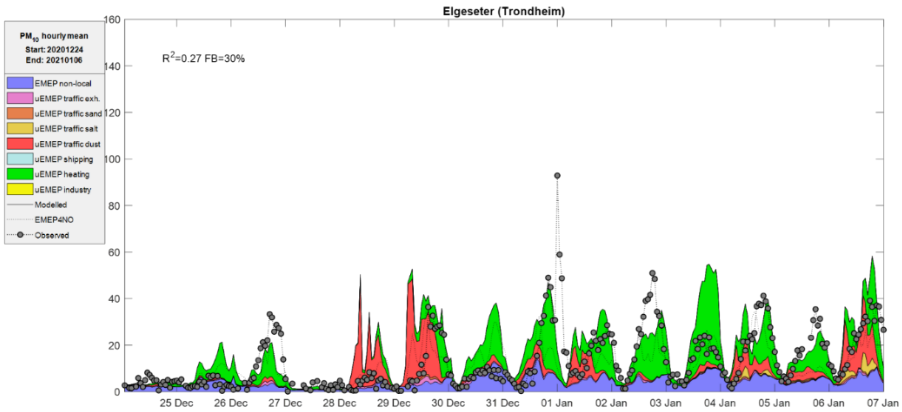

Figure 156. Caclulated and observed hourly PM10 concentrations for the period 24’th of December to 7’th of January at Elgeseter station. Modelled road dust contributions are shown in red, residential heating in green and background concentrations in violet. Observed concentrations are show as a dotted line with circles.

Not all binding episodes showed such clear results. This is due to other complicating factors as simple as errors in modelled wind direction, bias in modelled humidity, incorrect prediction of the road surface conditions, etc. Since there were so few dust binding events the overall impact of including dust binding in the model was less visible compared to these other model uncertainties.

Conclusions, dust binding modelling

The impact of dustbinding is modelled by NORTRIP. However, binding would appear to be more effective than the model indicates. This implies that the other properties of dust binding, such as its ’sticky’ mechanical properties, are also important, in addition to its hygroscopic properties. There is already a parameterisation in NORTRIP that relates the amount of dust binder to the retention that could simulate these properties. This has not been applied due to a lack of information on its exact nature. Laboratory experiments would help in this context but were not carried out during this project.

Implementation of NORTRIP and uEMEP models in Helsinki

The NORTRIP road dust emission model and the uEMEP model, used for the dispersion calculations, were implemented in Helsinki for use in the health impact analysis provided in Chapter Health impacts. This implementation was possible with the help of SYKE, who acquired the necessary input data. In addition, Helsinki is already within the Norwegian air quality assessment domain, allowing background pollutants and meteorology to be easily implemented.

Model setup

The following input data was acquired for implementation of the NORTRIP model in Helsinki:

- Traffic data from SYKE for NORTRIP:
    - Road network shapefiles with relevant traffic data including ADT, HDV%, Road type, Signed speed, road width, number of lanes and road structure type (City of Helsinki, 2023a; FTIA, 2023), Figure 157.
    - Studded tyre share and start and stop of the studded tyre season (City of Helsinki, 2023b; Unhola, 2020),Table 19.
    - Emission factors for PM exhaust and NO_X (HBEFA, 2023),Table 19.
    - Time variation data for 168-hour week temporal profiles (HSL, 2019)
- Residential combustion emissions from SYKE provided at 250 m resolution (Karvosenoja, 2008; Savolahti, 2019), Figure 160.
- Home address population data from Helsinki provided at 250 m resolution (Paituli, 2023), Figure 159.
- 2m resolution surface elevation data used to calculate shading in NORTRIP (Paituli, 2023, Figure 158.

The calculations made use of existing meteorological and air quality fields already calculated for the Norwegian air quality analysis that also covers Helsinki.

- NORTRIP made use of MEPS (Metcoop Ensemble Prediction System) meteorology (common meteorology for Norway, Finland and Sweden), Müller et al. (2017).
- Existing regional air quality modelling was applied (EMEP4NO at 2.5 km using EMEP emissions), Denby et al. (2020).
- uEMEP, high resolution modelling, was applied at 100 m for maps and 25 m for stations where the traffic and residential combustion emission sources were implemented, Denby et al. (2020).
- Hourly concentrations were calculated providing maps and a comparison of daily mean concentrations at 4 stations in Helsinki (HSY, 2023)

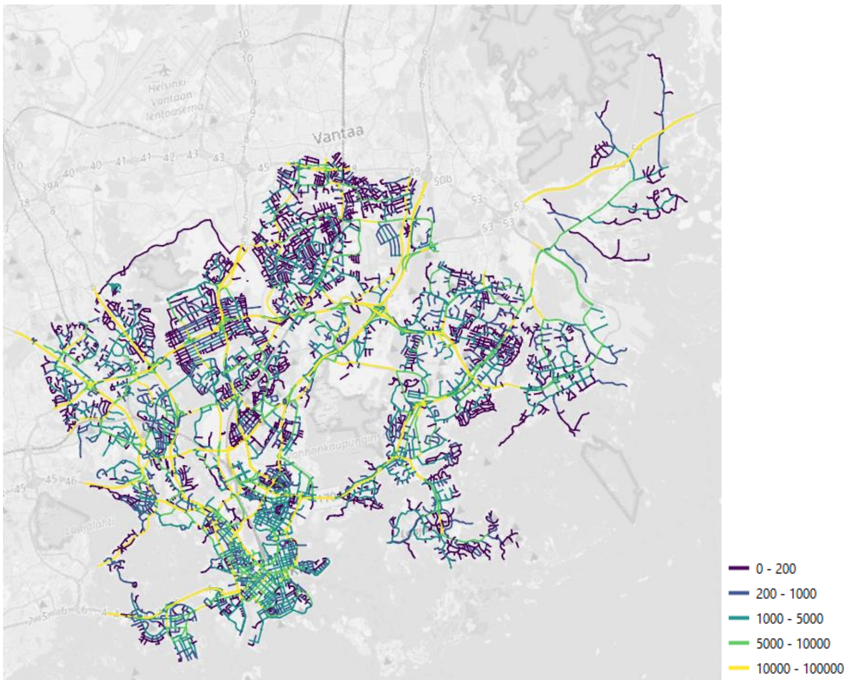

Figure 157. Road network data provided by SYKE for Helsinki. Colours indicate the road link ADT.

Figure 158. Detailed view of Helsinki city centre showing the 2 m resolution laser scanning surface elevation map (m) used in NORTRIP to calculate shading and long wave radiation. Also shown is the road network, as given in Figure 157

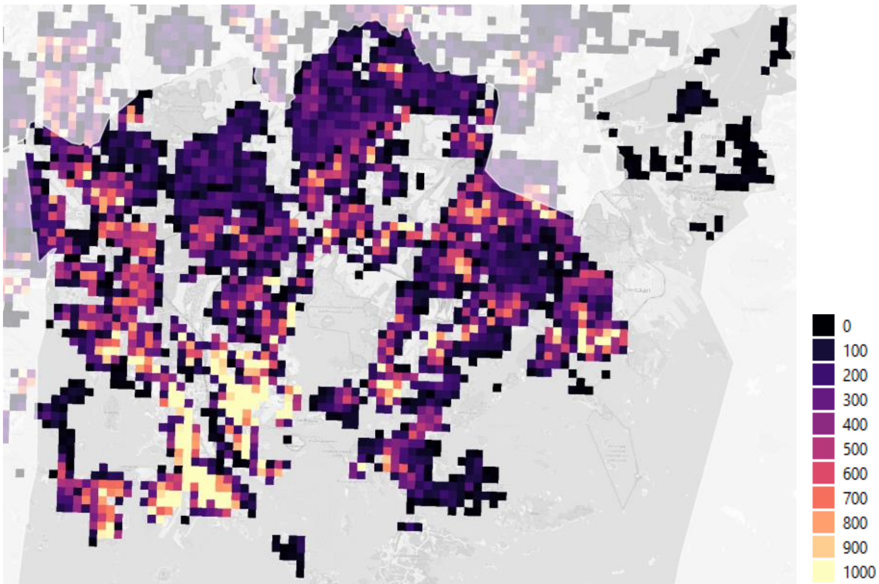

Figure 159. Population density data for Helsinki at 250 m resolution. Colours indicate inhabitants per grid.

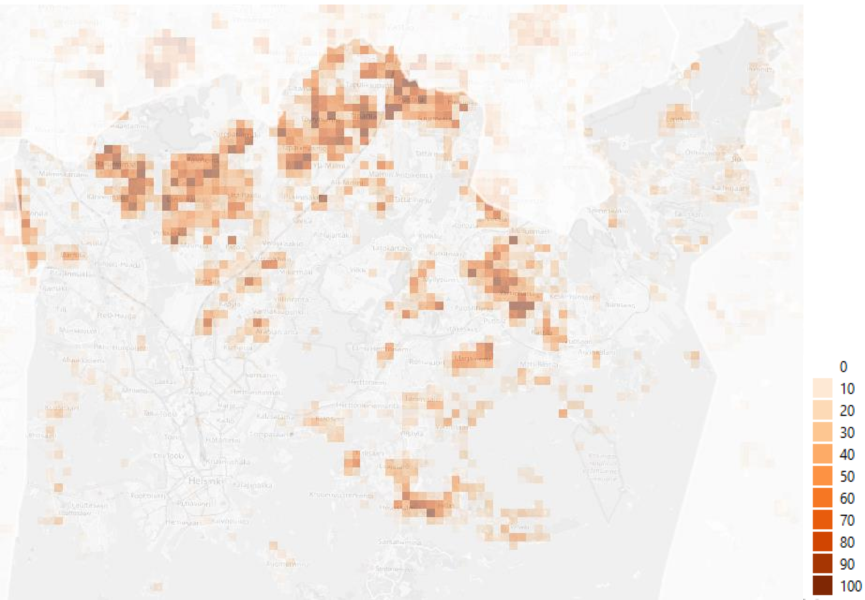

Figure 160. Residential combustion emissions for Helsinki at 250 m resolution (kg/year/grid).

Table 19. Emission factors for traffic and studded tyre share and season used in NORTRIP

Parameter	Value	Unit
Studded tyre share full, light vehicles	70	%
Studded tyre share full, heavy vehicles	0	%
Date start studded tyre season	10.15	mm.dd
Date start full studded tyre season	12.01	mm.dd

Date end full studded tyre season	04.01	mm.dd
Date end studded tyre season	05.01	mm.dd
NOX emission factor light	0.47	g/veh/km
NOX emission factor heavy	2.0	g/veh/km
PM exhaust emission factor light	0.013	g/veh/km
PM exhaust emission factor heavy	0.04	g/veh/km

Results

Maps of PM10 and PM2.5 concentrations are already shown in Chapter WP4 - Helsinki. In addition, we provide the calculated NO_2 concentrations here, Figure 161.

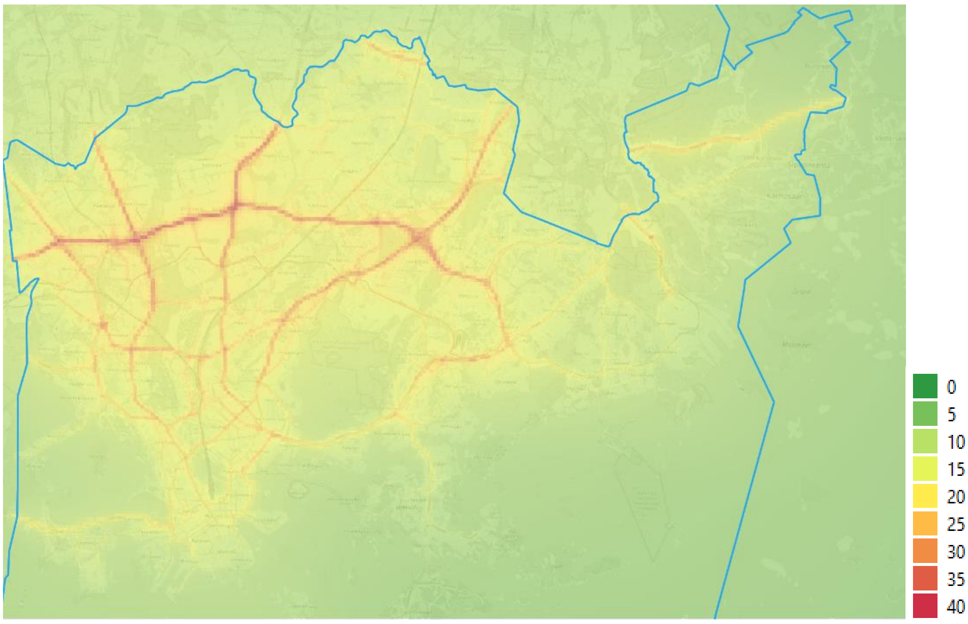

Figure 161. Calculated NO_2 concentrations for the Helsinki, 2021 annual mean.

Plots of daily mean concentrations at four stations are provided in Figure 162 - Figure 164 for PM10, PM2.5 and NO_2. The PM10 concentrations at 3 of the stations was reasonably well modelled. PM10 concentrations at Mannerheimintie were underestimated, particularly in the summer and autum period. Significant construction work was being undertaken at this site during this period.

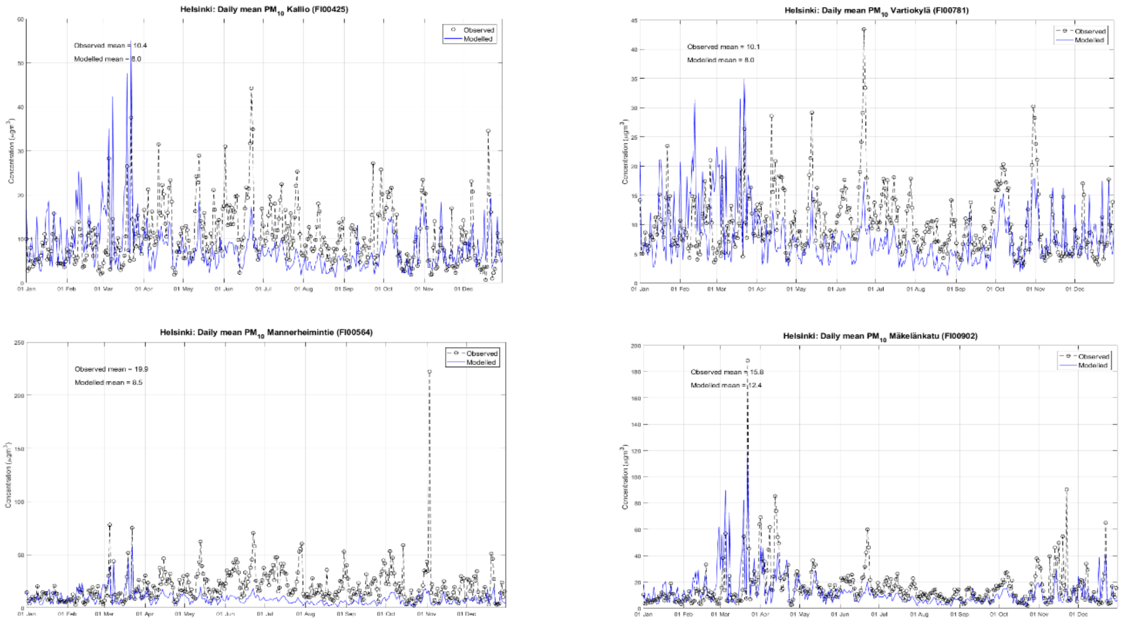

Figure 162. Calculated daily mean PM10 concentrations for the four the Helsinki stations, 2021.

The PM2.5 concentrations at 3 of the stations was reasonably well modelled. Concentrations at Mannerheimintie were underestimated, particularly in the summer and autum period. This may also be the result of significant construction work was being undertaken at this site during this period

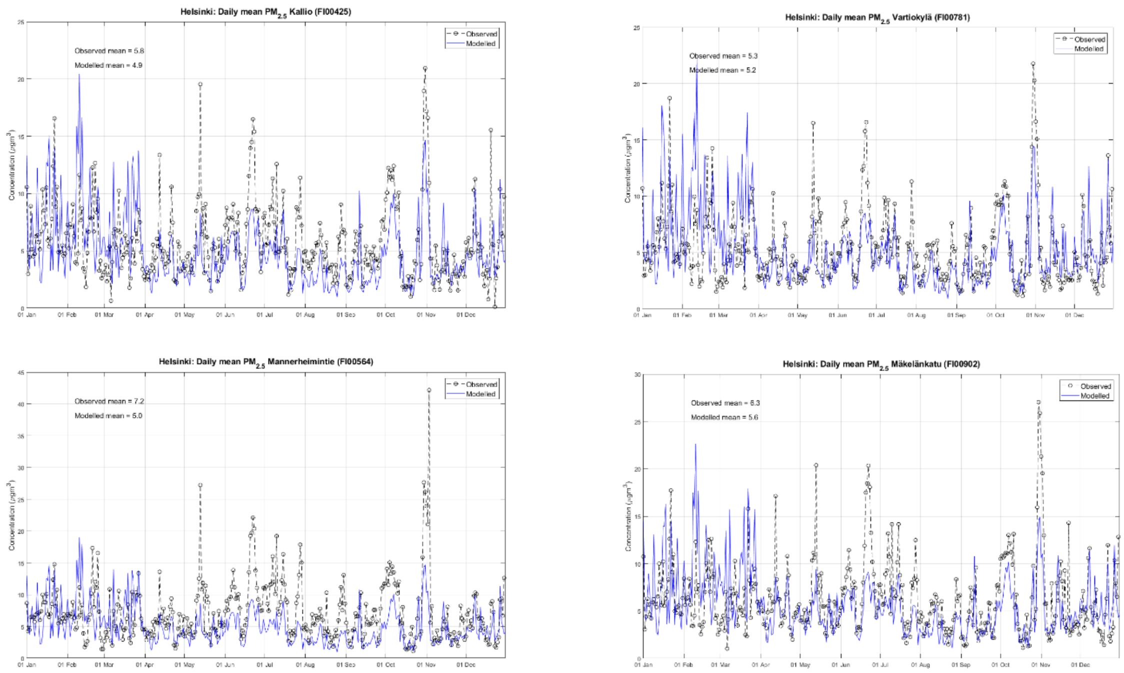

Figure 163. Calculated daily mean PM2.5 concentrations for the four the Helsinki stations, 2021.

The NO_2 concentrations at all 4 of the stations was reasonably well modelled with a slight overestimation at all sites.

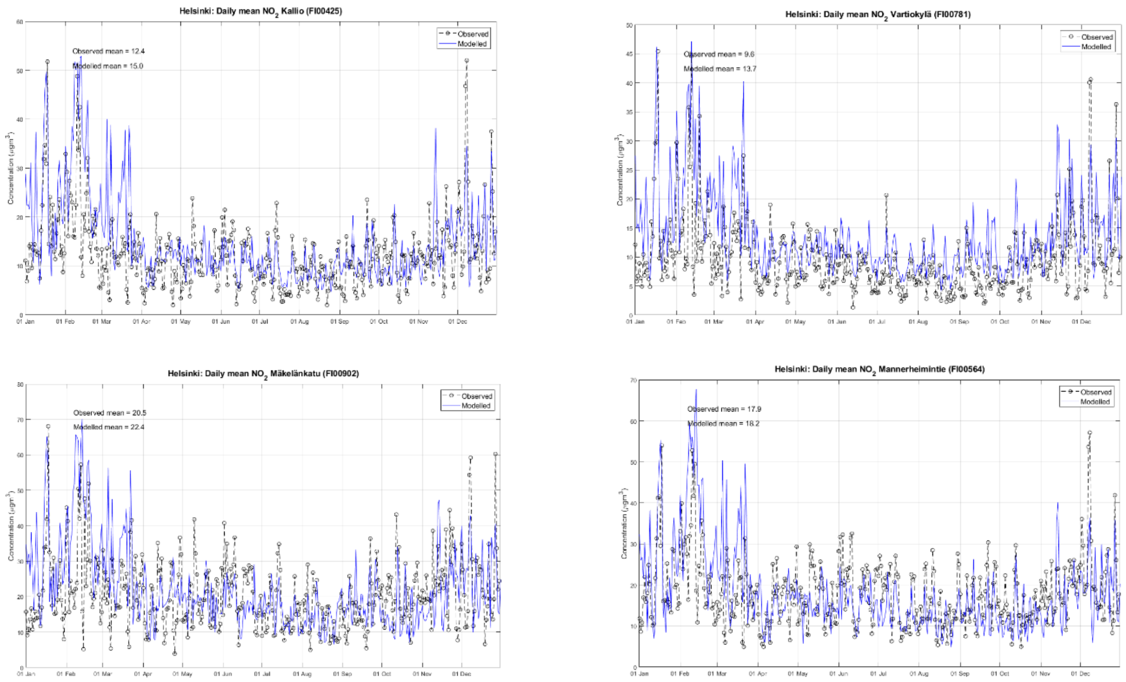

Figure 164. Calculated daily mean NO_2 concentrations for the four the Helsinki stations, 2021.

NORTRIP emissions were calculated for the Helsinki region and the total emissions are shown in Figure 165. Total PM10 emissions are just over 1100 tonnes. The model calculated that 3 800 tonnes of salt was applied to the roads in the year 2021.

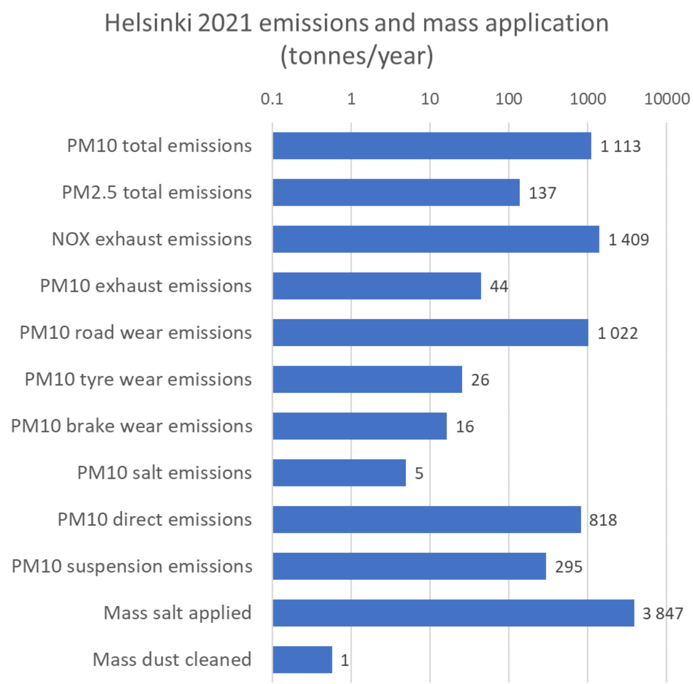

Figure 165. Emissions and mass balance calculated by NORTRIP in the Helsinki region, 2021.

Conclusions, modelling in Helsinki

NORTRIP has been implemented for the first time in Helsinki. Good input datasets were provided by SYKE, including laser scanning surface elevation data at 2 m resolution. This is the first time such a dataset has been used with NORTRIP. The calculated concentrations agreed well with the four measurement sites, with the exception of PM at Mannerheimintie where construction work was being undertaken during the modelling period. The PM2.5 emissions from residential heating were also included, though these seemed to be underestimated. Several long-range transport events seem to have occurred during 2021 and these were only partially reflected in the EMEP calculations.

The Helsinki modelling was found to be of sufficient quality for its use in health impact assessments in Chapter WP4 - Helsinki. It is hoped that this pilot study will lead to a more extensive use of NORTRIP in Finland in the future.

Parameterisation of sand crushing and road abrasion

Crushing

In Chapter WP2 – Crushing of winter sand, road simulator test, experiments in the road simulator were used to assess the rate and size distribution of sand crushing. In particular the plots shown in Figure 40 and reproduced here with new fitted curves, Figure 166, present the best data yet collected concerning crushing. The reduction in sand mass in the size range 5000 - 200 µm represents the production of particles in the smaller particle size ranges. Indeed, the increase in all these small size ranges can be seen in Figure 166. If crushing was to go on continuously then we would expect to see linear reductions in these graphs, at least for the < 10% crushing region. In the start they are indeed quite linear. However, the last two measurements at 1300 and 1700 wheel passages do not follow this linear trend and the crushing rate appears to slow. This is conjectured to be the result of rounding of the sand particle edges, limiting effectively the amount of crushing that can occur for a sand particle.

The appropriate equation describing this production of fine particles with a rate $f_{crushing}$ limited to a fraction of the total sand f_{sand} is given by

$$M_{sand}(x,i) = M_{sand}(all)\, f_{sand}(x)\, exp\left(-f_{crushing}(x)\, i\right) \quad (20)$$

Where $M_{sand}(x,i)$ is the mass of sand in the particles size fraction '*x*' after '*i*' wheel passage and $M_{sand}(all)$ is the total sand. For the largest size fraction 5000 – 200 µm, which is reduced by the sum of the increased fine particles, the same equation for reduction can be written:

$$M_{sand}(x,i) = M_{sand}(all)\, \left[1 - f_{sand}(x)\left(1 + exp\left(-f_{crushing}(x)\, i\right)\right)\right] \quad (21)$$

where *x* in this case is the size range 5000 – 200 µm. A simple geometric argument, the difference between the volume of a cube and a sphere, indicates that a cubic sand particle will lose 50% of its mass before becoming a sphere. This is likely an upper limit to the amount available for crushing. Based on the fits to the curves in Figure 166 we assess that the limit for sand mass available for crushing is 10% of the total mass and the rate of crushing is 1.2 x 10^{-3} $g_{<200}/g_{total}$/wheel passage. This 10% is divided between the finer fractions by 8%, 1.7% and 0.3% for $DL_{200\text{-}10}$, $DL_{10\text{-}2.5}$ and $DL_{<2.5}$ respectively. The rates of production of these fine fractions are similar, but not the same, to the total rate of production, namely 1.5 x 10^{-3} , 0.6 x 10^{-3} and 0.4 x 10^{-3} $g_{crushed}/g_{total}$/wheel passage. These results are based on visual fits to the data. Given the area of sanding is roughly 0.25 m^2 then this gives the same production rates for g/m^2/vehicle ≈ g_{total}/wheel passage. These results, along with the current default sand size distribution, are shown in Table 20 with observations are shown in Figure 166.

Table 20. Derived crushing parameters using Equations 20 and 21 and visually fitting to the observed data shown in Figure 166

Size bin (µm)	200 - 5000	200 - 10	10 – 2.5	< 2.5

f_{sand}	0.1	0.08	0.017	0.003
$f_{crushing}$	1.2×10^{-3}	1.5×10^{-3}	0.59×10^{-3}	0.43×10^{-3}
f_{sand} (default)	0.05	0.042	0.006	0.002

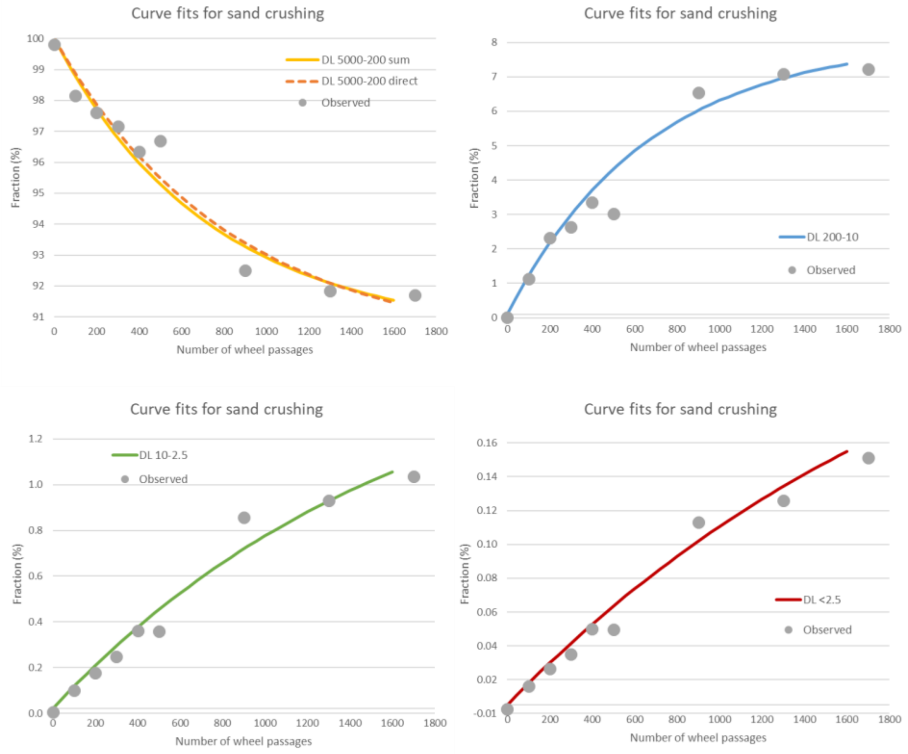

Figure 166. Fits to Equation 20 along with the observed fine particle fractions for the different size categories. For the size range 5000 – 200 µm range both the direct fits, using Equation 21, and the sum of the finer scale fits, using Equation 20, are shown.

What this infers for the model is that crushing occurs quite quickly but is limited in the amount of fine particle sand that can be produced, to just 10% of the applied sand. Whether 10% is a long term or just a short-term limit is not possible to derive from the collected data. Sampling of older well crushed sand would help to set these long-term crushing limits, if they exist.

Abrasion

In Figure 41, an increase in sampled mass is found on the road surface and it is conjectured to be due to the abrasion of the surface. If this is the case then the approximate rate of abrasion is found to be a 0.2% increase after 1600 wheel passages with 2 x 400 g sand on two slabs, equivalent to roughly 1600 g/m^2. This infers an abrasion rate of 3.1×10^{-6} /(g_{sand}/m^2)/wheel passage. For a vehicle this rate will be 4 times larger = 1.2×10^{-5} /(g_{sand}/m^2)/vehicle. These measurements were made at 2-3 km/h.

Sand removal

In addition to the size distribution measurements, estimates of the amount of sand leaving the pavement and nearby area were also made. Of these measurements in Figure 48 gives perhaps the most useful information, that at 30 km/h there is a total loss from the system of 240 g out of the initial 800 g after 400 wheel passages. Within the track itself the loss is much greater with only 50 g remaining after 400 wheel passages. Some of this loss may be due to suspension of the finer particles. This is indicated in Work package 2, Figure 48 to be at least 25 g. If we assume that 25% of the sand is removed after 400 wheel passages then this gives a coarse sand removal rate of 6×10^{-4} per wheel passage from the system and 2×10^{-3} per wheel passage for the wheel tracks. This is an important point for both crushing and abrasion. Under dry conditions the coarse sand is removed at rates similar to or higher than the rates of crushing and abrasion so the sand will contribute little to the finer fractions under dry conditions. When the road is wet or icey then the sand will remain in place and can contribute more to the dust load on the road surface through crushing.

NORTRIP modelling

A number of model runs are made to represent the impact of sand crushing and abrasion using these measured values. A data set for Hornsgatan 2009-2010 was selected as this season had a long wet/icey period where sand could typically be applied. For this experiment measured road wetness was used to inhibit suspension. Two sandings were applied, one at the start of August when the surface was mostly dry and one mid-December at the start of a 3-month wet/frozen period. Both applications were 400 g/m^2.

In Figure 167a the summary results are shown without any sanding. The model performs very well for this period. In Figure 167b sand is applied without crushing or abrasion but with the default size distribution used in NORTRIP for sand particles, these being: 4.2%, 0.6% and 0.2% for DL_{200-10}, $DL_{10-2.5}$ and $DL_{<2.5}$ respectively, see Table 20. These percentage distributions are roughly half of the derived available fractions. This leads to a 1 µg/m^3 increase in average PM concentrations. The largest contribution from sanding comes from the dry period. During the wet period sand particles can be removed by drainage and vehicle spray, so by the time the road drys up the fine sand loading is much reduced. The dust loading shown is for suspendable dust, i.e. < 200 µm.

In Figure 168a and b the impact of crushing with low ($6x10^{-4}$ veh^{-1}) and high ($2x10^{-3}$ veh^{-1}) sand removal rates is shown, using the 10% limit of sand available for crushing and the derived crushing rate of 1.2 x 10^{-3} /(g_{sand}/m^2)/vehicle. This leads to a further increase of 1.1 µg/m^3 for the low sand removal rate and 0.5 µg/m^3 for the high sand removal rate. The highest impact in this case comes from the wet period where retention of the sand leads to more crushing. Even so, in all cases the 10% of sand available for crushing is crushed within a day. Almost all sand is also removed from the road surface during the dry period within a day.

In Figure 169a and b the impact of sand abrasion is presented for the low and high sand removal rates. In this case we see an unrealistic increase in dust loading and emissions. This occurs in the wet period, where sand remains on the road surface and continuously wears the road surface. In the dry period the sand is quickly removed, and abrasion does not contribute significantly.

In Figure 170a we reduce the abrasion rate by a factor of 10, which still adds significantly to the road dust loading with a 50 g/m^2 increase in the wet period and a 4 µg/m^3 increase in total concentrations. In Figure 170b we show the impact on this abrasion calculation if we reduce the no road wear snow/ice depth parameter from 5 mm (always wear) to 1 mm (no road wear of any type when the surface snow/ice is > 1 mm). This impacts on both the abrasion and the normal road wear from studded tyres. This has only a small impact, a decrease of 1.5 ug/m^3, since the period when the road is covered with > 1 mm ice/snow is not long, just a few days.

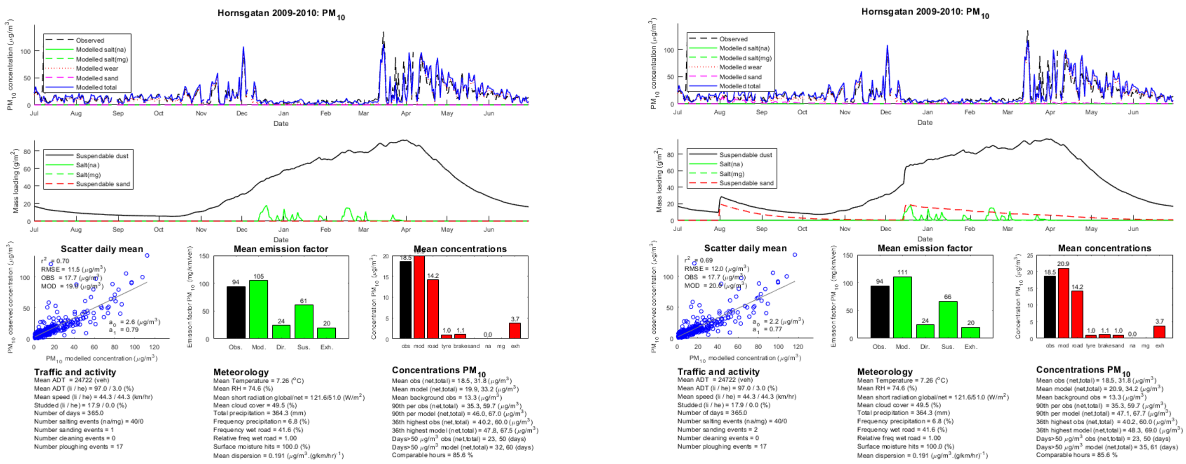

Figure 167. NORTRIP model calculation without sanding (left) and with two sanding applications of 400 g/m^2 without crushing or abrasion (right).

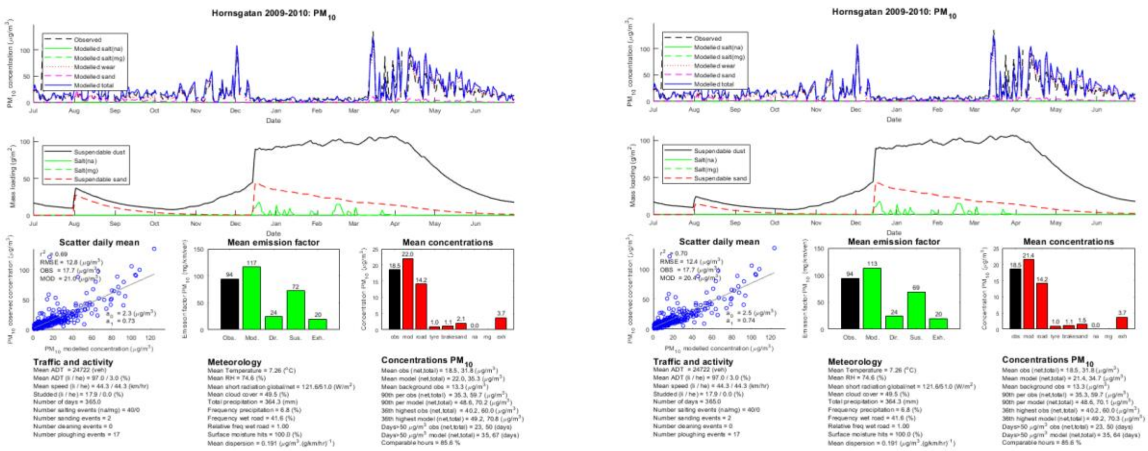

Figure 168. NORTRIP model calculations with two sanding applications of 400 g/m^2 including crushing but no abrasion. Left is with low sand removal rate and right with high sand removal rate.

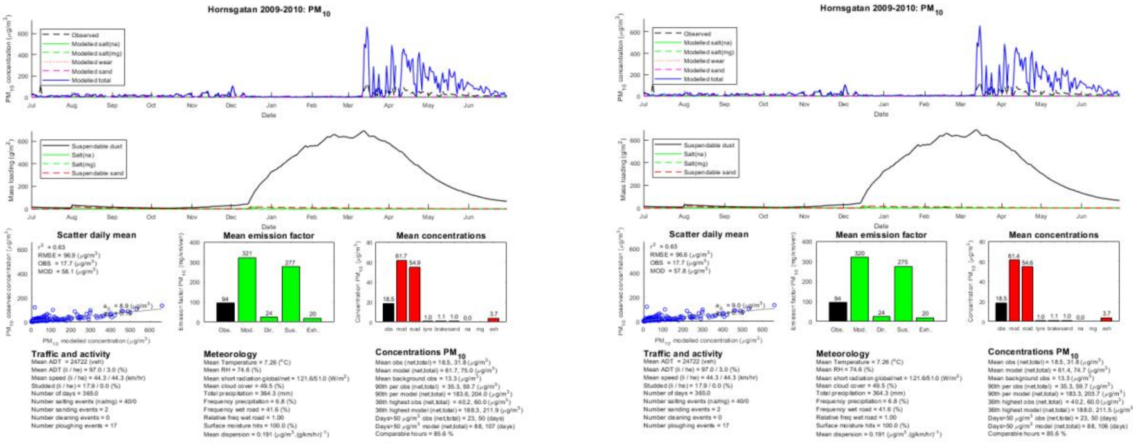

Figure 169. NORTRIP model calculations with two sanding applications of 400 g/m^2 including abrasion but no crushing. Left is with low sand removal rate and right with high sand removal rate.

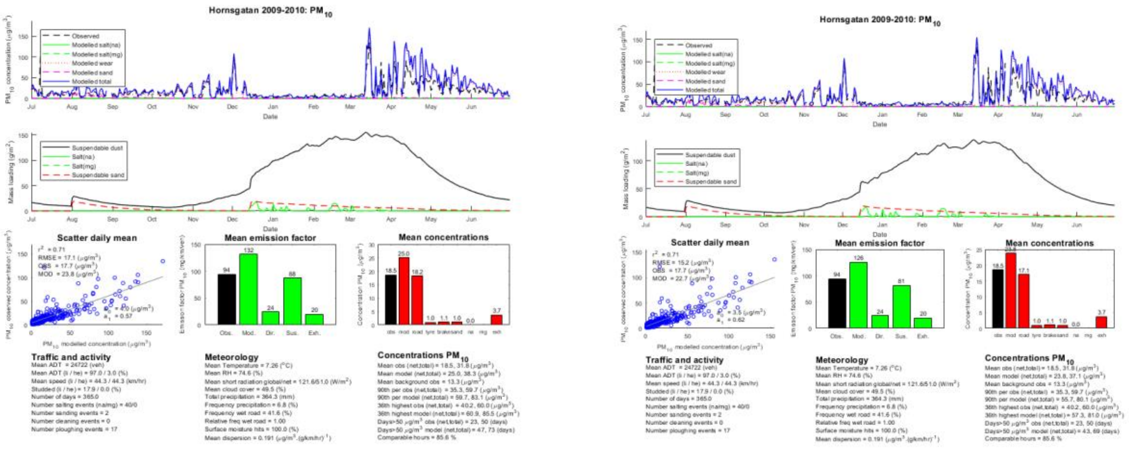

Figure 170. NORTRIP model calculations with two sanding applications of 400 g/m^2 including abrasion but no crushing using the low sand removal rate. Left is with the a reduced abrasion rate, factor of 10 reduction, and right is where the wear ice/snow threshold is set to 1 mm w.e..

Conclusion, sand crushing and abrasion

Based on these results the implication is that road wear through sand abrasion can be more significant than sand crushing. Though this seems counter intuitive, it is exactly these results that were found by Kupiainen (2007) where the road abrasion contribution was larger than the road sand contribution to PM10 under laboratory conditions for non-studded tyres. Unfortunately, the tests carried out in this project could not distinguish between road and sand dust. Even so, the abrasion results will require more work in the future, but the crushing results may serve as a basis for the new parameterisation in NORTRIP. The maximum amount of sand available for crushing into the different size ranges is still an open question. Recommended is the use of the low removal rate of sand, though results are not sensitive to the ranges when applied here.

Impact of vehicle weight on wear

Based on the findings in Chapter WP2 – Influence of weight on particle emissions, field tests, the dependence on road wear was determined to be linear, passing through 0 wear for 0 weight and with a relative scaling of 1 for vehicles weighing 1532 kg, based on the 2021 data from Stockholm, Chapter WP4 - Stockholm. This parameterisation is not directly implemented in the model, but the scaling factor is pre-calculated and applied to the road wear parameters in the parameter file based on the estimate of average vehicle fleet weight.

Application of the parameterisation has been used to calculate the health impacts of a shift from fossil to electric vehicles in Chapter WP4 - Stockholm.

References

City of Helsinki, 2023a. Traffic and street planning. Traffic volumes Helsinki. (Finnish name: Helsingin liikenteen määrät) https://kartta.hel.fi/paikkatietohakemisto/pth/?id=381

City of Helsinki 2023b. Winter tyre survey 2023. Kantar Public. Not published

Denby, B. R., Gauss, M., Wind, P., Mu, Q., Grøtting Wærsted, E., Fagerli, H., Valdebenito, A., and Klein, H.: Description of the uEMEP_v5 downscaling approach for the EMEP MSC-W chemistry transport model, Geosci. Model Dev., 13, 6303–6323, https://doi.org/10.5194/gmd-13-6303-2020, 2020.

FTIA, 2023. Finnish Transport Infrastructure Agency. Digiroad. https://vayla.fi/en/transport-network/data/digiroad/data

HBEFA, 2023. Handbook Emission Factors for Road Transport. https://www.hbefa.net/e/index.html

HSL Helsinki Region Transport 2019. Demand models for the Helsinki region commuting area traffic forecasting system 2017. HSL publications 5/2019 (in Finnish) https://www.hsl.fi/sites/default/files/helsingin_seudun_tyossakayntialueen_liikenne-ennuste_kysyntamallit_5_2019.pdf

HSY, 2023.Helsinki Region Environmental Services Authority. https://www.hsy.fi/en/airquality/

Karvosenoja, N., 2008. Emission scenario model for regional air pollution. Monographs of the Boreal Environment Research 32.

Kupiainen, Kaarle. (2007). Road Dust from Pavement Wear and Traction Sanding. Monographs of the Boreal Environment Research. 26.

Müller, M., Homleid, M., Ivarsson, K., Køltzow, M. A., Lindskog, M., Midtbø, K. H., Andrae, U., Aspelien, T., Berggren, L., Bjørge, D., Dahlgren, P., Kristiansen, J., Randriamampianina, R., Ridal, M., and Vignes, O.: AROME-MetCoOp: A Nordic Convective-Scale Operational Weather Prediction, Model, Weather Forecast., 32, 609–627, https://doi.org/10.1175/WAF-D-16-0099.1, 2017

Paituli, 2023. Download data from https://paituli.csc.fi/download.html

Savolahti, M., Lehtomäki, H., Karvosenoja, N., Paunu, V-V., Korhonen, A., Kukkonen, J., Kupiainen, K., Kangas, L., Karppinen, A. & Hänninen, O. 2019. Residential Wood Combustion in Finland: PM2.5 Emissions and Health Impacts with and without Abatement Measures. IJERPH 16, 2920. https://doi.org/10.3390/ijerph16162920

Unhola, T. 2020. Nastoin varustettujen autojen osuus liikennevirrasta Koillis-Helsingissä 2019–2020. The City of Helsinki Urban Environment Division, studded tyre share and season.

Synthesis

The NORDUST II project has been broad in its approach to elevate the knowledge on road dust emissions and involved a large number of investigations from laboratory and field and from measurement and sampling to parametrizations, modelling and future scenarios. The work has been made in diverse settings in Finland, Sweden, Norway and Iceland. Being a complex project, with a vast amount of data and results, this synthesis aims to give a brief overview of the main results and implications of NORDUST II.

Since the Nordic countries have been working for over a decade with mitigating the road dust problems on many scales, it was highly relevant to initiate the project with a state of the art work package, summarizing the current knowledge on how to mitigate road dust emissions. The work package compiled information from seventeen recent projects dealing with road operation mitigation measures, i.e. winter maintenance (sanding), dust binding and street sweeping. In acute dust episodes, the best way to control road dust emissions is the application of dust binding solutions. Sweeping is considered beneficial for lowering PM emissions on a seasonal basis, but not as acute measure. Instead of mitigating the symptoms (dust already on the road) efforts should be made to prevent the build-up of dust deposits during wet periods in autumn and winter. This would decrease the amount of dust that becomes airborne in spring when surfaces dry up.

An important part of the NORDUST II project, as for the preceding NORDUST project, has been to perform experiments that can help parametrising processes in the NORTRIP emission model, which so far has been based mainly on rudimental assumptions. In work package 2, efforts were made to investigate how vehicle weight influences PM emissions, how winter sand is crushed into airborne fractions and is removed from the wheel tracks and how the amount and distribution of an applied dust binder agent is affected by traffic.

Vehicle weight is of vital importance due to the ongoing developments of the vehicle fleet with continuously heavier vehicles due to trends and electrification. Both laboratory and field tests were used to address the question, and both studied were concurrent in that vehicle weight and speed significantly influence PM emissions, with heavier vehicles and higher speeds leading to increased emissions. Additionally, the type of tyre, particularly studded versus friction or summer tyres, plays a crucial role in the amount of PM emissions. Road surface properties (i.e. pavement type, dust load), also have a crucial role in PM emissions. These findings suggest that interventions aimed at reducing vehicle weight, controlling speeds, and encouraging the use of tyre types that wear less significantly reduce vehicular PM emissions. The relations found was used for parametrizations in work package 7.

A controlled study in the VTI road simulator was used to describe how a winter sand material is abraded and crushed into finer fractions from being run-over by tyres on a real road pavement. Only the coarsest fractions decreased while all finer fractions increased in mass with accumulating wheel over-runs. The decrease and accumulation of particles in the fractions relevant for the NORTRIP model could be described with mathematical functions and a new sand crushing parameterisation could be implemented based on the road simulator experiments. These experiments and resulting parametrization indicate that crushing occurs relatively quickly but is limited to just 10% of the sand mass, due to the physical properties of the sand. It should be noted that there is a need for more tests with different sand materials, amounts and speeds for an improved understanding of the processes. The sand removal study could conclude that removal of sand is a fast process and that the coarsest particle fractions are removed most efficiently. Finer fractions tend to accumulate at low speeds, but above 20 km/h all particles are depleted in wheel track. Only 5% remain after 400 wheel passages at 30 km/h.

In a field test in Linköping, Sweden, the removal of the dust binder CMA by traffic was studied by wet dust sampler (WDS) measurements. Despite the uncertainties in much of the input data and in the spreading of the CMA on the road surface, the results show that given the appropriate model parameters the NORTRIP model can largely reproduce the impact of traffic migration on the observed acetate concentrations from following the CMA development on the street for 30 hours after application. Interestingly, the model provides a quantification for the decay rate of dust binder on the road surface, based on the area where dust binder is applied and the traffic flow in and out of the applied area. The new module describes the along wheel tracks migration of road water and salt/dust-binder has been developed and assessed in work package 7. It helps describe the decay of dust binder based on the transport out of the dust bound region by traffic and may be further developed as a useful dust binding and winter road maintenance management tool.

At the same site in Linköping, the effect of dust binding with CMA on PM concentrations was investigated. By comparing the PM10/NO_X-ratio in Linköping and Norrköping, days when Linköping use dust binding while Norrköping did not, with days when neither of the two cities carried out dust binding, an effect of 16% reduction could be concluded. The evaluation method was not optimal, since no reference air quality station in street with no dust binding was available in Linköping.

The correlation between road dust load and PM concentrations in air is seldom straight-forward. Dust load is normally low in wheel tracks and higher outside due to stronger suspension forces in wheel tracks. But at high texture and low speeds, dust load can accumulate in wheel tracks without being suspended. The availability for suspension (suspension potential) and traffic properties controls how road dust contributes to airborne PM. Road dust suspension is inhibited by moist, can be hidden or cemented in road surface texture at prevailing traffic conditions or can accumulate in street sections unavailable for suspension. Road dust not available for suspension can be made available again by ineffective sweeping, loosening or moving the dust into wheel tracks where suspension forces are strongest. Even though it is possible to sample the total dust load by WDS-sampling or similar methods, the suspendible part is elusive. Measurement cars like Sniffer used in the project, is useful for emission measurements, but hard to relate to total dust load per surface area as well as to site specific surface properties. To overcome this, a measurement device called DUSTER II was evaluated in work package 5. The DUSTER II is used to suspend and measure dust from an enclosed road surface. The results could demonstrate that the suspension differs with different surface textures and a dry up sequence could also be followed. Remaining is to measure and/or calculate the corresponding suspension force, which so far has not been evaluated.

Tyre wear particles (TWP) have come into focus due to the concerns for microplastic and the huge global source related to wear of tyres. Only in Sweden, 11 000 tonnes of tyre debris are worn annually. From an analytical point of view, it is also one of the most challenging particle types to analyse, since standard microplastic analyses methods (like FTIR) do not apply to black particles. In work package 3, a dedicated study was made to characterize tyre wear particles using the VTI road simulator. It was found that TWP had a unimodal size distribution with the peak between 1 µm and 4 µm. Significantly, a predominant portion of the examined size fraction, ranging from 0.06 µm to 8 µm, corresponds to fine particles. Size distributions of PVC, NY and SBR pyrolysis products, species derived from constituents present in the tyre, resembled that established for TWP for coarser particles, but deviated for the finest particles. Attempts to quantify TWP from pyrolysis products of PVC, NY and SBR were inconclusive, likely due to differences in tyre polymer content and the quantification standard.

As have been mentioned earlier, the effects on electrification on NEE is of high interest, since increased vehicle weight was found to increase emissions of both tyre and road wear particles. In work package 4 future scenarios with different shares of electric vehicles in the cities of Stockholm, Helsinki and Trondheim, were investigated using the NORTRIP model. The three cities are quite different when it comes to share of studded tyre use (47, 70 and 18% respectively) as well as share of electric vehicles (14, 1 and 13%, respectively), yielding a wide range of scenarios. The studded tyre share of electric vehicles in the cities is significantly less than for fossil fuel vehicles. In Trondheim and Stockholm roughly half as many electric vehicles use studded tyres compared to fossil fuel vehicles. In Helsinki this number is less than a third. The introduction of electric vehicles into the traffic fleet is expected to occur at different rates in the different cities. By 2040 and 2050, respectively, the proportion of electric vehicles in Stockholm is expected to be 75% and 95%, Trondheim 90% and 95% and in Helsinki 39% and 63%. Since the vast majority of non-exhaust emissions of PM is due to studded tyre road wear, non-exhaust emissions in the future will, except for traffic volume and composition developments, be largely dependent on the different vehicle weights and the different studded tyre shares.

Several scenarios were modelled to determine the future of non-exhaust emissions. Scenarios where the current studded tyre share of electric and fossil fuel vehicles is maintained into the future show that there will be little change in the non-exhaust emissions. Scenarios where the assumed heavier electric vehicles (30–50% heavier than fossil fuel vehicles) have the same studded tyre share as fossil fuel vehicles showed a significant increase in non-exhaust emissions. Only scenarios with a reduction of studded tyre share for both electric and fossil fuel vehicles showed a decrease in non-exhaust emissions. In Trondheim and Helsinki, it was shown that a reduction in the studded tyre season can also have a significant impact on non-exhaust emissions. Health impact assessment indicated that currently the number of premature deaths due to non-exhaust emissions is around 4–5 premature deaths/year per 100 000 inhabitants in all three cities. This will increase or decrease depending on the chosen future scenario.

The plan for work package 6 on Iceland was to be able to characterise road dust load and properties in an environment rather different from the other Nordic countries. A wet dust sampler was shipped and set-up, but due to logistic complications, only an initial trial could be completed. The samples' turbidity was analysed and shown to follow the pattern of measurements in other Nordic streets and roads with accumulation outside wheel tracks and low amounts in wheel tracks. The NORTRIP model (NOn-exhaust Road Traffic Induced Particle Emissions), developed by the Nordic Institute for Air Research, was used to calculate the contribution of non-exhaust emissions to the urban particulate matter pollution in Reykjavik and to explore the effects of mitigation measures (Barr et al., 2021). The relationship between reduction in studded tyre use and speed reductions indicate that relatively large improvements can be made with relatively simple measures to reduce both. That is, reduction in speed within the city limits from 50 km/h to 30 km/h could lead to ~40% reduction in road wear from cars using studded tyres, and a similar reduction in particulate matter concentration in the atmosphere could be achieved if studded tyre use went from 45% to 20%. With the implementation of multi-lane NORTRIP model in the AirViro modeling package it is possible to get high resolution model results for various pollutants, including particulate matter. This can then be used to calculate exposure based on location. Preliminary run for the population weighted exposure gave a value of 3.4 µg/m3 in the capital area for PM2.5. This will be further used to calculate the morbidity and mortality associated with the pollution. It will also be used to calculate the cost and benefits of mitigation measures.

A main aim with the NORDUST project is to help further develop, parametrize, and refine the NORTRIP emission model. As have been described above, several activities in the project have been used for this purpose and the model has, in turn, been used for scenario analyses in all scientific partners' countries. Except for what has been previously described, the following improvements have been performed in work package 7:

- Existing datasets from Trondheim, where winter maintenance data is available, have been used to assess the dust binding description in the model. The model effectively models dust binding but the overall improvement in model performance is limited due to the impact of other processes.
- A large number of sensitivity studies have been carried out using air quality measurement data in Norway. This has led to changes in wet removal and suspension parameters in the model. The new model parameters have been applied in Norway with improved results. The same sensitivity studies indicate a real dependence of road dust emissions on vehicle speed.
- The NORTRIP model has been successfully implemented in Helsinki where it has been used to address the impact of a change in traffic fleet with the introduction of electric vehicles in WP4.

Research needs

Below are listed some of the research and development needs based on experience from the NORDUST II project.

WP1

The development of road dust mitigation solutions will continue in the Nordic countries. Tracking future advancements in the field and compiling knowledge will help plan and implement the most effective strategies for reducing road dust emissions.

WP2

Based on the results of work package 2 and also what was not included in the project, the following research and development needs are identified:

- Influence of vehicle weight is obvious in tests, but the knowledge about variation between and within different tyre types is low.
- Abrasion and crushing tests should be further developed based on the experiences from NORDUST II and a number of different materials (both regarding rock type, size distribution and shape properties) should undergo tests, to learn more about the variation.
- Optimal techniques for removing road dust in situ, without moving it into high resuspension areas like wheel tracks, should be further investigated.
- To better understand longitudinal dust binder (or salt) migration and to validate the migration module (see WP7), sampling should be performed along roads.
- There is need to investigate dust binders' physical characteristics under controlled conditions (see WP7)
- Influence of road surface properties, especially macro texture, on road dust availability and suspension needs further investigations. At present, the NORTRIP model does not take into account this parameter.
- Porous pavements have been shown to reduce dust suspension, but their function is delpeated by accumulating dust. If and how these pavements could actually be used for air quality improvement and how they should be maintained needs further research.
- Expand emissions testing to a broader range of real-world driving conditions (ie. road types) and vehicle (ie. size) and tyre (ie. different brands) types. This could provide a more comprehensive dataset for policymakers to base vehicle emissions standards and urban planning decisions on, also this would help to understand the effect of different tyre type and pavement type interaction and how these would effect PM emissions.
- How do different driving behaviours influence PM emissions? Understanding the impact of driving patterns, such as acceleration and braking frequency, could provide insights into how driver behavior modification could reduce emissions. Also, the effect of these parameters should be studied in the perspective of on-road measurements.

- How tyre wear over time influences PM emissions. Understanding the lifecycle emissions from tyres can guide regulations on tyre materials and designs to minimize environmental impact.

- Speed management strategies for reducing PM emissions in urban areas. This could support policies like variable speed limits and traffic calming measures to improve air quality.

WP3

Analyzing tyre wear particles (TWP) in the airborne fraction needs development of specific and quantitative methods, which are currently not available. As basis for method developments, there is a need for producing realistic TWP in proper amounts for different analyses techniques, preferably with as low contamination from other sources, as road wear, as possible.

WP4

The impact of electric vehicle on non-exhaust emissions has been quantified in this project for three Nordic cities. The findings indicate that non-exhaust emissions will continue, or increase, into the future unless significant reductions in studded tyres are implemented.

- These changes were assessed in terms of their health impact using PM2.5, as this component has the best health data available. However, the largest part of non-exhaust emissions is in PM10. Further health impact should be assessed for the coarse component of PM.

- The studies can be extended, in Norway at least, to the entire population of the country. This should also be possible in Sweden in the near future, and also possibly in Finland. Mapping the non-exhaust emissions for an entire country and its health impacts will provide useful information for policy decisions into the future since exhaust particle contributions will be negligible.

WP5

The possibilities to relate DUSTER resuspension results to suspension caused by traffic, would be valuable for investigating road dust load suspension in relation to total dust load at different ambient and traffic conditions.

WP6

For improved knowledge on Icelandic road dust properties in relation to other Nordic countries, WDS samplings need to be performed and evaluated. Further, more detailed input data for NORTRIP modelling are needed. Some specific research needs are:

- Understand better the effect of spraying and drainage.
- Iceland a good location because of wet conditions and frequent weather changes.
- Measure the dust load on a busy road with wet dust sampler (WDS) and compare to model results to improve modeling.
- Modeling of mitigation measures to get realistic estimates of reduction in non-exhaust pollution.
- Modeling of future scenarios, e.g., increased number of e-vehicles and total number of vehicles.
- Modeling of future scenarios due to changes in weather conditions.
- Calculate the health impacts and changes due to mitigation measures.
- Do cost benefits analysis of mitigation measures.
- Find ways to show effects of mitigation measures in measured concentrations of particulate matter; difficult because of high variability in concentrations.

WP7

Model development is a continual process. Some of the measurements carried out in this project have lead to new questions and some existing questions still need to be answered.

- Speed dependence of vehicle wear is difficult to assess in the field. Mobile measurements in this project indicated that there was little speed dependence. Assessment of existing data showed no clear relationship but indicated some dependence. As such the speed dependence question is not satisfactorily addressed in the model. Is the speed dependence linear or not at all speeds? Is the road wear acceleration dependent rather than speed dependent? Is the speed dependence only in the suspension or is it also in the wear?

- The migration module, part of the tunnel model being developed for NORTRIP, has shown it can reproduce the impact of the migration of dust binder given suitable model parameters. These parameters are not defined experimentally. Better information on the migration of dust binder and salt will help to improve effective management of these winter maintenance activities, to ensure the longevity of salt and dust binder application on the road surface by taking into account vehicle flow in the traffic system.

- The migration module also makes one of the first steps towards a multitrack version of NORTRIP, where the in and between wheel tracks, as well as shoulders, curbs and pedestrian/cycle ways, can be modelled separately but interact with each other. This avenue of modelling should be pursued into the future.

- The sand crushing experiments provide the first controlled experimental data on this process. The experiments indicate that just 10% of the total mass of sand is available for crushing. Additional measurements over longer periods are needed to assess if this is a real limitation over a long period of time.

- Whilst the model does reproduce the impact of dust binder, to a large extent, it still requires better information concerning the physical characteristics of the dust binding under controlled conditions. Experimental results for this still need to be obtained.

- Model sensitivity experiments were used to access the impact of wet removal processes. These processes have still yet to be quantified experimentally.

Acknowledgements

The NORDUST II project have involved a large number of activities which had not been possible without the skills and helpfulness of the following staff at involved scientific partners:

- VTI: Dennis Hydén, Tomas Halldin, Arne Johansson, Håkan Wilhelmsson, Gustav Danielsson, Håkan Arvidsson, Linda Corper
- Metropolia: Harri Nordlund, Kari Heikkilä, Kari Leskinen, Ville Arffman
- SLB-analys: Max Elmgren, Sanna Silvergren, Jennie Hurkman, Billy Sjövall

The project is also grateful to support and contribution from Thorsteinn Jóhannsson at Umhverfisstofnun, Iceland and Marketta Hyvärinen and Soile Knuuti at Väylävirasto, Finland.

NordFoU

Nordfou.org

C/O Vejdirektoratet

Carsten Niebuhrs Gade 43

1577 København V